Multi-omics characterization of pancreatic neuroendocrine neoplasms

by

Chi-Fu Kevin Yang

B.Sc. (Hons), Simon Fraser University, 2014

Thesis Submitted in Partial Fulfillment of the
Requirements for the Degree of
Doctor of Philosophy

in the
Department of Molecular Biology and Biochemistry
Faculty of Science

SIMON FRASER UNIVERSITY
Summer 2021

Declaration of Committee

Name:	**Chi-Fu Kevin Yang**
Degree:	**Doctor of Philosophy (Molecular Biology and Biochemistry)**
Thesis title:	**Multi-omics characterization of pancreatic neuroendocrine neoplasms**
Committee:	**Chair:** Esther Verheyen Professor, Molecular Biology and Biochemistry
	Sharon Gorski Supervisor Professor, Molecular Biology and Biochemistry
	Janel Kopp Committee Member Assistant Professor, Cellular and Physiological Sciences University of British Columbia
	Ryan Morin Committee Member Associate Professor, Molecular Biology and Biochemistry
	Ly Vu Examiner Assistant Professor, Molecular Biology and Biochemistry
	Dawn Quelle External Examiner Professor, Neuroscience and Pharmacology University of Iowa

Ethics Statement

The author, whose name appears on the title page of this work, has obtained, for the research described in this work, either:

a. human research ethics approval from the Simon Fraser University Office of Research Ethics

or

b. advance approval of the animal care protocol from the University Animal Care Committee of Simon Fraser University

or has conducted the research

c. as a co-investigator, collaborator, or research assistant in a research project approved in advance.

A copy of the approval letter has been filed with the Theses Office of the University Library at the time of submission of this thesis or project.

The original application for approval and letter of approval are filed with the relevant offices. Inquiries may be directed to those authorities.

Simon Fraser University Library
Burnaby, British Columbia, Canada

Update Spring 2016

Abstract

Pancreatic neuroendocrine neoplasms (PNENs) are biologically and clinically heterogeneous neoplasms in which pathogenic alterations are often indiscernible. Treatments for PNENs are insufficient in part due to lack of alternatives once current options are exhausted. Despite previous efforts to characterize PNENs at the molecular level, there remains a lack of molecular subgroups and molecular features with clinical utility for PNENs. In this work, I describe the identification and characterization of four molecularly distinct subgroups from primary PNEN specimens using whole-exome sequencing, RNA-sequencing and global proteome profiling. A Proliferative subgroup with molecular features of proliferating cells was associated with an inferior overall survival probability. A PDX1-high subgroup consisted of PNENs demonstrating genetic and transcriptomic indications of NRAS or HRAS activation. An Alpha cell-like subgroup, enriched in PNENs with deleterious *MEN1* and *DAXX* mutations, bore transcriptomic similarity to pancreatic α-cells and harbored proteomic cues of dysregulated metabolism involving glutamine and arginine. Lastly, a Stromal/Mesenchymal subgroup exhibited increased expression and activation of the Hippo signaling pathway effectors *YAP1* and *WWTR1* that are of emerging interest as potentially actionable targets in other cancer types. Whole-genome and whole-transcriptome analysis of PNEN metastases identified novel molecular events likely contributing to pathogenesis, including one case presumably driven by *MYCN* amplification. In agreement with the findings in primary PNENs, four of the metastatic PNENs displayed a substantial Alpha cell-like subgroup signature and all harboured concurrent mutations in *MEN1* and *DAXX*. Collectively, the identified subgroups present a potential stratification scheme that facilitates the identification of therapeutic vulnerabilities amidst PNEN heterogeneity to improve the effective management of PNENs.

Keywords: pancreatic neuroendocrine neoplasms; whole-genome sequencing; whole-exome sequencing; RNA-sequencing; proteomic profiling

Dedication

To the cancer patients who fearlessly battled through adversity and donated their samples to improve the health of others.

Acknowledgements

This thesis would not have been possible without my supervisor, Dr. Sharon Gorski, who took me in first as an Honours student and later as a PhD student. The road towards completing this thesis was not smooth, and I was often clueless of where this work may lead to. But despite a lengthy, rocky start followed by a lagging progression, Sharon has always encouraged my ideas and decisions and provided guidance that helped me through the difficult time. I am also truly grateful for her understanding of the many mistakes I have made throughout and her altruistic supports. I am thankful of Drs. Janel Kopp and Ryan Morin, who agreed to sit on my committee and provided valuable feedbacks throughout my research. I would like to also thank the examiners for taking the time to read this thesis and attend my defence. My gratitude extends to all the fantastic past and current members of the Gorski lab whom I have had the pleasure to work with, especially Dr. Suganthi Chittaranjan who has been endowing me with various technical skills and conceptual knowledge since I first joined the Genome Sciences Centre as a Co-op student.

The works presented in this thesis were made possible with the generous financial supports from various sources. The tremendous amount of works presented in Chapter 2 was supported by the 2017 Neuroendocrine Tumor Research Foundation-AACR Grant, Grant Number 17-60-33-GORS and the Pancreas Centre BC IDEAS Grant (2013-2015). I am thankful for the financial supports from SFU through Graduate Fellowships, President's PhD Scholarship, Special Graduate Entrance Scholarship and Marion Anderson Travel Award, and the John Bosdet Memorial Fund GSC Trainee Travel Awards from BC Cancer.

The data and results presented in Chapters 2 and 3 of this thesis were the outcomes of multi-team collaborations largely driven by Sharon. All individuals who contributed to the works in these chapters were instrumental, and their specific involvement are listed here in no particular order. For the works in Chapter 2: Steve Kalloger, Drs. John Aird and Michael Lee coordinated sample transfer and reviewed and compiled clinical and pathological data; Dr. Andrew Mungall oversaw sample preparation and sequencing; Karen Mungall oversaw variant calling analysis from whole-exome sequencing reads; Christopher Rushton performed RNA-sequencing quantification; Shane Colborne performed mass-spectrometry and proteomic profiling; Dr. Jörg

Schrader developed and provided the NT-3 cell line; Dr. Jing Xu performed cell culture work; Christine Chow and Dr. Dongxia Gao performed immunohistochemical staining and scoring of tissue microarray; Dr. Joanna Karasinska performed laser-capture microdissection of tissue specimens; Dr. Patrick MacDonald provided cadaveric islet extractions; Drs. Steven Jones, Ryan Morin and Marco Marra supervised the sequencing aspects of the study; Dr. Gregg Morin supervised the proteomic aspects of the study; Drs. Michael Lee, Jonathan Loree and Daniel Renouf provided clinician expertise; Drs. John Aird and David Schaeffer provided pathologist expertise. For Chapter 3: Drs. Hui-li Wong, Jonathan Loree, Hagen Kennecke, Howard Lim, Xiaolan Feng, Janine Davis and Daniel Renouf provided clinician expertise; Drs. Chen Zhou and David Schaeffer provided pathologist expertise; Steve Kalloger and Dr. Joanna Karasinska contributed to data acquisition and interpretation; Drs. Yaoqing Shen and Eric Zhao contributed bioinformatic analysis expertise; Drs. Aly Karsan, Steven Jones, Janessa Laskin, Marco Marra, David Schaeffer, Daniel Renouf and Sharon supervised the study; Drs. Hui-li Wong and Yaoqing Shen contributed to manuscript preparation and submission; other members of the Personalized OncoGenomics program team contributed to sample preparation, sequencing and derivation of data. I would like to also acknowledge and thank Dr. Gian Negri, Dr. Sandra Spencer, Richard Corbett and Dr. Elizabeth Chun for helpful discussion and technical advice on bioinformatic analysis; Drs. Mitsuhiro Komba and Dan Luciani for teaching me about pancreatic islets and how to isolate them; and the members of the Sequencing and Proteomics platforms and the Projects team at the Genome Sciences Centre for continuous supports.

I am sincerely grateful of the patience, support and company from my family. My mom, who still tries to understand what I do, has coached and prepared me for everything. My dad, who seldom shares thoughts, puts his caring into actions that speak louder than words. My sister, who has embraced my childishness, has always volunteered to take family duties away from me so I can focus on my study. My dog served an invaluable role in reducing all the stresses throughout this journey. Last but most importantly, I would like to thank my partner Morgana, who has always been there for me, and to whom I can share all the laughter and tears.

Table of Contents

Declaration of Committee ii
Ethics Statement iii
Abstract iv
Dedication v
Acknowledgements vi
Table of Contents viii
List of Tables xi
List of Figures xii
List of Acronyms xiv

Chapter 1. Introduction to pancreatic neuroendocrine neoplasms 1
1.1. Incidence and prevalence of PNENs 3
1.2. Evolution of cancer classification in PNENs 3
1.2.1. Classification of NENs based on embryological origin 4
1.2.2. Earlier editions of the WHO classification of PNENs 5
1.2.3. Current classification system 8
1.2.4. Cancer staging system 9
1.3. Clinical heterogeneity 9
1.3.1. Functional vs nonfunctional PNENs 9
1.3.2. Hereditary cancer syndromes 11
Multiple endocrine neoplasia type I syndrome 11
Von Hippel-Lindau syndrome 11
Neurofibromatosis type I 12
Tuberous sclerosis complex 12
1.3.3. Treatments and responses 12
PNECs 13
PNETs 13
1.4. Molecular heterogeneity 16
1.4.1. Early biological studies using mouse models 17
1.4.2. Recurrently mutated genes in PNENs 19
MEN1 22
DAXX and ATRX 23
PI3K/AKT/mTOR pathway 23
DNA damage repair 24
1.4.3. Copy number variations in PNENs 25
1.4.4. Transcriptome and subtyping studies of PNENs 29
1.4.5. Proteomic analysis of PNENs 34
1.5. Aims, objectives and chapters overview 35

Chapter 2. Proteotranscriptomic classification and characterization of PNENs 37
2.1. Introduction 37
2.2. Results 38

2.2.1. Whole-transcriptome and global proteome analyses identify four distinct proteotranscriptomic subgroups among PNENs 38
2.2.2. Analysis of a separate cohort of PNENs confirms the four proteotranscriptomic subgroups 43
2.2.3. Comparison of paired transcriptome and proteome profiles reveals modest single gene correlations but shared patterns of gene set enrichment 48
2.2.4. A Proliferative PNEN subgroup is associated with unfavourable clinicopathological characteristics and molecular features of cell cycle progression 51
2.2.5. Transcriptomic and proteomic analysis reveals differential enrichment of *ARX*, *PDX1* and organellar proteins between subgroups 54
2.2.6. The Stromal/Mesenchymal subgroup specimens are enriched in stromal and immune cells 57
2.2.7. Mutational differences between the proteotranscriptomic subgroups suggest distinct oncogenic drivers 59
2.2.8. Inferred activities of key cellular regulators are consistent with mutational differences and suggest involvement of the Hippo signaling pathway in the Stromal/Mesenchymal subgroup 62
2.3. Discussion 64
2.4. Methods 68
2.4.1. Case and clinical information accrual 68
Tumour specimens 68
Cell lines 69
Normal islet samples 69
Clinicopathological characteristics 69
2.4.2. Sample processing 70
FFPE tissue nucleic acid extraction 70
Snap-frozen tissue nucleic acid extraction 70
RNA-seq 70
Protein extraction and digestion 72
Peptide labeling and fractionation 73
MS analysis 73
Genomic library construction 74
WES 75
2.4.3. Data analysis 75
RNA quantification and sample exclusion 75
Protein quantification and preprocessing 76
cNMF 77
Differential analysis 78
Gene and protein ID conversions 78
Enrichment analysis 78
PCA 79
GSVA 79
CIBERSORT 79
Cellular regulator activity inference analysis 80
Variant calling and prioritization 80

IHC analysis 81
2.4.4. Data deposition and access 82
2.4.5. Key Resources Table 82

Chapter 3. Whole-genome and transcriptome analyses of metastatic PNENs .. 88
3.1. Introduction 88
3.2. Results 90
3.2.1. Clinical Presentation and Treatment Outcomes 90
Case 1 91
Case 2 92
Case 3 92
Case 4 93
Case 5 93
3.2.2. Genomic analyses 94
3.2.3. Shared molecular alterations 97
3.2.4. Case-specific molecular alterations of interest 98
Case 1 98
Case 2 99
Case 3 99
Case 4 101
Case 5 101
3.2.5. Proteotranscriptomic subgroup of metastatic PNENs 101
3.3. Discussion 106
3.4. Methods 111
3.4.1. Sample collection and processing 111
3.4.2. Sequencing and Bioinformatics 112
3.4.3. Gene expression analysis 113
3.4.4. Sequencing result visualization 113
3.4.5. Data deposition and access 114

Chapter 4. Conclusions and future directions 115
4.1. Novel alterations in PNENs 115
4.1.1. Activation of HRAS and NRAS in PDX1-high PNENs 115
4.1.2. Activation of Hippo signaling pathway effectors in Stromal/Mesenchymal PNENs 116
4.1.3. Dysregulated metabolism involving arginine and glutamine in Alpha cell-like PNENs 118
4.1.4. Focal amplification of *MYCN* concomitant with a *MCYN*-driven transcriptomic signature in a metastatic PNEN 119
4.2. Emerging molecularly based classifications 121
4.3. Expanding to other NENs 123
4.4. Concluding remarks 126

References 128

Appendix Supplemental Data File 158

List of Tables

Table 1.1. Evolution of WHO classification systems for PNENs. 6
Table 1.2. The proportional of functional vs nonfunctional PNENs in reported cohorts. 10
Table 1.3. Hereditary cancer syndromes leading to predisposition of PNENs. 11
Table 1.4. Recurrently mutated genes in PNENs. 20
Table 1.5. Existing PNEN subtyping studies and subtype characteristics. 26
Table 2.1. Clinicopathological characteristics of the PNEN cohorts 39
Table 2.2. Clinicopathological associations of the proteotranscriptomic subgroups using all 84 PNENs included in this study. 52
Table 3.1. Baseline characteristics of the five patients with metastatic PNENs. 90
Table 3.2. Sequence variants in genes previously implicated in PNENs. 98
Table 3.3. All metastatic PNENs enrolled in the POG program up to March 2021. 102
Table 3.4. Mutational status of *MEN1*, *DAXX* and *ATRX* in the 9 POG PNENs. ... 105
Table 3.5. Tumour content and sequencing coverage for the five metastatic PNENs 112

List of Figures

Figure 1.1. The exocrine and endocrine components of the pancreas. 2
Figure 1.2. Embryological classification of NENs. 5
Figure 2.1. cNMF rank survey of the Discovery cohort specimens based on transcriptomic profiles. 40
Figure 2.2. cNMF rank survey of the Discovery cohort specimens based on proteomic profiles. 41
Figure 2.3. Whole-transcriptome and global proteome analyses identify four distinct proteotranscriptomic subgroups among PNENs. 42
Figure 2.4. PCA of the Discovery cohort specimens. 43
Figure 2.5. cNMF rank survey of the Validation cohort specimens plus control samples based on transcriptomic profiles. 44
Figure 2.6. cNMF rank survey and comparison of subgroup assignments of the Validation cohort specimens. 45
Figure 2.7. cNMF rank survey and subgroup distribution of the Discovery and Validation cohort specimens. 46
Figure 2.8. cNMF rank survey and subgroup comparisons of the Sadanandam et al. dataset 47
Figure 2.9. Comparison of paired transcriptome and proteome profiles reveals modest single gene correlations. 49
Figure 2.10. Paired transcriptome and proteome profiles exhibit shared patterns of gene set enrichment. 50
Figure 2.11. Overall survival probability of all 84 PNEN patients included in this study. 51
Figure 2.12. The top cellular components enriched or depleted on the protein level in each proteotranscriptomic subgroup. 54
Figure 2.13. Subgroups are characterized by difference in enrichment of cell types. 57
Figure 2.14. Differences in enrichment of non-tumour cells between the four subgroups. 58
Figure 2.15. Mutational differences between the proteotranscriptomic subgroups suggest distinct genetic drivers 61
Figure 2.16. Inferred activities of cellular regulators are consistent with mutational differences and suggest involvement of the Hippo signaling pathway in the Stromal/Mesenchymal subgroup 64
Figure 3.1. Clinical evolution and treatment of the five patients with metastatic PNENs 91
Figure 3.2. Genome-wide copy-number architectures across the five cases. 95
Figure 3.3. Key molecular alterations and predicted upstream regulators across the five cases. 96
Figure 3.4. Illustration of the two structural variants involving *TSC2* identified in Case 3. 100

Figure 3.5. Comparison of mutation signature of case 3 to signature 30. 100
Figure 3.6 Correlation of POG PNENs to each of the proteotranscriptomic PNEN subgroups. 103
Figure 3.7. Transcriptomic similarity of each POG PNEN to the four proteotranscriptomic subgroups. 105
Figure 3.8. mRNA expression levels of *ARX*, *PDX1*, *YAP1* and *WWTR1* in the 9 POG PNENs. 106
Figure 4.1. Consensus hierarchical clustering result of the POG NENs. 126

List of Acronyms

5-HTP	5-hydroxytryptophan
AEBP1	AE binding protein 1
AJCC	American Joint Committee on Cancer
AKT1	AKT serine/threonine kinase 1
ALDH1	Aldehyde dehydrogenase 1
ALT	Alternative lengthening of telomere
ANXA6	Annexin A6
APC	APC regulator of WNT signaling pathway
AR	Androgen receptor
ARG2	Arginase 2
ARID2	AT-rich interaction domain 2
ARX	Aristaless related homeobox
ATM	ATM serine/threonine kinase
ATRX	ATRX chromatin remodeler
AXIN2	Axin 2
BEND2	BEN domain containing 2
BET	Bromodomain and extra-terminal subfamily
BRAF	B-Raf proto-oncogene, serine/threonine kinase
BRCA2	BRCA2 DNA repair associated
Cap/Tem	Capecitabine plus temozolomide
Carbo/Iri	Carboplatin plus irinotecan
CASP3	Caspase 3
CASR	Calcium sensing receptor
CD31	Platelet and endothelial cell adhesion molecule 1; also known as PECAM1
CD34	CD34 molecule
CDK4	Cyclin dependent kinase 4
CDK6	Cyclin dependent kinase 6
CDKN1B	Cyclin dependent kinase inhibitor 1B
CDKN2C	Cyclin dependent kinase inhibitor 2C
CgA	Serum chromogranin A
CHEK2	Checkpoint kinase 2

CHGA	Chromogranin A
ChIP-seq	Chromatin immunoprecipitation sequencing
CIN	Chromosomal instability
Cis/Etop	Cisplatin plus etoposide
cNMF	Consensus non-negative matrix factorization
CNPY2	Canopy FGF signaling regulator 2
CNV	Copy number variation
CT	Computed tomography
CTNNB1	Catenin beta 1
DAP	Differentially abundant protein
DAXX	Death domain associated protein
DEG	Differentially expressed gene
DEPDC5	DEP domain containing 5, GATOR1 subcomplex subunit
EGA	European Genome-phenome Archive
EMT	Epithelial-to-mesenchymal transition
EWSR1	EWS RNA binding protein 1
FDR	False discovery rate
FFPE	Formalin-fixed paraffin-embedded
FLI1	Fli-1 proto-oncogene, ETS transcription factor
FLT1	Fms related receptor tyrosine kinase 1
FOXM1	Forkhead box M1
G(1/2/3)	Grade 1/2/3
GAST	Gastrin
GATA6	GATA binding protein 6
GCG	Glucagon
GCK	Glucokinase
GEP	Gene expression profile
GEP-NEN	Gastroenteropancreatic neuroendocrine neoplasm
GI	Gastrointestinal
GLS	Glutaminase
GLUD2	Glutamate dehydrogenase 2
GLUL	Glutamate-ammonia ligase
GSA	Gene set analysis

GSVA	Gene set variation analysis
H3	Histone H3
H3.3	Histone H3 variant H3.3
H3K27ac	H3 lysine 27 acetylation
HGNC	HUGO Gene Nomenclature Committee
HIF1A	Hypoxia inducible factor 1 subunit alpha
HNF1B	HNF1 homeobox B
HR	Homologous recombination
HRAS	HRas proto-oncogene, GTPase
Igf1r	Insulin growth factor 1 receptor
Igf2	Insulin-like growth factor 2
IHC	Immunohistochemical
IHCT	International Histological Classification of Tumours
INA	Internexin neuronal intermediate filament protein alpha
Indel	Small insertion and deletion
INSM1 (Insm1)	Insulinoma-associated 1
IRX2	Iroquois homeobox 2
KDR	Kinase insert domain receptor
KMT2C	Lysine methyltransferase 2C
KRAS	KRAS proto-oncogenes, GTPase
LATS(1/2)	Large tumor suppressor kinase 1/2
LC	Large-cell type
LCM	Laser capture microdissection
LOH	Loss of heterozygosity
MAFA	MAF bZIP transcription factor A
MANEC	Mixed adeno-neuroendocrine carcinoma
MAP1B	Microtubule associated protein 1B
MAP2	Microtubule associated protein 2
MAPK	Mitogen-activated protein kinase
MCM	Minichromosome maintenance
MEN1 (Men1)	Menin 1
MEN1 syndrome	Multiple endocrine neoplasia type I
MGMT	O-6-methylguanine-DNA methyltransferase

MiNEN	Mixed non-neuroendocrine-neuroendocrine neoplasm
MKI67	Marker of proliferation Ki-67
MLP	Metastasis-like primary
MS	Mass spectrometry
MTAP	Methylthioadenosine phosphorylase
MTOR	Mechanistic target of rapamycin kinase
mTORC1	mTOR complex 1
MUTYH	MutY DNA glycosylase
MYC	MYC proto-oncogene, bHLH transcription factor
MYCL	MYCL proto-oncogene, bHLH transcription factor
MYCN	MYCN proto-oncogene, bHLH transcription factor
NEC	Neuroendocrine carcinoma
NEN	Neuroendocrine neoplasm
NET	Neuroendocrine tumour
NEUROD1	Neuronal differentiation 1
NEUROG3	Neurogenin 3
NF(1/2)	Neurofibromin 1/2
NF1 disorder	Neurofibromatosis type I
NRAS	NRAS proto-oncogene, GTPase
NTHL1	nth like DNA glycosylase 1
ONECUT(1/2)	One cut homeobox 1/2
OxPhos	Oxidative phosphorylation
PAX8	Paired box 8
PCA	Principal component analysis
PDAC	Pancreatic ductal adenocarcinoma
PDEC	Poorly-differentiated endocrine carcinoma
PDX1	Pancreatic and duodenal homeobox 1
PIK3CA	Phosphatidylinositol-4,5-bisphosphate 3-kinase catalytic subunit alpha
PNEC	Poorly-differentiated pancreatic neuroendocrine carcinoma
PNEN	Pancreatic neuroendocrine neoplasm
PNET	Well-differentiated pancreatic neuroendocrine tumour
POG	Personalized oncogenomics
PRRT	Peptide receptor radionuclide therapy

PRRX2	Paired related homeobox 2
PTEN	Phosphatase and tensin homolog
PTF1A	Pancreas associated transcription factor 1a
RAB11B	RAB11B, member RAS oncogene family
RB1 (Rb1)	RB transcriptional corepressor 1
RECIST	Response Evaluation Criteria in Solid Tumors
RET	Ret proto-oncogene
RNA-seq	RNA-sequencing
RPKM	Reads per kilobase of transcript per million mapped reads
RTK	Receptor tyrosine kinase
SC	Small-cell type
SLC2A(1/2)	Solute carrier familiar 2 member 1/2
SMARACA4	SWI/SNF related, matrix associated, actin dependent regulator of chromatin, subfamily a, member 4
SNP	Single nucleotide polymorphism
SNV	Single nucleotide variant
SOX9	SRY-box transcription factor 9
SPIA	Signaling pathway impact analysis
SSA	Somatostatin analog
SST	Somatostatin
SSTR(1~5)	Somatostatin receptor (1~5)
STK(3/4)	Serine/threonine kinase 3/4
SV	Structural variation
SYP	Synaptophysin
TCA	Tricarboxylic acid
TCF3	Transcription factor 3
TCGA	The Cancer Genome Atlas
TFEA	Transcription factor enrichment analysis
TIL	Tumour infiltrating lymphocyte
TMA	Tissue microarray
TMB	Tumour mutation burden
TME	Tumour microenvironment
TMT	Tandem mass tag
TP53	Tumor protein p53

TPD52	Tumor protein D52
TPM	Transcript per million
TRAF7	TNF receptor associated factor 7
Trp53	Transformation related protein 53
TSC	Tuberous sclerosis complex
TSC(1/2)	TSC complex subunit (1/2)
TUBB3	Tubulin beta 3 class III
UBC	University of British Columbia
UCHL1	Ubiquitin C-terminal hydrolase L1
VCAN	Versican
VEGFR	Vascular endothelial growth factor receptor
VHL	von Hippel-Lindau tumour suppressor
VHL syndrome	von Hippel-Lindau syndrome
VIP	Vasoactive intestinal peptide
WDEC	Well-differentiated endocrine carcinoma
WDET	Well-differentiated endocrine tumour
WES	Whole-exome sequencing
WGS	Whole-genome sequencing
WHO	World Health Organization
WTS	Whole-transcriptome sequencing
WWTR1	WW domain containing transcription regulator 1; also common known as TAZ
Y-90	^{90}yttrium
YAP1	Yes1 associated transcription regulator
YY1	YY1 transcription factor

Chapter 1.

Introduction to pancreatic neuroendocrine neoplasms

Neuroendocrine neoplasms (NENs) are a group of rare but heterogeneous tumours arising from neuroendocrine cells that can be found within dedicated endocrine tissues and diffusely throughout the body (Oronsky et al., 2017). The endocrine compartment of the pancreas, the islets of Langerhans, (Figure 1.1) is an example of dedicated endocrine tissue from which pancreatic NENs (PNENs) can arise. The history of NENs began in the mid-to-late 19th century with the repeated post-mortem observations of atypical masses in the small intestine. In contrast to the aggressive behaviours typically seen with carcinomas, these masses had no or low-grade invasion into the surrounding tissues and were referred to as “benign carcinomas” by the German physician and pathologist Siegfried Oberndorfer (Modlin et al., 2004). These “benign carcinomas” were rarely observed, and as such the indications and characteristics of these tumours remained cryptic until an entity-defining publication by Oberndorfer in 1907 (Modlin et al., 2004). In his seminal paper, Oberndorfer proposed that these rare growths belong to a novel disease entity and coined the term “karzinoide”, now referred to as carcinoid, to describe their “carcinoma-like” characteristics while distinguishing them from the classical carcinomas with highly aggressive clinical behaviours (Modlin et al., 2004; Oberndorfer, 1907). Nearly a decade later, it was found that carcinoid tumours shared biochemical properties with a neuroendocrine cell type in the small intestine, specifically in their ability to reduce silver salts (ie. argentaffin). This similarity suggested neuroendocrine cells as the likely cells-of-origin of carcinoid tumours (Modlin et al., 2004) and marked the first evidence supporting the probable neuroendocrine origin of carcinoid tumours.

Subsequent to the discoveries of small intestinal carcinoid tumours, tumours of similar clinical and biochemical behaviours were observed in other organs such as the stomach and pancreas (Feyrter, 1938). It is now recognized that tumours can originate from neuroendocrine cells found throughout the body (Oronsky et al., 2017). Despite their rather short history since discovery, the terminologies for these neuroendocrine

cell-derived neoplasms have gone through considerable modifications. For the purpose of this thesis, they are generically referred to as NENs, which include any neoplasms with neuroendocrine differentiation.

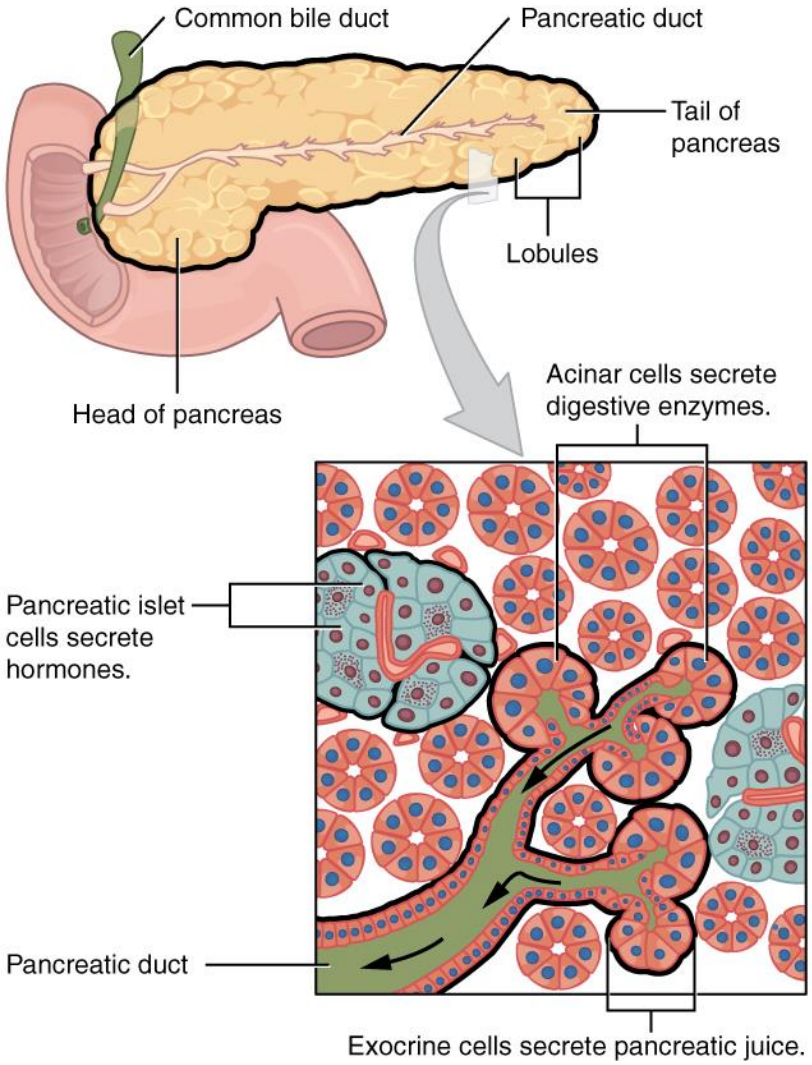

Figure 1.1. The exocrine and endocrine components of the pancreas.
The pancreas consists of an exocrine component, acinar and duct cells, and an endocrine component, islets. The islets are scattered throughout the pancreas and are clusters of different cell types that secrete various hormones for maintaining body homeostasis. The image was adapted from the original work by OpenStax College, obtained from the public domain Wikimedia (under the license CC BY 3.0).

Among NENs of different primary sites, those arising from the gastrointestinal (GI) tract and the pancreas were typically combined in earlier studies and referred to as gastroenteropancreatic NENs (GEP-NENs) due to the anatomical proximity and similar cells of origins of these organs (Modlin et al., 2008). However, it was later recognized that PNENs differed from extrapancreatic NENs in their responses to therapies (Kulke et

al., 2011), warranting separate assessments and considerations for PNENs (Kunz, 2015). Since PNENs have been analyzed separately from other NENs in the last decade only, studies focusing solely on PNENs have been limited; many of the early studies included PNENs as part of a study on NENs of all sites or GEP-NENs. Our knowledge of PNENs has therefore lagged and there is a dire need for the clinical, biological, and the integrated understanding of this under-studied disease to facilitate clinical management of PNENs. In this chapter, an abundance of background information referenced and introduced relates to NENs in general or GEP-NENs. Where applicable, studies or results specific to PNENs are indicated.

1.1. Incidence and prevalence of PNENs

NENs are considered rare neoplasms accounting for ~1.5% of new cancer diagnoses, but the annual incidence of NENs increased 6.4-fold while the incidence of all malignancies remained stable between 1973 and 2012 (Dasari et al., 2017). This rising NEN incidence has largely been due to expanded availability of advanced imaging technologies and has led to increased diagnosis of early-stage diseases, suggesting the prevalence of NENs is higher than originally expected despite their low incidence (Dasari et al., 2017; Hallet et al., 2015). Indisputably, due to their typically slow-growing nature, the prevalence of NENs has exceeded those of esophageal, gastric, pancreatic and hepatobiliary cancers (Yao et al., 2008). For PNENs, the annual incidence increased substantially from less than 0.2 to 0.84 per 100,000 individuals in the United States between 1973~2012 (Dasari et al., 2017) and from 0.1 to 0.6 per 100,000 individuals in Canada (Ontario) between 1994~2009 (Hallet et al., 2015). The proportion of metastatic disease among new diagnoses, however, decreased during the period while more patients presented with localized disease, supporting the hypothesis that increased detection of early-stage disease is leading to higher incidence (Dasari et al., 2017; Hallet et al., 2015).

1.2. Evolution of cancer classification in PNENs

A cancer classification system not only divides a cancer type into classes based on similar presentations and anatomical locations but also aids in providing prognostic and therapeutic implications for a given class to facilitate clinical management (Carbone,

2020). Our initial paucity and recent exponential gain of knowledge of PNENs is perhaps best represented by the numerous attempts to devise a classification system, initially for NENs and more recently for PNENs specifically, over the course of the past 6 decades.

1.2.1. Classification of NENs based on embryological origin

Establishment of a cancer classification system relies on, and is built upon, prior clinical observations and evidence, which were seemingly lacking during the early years following the first recognition of NENs. The first classification system for NENs was proposed by Williams and Sandler in 1963, 56 years after Oberndorfer coined the term “karzinoide” (Modlin et al., 2004). In their paper, Williams and Sandler suggested that NENs could be grouped based on the embryological origin of the organ from which a NEN arose from. This stratified NENs into foregut, midgut and hindgut NENs (Figure 1.2). Their recommendation was based on the observations that NENs could vary in histological structures, frequency of cells being argentaffin, secretion of 5-hydroxytryptophan (5-HTP) and accompanying carcinoid syndrome in patients (Williams and Sandler, 1963). Formulated on the combination of these characteristics, NENs arising from the foregut (eg. bronchus, stomach and pancreas), midgut (eg. mid-duodenum, cecum and mid-transverse colon), or hindgut (eg. descending colon and rectum) were found more similar to those arising from organs of the same embryological origin than those that differed (Williams and Sandler, 1963). Although this classification system is now considered superficial, it was a pioneering effort to classify NENs based on histopathology, which remains the foundation for the current NEN classification system established by the World Health Organization (WHO).

1907 Oberndorfer

"Karzinoide" (Carcinoid)
Little to no invasion
Generally small in size
Extremely slow growing

1963 Williams & Sandler

	Foregut	Midgut	Hindgut
Argentaffin	*Usually negative*	*Mostly positive*	*Often negative*
Carcinoid syndrome	*Frequent*	*Frequent*	*None*
5-HTP secretion	*Frequent*	*Rare*	*None*
Histology	*Trabecular*	*Nesting*	*Trabecular*

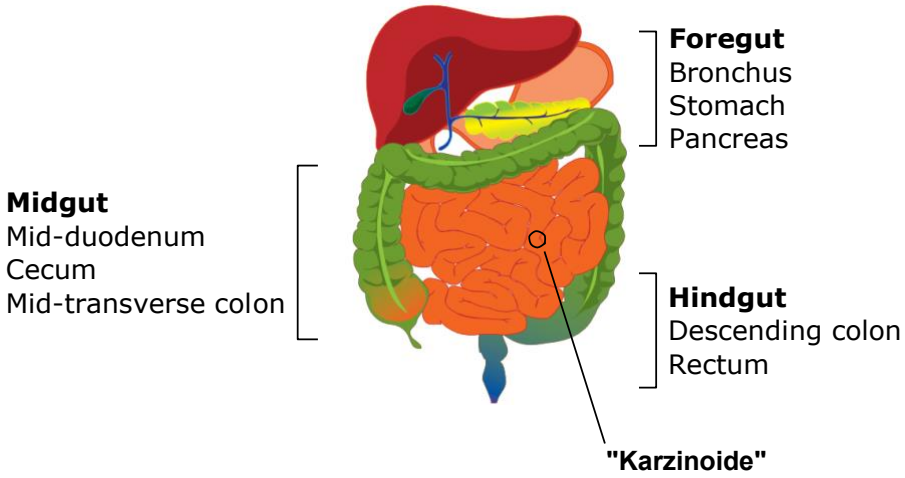

Figure 1.2. Embryological classification of NENs.
The carcinoid tumours first identified by Siegfried Oberdorfer in 1907 in the small intestine were subsequently found in other organs and later classified by Williams and Sandler in 1963 based on embryological origins. The foregut, midgut and hindgut carcinoid tumours were found to differ in frequencies of being argentaffin, accompanying carcinoid syndrome and 5-HTP and histological presentations. Note that a recent study identified a greater proportion of small intestinal NENs with carcinoid syndrome compared to NENs of the lungs or other primary sites (Halperin et al., 2017). Image of the gut was adapted from the original work by Mikael Häggström, obtained from the public domain Wikimedia Human body diagrams (under the license CC0).

1.2.2. Earlier editions of the WHO classification of PNENs

The WHO classification system is currently the only clinically relevant and standardized classification for PNENs. Its antecedent, the International Histological Classification of Tumours (IHCT), commenced in 1967 and primarily relied on histological examinations (Sobin, 1981) which later incorporated immunohistochemical (IHC) assessments in the subsequent edition (Sobin, 1989). The first and second editions of IHCT on GI cancer were published in 1976 and 1990, respectively. The later

edition improved on a few key cancer types, including GEP-NENs (still referred to as carcinoids at the time) for which the IHC assessments of hormones (eg. gastrin, somatostatin, pancreatic polypeptides) superseded the traditional silver staining in subclassifying GEP-NENs (Jass et al., 1990) (Table 1.1).

Table 1.1. Evolution of WHO classification systems for PNENs.

Classification System	Well-differentiated			Poorly-differentiated	Mixed Histology
IHCT 1976/1990	**Carcinoid** Argentaffinity (1st edition) IHC of specific hormones (2nd edition) Histology (for diagnosis only)				
2000/2004 WHO (PNEN)	**WDET** <u>Benign</u> Confined to pancreas No perineural invasion No angioinvasion < 2 cm in diameter < 2 mitotic rate[b] or < 2% Ki67 <u>Uncertain Behaviour</u> Confined to pancreas At least one of: perineural invasion, angioinvasion, > 2cm in diameter, 2-10 mitotic rate or > 2% Ki67 **WDEC** Local invasion and/or metastases			**PDEC** > 10 mitotic rate	
2010 WHO (GEP-NEN)[a]	**NET-G1** < 2 mitotic rate or ≤ 2% Ki67	**NET-G2** 2-20 mitotic rate or 3-20% Ki67	**NEC-G3** > 20 mitotic rate or > 20% Ki67 LC or SC		**MANEC** ≥ 30% are NE cells
2017/2019 WHO (PNEN)	**NET-G1** < 2 mitotic rate or < 3% Ki67	**NET-G2** 2-20 mitotic rate or 3-20% Ki67	**NET-G3** > 20 mitotic rate or > 20% Ki67	**NEC** LC or SC type	**MiNEN** ≥ 30% are NE cells

[a]The hyperplasia/dysplasia class from the WHO 2010 classification referred to pre-neoplastic lesions and is excluded from this table. [b]Mitotic rate: number of mitotic cells / 10 high power fields. IHC: immunohistochemistry, NE: neuroendocrine, NEN: NE neoplasm, NEC: NE carcinoma, NET: NE tumour, GEP-NEN: gastroenteropancreatic NEN, PNEN: pancreatic NEN, MANEC: mixed adeno-neuroendocrine carcinoma, MiNEN: mixed neuroendocrine-nonneuroendocrine neoplasm, WDET: well-differentiated endocrine tumour, WDEC: well-differentiated endocrine carcinoma, PDEC: poorly-differentiated endocrine carcinoma, LC: large cell, SC: small cell, WHO: World Health Organization.

Ten years later, the WHO Classification of Tumours project replaced and continued the mission of the IHCT in standardizing cancer classifications based on histopathology with the addition of molecular genetics to facilitate clinical management (Kleihues and Sobin, 2000). This refreshed classification system also included the first WHO classification section dedicated to PNENs (published in 2004). The 2000/2004 WHO classification system proposed to classify PNENs based on histological differences, prognostic markers and stage of the disease into three groups: well-differentiated endocrine tumour (WDET), well-differentiated endocrine carcinoma (WDEC) and poorly-differentiated endocrine carcinoma (PDEC); this classification was similarly proposed for other GEP-NENs. For PNENs, WDETs were those confined to the pancreas and were further subclassified into benign or tumours of uncertain behaviour based on size, proliferative potential, and presence of vascular and perineural invasions. WDECs were NENs with evidence of gross local invasion and/or metastases, while PDECs were those of poorly-differentiated histology and high proliferative potential (Heitz et al., 2004) (Table 1.1). The criteria implemented in this system, however, overlapped largely with cancer staging (eg. local invasion and distant metastasis), and the intrinsic ambiguities associated with WDETs of uncertain behaviour could potentially lead to confusions between clinicians and pathologists. Updates to the WHO classification for GEP-NENs were therefore proposed to address these concerns (Rindi et al., 2014).

In 2010, a new edition of the WHO classification for GEP-NENs was published and similarly implemented the histological differentiation and proliferative potential criteria of its predecessor. However, it also proposed major rectifications, including the use of “neuroendocrine” instead of “endocrine” to better reflect the biological nature of NENs. Therein, GEP-NENs were grouped into five classes: 1) neuroendocrine tumour (NET)-G1, 2) NET-G2, 3) neuroendocrine carcinoma (NEC)-G3, 4) mixed adeno-neuroendocrine carcinoma (MANEC), and 5) hyperplastic/dysplastic neoplasm. The term “carcinoma” implies poorly-differentiated histology and NECs may be of small cell or large cell type (Rindi et al., 2010). The term “NENs” was used as a generic term to refer to both NETs and NECs, and this usage is adopted throughout this thesis.

Among the five classes, NET-G1/2 and NEC-G3 were defined according to proliferative potential (based on Ki67 or mitotic index), while MANEC and hyperplastic/dysplastic neoplasm (Rindi and Solcia, 2007) were defined based on histological and morphological assessments (Table 1.1). The grading-based grouping of the first three classes proved to be prognostically significant, however, it was later determined inadequate due to a Ki67 categorization gap between NET-G1 (≤ 2% Ki67 index) and NET-G2 (3–20% Ki67 index) and the assumption that all NECs-G3 were poorly-differentiated and with high proliferative potential (Rindi et al., 2014). These limitation and assumption were particularly evident for NENs in the pancreas, where the histological differentiation status is highly correlated with responses to different therapies (Inzani et al., 2018).

1.2.3. Current classification system

Subsequently in 2017, the WHO classification was updated for PNENs to include a NET-G3 class to accommodate well-differentiated PNENs (ie. PNETs) with a proliferative potential greater than the G2 range. The grading threshold of NET-G1 was also increased from ≤ 2 to < 3% Ki67 index (Lloyd et al., 2017). In addition, the updates in the 2017 classification system included removal of the hyperplastic/dysplastic class and redefinition of MANEC into mixed non-neuroendocrine-neuroendocrine neoplasm (MiNEN) that encompasses NENs with substantial neuroendocrine and non-neuroendocrine components (Table 1.1).

At the time of writing this thesis, the release of the new edition of the WHO Classification of Tumours series has commenced, with the first volume published in 2019 covering cancers of the GI tract including GEP-NENs. In this most up-to-date version, GEP-NENs are classified similar to the 2017 WHO classification for PNENs, and no specific changes were proposed for PNENs. This 2017/2019 WHO classification of PNENs has been widely adapted, and the works that will be introduced in the subsequent chapters of this thesis are based on the criteria and terminologies of this updated classification system. That is, PNENs are divided based on their histological differentiation into well-differentiated PNETs and poorly-differentiated PNECs, where PNETs may be further classified into G1-3 based on proliferative potential and PNECs may be of small-cell type (PNEC-SC) or large-cell type (PNEC-LC) (Table 1.1).

1.2.4. Cancer staging system

In addition to the WHO classification, it is worth mentioning that PNENs are TNM-staged like other cancer types as of 2009 using the American Joint Committee on Cancer (AJCC) 7th edition staging system (Kulke et al., 2010a). The TNM staging describes the size (T), and evidence of local spread (N) and distant metastasis (M) of any given tumour to aid with its clinical management. This TNM staging system is used complementarily to the WHO classification system for clinical management.

1.3. Clinical heterogeneity

A major hurdle in the management of PNENs is clinical heterogeneity, where patients present with a wide spectrum of clinical manifestations and the neoplasms have variable characteristics and responses to therapies. Although NENs were initially described as “benign carcinoma” due to their usually indolent clinical nature, disease-related mortality has become evident, especially in patients with PNENs diagnosed in a metastatic setting or eventually becoming metastatic (Hallet et al., 2015; Niederle et al., 2010). Indeed, patients with PNENs have among the shortest median overall survival time (3.6 years) compared to patients with NENs in general (9.3 years), but the 5-year overall survival probabilities for patients with PNENs have been reported to range from 26% to 100% depending on various clinical phenotypes (Halfdanarson et al., 2008; Yao et al., 2008). Variables such as the spread of the disease at the time of diagnosis, the spectrum of symptoms patients present with, the underlying hereditary cancer syndromes leading to predisposition of PNENs and the variable responses to treatments all contribute to the often unpredictable disease prognosis and behaviours of PNENs.

1.3.1. Functional vs nonfunctional PNENs

PNENs can be clinically defined as functional or nonfunctional, which is independent from their WHO classification designation. Functional PNENs are found in patients presenting with hormonal syndromes resulting from the hypersecretion of one or more amines or peptides by the neoplasms. In comparison, nonfunctional PNENs do not result in specific hormonal syndromes and are more clinically silent but account for the majority of PNEN incidences (Halfdanarson et al., 2008) (Table 1.2). Functional PNENs are named according to the hormone they secrete in excess, and the most common

functional PNENs are insulinomas and gastrinomas with hypersecretion of insulin and gastrin, respectively (Halfdanarson et al., 2008; Ito et al., 2012). Each of these hormones, when secreted in excess, leads to a particular syndrome often with nonspecific manifestations. For example, a patient with insulinoma may suffer from hypoglycemia due to excessive insulin secretion by the neoplasms (Hofland et al., 2020a). Hypersecretion of more than one hormone in functional PNENs is rare and has only been observed in metastatic cases (Crona et al., 2016).

Table 1.2. The proportional of functional vs nonfunctional PNENs in reported cohorts.

	Proportion of all PNENs
Functional PNENs	
Insulinoma	30-45%
Gastrinoma	16-30%
VIPoma	< 10%
Glucagonoma	< 10%
Nonfunctional PNENs	25-100%

Data adapted from (Halfdanarson et al., 2008). The data had originally been compiled by Halfdanarson et al. from 25 prior studies. For functional PNENs, only the four most common types are shown. VIP: vasoactive intestinal peptide.

The indication of whether a PNEN is functional or nonfunctional is strictly defined within the clinical setting: nonfunctional PNENs may still be secretory, but their secretions do not result in clinically significant syndromes (Ito et al., 2012). This functional status indication is important from a clinical perspective, as the resultant hormonal syndrome often needs to be controlled concurrent with the anti-cancer regimen directed at the PNENs (Ito et al., 2012). Yet, despite functional PNENs causing hormonal syndromes, the prognoses of functional PNENs are typically better than nonfunctional PNENs (Wang et al., 2011a). For instance, patients with benign insulinomas have a 10-year overall survival rate of 78%, while patients with nonfunctional PNENs have a 5-year overall survival rate of 26-58% (Halfdanarson et al., 2008). The reasons behind this survival difference are not entirely known but may be partly attributed to a greater proportions of functional PNENs (insulinomas in particular) being benign and most nonfunctional PNENs becoming only symptomatic and detected at later disease stage (Cloyd and Poultsides, 2015; Halfdanarson et al., 2008; Vinik et al., 2010).

1.3.2. Hereditary cancer syndromes

The vast majority of PNENs are sporadic, but it has been well-established that a few hereditary cancer syndromes can lead to predisposition of, and contribute to, up to 10% of PNENs (de Wilde et al., 2012). These syndromes are the consequences of germline alterations to tumour suppressor genes menin 1 (*MEN1*), von Hippel-Lindau tumour suppressor (*VHL*), TSC complex subunit 1/2 (*TSC1/2*) and neurofibromin 1 (*NF1*) that result in a multitude of hyperplastic/neoplastic growths in certain organs (Alexakis et al., 2004) (Table 1.3). The degrees to which PNENs contribute to the mortality of the patients with these hereditary cancer syndromes among various manifestations are not well-known, but the presence of PNENs was associated with an inferior survival outcome in patients with multiple endocrine neoplasia type I (MEN1) syndrome (Jensen et al., 2008), suggesting PNENs contribute, at least partially, to the mortality of patients presenting with these hereditary cancer syndromes.

Table 1.3. Hereditary cancer syndromes leading to predisposition of PNENs.

Hereditary cancer syndrome	Affected gene	Prevalence among population	Frequency of PNENs in affected individuals
Multiple endocrine neoplasia type I	*MEN1*	1-10 / 100,000	60%
Von Hippel-Lindau syndrome	*VHL*	2-3 / 100,000	< 20%
Neurofibromatosis type I	*NF1*	1 / 3,000-4,000	< 10%
Tuberous sclerosis complex	*TSC1/2*	1 / 10,000	Rare

Data adapted from (Alexakis et al., 2004; Ito et al., 2012; de Wilde et al., 2012).

Multiple endocrine neoplasia type I syndrome

MEN1 syndrome is a rare autosomal dominant condition that results from germline alterations in the *MEN1* gene and is characterized by hyperplastic/neoplastic growths in the parathyroid, enteropancreatic tissues and pituitary. PNENs are evident in more than 60% of MEN1 patients. And similar to sporadic PNENs, MEN1-associated PNENs may be functional or nonfunctional, with the latter constituting the majority of observations (Ito et al., 2012; Jensen et al., 2008).

Von Hippel-Lindau syndrome

Von Hippel-Lindau (VHL) syndrome is also a rare autosomal dominant condition. Patients with VHL syndrome harbour germline alterations in the *VHL* genes and typically present with multiple tumours and/or cysts of various phenotypes. PNENs are observed

in less than 20% of patients with VHL syndrome, but nearly all VHL syndrome-associated PNENs are nonfunctional (Alexakis et al., 2004; Ito et al., 2012; Jensen et al., 2008).

Neurofibromatosis type I

Neurofibromatosis type I (NF1) disorder results from germline alterations in the *NF1* gene and is a relatively common condition compared to MEN1 and VHL (Alexakis et al., 2004). Common clinical manifestations of NF1 include disorders of the nervous system such as benign or malignant tumours of the central and peripheral nervous systems. Only up to 10% of patients with NF1 disorder develop PNENs, and these PNENs can be functional or nonfunctional (Ito et al., 2012; Jensen et al., 2008).

Tuberous sclerosis complex

Tuberous sclerosis complex (TSC) is an autosomal dominant condition and occurs as a results of germline alterations in the *TSC1* or *TSC2* genes. Patients with TSC often present with hamartomas and neoplasms in multiple organs (Alexakis et al., 2004; Ito et al., 2012; Jensen et al., 2008). Pancreatic involvement is not common in patients with TSC, but PNENs are the most common pancreatic lesion in patients with TSC and may be functional or nonfunctional (Ito et al., 2012; Larson et al., 2012).

1.3.3. Treatments and responses

Clinical management of PNENs is complicated by multiple factors such as the functional status, the spread of the disease and the WHO classification. All of these contribute to the clinical behaviour of PNENs and thus largely dictate the optimal treatment regimen for each patient. In general, removal of tumour mass is the mainstay when feasible, and a surgical resection with curative intent is standard for localized PNENs. For metastatic cases, cytoreductive surgery and/or liver-directed therapies may be recommended to target the primary and secondary lesions, respectively (Kunz, 2015). For progressive, unresectable, metastatic and/or symptomatic PNENs, systemic treatments are administered, where the particular therapeutic agents considered depend on the WHO classification and the functional status of the tumour (Kunz, 2015; Li et al., 2020).

PNECs

PNECs are generally treated differently from PNETs due to historically observed differences in treatment responses between NENs of different histological differentiation. In most cases, NECs are treated similarly regardless of their primary sites, while different targeted treatments are recommended for NETs depending on their primary sites (Kunz, 2015). The current standard systemic treatment for NECs is cisplatin with etoposide, which had originally been administered for patients with small cell lung cancer, a type of lung NEC (Strosberg et al., 2010). This combination achieved an excellent response rate in patients with NECs (67% overall tumour regression rate) but dreadful response rate in patients with NETs (7% overall tumour regression rate) (Moertel et al., 1991). A retrospective study of GEP-NECs-G3 (2010 WHO classification) found increased median overall survival time in patients treated with a combination of platinum-based agent (cisplatin or carboplatin) and etoposide (11 months; 95% CI of 9.4-12.6 months) versus patients under best supportive care (1 month; 95% CI of 0.3-1.8 months). Of note, a lower response rate to the treatment combination was observed in GEP-NECs-G3 with <55% Ki67 index (15% vs 42%), though GEP-NECs-G3 with <55% Ki67 index were associated with a slightly better survival outcome compared to >55% Ki67 index (Sorbye et al., 2013). However, this study did not examine or distinguish the histological differentiation status of the specimens. Among PNENs, NETs-G3 often have <55% Ki67 index, whereas most NECs have >55% Ki67 index (Basturk et al., 2015; Tang et al., 2016). While randomized clinical trials specifically for PNECs are lacking, the greater response rate to platinum-based therapy observed in GEP-NECs-G3 with >55% Ki67 index likely suggests a similarly differential response rate to cisplatin-based therapy in PNECs vs PNETs-G3.

PNETs

Systemic therapies for PNETs are administered to control tumour growth and/or symptoms, where the latter are mostly attributed to the functional status of the tumour. For the purpose of this thesis, only tumour-controlling therapeutic agents for PNETs are discussed.

Somatostatin analogues

Somatostatin (SST) is a cyclic peptide that binds to somatostatin receptors 1~5 (SSTR1~5) and regulates the release of multiple hormones, many of which cause

hormonal syndromes in patients with functional NENs (Günther et al., 2018). Given the inhibitory role of SST in releases of hormones and abundant expression of SSTRs on NEN cells, SST was expected to be of therapeutic value in patients with functional NENs. Due to the extremely short half-life of SST (< 3 minutes), attempts were made to synthesize SST analogs (SSAs) suitable in clinical settings (Lamberts et al., 1996). Octreotide was the first SSA introduced and has been used in the clinics since the 1980s (Kunz, 2015). Another SSA, lanreotide, was later approved and showed similar efficacy as octreotide but with easier administration (O'Toole et al., 2000). SSAs inhibit SSTR2/5 and elicit clinical benefits in patients with functional NENs by suppressing their levels of circulating hormones such as insulin and glucagon thereby alleviating the associated symptoms (Kvols et al., 1987; Lamberts et al., 1996; O'Toole et al., 2000). Considering their clinical benefits and historical success, SSAs are the mainstays for alleviating functional syndromes in patients with functional NENs (Hofland et al., 2020b; Kunz, 2015; Li et al., 2020).

In addition to their suppressive effects on hormone secretion, SSAs were found to elicit antitumour effects. In a randomized, double-blind phase 3 trial involving patients with metastatic nonfunctional enteropancreatic NETs, treatment with lanreotide improved progression-free survival compared to treatment with placebo (median survival time not reached vs 18.0 months). Among the patients with metastatic nonfunctional PNETs (n = 91), multivariate analysis showed improved progression-free survival rate in those treated with lanreotide vs placebo (hazard ratio of 0.58; 95% CI of 0.32~1.04) (Caplin et al., 2014).

Building upon the abundance of SSTRs on the NEN cell surface, radiolabeled SSAs have been exploited for targeted therapy. This approach, called peptide receptor radionuclide therapy (PRRT), uses SSAs chelated with radionuclide to introduce localized radiation to SSTR-positive NEN cells (Hofland et al., 2020b). Two radiolabeled SSAs, ^{90}Y-DOTATOC and ^{177}Lu-DOTATATE, were investigated in several clinical trials and showed survival benefits in patients with metastatic SSTR-positive NENs (Brabander et al., 2017; Imhof et al., 2011). A phase 3 trial involving midgut NETs found increased progression-free survival (65.2% vs 10.8% at month 20) in patients treated with ^{177}Lu-DOTATATE compared to octreotide (Strosberg et al., 2017). A phase 3 trial investigating the efficacy of ^{177}Lu-DOTATATE in locally advanced or metastatic NETs-G2/3 is still in recruitment phase at the time of writing (CinicalTrials.gov Identifier:

NCT03972488). While no randomized, prospective trial of PRRT exists for patients with PNENs, PRRT has been used for the treatment of metastatic SSTR-positive NENs in Europe since the 1990s (Kunz, 2015). A retrospective analysis of 68 patients with metastatic SSTR-positive PNETs treated with ^{177}Lu-DOTATATE reported a disease control rate (sum of partial response, minor response and stable disease) of 81% (Ezziddin et al., 2014), suggesting patients with SSTR-positive PNENs are likely to benefit from PRRT.

Chemotherapies

Cytotoxic agents are considered for the treatment of advanced stage PNETs, and a combination of an alkylating agent and an antimetabolite is used. Historically, the combination of streptozocin and fluorouracil was used for the treatment of advanced PNENs (Moertel et al., 1992). However, due to limited response rate and toxicity, capecitabine plus temozolomide (Cap/Tem) has become the combination of choice for patients with advanced PNETs (Kunz, 2015). No phase 3 trials involving Cap/Tem have been conducted in patients with PNENs, but preliminary results from a recent phase 2 trial (ClinicalTrials.gov Identifier: NCT01824875) involving patients with unresectable or metastatic PNETs-G2/3 suggested that treatment with Cap/Tem was favoured over temozolomide alone in improving progression-free survival (22.7 vs 14.4 months; HR = 0.58) and overall survival (median overall survival not reached vs 38 months) with a response rate of 33% (Kunz et al., 2018; Li et al., 2020).

Targeted therapies

Aside from SSAs and cytotoxic agents, two molecularly targeted therapeutic agents have been approved for the treatment of advanced stage PNETs: everolimus and sunitinib. Targeted therapeutic agents exploit certain molecular vulnerabilities such as dysregulated signaling pathways to preferentially distress the tumours growth and/or viability. Everolimus is an inhibitor of the mechanistic target of rapamycin kinase (MTOR) that suppresses the PI3K/AKT/mTOR signaling pathway (Bhaoighill and Dunlop, 2019). A phase 3 trial involving patients with unresectable or metastatic PNETs-G2/3 showed increased progression-free survival (11 vs 4.6 months; HR = 0.35) but no overall survival benefit in patients treated with everolimus vs placebo. The authors remarked that the clinical benefits of everolimus treatment in patients with advanced PNETs were primarily stabilization or minor shrinkage of the tumours (Yao et al., 2011). Sunitinib is an inhibitor

of receptor protein-tyrosine kinases, among which include vascular endothelial growth factor receptors (VEGFRs) that induce angiogenesis (Roskoski, 2007). In a phase 3 trial involving patients with unresectable or metastatic PNETs of any grade, sunitinib treatment similarly increased progression-free survival (11.4 vs 5.5 months; HR = 0.42) compared to placebo treatment (Raymond et al., 2011). Although everolimus and sunitinib were shown to improve progression-free survival in patients with advanced PNETs, the tumour response rate to either agent was dismal (5% and 9.3%, respectively) suggesting these agents only provide therapeutic benefits in a small subset of patients with PNETs (Raymond et al., 2011; Yao et al., 2011).

1.4. Molecular heterogeneity

As with the evolution of their classification, our growing understanding of the molecular alterations underlying PNENs has revealed the highly heterogeneous nature of their molecular landscapes. Earlier studies identified potential driver genes contributing to PNEN development from investigating hereditary cancer syndromes (described in Section 1.3.2). These studies led to the identification of *MEN1*, *VHL*, *NF1* and *TSC1/2* as putative driver genes in PNENs (Mafficini and Scarpa, 2019; Pipinikas et al., 2019). However, only less than 10% of PNENs are associated with cancer hereditary syndromes (de Wilde et al., 2012), and PNENs have a low tumour mutation burden (TMB; 0.82 mutations per megabase with a range of 0.04~4.56, compared to 2.64 with a range of 0.65~28.2 in pancreatic ductal adenocarcinoma [PDAC]), suggesting there are other molecular alterations beyond gene mutations that contribute to PNEN etiology and pathogenesis (Banck et al., 2013; Jiao et al., 2011; Scarpa et al., 2017). Omic approaches have become increasingly popular in molecular characterization studies over the past decade due to advancing technologies and declining costs. Accordingly, microarray and high-throughput sequencing technologies have been exploited to characterize the genome, epigenome and transcriptome of PNENs in attempts to identify clinically relevant molecular alterations. The results of these studies have culminated in the identification of recurrently altered genes, dysregulated signaling pathways and chromosomal anomalies among PNENs (Cao et al., 2013; Hong et al., 2020; Jiao et al., 2011; Lawrence et al., 2018; Missiaglia et al., 2010; Roldo et al., 2006). More recently, different molecular subtypes of PNENs with prognostic implications were identified and described by separate groups (Cejas et al., 2019; Chan et al., 2018; Lawrence et al.,

2018), including one study that compared patient PNENs with neoplasms from a genetically engineered mouse model with spontaneous PNEN development (Sadanandam et al., 2015).

1.4.1. Early biological studies using mouse models

Early pathogenesis studies of PNENs were enabled by the development of the RIP-Tag mouse model by Douglas Hanahan during the 1980s. Hanahan created a fusion construct RIP-Tag by combining rat insulin promoter with SV40 large T antigen (Tag) and injected the fusion construct into mouse embryos. The resultant RIP-Tag litter had heritable tumour formations in the pancreas and died at an age of 9~12 weeks. The pancreatic lesions were confirmed as insulinomas and NECs (then-called “islet cell carcinomas”) that arose from transformed pancreatic β-cells (Hanahan, 1985). This mouse model provided the first evidence supporting the capability of pancreatic β-cells to give rise to PNENs. Subsequently, various genetically engineered mouse models provided evidence that PNENs may arise from the endocrine compartment of the pancreas depending on the genetic alterations introduced and the cells of targeted expression. Glucagonomas could arise from expression of Tag or deletion of tumour suppressor genes RB transcriptional corepressor 1 (*Rb1*) and transformation related protein 53 (*Trp53*) in pancreatic α-cells (Efrat et al., 1988; Glenn et al., 2014), and insulinomas could arise from β-cell-specific deletion of *Men1* (Bertolino et al., 2003a). Interestingly, heterozygous *Men1* mice developed PNENs with varying biochemical and histological characteristics including insulinomas, glucagonomas, NECs, as well as PNETs expressing both insulin and glucagon (Bertolino et al., 2003b). Recently, the insulinoma-associated 1 (*Insm1*) gene was linked to the development of metastatic nonfunctional PNENs using the RIP-Tag mouse model, suggesting pancreatic endocrine cells may give rise to functional and nonfunctional PNENs (Kobayashi et al., 2019).

The RIP-Tag mouse was an exemplary model to elucidate not only the development of PNENs but also the progression of cancer in general, as it sustained a spectrum of pre-malignant and malignant lesions and showcased a continuum of progressive lesions reminiscent of cancer progression (Hanahan, 1985; Hanahan and Folkman, 1996). Hence, studies using this model system led to the identification of several cancer hallmarks (Hanahan and Folkman, 1996; Hanahan and Weinberg, 2000, 2011). Using histological, temporal and statistical assessments of the pancreatic lesions

from the RIP-Tag model, Hanahan proposed two distinct pre-cancerous stages, hyperplastic and angiogenic, between normal islets and PNENs. It was found that ~50% of the islets in RIP-Tag mice became hyperplastic with hyperproliferation (Teitelman et al., 1988), possibly driven by aberrant insulin-like growth factor 2 (*Igf2*) gene expression (Christofori et al., 1994, 1995). Only a small percentage (1~2%) of the hyperplastic islets became angiogenic with evidence of neovasculatures and ultimately developed into PNENs upon loss of E-cadherin (Perl et al., 1998). Elevated expression of insulin growth factor 1 receptor (*Igf1r*) could accelerate the development of the PNENs (Lopez and Hanahan, 2002). The “angiogenic switch” was required for the progression of hyperplastic islets into adenomas that subsequently progressed into PNENs (Folkman et al., 1989). Treatment of RIP-Tag mice with sunitinib inhibited tumourigenesis and stabilized established tumours improving survival outcomes (Casanovas et al., 2005; Pietras and Hanahan, 2005). However, similar to the treatment outcomes in patients, tumour progression eventually ensued in RIP-Tag mice treated with sunitinib, and the tumour regrowth accompanied increased invasive and metastatic potentials (Pàez-Ribes et al., 2009).

While these mouse models provided possible etiology and pathogenesis of PNENs, they are not fully representative of PNENs found in patients. The genetic modulations introduced into the genetically engineered PNEN mouse models are only observed in subsets of patient PNENs. For instance, transformation driven by Tag was primarily mediated through inhibition of *Rb1* and *Trp53* (Ali and DeCaprio, 2001), and alterations to tumour suppressor genes *RB1* and tumor protein p53 (*TP53*) are common in PNECs but rare in PNETs among patients (Yachida et al., 2012), though the cyclin dependent kinases 4 and 6 (*CDK4*; *CDK6*) that act downstream of *RB1* were found to be overexpressed or amplified in a subset of PNETs (Tang et al., 2012). Moreover, the majority of murine PNEN models give rise to functional PNENs, while most sporadic PNENs in patients are nonfunctional (Halfdanarson et al., 2008). Most murine PNENs also do not fully recapitulate patient PNENs (Yu, 2016), and the human and murine endocrine pancreas are different in structures and cell-type proportions (Dolenšek et al., 2015). A microarray-based study of mRNA and miRNA identified three subtypes among patient PNENs, only two of which were observed among PNENs found in RIP-Tag mice (Sadanandam et al., 2015). Careful extrapolation of PNEN etiology from murine models

is therefore warranted, and recent interests in the molecular underpinnings of patient PNENs have shifted towards direct investigations using patient specimens.

1.4.2. Recurrently mutated genes in PNENs

DNA-sequencing studies of sporadic PNENs have identified a few recurrently mutated genes and mutational differences between PNETs and PNECs (Table 1.4). Using whole-exome sequencing (WES) and Sanger sequencing, Jiao et al. (2011) identified recurrent somatic gene mutations in *MEN1*, death domain associated protein (*DAXX*), ATRX chromatin remodeler (*ATRX*), and genes of the PI3K/AKT/mTOR pathway (including *TSC2*, phosphatase and tensin homolog [*PTEN*] and phosphatidylinositol-4,5-bisphosphate 3-kinase catalytic subunit alpha [*PIK3CA*]) in 44.1%, 25%, 17.6% and 14% of 68 PNETs-G1/2, respectively. The identified mutations in *MEN1*, *DAXX* and *ATRX* were mostly inactivating, suggesting their tumour suppressive roles. The mutations in *DAXX* and *ATRX* were mutually exclusive and collectively affected 42.6% of the sequenced specimens. Later, Scarpa et al. (2017) performed whole-genome sequencing (WGS) on 98 sporadic PNETs and similarly identified somatic mutations affecting *MEN1*, *DAXX*/*ATRX* and the PI3K/AKT/mTOR pathway (including *PTEN* and *DEPDC5* [DEP domain containing 5, GATOR1 subcomplex subunit]) in 36.7%, 33.7% and 9.2% of sequenced specimens, respectively. Each sequenced specimen on average harboured 23.5 somatic coding mutations. Interestingly, 17% of the sequenced PNETs harboured germline pathogenic mutations affecting putative tumour suppressor genes including *MEN1*, *VHL*, mutY DNA glycosylase (*MUTYH*), checkpoint kinase 2 (*CHEK2*) and *BRCA2* (BRCA2 DNA repair associated), all coupled with somatic loss of heterozygosity (LOH) and resulted in biallelic loss of the respective gene (Scarpa et al., 2017).

Another study performed targeted sequencing of 637 genes among 42 PNETs and identified 52.4%, 11.9% and 7.1% of the sequenced specimens with mutations in *MEN1*, *DAXX/ATRX* and *PTEN*, respectively (Lawrence et al., 2018). A WES or targeted sequencing study of 65 PNETs from the previously mentioned phase 3 everolimus trial (Section 1.3.3) revealed mutations in *MEN1*, *DAXX/ATRX* and genes of the PI3K/AKT/mTOR pathway in 43.1%, 38.5% and 10.8% of the specimens (Yao et al., 2019). Targeted sequencing of cancer-related genes in 96 tumour samples from 80 patients with metastatic PNETs who had received prior treatments revealed 56.3%,

40%, 25%, 25% and 12.5% of the cohort with mutations in *MEN1*, *DAXX*, *ATRX*, *TSC2* and *PTEN*, respectively (Raj et al., 2018). In addition, 7.5% of the cohort harboured mutations in *BRAF* (B-Raf proto-oncogene, serine/threonine kinase), two of which resulted in p.V600E, an activating variant commonly associated with melanoma and colorectal cancer (Cantwell-Dorris et al., 2011). Notably, this cohort had a median TMB of 2.95 mutations per megabase, substantially higher than a TMB of 0.82 reported by other studies, possibly due to prior treatments (Raj et al., 2018).

While there were differences in the recurrence of mutations affecting *MEN1*, *DAXX/ATRX* and genes of the PI3K/AKT/mTOR pathway between cohorts and studies, the results from all studies support that these genes are recurrently altered in PNETs. The majority of the PNETs included in the above sequencing studies were nonfunctional. Analyses of insulinomas alone, however, did not identify recurrent mutations affecting any of these genes. In fact, few somatic coding mutations (average of 3.7-10.7 per specimen) were identified among insulinomas, but a recurrent hotspot mutation affected the YY1 transcription factor (*YY1*) gene. This hotspot mutation resulted in a p.T372R variant and was found in 15.4-32.6% of insulinomas (Cao et al., 2013; Cromer et al., 2015; Hong et al., 2020; Lichtenauer et al., 2015; Wang et al., 2017).

Table 1.4. Recurrently mutated genes in PNENs.

	PNEN subset	Somatic mutation frequency	Germline mutation frequency	References
MEN1	NETs	38-56%	5%	(Jiao et al., 2011; Lawrence et al., 2018; Raj et al., 2018; Scarpa et al., 2017; Yao et al., 2019)
DAXX/ATRX	NETs	11-58%	-	(Jiao et al., 2011; Lawrence et al., 2018; Raj et al., 2018; Scarpa et al., 2017; Yao et al., 2019)
YY1 (p.T372R)[a]	Insulinomas	15-33%	-	(Cao et al., 2013; Cromer et al., 2015; Hong et al., 2020; Lichtenauer et al., 2015; Wang et al., 2017)

	PNEN subset	Somatic mutation frequency	Germline mutation frequency	References
PI3K/AKT/mTOR pathway[b]	NETs	7-43%	-	(Jiao et al., 2011; Lawrence et al., 2018; Raj et al., 2018; Scarpa et al., 2017; Yao et al., 2019)
RB1	NECs	71%	-	(Yachida et al., 2012)
TP53	NECs	57-60%	-	(Vijayvergia et al., 2016; Yachida et al., 2012)
KRAS (activating)	NECs	28-30%	-	(Vijayvergia et al., 2016; Yachida et al., 2012)
MUTYH	NETs	-	5%	(Scarpa et al., 2017)
CHEK2	NETs	-	4%	(Scarpa et al., 2017)
BRCA2	NETs	-	1%	(Scarpa et al., 2017)
CDKN1B	NETs	-	1%	(Scarpa et al., 2017)
VHL	NETs	-	1%	(Scarpa et al., 2017)

[a]In *YY1*, only hotspot mutations resulting in p.T372R have been reported. [b]Includes *DEPDC5*, *PIK3CA*, *PTEN* and *TSC2*.

Sequencing studies involving PNECs are scarce. A targeted sequencing study of 9 cancer-related genes identified activating *KRAS* (KRAS proto-oncogenes, GTPase) mutations, inactivating *TP53* mutations and inactivating *RB1* mutations in 28.6%, 57.1% and 71.4% of 7 PNECs, respectively. None of the 11 PNETs also included in the study had mutations in these three genes suggesting genetic distinctions between PNETs and PNECs (Yachida et al., 2012). In another study that performed targeted sequencing of 50 cancer-related genes among 23 NECs of various primary sites, 60.1% and 30.4% of the specimens harboured mutations in *TP53* and *KRAS*, respectively (Vijayvergia et al., 2016). Together, these findings suggest genetic distinctions between PNETs and PNECs, where PNECs are genetically more similar to extrapancreatic NECs than to PNETs.

In addition to single nucleotide variations (SNVs) or small insertions and deletions (Indels) that affect local sequences, a few structural variations (SVs) with

predicted functional impacts were reported in PNETs. These included rearrangements leading to inactivation of *MTAP* (methylthioadenosine phosphorylase; 4.1%), *ARID2* (the AT-rich interaction domain 2*;* 5.1%), *SMARCA4* (SWI/SNF related, matrix associated, actin dependent regulator of chromatin, subfamily a, member 4*;* 3.1%) and *KMT2C* (lysine methyltransferase 2C*;* 3.1%). Gene fusions involving *EWSR1* (EWS RNA binding protein 1) were found in three PNETs, where two were due to in-frame fusion with the *BEND2* (BEN domain containing 2) and another with *FLI1* (Fli-1 proto-oncogene, ETS transcription factor) (Scarpa et al., 2017). The latter is common in Ewing's sarcoma (Sankar and Lessnick, 2011).

MEN1

MEN1 encodes a ubiquitously expressed scaffold protein with predominant nuclear localization (Guru et al., 1998) and has been associated with transcriptional regulation, cellular signaling and DNA repair (Agarwal, 2017). The mutations in *MEN1* observed among PNETs were largely inactivating mutations suggesting *MEN1* poses inhibitory roles on PNET development, but the mechanisms by which it suppresses tumourigenesis from the endocrine pancreas remain elusive. In the context of PNENs and the endocrine pancreas, MEN1 indirectly regulates the gene expression of cell cycle inhibitors, cyclin dependent kinase inhibitor 1B (*CDKN1B*) and cyclin dependent kinase inhibitor 2C (*CDKN2C*), through histone H3 (H3) lysine 4 trimethylation at the *CDKN1B* and *CDKN2C* promoter regions (Karnik et al., 2005). Loss of CDKN2C was found in 67.3% of 61 PNENs from patients with MEN1 syndrome (Conemans et al., 2018). The Wnt signaling pathway inhibits proliferation of mouse PNEN cells, and MEN1 interacts with members of the Wnt signaling pathway, including catenin beta 1 (CTNNB1) and transcription factor 3 (TCF3), and regulates the expression of Wnt pathway target gene axin 2 (*AXIN2*) (Chen et al., 2008). MEN1 likely also regulates the PI3K/AKT/mTOR pathway as it inhibits the activation of AKT serine/threonine kinase 1 (AKT1) by preventing its translocation from cytoplasm to the plasma membrane during growth factor stimulation (Wang et al., 2011b). Hotspot activating mutations in *KRAS* are found in nearly all PDACs but are virtually nonexistent in PNETs (Jiao et al., 2011). MEN1 was found to act downstream of KRAS and assumed an anti-proliferative role thereby suppressing pancreatic endocrine cell proliferation upon KRAS activation (Chamberlain et al., 2014).

DAXX and *ATRX*

The mutually exclusive occurrence of inactivating mutations in *DAXX* and *ATRX* among PNETs suggested their cooperative roles in suppressing PNET development. DAXX and ATRX coordinately deposit histone H3 variant H3.3 (H3.3) at telomeric and pericentric heterochromatin in a replication-independent manner (Drané et al., 2010; Goldberg et al., 2010; Lewis et al., 2010; Wong et al., 2010). Both DAXX and ATRX as well as telomeric H3.3 deposition are required to suppress the alternative lengthening of telomere (ALT) pathway. ALT is a homologous recombination (HR)-dependent but telomerase-independent mechanism that promotes cancer cell immortality (Clynes et al., 2015). Loss of DAXX or ATRX protein expression is associated with chromosomal instability (CIN) in PNETs (Marinoni et al., 2014). Analysis of 41 PNETs using fluorescence in situ hybridization revealed 61.0% with ALT, all of which harboured mutation in *DAXX*/*ATRX* and/or lost nuclear localization of DAXX/ATRX (Heaphy et al., 2011). Three independent studies of PNETs congruously reported the prognostic utility of ALT in PNETs where ALT positivity was associated with reduced disease-free survival, larger tumour size and higher WHO grade (Kim et al., 2017b; Marinoni et al., 2014; Singhi et al., 2017). A subsequent study using an international cohort of over 600 nonfunctional PNETs showed loss of DAXX/ATRX staining or ALT positivity was independently associated with reduced recurrence-free survival. The 5-year recurrence-free survival rates were 40% for DAXX/ATRX-loss and 42% for ALT-positive subsets compared to 85% and 86% in the opposed subsets, respectively (Hackeng et al., 2021).

PI3K/AKT/mTOR pathway

The PI3K/AKT/mTOR pathway is involved in numerous cellular processes including stress adaptation, cell proliferation and regulation of bioenergetics for cell growth and survival. The pathway is dysregulated in multiple cancer types and is a target of interest among PNETs (Porta et al., 2014). A few somatic mutations in genes of the PI3K/AKT/mTOR pathway were identified and collectively affected 7~14% of sequenced PNETs (Jiao et al., 2011; Lawrence et al., 2018; Scarpa et al., 2017). In addition to gene mutations, microarray analysis comparing PNENs to normal islets identified reduced *TSC2* expression in the tumours. IHC analysis of TSC2 and PTEN showed lower levels of these proteins in PNENs compared to islets, and PNENs with lower TSC2 or PTEN IHC scores were associated with poor clinical outcomes (Missiaglia et al., 2010). IHC positivity of phosphorylated MTOR and phosphorylated ribosomal protein S6, markers

indicative of PI3K/AKT/mTOR pathway activation, were also associated with clinicopathological characteristics of poor clinical outcomes (Komori et al., 2014). However, there is currently no data to support whether aberrant activation of PI3K/AKT/mTOR pathway leads to susceptibility to the MTOR inhibitor everolimus in PNENs (Yao et al., 2019).

DNA damage repair

There have been few but consistent reports supporting alterations in DNA damage response and repair pathways among PNETs. Sanger sequencing of 35 kinase genes among 36 PNENs identified somatic mutations affecting the ATM serine/threonine kinase gene (*ATM*) in 5.6% of the specimens (Corbo et al., 2012). *ATM* as well as *BRCA2*, *CHEK2* and *MUTYH*, described above in which germline mutations were found among PNETs, are involved in DNA damage response and repair pathways. The ATM-CHEK2 pathway is stimulated in response to DNA double stranded breaks to activate checkpoint responses that facilitate DNA repair and cell survival (Smith et al., 2010b). BRCA2 acts downstream of CHEK2 and regulates the HR repair of DNA double stranded breaks (Bahassi et al., 2008; Thorslund and West, 2007; Yang et al., 2002). MUTYH is a DNA glycosylase involved in base excision repair pathway that prevents G:C>T:A transversion, and germline mutations in *MUTYH* lead to colorectal polyposis (Al-Tassan et al., 2002; Shinmura et al., 2000). In addition to regulation of ALT, DAXX, ATRX and H3.3 were recently associated with DNA damage repair. DAXX, ATRX and their coordinated deposition of H3.3 were required during extended DNA repair synthesis at exogenously induced DNA double stranded breaks (Juhász et al., 2018). Together, these findings point to potentially defective DNA damage response pathways in some PNETs. PNECs frequently harboured mutations in *TP53* and *RB1*, which can also lead to elevated DNA damage. Deletion of *RB1* results in increased double stranded breaks due to reduced HR-mediated and non-homologous end-joining-mediated DNA damage repairs (Cook et al., 2015; Marshall et al., 2019). *TP53* has been connected to various DNA damage repair mechanisms including base excision repair and HR-mediated repair (Williams and Schumacher, 2016). *MUTYH* is transcriptionally regulated by *TP53* and potentially mediates the tumour suppressor functions of *TP53* (Oka et al., 2014), suggesting potential molecular similarities between certain PNETs and PNECs despite distinctions in recurrently mutated genes between the two entities.

1.4.3. Copy number variations in PNENs

Chromosomal alterations in PNETs have been investigated by a few studies and used to identify copy number variation (CNV)-based subtypes associated with clinicopathological characteristics (Table 1.5). A single nucleotide polymorphism (SNP) array study of 15 PNETs identified recurrent loss of chromosomes 1 (40%), 3 (46.7%), 11 (53.3%) and 22 (40%) and recurrent gain of chromosomes 5 (46.7%), 7 (60%), 12 (46.7%), 14 (53.3%), 17 (53.3%) and 20 (46.7%). Recurrent LOH of 11q was observed in 46.7% of the analyzed PNETs. While the sample size was small, the PNETs with more than four chromosomal gains/losses had larger tumour size (5.4 cm vs 2.3 cm) compared to those with four or less chromosomal gains/losses (Nagano et al., 2007). In their study of 98 PNETs, Scarpa et al. (2017) similarly used SNP array for copy number analysis and identified four discrete groups based on unsupervised clustering of chromosomal arm copy number patterns. Approximately one third of the cohort had limited CNV events, and the other two thirds had a recurrent pattern of either whole chromosomal loss or gain. A small subset of PNETs with recurrent chromosomal gain formed a polyploid group and was associated with a higher somatic mutation rate with an average of 1.98 mutations per megabase compared to an average of 0.82 mutations per megabase across the cohort. Among the recurrent chromosomal loss regions across the sequenced cohort were 11q13.1 and 9q21.3 that included *MEN1* and *CDKN2A*, respectively (Scarpa et al., 2017). A separate study analyzing somatic CNVs from WGS or WES data of 127 nonfunctional PNETs similarly identified three groups either with limited CNV events or recurrent chromosomal gain or loss. The group with limited CNV events was associated with a better relapse-free survival and fewer cases with mutations in *DAXX/ATRX* compared to the other two (Table 1.5; Hong et al., 2020). Lawrence et al. (2018) also identified three CNV-based groups from targeted sequencing data of 637 genes from 42 PNETs. One group (Group 1) was characterized with recurrent pattern of LOH affecting chromosomes 1, 2, 3, 6, 8, 10, 11, 16, 21 and 22 and PNETs with lymphovascular invasion and *MEN1* mutation. The two other groups had limited CNV events, where Group 2 contained PNETs with *MEN1* mutation and LOH affecting chromosome 11 while Group 3 PNETs did not harbour *MEN1* mutation and had higher *MEN1* mRNA expression (Table 1.5; Lawrence et al., 2018). Unsupervised clustering of CNV events also identified three groups among 65 PNETs from the phase 3 everolimus trial introduced in Section 1.3.3. Two of the three groups displayed LOH in

chromosomes 1, 2, 3, 6, 8, 10, 11, 15, 16, 21 and 22 and contained mostly PNETs harbouring *MEN1* mutation with high CIN score. Patients of these two groups with recurrent LOH also had a better overall survival probability (Yao et al., 2019).

Despite nonfunctional PNETs being consistently categorized into three CNV-based groups, clustering of CNV events among 84 insulinomas revealed only a group with limited CNV events and another with recurrent chromosomal gain. The hotspot *YY1* p.T372R was more common among insulinomas with limited CNV events (59% vs 7%), while the majority of insulinomas with chromosomal gains harboured amplification of *TSC1/2* (Table 1.5). No difference in relapse-free survival was observed between the two insulinoma groups (Hong et al., 2020).

Table 1.5. Existing PNEN subtyping studies and subtype characteristics.

Study	PNEN/subset	Identification method	Subtype	Characteristics[a]
(Sadanandam et al., 2015)	PNENs	Unsupervised clustering of miRNA and mRNA microarrays	Normal islet-like	Clustered with normal islets
			Insulinoma-like	Enriched in insulinomas No *DAXX/ATRX* mutations
			Intermediate	Enriched in specimens with mutant *MEN1* and *DAXX/ATRX*
			Metastasis-like primary-1	Enriched with liver or lymph node metastases
			Metastasis-like primary-2	
(Chan et al., 2018)	PNETs-G1-2	Unsupervised clustering of RNA-seq and DNA methylation microarray	A-D-M Wildtype	Wildtype *MEN1*, *DAXX* and *ATRX* Heterogeneous gene expression profiles High *PDX1* expression
			A-D-M Mutant	Mutant *MEN1*, *DAXX* or *ATRX* Gene signatures of α-cells High *ARX* expression
(Cejas et al., 2019)	Nonfunctional PNETs (grades unreported)	Pairwise correlations based on H3K27ac profiles	Type A	High *ARX* expression Enriched with ALT+ specimens
			Type B	High *PDX1* expression Few ALT+ specimens
			Type C	Uncharacterized

Study	PNEN/subset	Identification method	Subtype	Characteristics[a]
(Lawrence et al., 2018)	PNETs-G1-2	Unclear stratification based on CNVs	Group 1	Recurrent LOH affecting chromosomes 1, 2, 3, 6, 8, 10, 11, 16, 21, 22 Enriched in specimens with mutant *MEN1* and *DAXX/ATRX* Enriched in specimens with LVI
			Group 2	Limited CNV with recurrent LOH affecting chromosome 11 Enriched in specimens with mutant *MEN1.*
			Group 3	Contained specimens of variable aneuploidy Variable clinical outcomes
(Hong et al., 2020)	PNETs	Unsupervised clustering of CNVs followed by separation based on insulinoma indication	NF-Del	Higher TMB More frequent inactivating of TSGs due to LOH and mutation
			NF-Neutral	Limited CNVs Contained higher proportion of tumours smaller in size and lower in grade.
			NF-Amp	Recurrent chromosomal gains Enriched in specimens with mutant *MEN1* and *DAXX/ATRX*
			Ins-Neutral	Limited CNVs Enriched in specimens with *YY1* p.T372R
			Ins-Amp	Recurrent chromosomal gains Enriched in specimens with *TSC1/2* amplification
(Di Domenico et al., 2020)	PNETs-G1-2	Phyloepigenetic analysis of differentially methylated sites between α-cells and β-cells	α-like	Clustered with α-cells IHC positivity for ARX but not PDX1 Enriched in specimens with mutant *MEN1*
			β-like	Clustered with β-cells IHC positivity for PDX1 but not ARX

Study	PNEN/subset	Identification method	Subtype	Characteristics[a]
			Intermediate	Majority of specimens were positive for ARX IHC Enriched in specimens with mutant *MEN1* and *DAXX/ATRX* Reduced DFS compared to the other two subtypes
(Lakis et al., 2021)	PNETs	Unsupervised clustering of variable, disease-specific methylation sites	T1	Few mutant *MEN1 or DAXX/ATRX* Enriched in functional tumours
			T2	Enriched in specimens with mutant *MEN1* and *DAXX/ATRX* Enriched with ALT+ specimens Recurrent LOH in chromosomes 1, 2, 3, 6, 8, 10, 11, 15, 16, 21 and 22
			T3	Enriched in specimens with mutant *MEN1* Recurrent loss of chromosome 11
(Boons et al., 2020)	PNETs	Unsupervised clustering of methylation status at PDX1 gene region	Subtype A	Clustered with α-cells Enriched in specimens with mutant *MEN1* or *DAXX/ATRX* Reduced overall survival probability Recurrent loss of chromosomes 1, 2, 6, 10, 16 and 22
			Subtype B	Clustered with β-cells Enriched in specimens with wildtype *MEN1*, *DAXX* and *ATRX* Recurrent loss of chromosome 11

[a]Subtype characteristics were extracted from the corresponding publications and may simply be based on comparisons between subtypes from the same study. ALT: alternative lengthening of telomeres. LVI: lymphovascular invasion, DFS: disease-free survival, TSG: tumour suppressor gene, LOH: loss of heterozygosity, TMB: tumour mutation burden.

1.4.4. Transcriptome and subtyping studies of PNENs

With the advent of affordable molecular profiling technologies, numerous studies have been conducted to characterize different cancer types on molecular levels. As a result, molecular subtyping has been used to identify groups of tumours based on common molecular characteristics and that correlate with clinical outcomes for potential prognostic and predictive utility in clinical settings. This approach has precipitated clinically relevant subtypes in various cancer types such as colorectal cancer (Guinney et al., 2015), exocrine pancreatic cancer (Bailey et al., 2016; Collisson et al., 2011) and breast cancer (Sørlie et al., 2001). Similar attempts have recently been made to identify PNEN subtypes, albeit with inter-study variations.

The earliest clustering analysis performed on PNENs was done with miRNA profiles. A custom miRNA microarray that included probes for 235 human mature miRNAs was used to determine the miRNA expression patterns in rare pancreatic cancer types. The profiled specimens included 28 nonfunctional PNETs (11 WDETs and 17 WDECs based on 2000/2004 WHO classification), 12 insulinomas (11 WDETs and 1 WDEC), 4 acinar carcinomas and 12 normal pancreas. Unsupervised clustering of the miRNA profiles predictably distinguished normal pancreas from all included tumour samples but did not identify any distinction between nonfunctional PNETs vs insulinomas or WDETs vs WDECs (Roldo et al., 2006). Considering the endocrine pancreas is the likely precursor of PNETs, and the endocrine component only makes up to 5% of the pancreas volume (Ionescu-Tirgoviste et al., 2015), the finding that the normal pancreas samples clustered away from the tumours was unsurprising due to distinctions between endocrine and exocrine pancreas. Analysis between nonfunctional PNETs and insulinomas only identified differential expression of miR-203, miR-204 and miR-211, all of which were more highly expressed in insulinomas. In particular, the expression of miR-204 was found to positively correlate with insulin IHC score. Among all miRNAs profiled, only miR-21 level was found to associate with presence of metastases and Ki67 > 2% (Roldo et al., 2006).

A microarray-based mRNA profiling study was subsequently performed and used to analyze the gene expression patterns of 72 primary PNENs (including both PNETs and PNECs, 15 of which were insulinomas), 7 matched metastases and 10 normal pancreatic samples (5 bulk pancreas and 5 islet preparations). Similar to miRNA-based

analysis, unsupervised clustering of the mRNA expression profiles distinguished normal pancreatic samples from the PNENs, while the nonfunctional WDETs, WDECs and PDECs (2000/2004 WHO classification) fell into overlapping clusters that also included the matched metastases (Missiaglia et al., 2010). Interestingly, the insulinomas clustered away from the other PNENs suggesting profound mRNA but subtle miRNA level differences between insulinomas and nonfunctional PNENs (Missiaglia et al., 2010; Roldo et al., 2006). Differential analyses identified downregulation of *TSC2* in both insulinomas and nonfunctional PNENs compared to normal samples. As mentioned in the previous subsection, IHC analysis of TSC2 and PTEN further established a correlation between low level staining of these markers and reduced overall survival and progression-free survival and suggested a dysregulated PI3K/AKT/mTOR pathway in PNENs (Missiaglia et al., 2010).

The first formal class discovery study of PNENs was conducted by incorporating miRNA and mRNA expression data from patient PNENs and correlating with the PNENs from the RIP-Tag mouse model. A qPCR array had previously been used to quantitatively measure the levels of 430 miRNAs from RIP-Tag specimens and confirmed distinct miRNA profiles between specimens at various disease stages. Clustering of miRNAs from RIP-Tag mouse tumour specimens revealed a small subset of primary tumours, termed metastasis-like primary (MLP) tumours, more similar to liver metastases than other primary tumours based on miRNA profiles (Olson et al., 2009). Using the microarray data previously generated from patient PNENs, Sadanandam et al. (2015) identified three subtypes from miRNA profiles, one of which had high expression of miRNAs also elevated in the MLP tumours from the RIP-Tag mouse. A similar analysis approach applied to the mRNA microarray data from the study by Missiaglia et al. (2010) identified five clusters: normal islet-like, insulinoma-like, intermediate, MLP-1 and MLP-2 (Table 1.5). The normal islet-like cluster consisted primarily of normal islet samples while insulinomas were predominant in the insulinoma-like cluster. The two MLP clusters contained largely metastasis specimens or primary tumours from patients with metastatic PNENs and therefore inherited the MLP terminology from the RIP-Tag specimen clustering study (Olson et al., 2009; Sadanandam et al., 2015).

A PanNETassigner-miR signature (n = 30) and a PanNETassigner-mRNA signature (n = 221) were derived from the miRNA and mRNA profiles, respectively, and used to validate the subtypes in additional cohorts. Analysis of specimens with paired

miRNA and mRNA expression data suggested significant enrichment between the three miRNA-based subtypes and the four mRNA-based subtypes (excluding the normal islet-like subtype). Combined analysis of mRNA expression profiles from human and RIP-Tag PNENs revealed transcriptomic similarities of insulinoma-like and MLP subtypes to RIP-Tag insulinomas and MLP tumours, respectively (Sadanandam et al., 2015). Targeted sequencing of genes recurrently mutated in PNENs (Jiao et al., 2011) found roughly half of the intermediate subtype PNENs with mutations in *MEN1* and *DAXX/ATRX* while only 12.5% of insulinoma-like PNENs had mutations in *MEN1* and none in *DAXX/ATRX* (Sadanandam et al., 2015). Given the abundance of specimens with MEN1 and *DAXX/ATRX* mutations in the intermediate subtype PNENs and their clustering away from insulinoma-like and MLP subtype PNENs, the intermediate subtype of specimens was proposed to be absent from the RIP-Tag mouse model, which does not harbour mutations in *MEN1* and *DAXX/ATRX* (Sadanandam et al., 2015). The MLP subtypes were associated with PNENs of higher WHO grade (2010 edition) and characterized with relatively higher expression of pancreatic progenitor genes HNF1 homeobox B (*HNF1B*) and GATA binding protein 6 (*GATA6*). The insulinoma-like PNENs, on the contrary, had higher expression of β-cell marker genes pancreatic and duodenal homeobox 1 (*PDX1*), insulin (*INS*), glucokinase (*GCK*) and solute carrier familiar 2 member 2 (*SLC2A2*) as well as insulinoma-specific gene *INSM1* (Sadanandam et al., 2015).

In their WGS study, Scarpa et al. (2017) applied RNA-sequencing (RNA-seq) to 30 of the PNENs and identified three clusters from unsupervised analysis. Two of the clusters were moderately similar to the intermediate and MLP subtypes based on enrichment analysis using the PanNETassigner-mRNA signature genes. However, the cluster most similar to the intermediate subtype was not enriched in PNENs with *MEN1* and *DAXX/ATRX* mutations, and the third cluster was not particularly similar to any of the subtypes identified by Sadanandam et al. (2015) (Scarpa et al., 2017).

Five studies subsequently identified two to three PNEN subtypes using RNA-seq, methylation profiles, enhancer profiles, or a combination of these methods (Boons et al., 2020; Cejas et al., 2019; Chan et al., 2018; Di Domenico et al., 2020; Lakis et al., 2021; Table 1.5). In all except one of these studies, the subtypes were partly dictated by the potential cell-of-origin.

Unsupervised hierarchical clustering of RNA-seq or DNA methylation microarray data from 33 PNETs-G1/2 (of functional or nonfunctional status) identified two clusters characterized by presence or absence of mutations in any of *MEN1*, *DAXX* or *ATRX*. The correlation between the mutational status of the genes and the two clusters were confirmed in external gene expression datasets. The PNET subtype characterized with mutations, the A-D-M mutant subtype, was associated with reduced recurrence-free survival and exhibited gene expression signatures of pancreatic α-cells. Pancreatic α-cell-specific genes aristaless related homeobox (*ARX*) and iroquois homeobox 2 (*IRX2*) were highly expressed while β-cell-specific genes *PDX1*, MAF bZIP transcription factor A (*MAFA*) and *INS* were lowly expressed in this A-D-M mutant subtype compared to the A-D-M WT subtype. The A-D-M WT PNETs were found to be heterogeneous in both gene expression profiles and expression of pancreatic cell-type-specific genes (Chan et al., 2018).

Cejas et al. (2019) examined the super-enhancer profiles marked by H3 lysine 27 acetylation (H3K27ac) using chromatin immunoprecipitation sequencing (ChIP-seq) among 8 nonfunctional PNETs and identified three subtypes: Type A, B and C. Comparison between Type A and B revealed significantly higher H3K27ac in the *ARX* and *IRX2* loci of Type A PNETs and in the *PDX1* locus of Type B PNETs; Type C PNETs had variable H3K27ac signals at these loci. RNA-seq confirmed relatively higher *ARX* and *PDX1* mRNA expression in Type A and B PNETs, respectively, and further suggested transcriptomic similarity of Type A PNETs to α-cells and Type B PNETs to β-cells. Subtyping 61 *MEN1*-mutant PNETs based on ARX and PDX1 IHC analysis revealed reduced relapse-free survival in PNETs either with only ARX positivity or neither ARX and PDX1 (double-negative). Mutation status of *DAXX* and *ATRX* was not assessed among the MEN1-mutant cohort, but 48.1% of ARX-positive or double-negative PNETs were positive for ALT while only 14.3% of PDX1-positive or PDX1-positive-ARX-positive were positive for ALT (Cejas et al., 2019). However, no prognostic differences were found between PDX1-positive and ARX-positive PNETs in an international cohort of 668 nonfunctional PNET specimens (Hackeng et al., 2021).

A subsequent study analyzed the methylation status of the *PDX1* gene region among 83 PNETs and identified two hierarchical clusters: subtype A and subtype B. Subtype A was enriched with PNETs harbouring mutant *MEN1*, *DAXX* or *ATRX* and associated with a higher rate of disease recurrence similar to the A-D-M mutant subtype

reported by Chan et al. (Boons et al., 2020; Chan et al., 2018). Inference of CNV from methylation array identified shared and different CNV patterns between the two subtypes. Recurrent loss of chromosome 11 was observed in all PNETs. Recurrent loss of chromosomes 1, 2, 6, 10, 16 and 22 and gain of chromosomes 4, 12, 14, 17, 18, 19, 20 and 21 were observed in subtype A PNETs. Subtype B PNETs, on the other hand, had low frequencies of chromosome loss and recurrent gain of chromosome 21. Further, subtype B PNETs were associated with a reduced overall survival probability compared to subtype A PNETs (Boons et al., 2020).

Phyloepigenetic analysis of 125 PNETs-G1/2 (including functional and nonfunctional) and normal α-cells and β-cells distinguished α-cell-like and β-cell-like groups from an intermediate group of PNETs. The methylomes of PNETs and isolated α-cells and β-cells were profiled using microarray, and the differentially methylated sites between α-cells and β-cells were used to perform phyloepigenetic analysis. Hierarchical relationships were observed between the PNETs and normal cells, where α-cells and β-cells sat at two extremities. Subsets of PNETs grouped with normal α-cells or β-cells were named as α-like or β-like PNETs, respectively. The majority of the profiled PNETs (n = 92), however, were intermediate to the two subtypes and were weakly similar to α-cells or β-cells. The α-like, β-like and intermediate subtypes exhibited mutational differences in *MEN1* and *DAXX/ATRX*, where 67.4% of the intermediate PNETs harboured mutations in *MEN1* and/or *DAXX/ATRX* and 57.9% of α-like PNETs harboured mutations in *MEN1*. Mutations in *DAXX/ATRX* were absent among α-like PNETs, and nearly all β-cell PNETs had wildtype *MEN1*, *DAXX* and *ATRX*. In addition, the intermediate PNETs were characterized with numerous CNV events, while α-like and β-like PNETs had limited CNV events. IHC of ARX and PDX1 confirmed positivity in α-like and β-like PNETs, respectively, but also found 86% of the intermediate PNETs positive for ARX. Survival analysis of the PNETs stratified by phyloepigenetic groups showed the intermediate PNETs associated with reduced disease-free survival compared to α-like and β-like PNETs (Di Domenico et al., 2020).

The Scarpa group followed up their WGS study (Scarpa et al., 2017) with a microarray-based methylome profiling study. Tumour-specific methylation sites in promoter regions were identified from 84 sporadic PNETs after comparative analysis to adjacent normal pancreatic tissues and used to perform unsupervised cluster analysis that identified three methylation subtypes: T1, T2 and T3. The T1 PNETs were

characterized by few mutations in *MEN1* and *DAXX/ATRX* and included 7 of the 11 functional PNETs included in the cohort. The T2 subtype of PNETs had recurrent mutations in *MEN1* and *DAXX/ATRX*, high frequency of tumours with ALT and tumours of larger size and higher TMB. Mutations in *MEN1* were also common in the T3 subtype, but the T3 subtype contained a higher proportion of NETs-G1 and cases without extra-pancreatic spread of perineural/vascular invasion. Analysis of CNV events found recurrent loss of chromosome 11 among T3 PNETs and recurrent LOH in chromosomes 1, 2, 3, 6, 8, 10, 11, 15, 16, 21 and 22 among T2 PNETs (Lakis et al., 2021), potentially matching the T2 and T3 subtypes to Group 1 and 2 described by Lawrence et al. (2018).

1.4.5. Proteomic analysis of PNENs

There is currently no large-scale global proteomic study on PNENs. A literature search discovered only three studies that employed a proteomic approach to identify proteins either of potential prognostic utility or with metastasis associations. A two-dimensional gel electrophoresis approach following tissue microdissection was used for comparative proteomic analysis between 6 benign and 6 metastatic insulinomas. Eight candidate proteins were found more abundant and another eight less abundant in the metastatic insulinomas relative to the benign specimens. IHC validation of the candidates on a tissue microarray (TMA) of 62 insulinomas confirmed higher levels of aldehyde dehydrogenase 1 (ALDH1) and tumor protein D52 (TPD52) in malignant insulinomas and benign insulinomas, respectively. TPD52 IHC scores were positively correlated with better recurrence-free survival and overall survival in multivariate analysis (Alkatout et al., 2015). A comparative analysis of global proteomes of four insulinomas and paired pancreatic tissues identified 219 more abundant and 62 less abundant proteins in insulinomas among 3,476 identified proteins. Among the more abundant proteins in insulinomas, IHC analysis of ubiquitin C-terminal hydrolase L1 (UCHL1), microtubule associated protein 1B (MAP1B), microtubule associated protein 2 (MAP2), versican (VCAN) and CDK4 confirmed higher abundance or specific expression in 40 PNETs (including functional and nonfunctional) relative to surrounding normal tissues. PDX1 and calcium sensing receptor (CASR) were also identified to be more abundant from proteomic analysis of PNETs vs normal tissues but were only detected in insulinomas and not in other PNETs. In addition, concurrent expression of UCHL1 and internexin neuronal intermediate filament protein alpha (INA) was associated with a

better overall and disease-free survival outcome (Song et al., 2017). Another comparative study of global proteomes of 7 pairs of primary tumours and metastases from patients with PNENs found 33 and 76 proteins (among 3,722 identified proteins) more abundant in primary tumours or metastases, respectively. IHC of candidate proteins associated with metastases confirmed up-regulation of annexin A6 (ANXA6), canopy FGF signaling regulator 2 (CNPY2), RAB11B (RAB11B, member RAS oncogene family) and tubulin beta 3 class III (TUBB3) in the liver metastases, with CNPY2 absent in normal islet cells. Positivity in either CNPY2 and RAB11B was associated with PNENs of higher grade. In addition, CNPY2 IHC positivity was an independent prognostic marker of reduced liver recurrence-free survival (Shimura et al., 2018).

1.5. Aims, objectives and chapters overview

The clinical and molecular heterogeneity of PNENs are now well-appreciated and are the major hurdles in the effective clinical management of PNENs. A few therapeutic options are available for patients with PNENs, but the response rate is often limited with nonexistent molecular predictive biomarkers. Despite mounting efforts over recent years to characterize PNENs at the molecular level, the results from existing studies examining the genome, epigenome, transcriptome or proteome of PNENs have largely been limited to the identification of potential prognostic indicators for patients with PNENs. Little advance has been made towards the identification of new therapeutic vulnerabilities and, by extension, potential targeted therapeutic agents that may modify the projected prognosis in this disease.

Molecular profiling studies of PNENs using either DNA and/or RNA level information have identified up to 5 potential subtypes with mutational and/or prognostic differences. However, inconsistencies between various subtyping schemes and limitations in their therapeutic implications from various studies hamper their potential translational utility. In spite of three studies that examined the proteomic alterations in a small number of PNENs, the proteomic landscape of PNENs remains practically unknown. Investigation into the multi-omic space of PNENs using DNA-, RNA- and protein- level data may lead to a more robust and versatile PNEN stratification and further dissect the pathogenesis of this disease to identify novel therapeutic vulnerabilities.

The majority of patients with PNENs present with distant metastases at the time of diagnosis, and the presence of metastases is significantly associated with disease-specific mortality in these patients. Ironically, molecular studies on the distant metastases from these patients are scarce due to specimen availability, where limited tissues from biopsies were typically devoted to diagnostic and pathological examinations. Elucidating the molecular alterations in metastases from patients with PNENs can bolster our knowledge in the biology of these deadly neoplasms to foster effective management of PNENs in the metastatic setting.

The overarching objective of this thesis project was to unravel the molecular heterogeneity of PNENs to enable molecular associations with clinicopathological characteristics and to identify potential novel therapeutic vulnerabilities in this disease. I hypothesized that 1) PNENs can be stratified into clinically relevant molecular subgroups based on their proteotranscriptomic profiles and 2) WGS and whole-transcriptome sequencing (WTS) of PNEN metastases can identify molecular alterations that offer additional insights into the pathogenesis of PNENs. The investigations to support these hypotheses resulted in a submitted manuscript (Yang et al., in revision) and a published report (Wong et al., 2018) that are described in Chapter 2 and 3, respectively. Chapter 2 details the molecular identification and characterization of four proteotranscriptomic subgroups from one of the largest PNEN cohorts to date. The discovery of these four PNEN subgroups accompanies potential novel oncogenic drivers and pathway alterations with therapeutic implications. Chapter 3 catalogues the genomic and transcriptomic aberrations identified from a small but unique cohort of PNEN metastases where two cases were presumably driven by novel oncogenic drivers. This is followed by unpublished results correlating the metastatic cases to the subgroups detailed in Chapter 2. Finally in Chapter 4, I discuss the roles and potential contributions of these findings to the current state of knowledge in PNEN research and suggest potential avenues for future research in this disease and other NENs.

Throughout this thesis, the conventional nomenclatures for genes and proteins are used, and the approved gene names from HUGO Gene Nomenclature Committee (HGNC) are used. Where applicable, the term “disorder” or “syndrome” is added to mentions of hereditary cancer syndromes to differentiate them from the protein products of the underlying causative genes.

Chapter 2.

Proteotranscriptomic classification and characterization of PNENs

This chapter is modified from a manuscript submitted to *Cell Reports* and is in revision at the time of writing this thesis. The study culminating in the submitted manuscript was a combined effort from multiple individuals as detailed in the Acknowledgements. My specific roles in this particular study included its conceptualization and design (jointly with my supervisor Dr. Sharon Gorski), sample coordination, data curation and analysis, results interpretation, figure generation and preparation of the submitted manuscript.

2.1. Introduction

PNENs are pancreatic neoplasms with neuroendocrine differentiation, in which substantial molecular and clinical heterogeneity has caused challenges for disease management. The WHO classification system has proven prognostic utility; the histological differentiation status in particular has been used to guide treatment regimens (Kunz, 2015). While both the functional status and the WHO classification system were shown to correlate with particular molecular alterations (Cao et al., 2013; Hong et al., 2020; Yachida et al., 2012), the roles of molecular features in the management of this disease have been limited, and responses to therapies often vary between tumours of the same histopathological class (Raymond et al., 2011; Yao et al., 2011). Moreover, the categorization of borderline or ambiguous cases based on the presence/absence of clinical syndromes and histopathology can be difficult and subjective, thus hindering their effective management.

Data from omics profiling studies have facilitated characterization of the molecular landscape of PNENs. WES and WGS of PNEN specimens have identified recurrent somatic mutations in *MEN1*, *DAXX*, *ATRX* and negative regulators of the PI3K/AKT/mTOR pathway, as well as recurrent germline mutations in *MEN1*, *VHL* and DNA repair genes *MUTYH*, *BRCA2* and *CHEK2* (Jiao et al., 2011; Scarpa et al., 2017). Differential gene expression analysis has identified metastasis-associated gene

signatures of PNENs (Scott et al., 2020). Several studies have identified altered signaling pathways, distinct chromosomal abnormalities and epigenomic profiles among PNENs, and up to 5 molecular subtypes with mutational and/or prognostic differences (Cejas et al., 2019; Chan et al., 2018; Di Domenico et al., 2020; Missiaglia et al., 2010; Sadanandam et al., 2015). However, most of these studies were restricted to pre-defined subsets of PNENs based on either histological differentiation (Cejas et al., 2019; Chan et al., 2018; Di Domenico et al., 2020) or both histological differentiation and functional status (Hong et al., 2020). The restriction to pre-defined subsets of PNENs may limit the relevance of results to other PNEN cohorts and likely contributed to the observed discrepancies among the PNEN subtypes reported by different groups (Cejas et al., 2019; Chan et al., 2018; Di Domenico et al., 2020; Sadanandam et al., 2015). With the proteome of PNENs as yet virtually unexplored, along with the previous inconsistent PNEN subtyping based on transcriptome and/or epigenome profiling of pre-defined PNEN subsets, we set out to identify and characterize a non-selected group of PNENs by incorporating RNA-seq and global proteome data from patient specimens. Combined with WES and inference analysis, four molecularly distinct proteotranscriptomic subgroups of PNENs emerged. In this chapter, I present the identification and characterization of the four proteotranscriptomic subgroups of PNENs with mutational, transcriptomic, proteomic, molecular pathway and potential oncogenic driver differences.

2.2. Results

2.2.1. Whole-transcriptome and global proteome analyses identify four distinct proteotranscriptomic subgroups among PNENs

Consensus non-negative matrix factorization (cNMF)-based clustering was used to survey the optimal number of clusters and identify molecularly distinct subgroups. cNMF was initially performed on a Discovery cohort of PNEN specimens (n = 36; Table 2.1 and Supplemental Table 1), 6 islet samples (five cadaveric and one matched to a Discovery cohort PNEN) and 2 cell line samples (BON-1 and QGP-1) using the top 25% variably expressed mRNAs from RNA-seq. Five clusters were identified, where one consisted exclusively of the normal islet samples, and another included the two cell lines with a few of the Discovery cohort PNENs (Figure 2.1A). Repeating cNMF on the Discovery cohort specimens alone essentially reproduced the same four PNEN clusters indicating robust separations between the four subgroups of PNENs (Figure 2.1B).

Table 2.1. Clinicopathological characteristics of the PNEN cohorts

Characteristics	Discovery N = 36	Validation N = 48	Total N = 84
Median Follow-up Time – mo. (Range)	**83.5 (2-211)**	**58 (0-87)**	**64 (0-211)**
Sex – no. (%)			
Male	**18 (50)**	**18 (37.5)**	**36 (43)**
Female	**18 (50)**	**30 (62.5)**	**48 (57)**
Functional Status – no. (%)			
Functional	**3 (8)**	**7 (15)**	**10 (12)**
Nonfunctioning	**33 (92)**	**41 (85)**	**74 (88)**
All-cause Mortality – no. (%)			
Censored	**21 (58)**	**41 (85)**	**62 (74)**
Deceased	**15 (42)**	**7 (15)**	**22 (26)**
Histological Differentiation – no. (%)			
Well Differentiated	**33 (91.7)**	**45 (94)**	**78 (93)**
Poorly Differentiated	**3 (8.3)**	**3 (6)**	**6 (7)**
Ki67 Index – no. (%)			
<3%	**19 (53)**	**22 (46)**	**41 (49)**
3-20%	**14 (39)**	**23 (48)**	**37 (44)**
>20%	**3 (8)**	**3 (6)**	**6 (7)**
pT[a]: Primary Tumour – no. (%)			
pT1	**4 (11)**	**19 (40)**	**23 (27)**
pT2	**12 (33)**	**15 (31)**	**27 (32)**
pT3	**15 (42)**	**10 (21)**	**25 (30)**
pT4	**5 (14)**	**3 (11)**	**8 (10)**
pTX	**-**	**1 (2)**	**1 (1)**
pN[a]: Regional Lymph Nodes – no. (%)			
pN0	**14 (39)**	**25 (69)**	**39 (46)**
pN1	**22 (61)**	**9 (19)**	**31 (37)**
pNX	**-**	**14 (29)**	**14 (17)**
Metastases at Diagnosis – no. (%)			
Absent	**25 (69)**	**36 (75)**	**61 (73)**
Present	**5 (14)**	**12 (25)**	**17 (20)**
Unknown	**6 (17)**	**-**	**6 (7)**
All-time Metastases – no. (%)			
Absent	**16 (44)**	**26 (54)**	**42 (50)**
Present	**19 (53)**	**22 (46)**	**41 (49)**
Unknown	**1 (3)**	**-**	**1 (1)**

a. pT and pN were defined according to the 8th edition of American Joint Committee on Cancer Pancreas Cancer Staging system. pTX or pNX denotes specimens with insufficient information, due to specimens being biopsy material or absence of lymph nodes in the specimens. mo.: months; no.: number. The case-by-case clinicopathological characteristics are included in Supplemental Table 1.

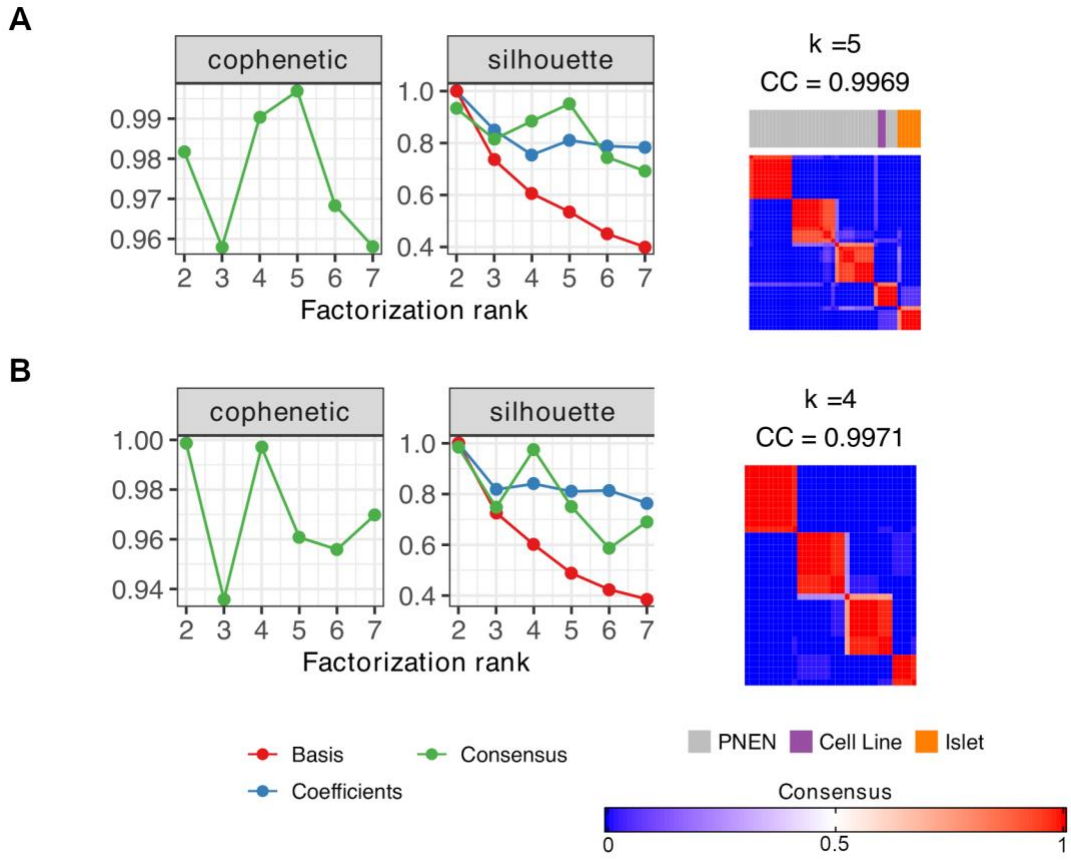

Figure 2.1. cNMF rank survey of the Discovery cohort specimens based on transcriptomic profiles.

cNMF was used to perform unsupervised clustering of the transcriptome data from the Discovery cohort PNEN specimens (n = 36). Cophenetic coefficients were used to evaluate how well the clustering results represented the original data, and silhouette coefficients were used to assess how similar a given sample was to its cluster compared to other clusters, respectively. A rank survey was performed to estimate the optimal rank based on cophenetic and silhouette coefficients (left). The consensus heatmap from the selected rank (right) was visually inspected for robust inter-cluster separation. The rank survey results are shown for the analysis of (A) the Discovery cohort specimens plus control samples or (B) the Discovery cohort specimens alone. Control samples included 6 normal islet and 2 cell line, BON-1 and QGP-1, samples.

Global proteome profiling was used to augment the transcriptome data from the Discovery cohort specimens. A total of 86,439 unique peptides mapped to 10,656 unique proteins were identified, 6,036 of which were quantified across all specimens. cNMF analysis using the top 25% variably abundant proteins similarly identified four clusters (Figure 2.2). Comparison between transcriptome- and proteome- based clustering results obtained from 35 Discovery cohort specimens with paired transcriptome and proteome data (Figure 2.3A-B) confirmed significant overlaps in the transcriptome- and proteome- based cluster assignments (Figure 2.3C), supporting the existence of four molecularly distinct proteotranscriptomic subgroups. Principal

component analysis (PCA) using either mRNA expression or protein abundance confirmed the molecular distinctions between the four subgroups and revealed one subgroup with greater intra-subgroup heterogeneity and inter-subgroup differences (Figure 2.4; purple).

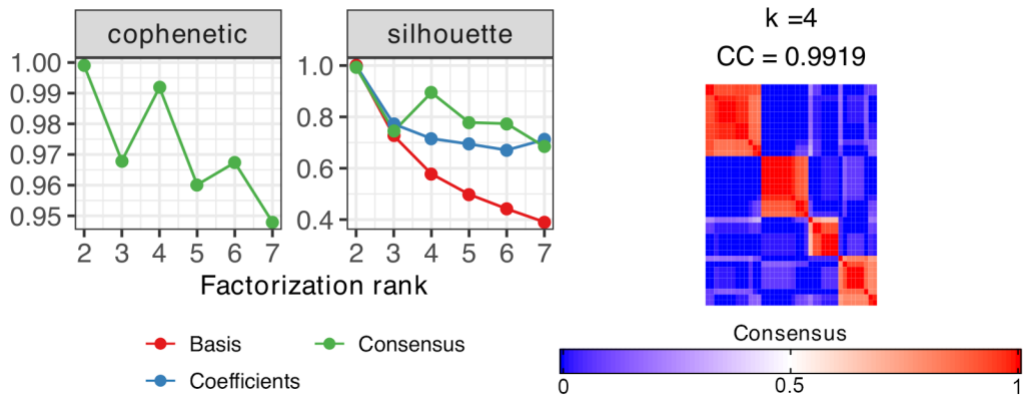

Figure 2.2. cNMF rank survey of the Discovery cohort specimens based on proteomic profiles.

cNMF-based rank survey was performed to estimate the optimal rank based on cophenetic and silhouette coefficients (left) from the proteome data of 40 PNENs, including 35 of the Discovery cohort PNEN specimens. The consensus heatmap from the selected rank (right) was visually inspected for robust inter-cluster separation.

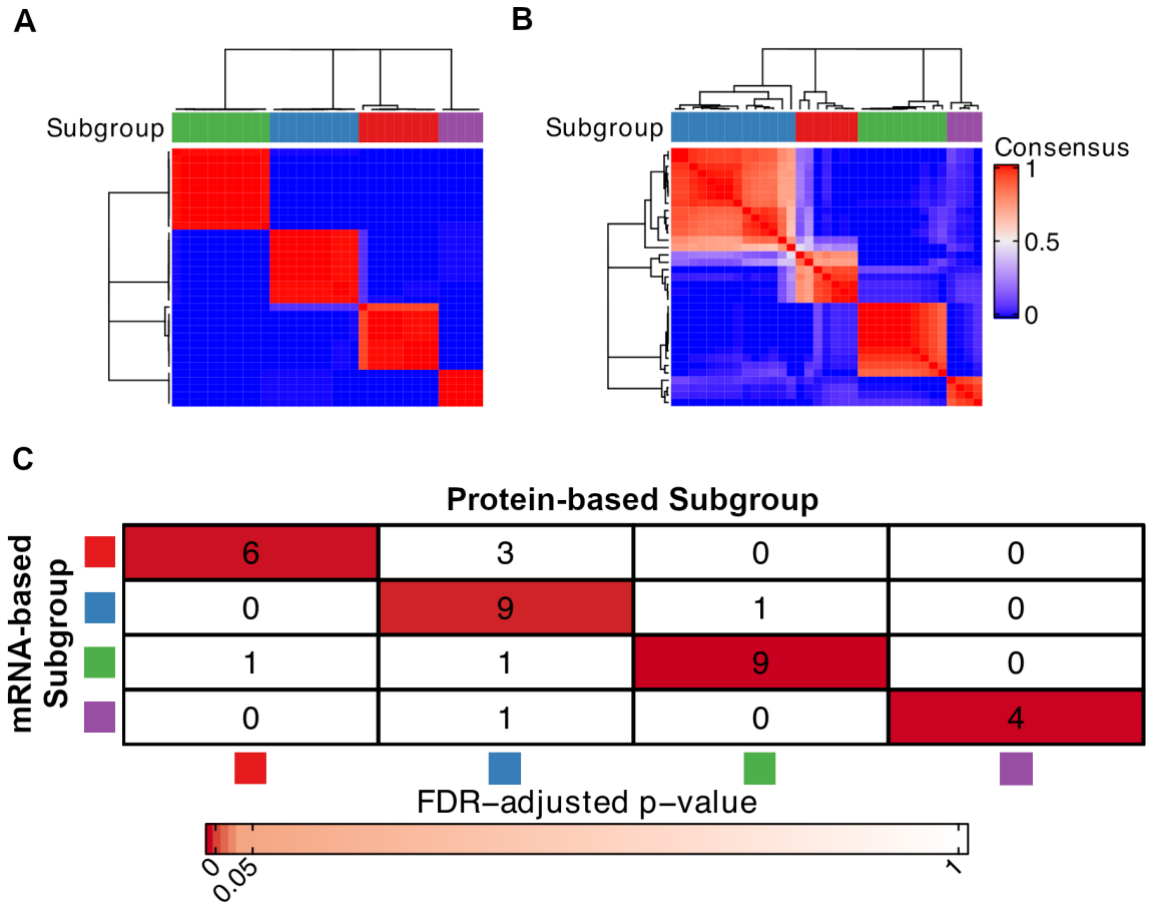

Figure 2.3. Whole-transcriptome and global proteome analyses identify four distinct proteotranscriptomic subgroups among PNENs.

cNMF analysis was independently performed using (A) transcriptome or (B) proteome data from 35 Discovery cohort PNEN specimens with paired information at the estimated optimal rank (k = 4). Shown are the consensus heatmap with the subgroup assignments derived from each analysis colour-coded at the top. (C) A 4x4 table summarizes the mRNA- and protein- based subgroup assignments of each Discovery cohort specimen, where the intersections indicate the number of specimens assigned to a particular mRNA- and protein- based subgroup. The significance of each mRNA- and protein- based subgroup intersection (ie. overlap) is colour-coded to reflect p-value computed from hypergeometric test with FDR correction. Comparisons were only made for the 35 Discovery cohort specimens with paired transcriptome and proteome information.

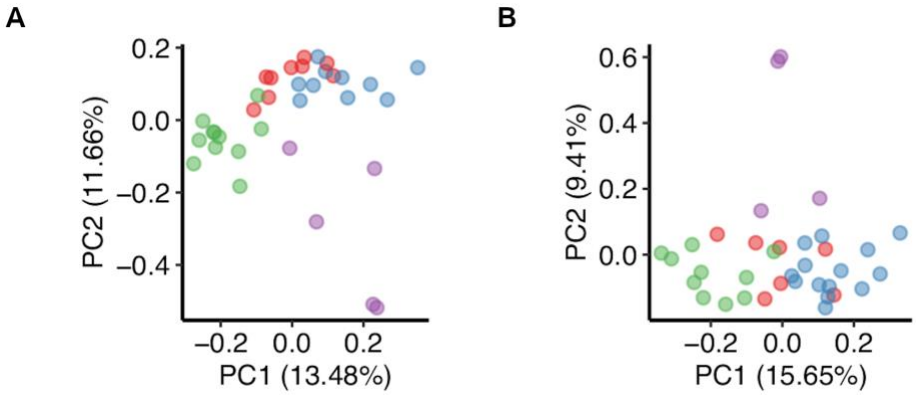

Figure 2.4. PCA of the Discovery cohort specimens.
PCA was performed for the Discovery cohort specimens with paired transcriptome and proteome data using either all expressed (A) mRNAs (n = 19,053) or (B) all quantified proteins (n = 6,036). Each dot represents a specimen and is colour-coded according to the subgroup assignments in Figure 2.3A-B.

To identify mRNAs and proteins that differed significantly between the four subgroups, I used differential expression/abundance analysis. A total of 1,637 differentially expressed genes (DEGs) and 354 differentially abundant proteins (DAPs) were identified between the subgroups among the Discovery cohort specimens. The list of DEGs and DAPs as well as their differential analysis statistics are available in Supplemental Table 2.

2.2.2. Analysis of a separate cohort of PNENs confirms the four proteotranscriptomic subgroups

To confirm the four proteotranscriptomic subgroups, a Validation cohort of 48 PNEN cases was identified (Table 2.1). Specimens from this cohort were collected, processed, sequenced and analyzed independently from the Discovery cohort to enable cross comparisons. cNMF analysis of the Validation cohort specimens, 4 islet samples and two NT-3 cell line (Benten et al., 2018) samples using the top 25% variably expressed mRNAs revealed six clusters where four consisted only of PNENs and two of either normal islet or cell line samples (Figure 2.5). Different from BON-1 and QGP-1, the NT-3 cell line samples formed a distinct cluster, which did not include any of the patient specimens. Repeating cNMF solely on the PNENs confirmed the existence of four clusters among the Validation cohort specimens (Figure 2.6A). To compare the subgroups identified from independent cluster analyses of the Discovery and Validation cohort specimens, the Discovery cohort-derived DEGs (Supplemental Table 2) were

used to perform cNMF on the Validation cohort specimens. This resulted in four subgroups (Figure 2.6B) that recapitulated the subgroups identified using Validation cohort variably expressed mRNAs (Figure 2.6C). Hence, I identified the same four subgroups of PNENs in two separate cohorts confirming the existence of four proteotranscriptomic subgroups among PNENs. Finally, I used the DEGs to perform cNMF to determine the final subgroup assignment of each of the 84 PNEN specimens included in this study. Four subgroups were identified (Figure 2.7A) and consisted of roughly equal numbers of specimens from the Discovery and Validation cohorts (Figure 2.7B). I proceeded with these DEGs-defined subgroups for downstream analysis while keeping the molecular analysis independent between the two cohorts.

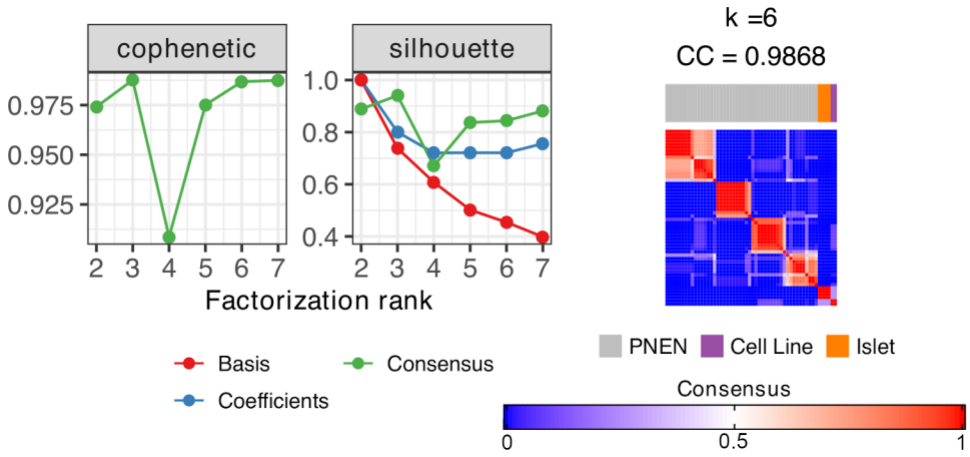

Figure 2.5. cNMF rank survey of the Validation cohort specimens plus control samples based on transcriptomic profiles.

cNMF-based rank survey was performed to estimate the optimal rank based on cophenetic and silhouette coefficients (left) from the transcriptome data of the Validation cohort PNEN specimens (n = 48) plus control samples. The consensus heatmap from the selected rank (right) was visually inspected for robust inter-cluster separation. Control samples included 4 normal islet and 2 NT-3 cell line samples.

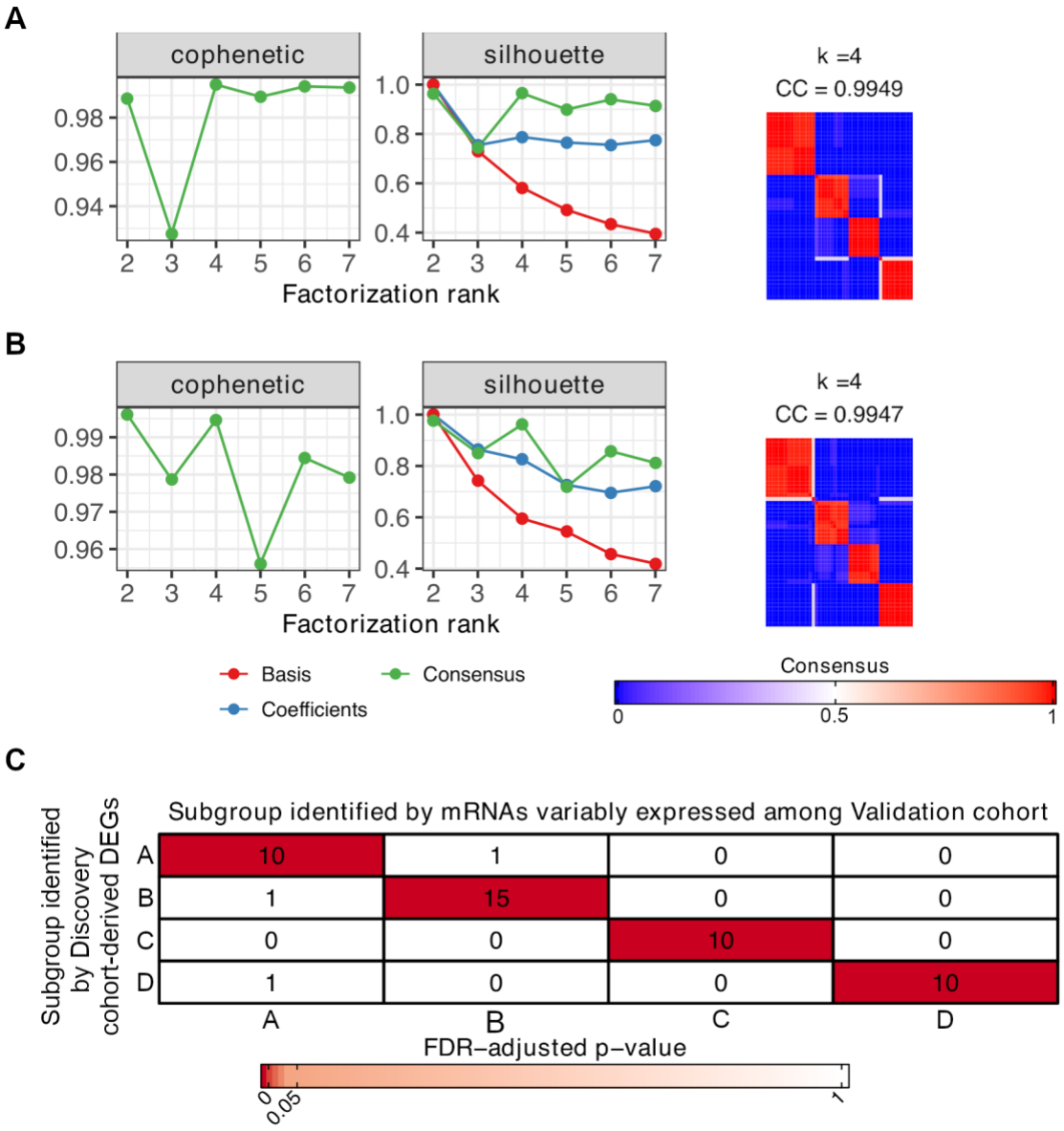

Figure 2.6. cNMF rank survey and comparison of subgroup assignments of the Validation cohort specimens.

cNMF-based rank survey was performed using either (A) variably expressed mRNAs or (B) the Discovery cohort-derived DEGs to estimate the optimal rank based on cophenetic and silhouette coefficients (left) from the transcriptome data of the Validation cohort PNEN specimens. The consensus heatmap from the selected rank (right) was visually inspected for robust inter-cluster separation. (C) A 4x4 table summarizes the number of Validation cohort specimens that were assigned to each of the subgroups identified using variably expressed mRNAs or the Discovery cohort-derived DEGs, where the intersections indicate the number of specimens assigned to a particular subgroup. The significance of each intersection (ie. overlap) is colour-coded to reflect p-value computed from hypergeometric test with FDR correction.

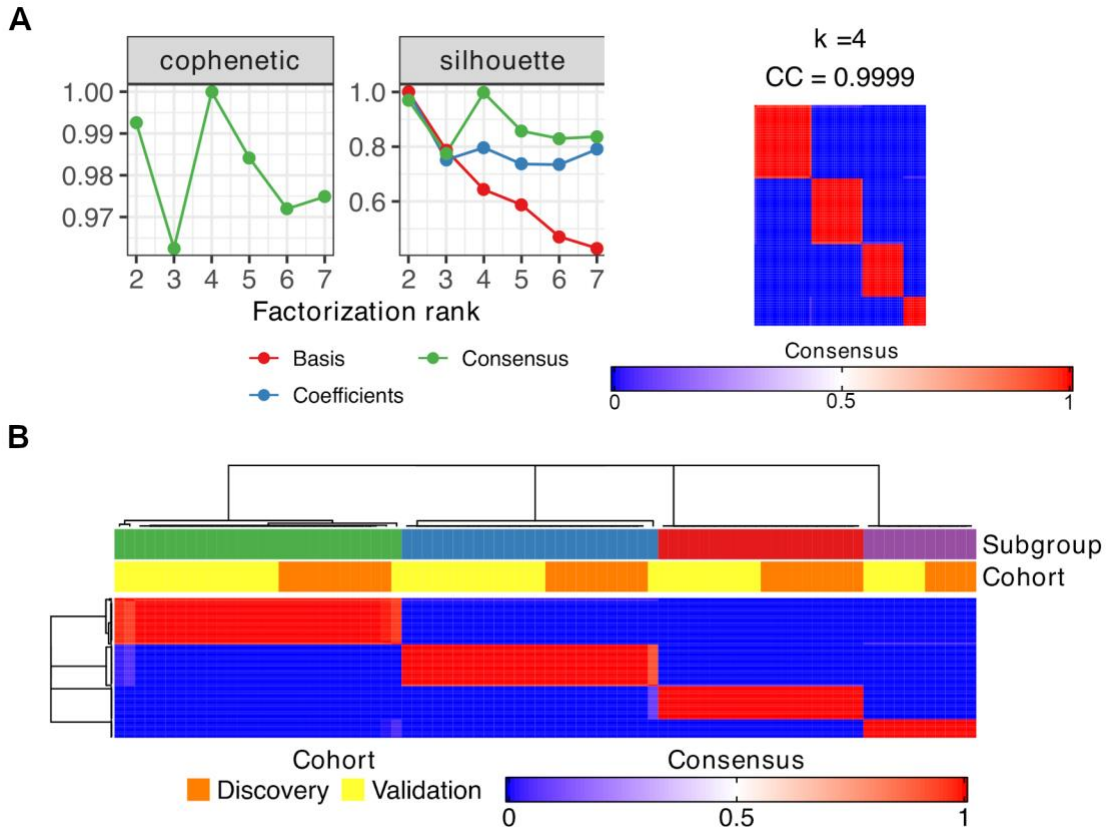

Figure 2.7. cNMF rank survey and subgroup distribution of the Discovery and Validation cohort specimens.

(A) cNMF-based rank survey was performed using the Discovery cohort-derived DEGs to estimate the optimal rank based on cophenetic and silhouette coefficients (left) from the transcriptome data of the Discovery and Validation cohort PNEN specimens (n = 84). The consensus heatmap from the selected rank (right) was visually inspected for robust inter-cluster separation. (B) The consensus heatmap from the cNMF analysis of the Discovery and Validation cohort specimens overlaid with subgroup assignments and cohort designations colour-coded at the top.

Sadanandam et al. previously analyzed microarray-based gene expression profiles (GEPs) from a non-selected cohort of PNENs (Missiaglia et al., 2010) but identified five subtypes: normal islet-like, insulinoma-like, MLP-1, MLP-2, and intermediate (Sadanandam et al., 2015). I reanalyzed their PNEN GEPs using my bioinformatic workflow and the Discovery cohort-derived DEGs and identified five subgroups that partially recapitulated the five Sadanandam subtypes (Figures 2.8A). While two of the DEGs-defined subgroups largely resembled the intermediate and MLP-2 subtypes, one DEGs-defined subgroup combined normal islet-like and insulinoma-like samples together, and two DEGs-defined subgroups constituted the MLP-1 (Figure 2.8B). The latter refinement of one subtype into two subgroups was likely due to my

approach using a greater number of genes in subgroup identification (1,637 vs 221 with 155 overlap) and RNA-seq which has enhanced dynamic range over microarrays thus capturing other molecular differences between the subgroups.

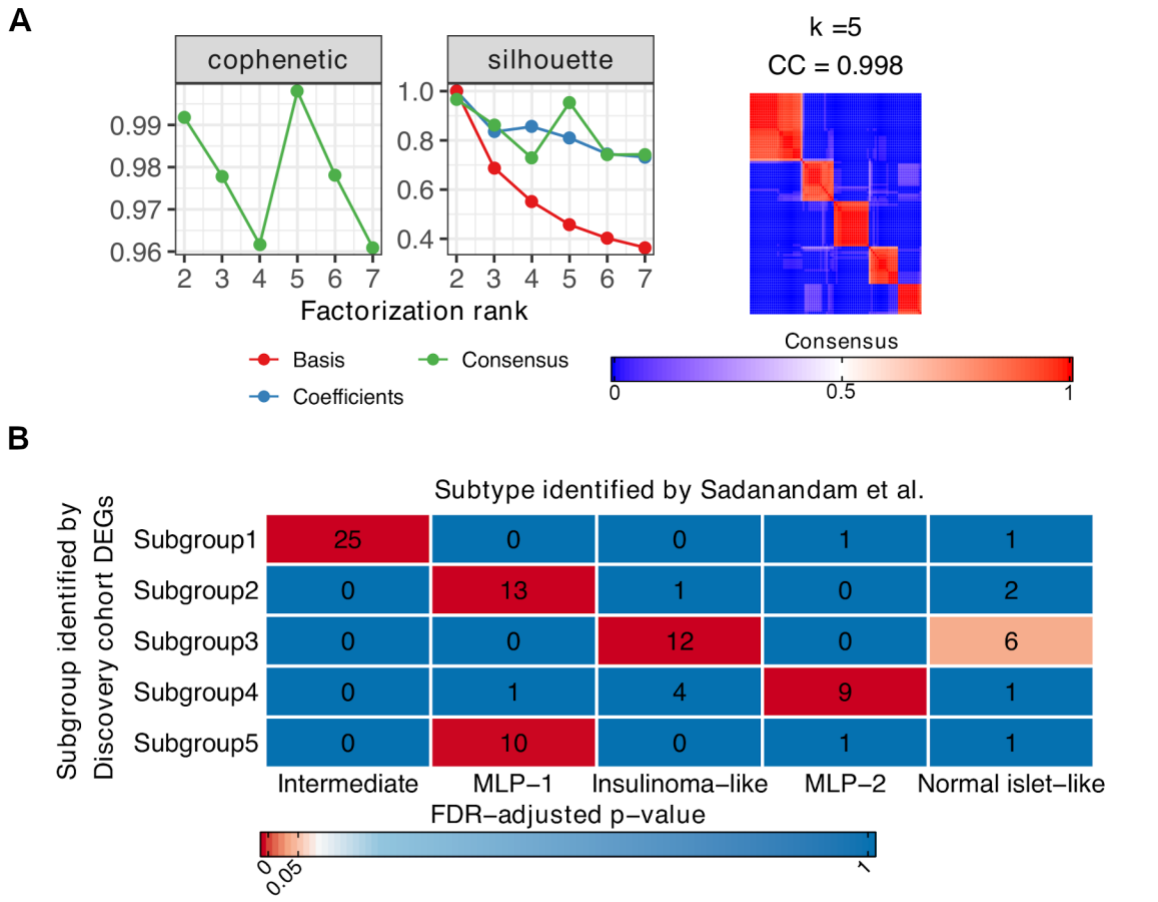

Figure 2.8. cNMF rank survey and subgroup comparisons of the Sadanandam et al. dataset.

cNMF-based rank survey was performed using the Discovery cohort-DEGs to estimate the optimal rank within the microarray dataset from Sadanandam et al.. (A) The cophenetic and silhouette coefficients at the tested ranks, and (B) the consensus heatmap at the selected rank. (C) Enrichment of the subgroups identified using the Discovery cohort-derived DEGs (rows) in the five subtypes previously identified by Sadanandam et al. (columns). The colour of each block reflects the significance of the enrichment computed by hypergeometric test followed by FDR correction. MLP: metastasis-like primary

2.2.3. Comparison of paired transcriptome and proteome profiles reveals modest single gene correlations but shared patterns of gene set enrichment

Analogous results obtained from the transcriptome- and proteome- based clustering analyses suggested distinct mRNA and protein features between the four proteotranscriptomic subgroups. Comparison between global transcriptomes and proteomes of the Discovery cohort samples showed modest but positive correlations (median Spearman's rho = 0.2776; Figure 2.9A). Comparison of paired mRNA expression and protein abundance from 5,931 available genes showed a wide spectrum of correlations between mRNA and protein variation (-0.4406~0.8840; Figure 2.9B) similar to previous studies in colorectal cancer (Mertins et al., 2016) and breast cancer (Zhang et al., 2014). Consistent with a low but variable number of genes showing concordant mRNA- and protein- level enrichment across normal tissues (Jiang et al., 2020), the majority of DEGs and DAPs were mutually exclusive with only 121 genes in common (Figure 2.9C). However, the correlations between mRNA and protein variation of these 121 intersecting genes were significantly higher compared to the correlations between global mRNA and protein variation (median Spearman's rho of 0.6807 vs. 0.3804, $p < 2.2 \times 10^{16}$, Kolmogorov-Smirnov test; Figure 2.9B) suggesting that a subset of subgroup-specific genes was under concerted directional regulation. Indeed, gene set analysis (GSA) independently performed with transcriptome or proteome data using the Hallmark gene sets from MSigDB (Liberzon et al., 2015) produced results with similar patterns and revealed distinct molecular features of each subgroup (Figure 2.10; Supplemental Table 3). Analysis of the Validation cohort specimens identified similarly enriched or depleted gene sets between the subgroups (Supplemental Table 3). Based on these prominent molecular features, as well as similarities to two previously reported PNEN subtypes (Cejas et al., 2019; Chan et al., 2018), the four subgroups were named as follow: Proliferative (purple), Alpha-cell-like (green), PDX1-high (red) and Stromal/Mesenchymal (blue), where the colours correspond to the subgroups in all relevant figures.

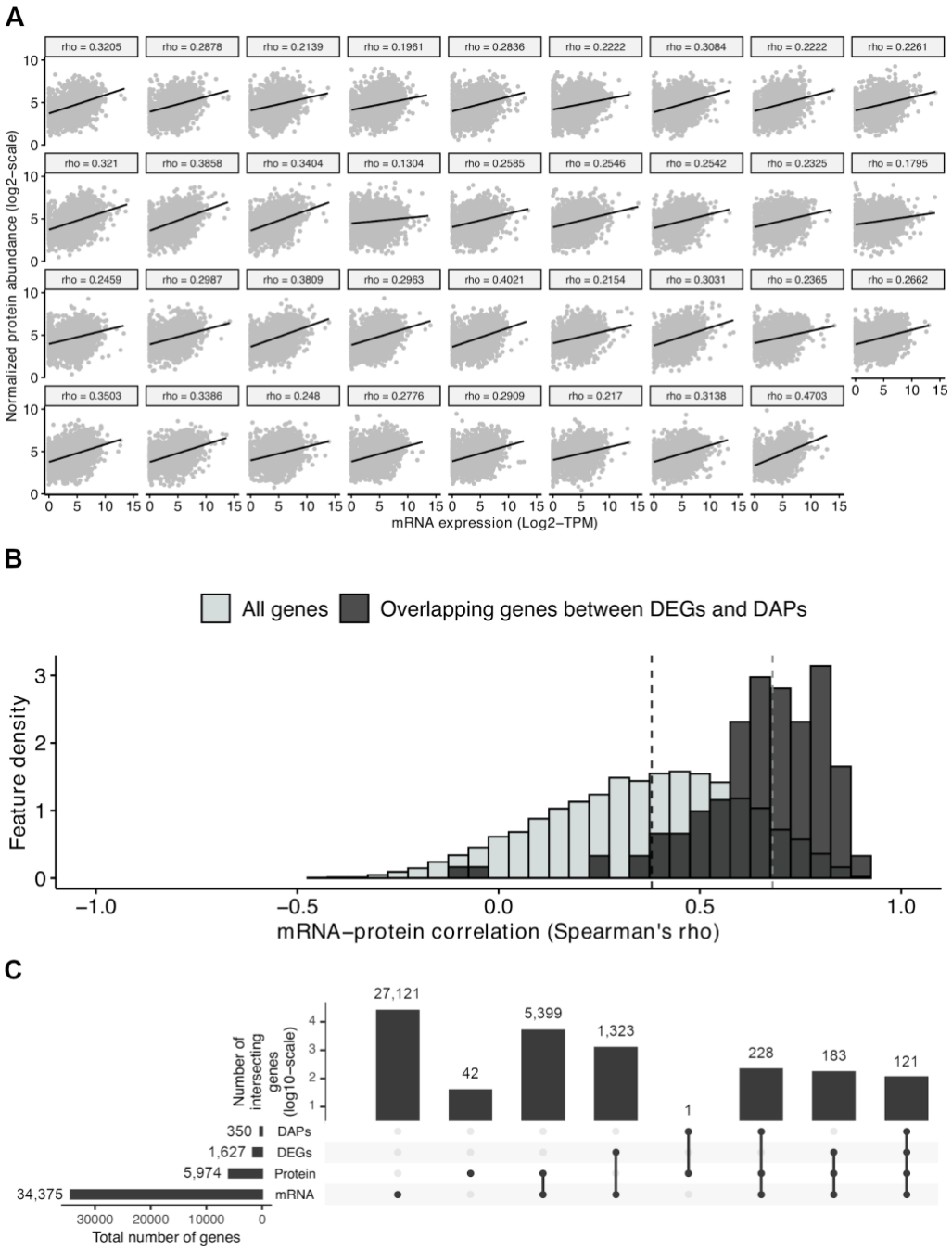

Figure 2.9. Comparison of paired transcriptome and proteome profiles reveals modest single gene correlations.

Comparisons between mRNA expression and protein abundance were made for 5,931 genes from the 35 Discovery cohort specimens with paired transcriptome and proteome data to evaluate (A) the correlation between steady state mRNA expression and protein abundance for each of the specimens, and (B) the correlations between mRNA and protein variation. For (B), shown in light grey are Spearman's rho for all genes, and shown in dark grey are Spearman's rho for the 121 genes that overlap between DEGs and DAPs. (C) is an UpSet plot that details the number of genes overlapping between whole-transcriptome (mRNA), proteome (protein), the list of DEGs and the list of DAPs. The complete list of DEGs and DAPs are included in Supplemental Table 2.

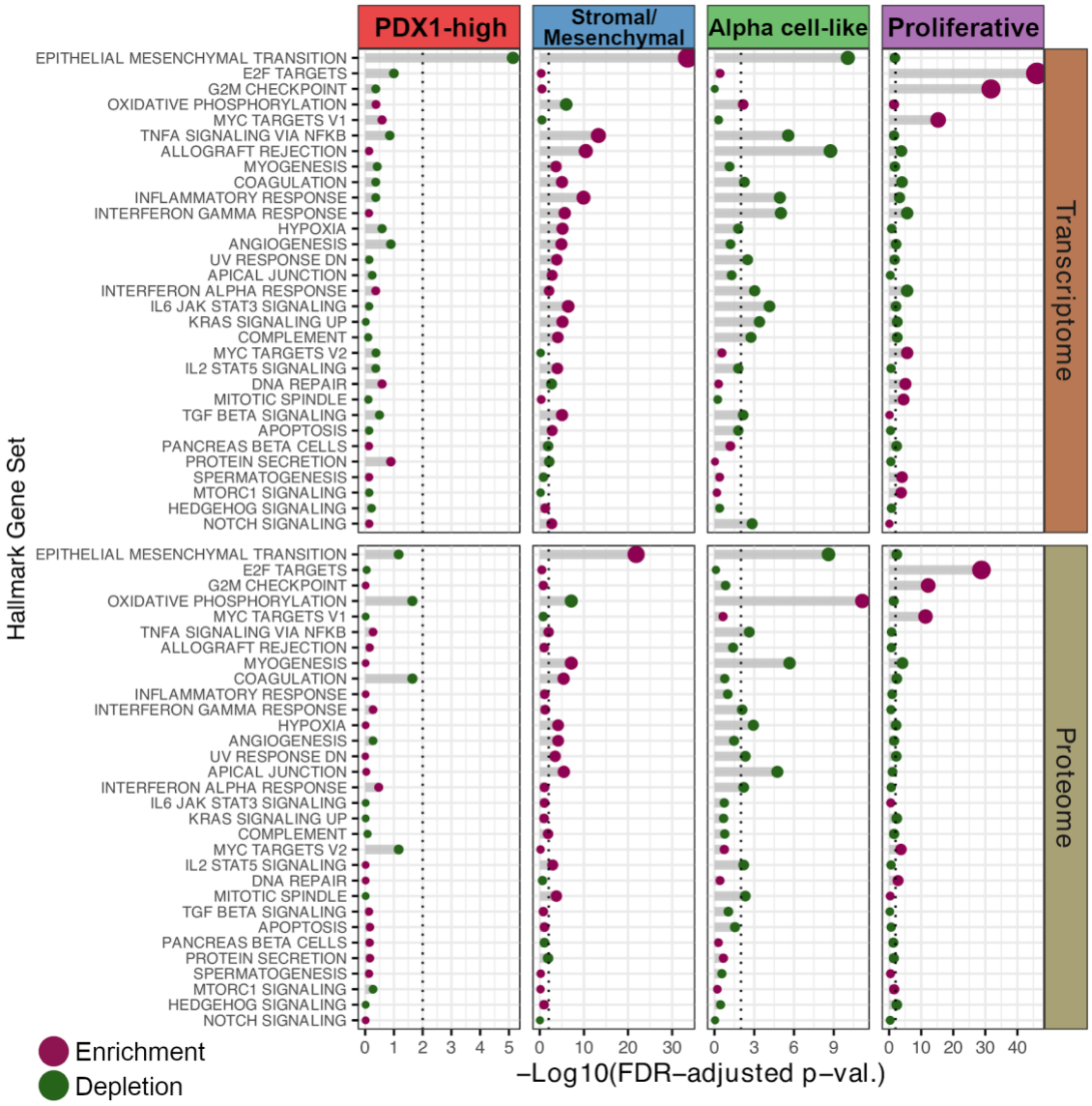

Figure 2.10. Paired transcriptome and proteome profiles exhibit shared patterns of gene set enrichment.

Gene set analysis using the Hallmark gene sets from MSigDB identified subgroup-specific features and revealed consistency between mRNA- (top) and protein- (bottom) level gene set enrichments among the Discovery cohort specimens. Each dot describes the enrichment (pink) or depletion (green) of each Hallmark gene set (rows) in each of the four proteotranscriptomic subgroups (columns), where its size and the length of its trailing grey bar are proportional to the significance of the enrichment/depletion. The same gene sets and order are shown in both the mRNA and protein plots. Only gene sets significantly enriched or depleted (FDR-adjusted p-value < 0.01; vertical dotted line) in at least one subgroup are shown. The complete results, including those from the Validation cohort comparison, are included in Supplemental Table 3.

2.2.4. A Proliferative PNEN subgroup is associated with unfavourable clinicopathological characteristics and molecular features of cell cycle progression

To increase statistical power and clinicopathological diversity, the associations between subgroups and available characteristics were evaluated using all 84 PNENs included in this study (Table 2.1). The Proliferative subgroup was associated with a reduced overall survival probability (p = 0.0024; logrank test; Figure 2.11), and significantly enriched with specimens of poorly-differentiated histology (i.e. PNECs) and Ki67 index > 20% (Table 2.2). Although PNECs are known to be genetically distinct from PNETs (Yachida et al., 2012), more than half of the Proliferative subgroup specimens had a well-differentiated histology and included one PNET-G1, four PNETs-G2, and one PNET-G3 (Supplemental Table 1). This observation suggests that a subset of PNETs may be more similar to PNECs than other PNETs at least at the transcriptome level. All four PNENs that had initially clustered with the BON-1 and QGP-1 cell line samples also fell within the Proliferative subgroup.

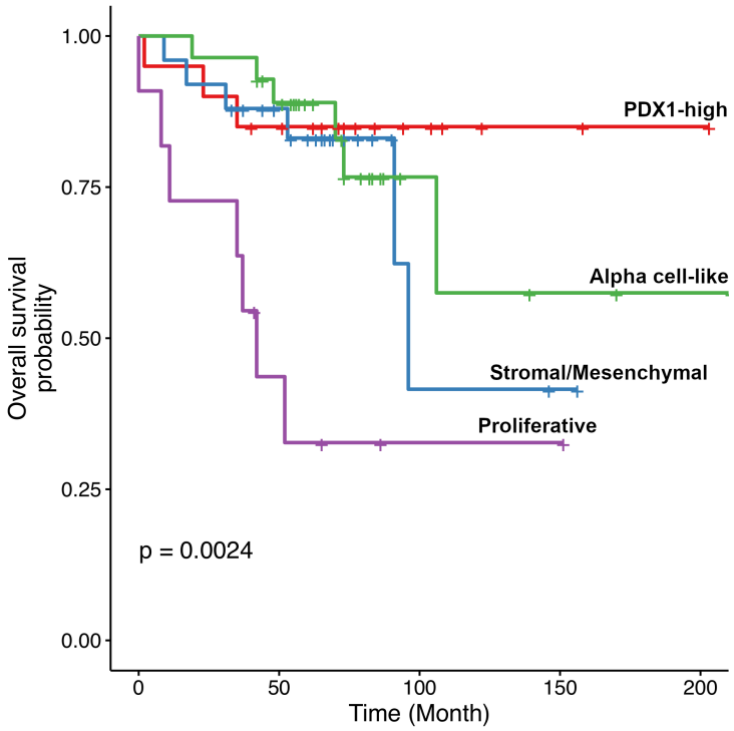

Figure 2.11. Overall survival probability of all 84 PNEN patients included in this study.
Patients were stratified by the proteotranscriptomic subgroup assignment of their specimens. Logrank test was used to evaluate whether the survival probabilities between the four subgroups were significantly different, and the resultant p-value is shown.

Table 2.2. Clinicopathological associations of the proteotranscriptomic subgroups using all 84 PNENs included in this study.

Characteristic		PDX1-high	Stromal/ Mesenchymal	Alpha cell-like	Proliferative	p-value
Sex						
	Female	13	12	17	6	0.69
	Male	7	13	11	5	
Functional Status						
	Functional	5	1	3	1	0.47
	Nonfunctional	10	11	11	7	
All-cause mortality						
	Censored	17	19	22	4	3.3×10^{-2}
	Deceased	3	6	6	7	
Histological Differentiation						5.2×10^{-5}
	Well	20	24	28	6	
	Poor	0	1	0	5	
Ki67						
	< 3%	14	12	14	1	4.7×10^{-4}
	3 – 20%	6	12	14	5	
	> 20%	0	1	0	5	
pT[a]						
	pT1	4	7	10	2	
	pT2	4	10	10	3	0.28
	pT3	11	4	6	4	
	pT4	1	4	2	1	
pN[a]						
	pN0	7	14	14	4	0.26
	pN1	11	8	7	5	
Metastases at Diagnosis						0.88
	No	13	20	20	8	
	Yes	4	4	6	3	
All-time Metastases						
	No	10	15	13	4	0.59
	Yes	9	10	15	7	

a. pT and pN were defined according to the 8th edition of American Joint Committee on Cancer Pancreatic Cancer Staging System. Cases with insufficient information were excluded. p-values were obtained from Fisher's exact test with Monte Carlo simulation.

The molecular features of the Proliferative subgroup included enrichment of cell cycle-related gene sets such as E2F targets and G2M checkpoints, which were evident at both the mRNA and protein levels (Figure 2.10). The mRNA expression and protein abundance of marker of proliferation Ki-67 (*MKI67*) were also significantly higher in the specimens of this subgroup consistent with their higher Ki67-based grading (Supplemental Table 2). Signaling pathway impact analysis (SPIA) was used to identify KEGG pathways enriched among the subgroup-specific DEGs and infer the relative activation state of each pathway (Tarca et al., 2008). The results from SPIA further supported the activation of cell cycle pathways in the Proliferative subgroup (Supplemental Table 4). GSA using cellular component gene ontologies revealed enrichment of proteins involved in chromosomes and spliceosomes suggesting increased DNA replication and active transcription (Figure 2.12; Supplemental Table 5). In particular, the mRNA and protein levels of multiple members of the minichromosome maintenance (MCM) family were higher in the Proliferative subgroup (Supplemental Table 2). The MCM family of proteins are involved in DNA replication initiation and elongation as well as chromosome maintenance (Forsburg, 2004). Altogether, the Proliferative subgroup was associated with a reduced overall survival probability and exhibited histology-, mRNA- and protein- level evidence of increased cell proliferation consistent with poorer outcomes typically observed in patients with PNECs or PNETs of higher grade (Dasari et al., 2017).

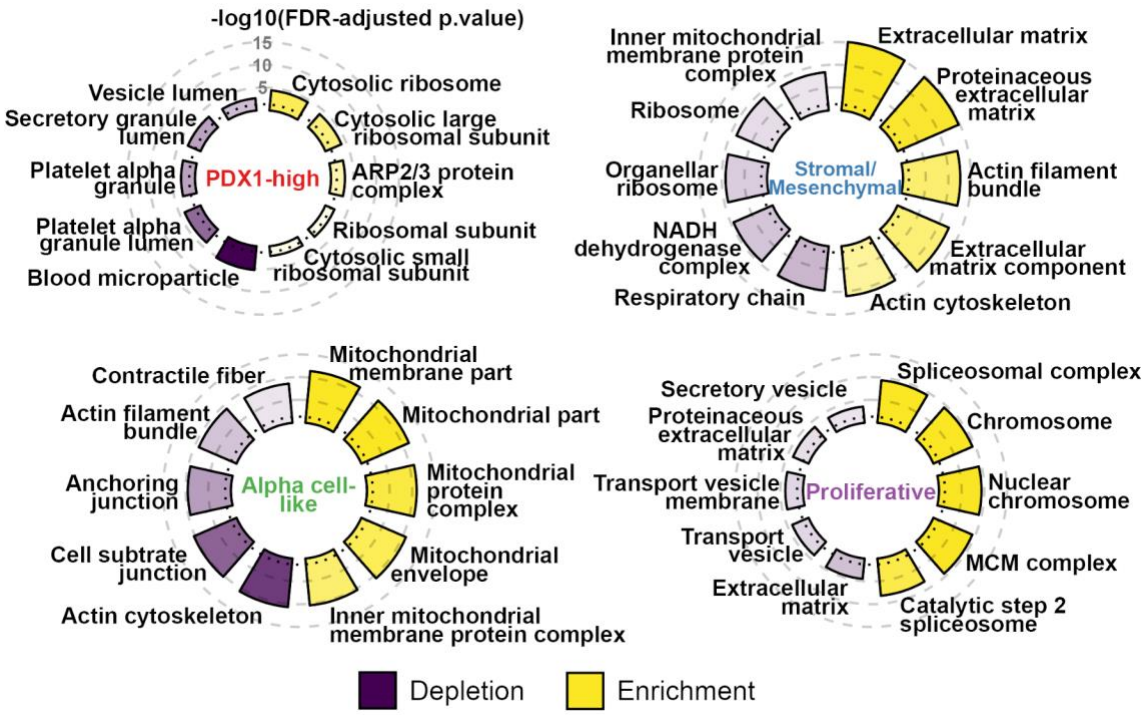

Figure 2.12. The top cellular components enriched or depleted on the protein level in each proteotranscriptomic subgroup.

The five highest ranking cellular component gene ontologies enriched (yellow) or depleted (purple) on the protein level in each of the four proteotranscriptomic subgroups depicted using circular barplot. The height and colour fill of each bar corresponds to the significance of the enrichment/depletion. Axis for the significance levels (FDR-adjusted p-values) are depicted as circular dashed lines for reference. All ontologies shown have FDR-adjusted p-value less than 0.05. The complete results are included in Supplemental Table 5.

2.2.5. Transcriptomic and proteomic analysis reveals differential enrichment of *ARX*, *PDX1* and organellar proteins between subgroups

Similar to two PNET subtypes previously reported (Cejas et al., 2019; Chan et al., 2018), the Alpha cell-like and PDX1-high subgroups showed increased expression of the transcription factors *ARX* and *PDX1*, respectively, in both the Discovery and Validation cohorts. The expression levels of *ARX* and *PDX1* in these two subgroups were also significantly higher ($p = 0.014$ and 0.023, respectively; Figure 2.13A) compared to levels observed in normal islets, indicating these transcription factors were selectively dysregulated. Considering that *PDX1* and *ARX* are cell fate-determining transcription factors, I evaluated the transcriptomic similarity of the samples to major pancreatic cell types using gene set variation analysis (GSVA). The results indicated significant similarity of the Alpha cell-like subgroup to pancreatic alpha cells, while none

of the four PNEN subgroups were similar to pancreatic beta cells or other endocrine cell types across both cohorts (Figure 2.13B-C). The Alpha cell-like subgroup was further characterized by increased mRNA expression and protein abundance of genes involved in oxidative phosphorylation (OxPhos; Figure 2.10) and increased abundance of mitochondrial proteins (Figure 2.12). Notably, the protein abundance of arginine (arginase 2; ARG2) and glutamine/glutamate metabolic enzymes (glutaminase, GLS; glutamate-ammonia ligase; GLUL; and glutamate dehydrogenase 2, GLUD2) was significantly higher in the Alpha cell-like subgroup (Supplemental Table 2), suggesting a potential reliance on these amino acids.

Given the differential expression of *PDX1* and *ARX* and their known roles in transcriptional regulation, I performed transcription factor enrichment analysis (TFEA) using ChEA3 (Keenan et al., 2019) to identify other transcription factors that may contribute to the molecular differences between the subgroups. Among the 1,632 transcription factors used by ChEA3 computation, one cut homeobox 1 (ONECUT1), paired related homeobox 2 (PRRX2), AE binding protein 1 (AEBP1) and forkhead box M1 (FOXM1) were the highest ranking in the PDX1-high, Stromal/Mesenchymal, Alpha cell-like and Proliferative subgroup, respectively. Both ARX and PDX1 were ranked among the top 10% transcription factors for both the Alpha cell-like and PDX1-high subgroups. The results from ChEA3 also suggested potential roles of ONECUT1/2, pancreas associated transcription factor 1a (PTF1A), SRY-box transcription factor 9 (SOX9) and neurogenin 3 (NEUROG3), all reported to be expressed in pancreatic progenitor cells (Bastidas-Ponce et al., 2017; Shih et al., 2013), in shaping the GEPs of the PDX1-high subgroup specimens (Supplemental Table 6). The expression of *NEUROG3* in human pancreas is transiently detected in endocrine progenitor and newly-differentiated endocrine cells (Jennings et al., 2013). The relatively higher mRNA levels of *PDX1* and *NEUROG3* observed in the PDX1-high subgroup specimens (Figure 2.13A; Supplemental Table 2) further support that this subgroup may be relatively similar to endocrine progenitor cells. Together, these results support that the Alpha-cell-like subgroup specimens resemble pancreatic alpha cells and exhibit increased abundance of mitochondrial proteins and expression of OxPhos-related genes, while the PDX1-high subgroup is characterized by high mRNA expression of PDX1 and involvement of other transcription factors typically expressed in pancreatic progenitor cells.

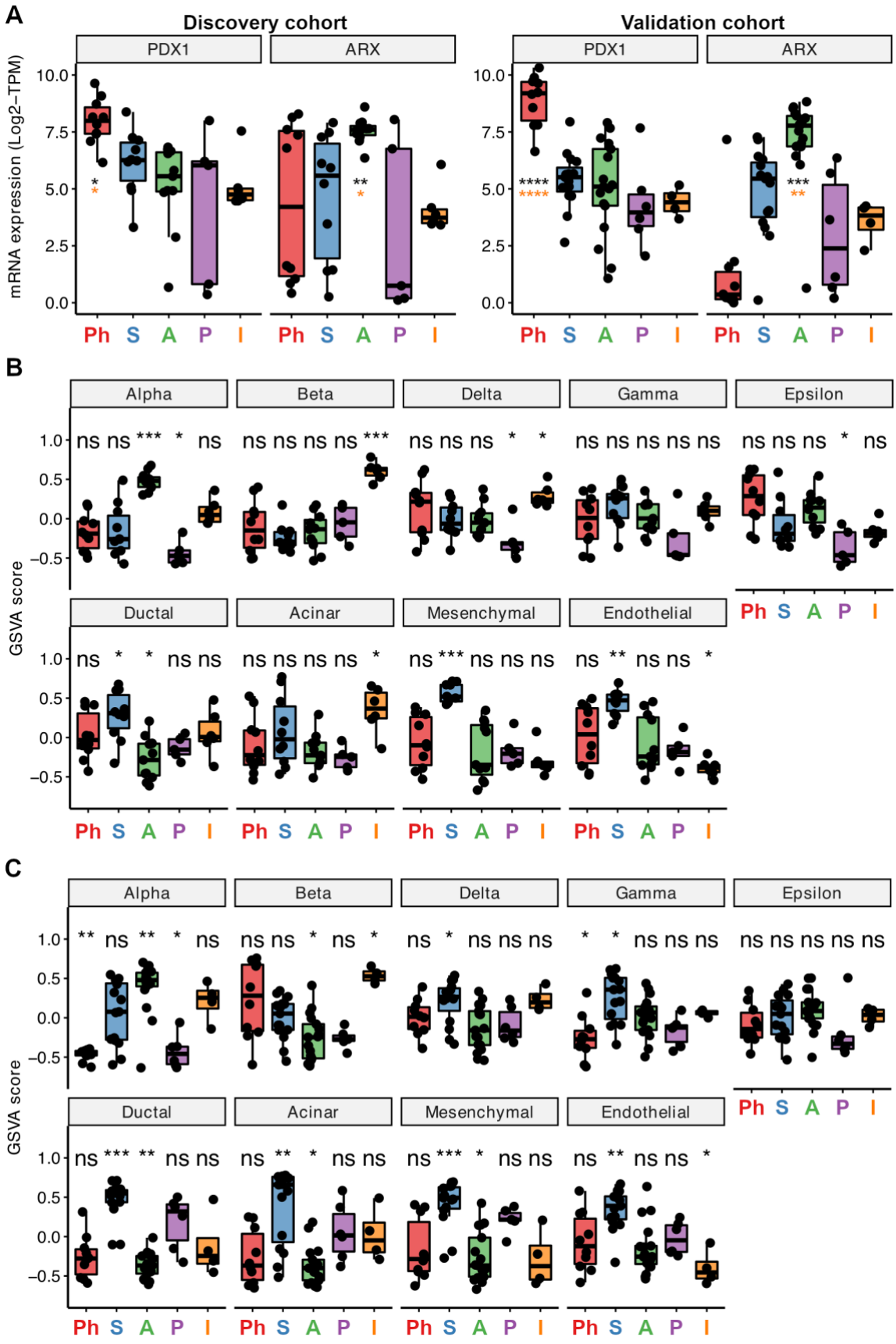
A
Discovery cohort
Validation cohort
PDX1
ARX
mRNA expression (Log2−TPM)
10.0
7.5
5.0
2.5
0.0
Ph S A P I
B
Alpha
Beta
Delta
Gamma
Epsilon
Ductal
Acinar
Mesenchymal
Endothelial
GSVA score
1.0
0.5
0.0
−0.5
C

Figure 2.13. Subgroups are characterized by difference in enrichment of cell types.

(A) The mRNA expression of *PDX1* and *ARX* between the four subgroups in the Discovery (left) or Validation (right) cohort. Statistical significance from differential expression analysis is shown for the PDX1-high subgroups (in the case of *PDX1*) or Alpha cell-like subgroups (in the case of *ARX*) vs. other PNENs (black asterisks) or normal islets (orange asterisks). (B) and (C) show the transcriptomic similarity of each (B) Discovery cohort or (C) Validation cohort (C) PNEN specimen to each of the 9 tested pancreatic cell types. Statistical significance in (B) and (C) was computed using Wilcoxon test to compare the scores from each subgroup of specimens to the rest. *: $p < 0.05$; **: $p < 0.01$; ***: $p < 0.001$; ****: $p < 0.0001$. Ph: PDX1-high subgroup; S: Stromal/Mesenchymal subgroup; A: Alpha cell-like subgroup; P: Proliferative subgroup; I: Normal Islet. Each box marks the median, 25th quartile and 75th quartile, and the whiskers extend to 1.5 times the inter-quartile range.

2.2.6. The Stromal/Mesenchymal subgroup specimens are enriched in stromal and immune cells

Most sporadic PNETs present as well-demarcated solitary masses and are vascularized with small vessels and little fibrotic stroma (Capelli et al., 2009; Kasajima et al., 2015). PNETs often contain few tumour infiltrating lymphocytes (TILs) compared to PNECs or PDACs, but a subset of PNETs was previously observed with higher abundance of TILs (Takahashi et al., 2018). Among the specimens in this study, I identified a Stromal/Mesenchymal subgroup that showed mRNA- and protein- level enrichment of genes involved in epithelial-to-mesenchymal transition (EMT) and immune responses (Figure 2.10, Supplemental Table 3). In combination with inferred activation of focal adhesion and gap junction pathways (Supplemental Table 4), as well as increased abundance of proteins associated with the extracellular matrix (Figure 2.12), these results suggested a relatively higher involvement of tumour microenvironment (TME) and/or mesenchymal cell-related molecular features in this particular subgroup. The Stromal/Mesenchymal subgroup specimens also exhibited significantly higher transcriptomic similarities to mesenchymal and endothelial cells (Figure 2.13B-C), though platelet and endothelial cell adhesion molecule 1 (PECAM1/CD31) and CD34 molecule (CD34) IHC staining of the primary specimens showed no evidence of increased microvessel densities ($p = 0.81$ and 0.26, respectively) (Figure 2.14A). GEP-based stromal and immune cell inference analysis using ESTIMATE (Yoshihara et al., 2013) and CIBERSORT (Newman et al., 2015) also found higher stromal and immune fractions in the specimens of this subgroup (Figure 2.14B-C). Together, these data indicate that the Stromal/Mesenchymal subgroup exhibited molecular characteristics suggestive of increased TME association and/or cellular phenotypes more akin to mesenchymal cells.

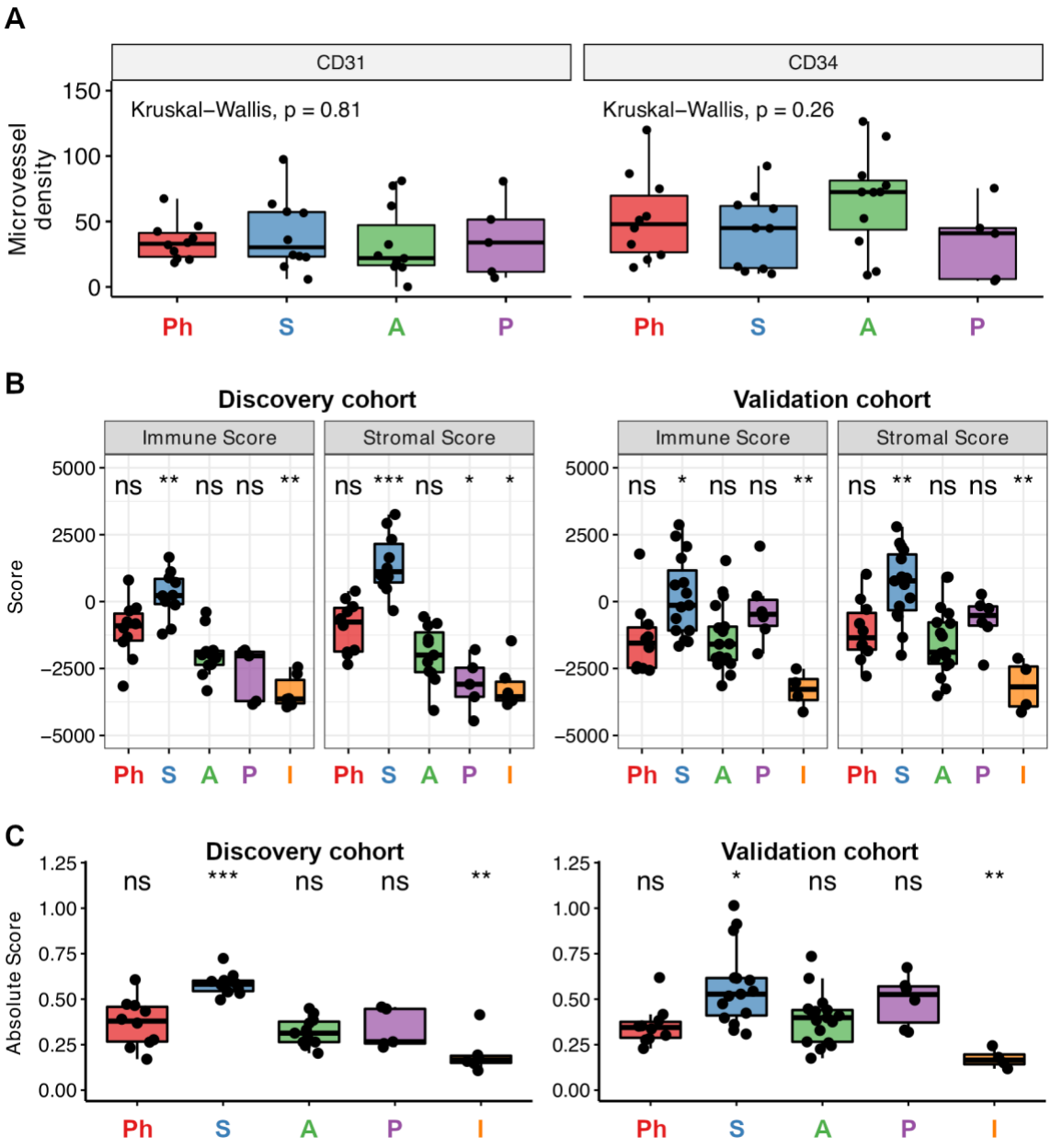

Figure 2.14. Differences in enrichment of non-tumour cells between the four subgroups.

(A) Microvessel density in each available Discovery cohort specimen (n = 36) assessed using either immunohistochemical staining of CD31 or CD34. The statistical significance was computed using Kruskal-Wallis test to test for differences between the subgroups. (B) The immune and stromal scores for each Discovery cohort (left) or Validation cohort (right) specimen from ESTIMATE analysis. (C) The absolute score from CIBERSORT for each Discovery cohort (left) or Validation cohort (right) specimen. In all panels, the specimens were stratified based on their subgroup assignments. In (B) and (C), the results from normal islet samples are included for reference, and the statistical significance was computed using Wilcoxon test to compare the scores from each subgroup of specimens to the rest. *: $p < 0.05$; **: $p < 0.01$; ***: $p < 0.001$. Ph: PDX1-high subgroup; S: Stromal/Mesenchymal subgroup; A: Alpha cell-like subgroup; P: Proliferative subgroup; I: Normal Islet. Each box marks the median, 25th quartile and 75th quartile, and the whiskers extend to 1.5 times the inter-quartile range.

2.2.7. Mutational differences between the proteotranscriptomic subgroups suggest distinct oncogenic drivers

To identify recurrent and potentially pathogenic sequence variants between the four subgroups, WES was performed on the 35 Discovery cohort specimens with paired transcriptome and proteome data. A total of 355 mutations in 227 cancer-related genes were identified among the 35 Discovery cohort specimens, where 10 (4.4%) cancer-related genes were mutated in more than 10% of the cohort (Supplemental Table 7). Among the most recurrently mutated cancer-related genes were those previously implicated in PNENs such as *MEN1*, *DAXX*, *ATRX* and *VHL*, with mutation frequencies of 22.9%, 17.1%, 8.6% and 11.4%, respectively (Figure 2.15). Comparison between the four subgroups showed a trend toward enrichment of deleterious *MEN1* mutations ($p = 0.066$; Fisher's exact test) and significant enrichment of deleterious DAXX mutations ($p = 0.013$; Fisher's exact test) in the Alpha cell-like subgroup specimens. The Alpha cell-like subgroup was also the only subgroup with *ATRX* mutations or deleterious *TSC1/2* mutations. IHC staining of DAXX and ATRX showed no significant association between the detected DNA mutations and DAXX/ATRX scores (Figure 2.15).

Germline mutations in *VHL* or *NF1* can cause VHL syndrome or NF1 disorder, both potentially leading to PNEN development (Alexakis et al., 2004; Hammel et al., 2000). There were four cases with VHL syndrome among the Discovery cohort patients all of which fell within the Stromal/Mesenchymal subgroup (Figure 2.15; Supplemental Table 1), consistent with the prominence of small vessels and stroma in VHL-associated neoplasms (Lubensky et al., 1998). In three of these VHL patients, at least one missense mutation in *VHL* was found in their sequenced specimens. None of the patients in our cohorts were diagnosed with neurofibromatosis, but a truncating mutation affecting *NF1* was found in one PDX1-high case (Figure 2.15; Supplemental Table 7).

Missense mutations in proto-oncogenes, experimentally shown to be hypermorphic in previous reports, were also found among the sequenced PNENs. These include a Proliferative subgroup specimen with a *CTNNB1* p.D32N variant (Al-Fageeh et al., 2004) concomitant with high mRNA expression (470.7 transcripts per million (TPM) vs cohort average = 114.5, SD = 71.1) and protein abundance (normalized, log2-scale abundance of 7.1 vs cohort average = 5.7, SD = 0.5) of *CTNNB1*, two PDX1-high specimens with an activating *HRAS* (HRas proto-oncogene, GTPase) or *NRAS* (NRAS

proto-oncogene, GTPase) p.Q61R variant (Burd et al., 2014; Geyer et al., 2018; Muñoz-Maldonado et al., 2019), another PDX1-high specimen with a weakly activating *RET* (ret proto-oncogene) p.V292M variant (Castellone et al., 2010), and a Stromal/Mesenchymal specimen with weakly activating *KRAS* p.L19F and p.Q22K variants (Smith et al., 2010a; Tsukuda et al., 2000) (Supplemental Table 7). Collectively, hypermorphic mutations affecting proto-oncogenes were identified in five of the sequenced specimens, all of which were histologically defined as PNETs (Figure 2.15).

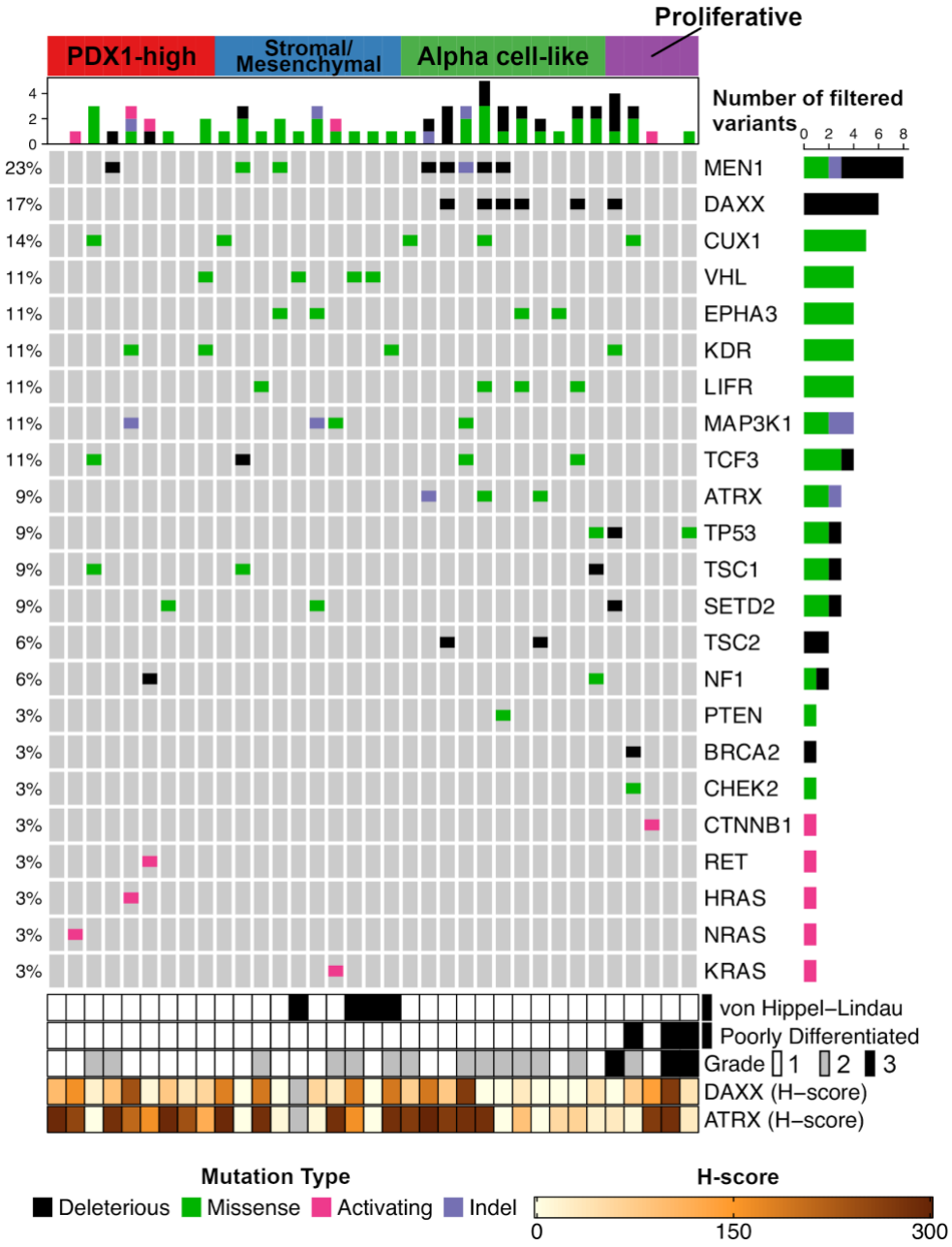

Figure 2.15. Mutational differences between the proteotranscriptomic subgroups suggest distinct genetic drivers

Oncoprint depicting the mutational status and the types of mutation in select genes among the 35 Discovery cohort specimens with paired transcriptome and proteome data. The genes were selected based on mutational frequency > 10%, known relevance to PNENs or known roles as proto-oncogenes in which at least one hypermorphic mutation was found (see also Table S7). Samples are ordered and colour-coded according to their subgroup assignments (top row). The barplot (second row) shows, in each patient sample, the total number and types of variants affecting the genes shown. The barplot on the far right shows the total number and types of variants affecting the indicated gene. Additional clinicopathological characteristics of interest are shown at the bottom. Shown mutations are categorized into Deleterious mutations: nonsense or frameshift mutations, Indel: inframe insertions or deletions, Missense mutations, or Activating mutations: point mutations experimentally shown to be hypermorphic.

2.2.8. Inferred activities of key cellular regulators are consistent with mutational differences and suggest involvement of the Hippo signaling pathway in the Stromal/Mesenchymal subgroup

To evaluate the functional impacts of the identified mutations and particularly their effects on GEPs, I used VIPER (Alvarez et al., 2016) to infer the activity of key cellular regulators based on subgroup-specific gene expression signatures. The VIPER results are included in Supplemental Table 8. Consistent with the observed mutations and mutational differences, MEN1, DAXX and ATRX were relatively inhibited in the Alpha cell-like subgroup, while the PDX1-high subgroup showed relative activation of HRAS and NRAS along with inhibition of NF1. Similarly, the identified activating *KRAS* mutations and deleterious *TSC2* mutations in the Stromal/Mesenchymal subgroup specimens were supported by the relative activation of KRAS and inhibition of TSC2 in this subgroup (Figures 2.15 and 2.16A).

I further exploited the VIPER results and found Yes1 associated transcription regulator (YAP1) and WW domain containing transcription regulator 1 (WWTR1) to be the top 1 and 3 activated regulators, respectively, in the Stromal/Mesenchymal subgroup (Figure 2.16A; Supplemental Table 8). WWTR1, also known as TAZ, along with YAP1 are transcriptional coactivators and downstream effectors of the Hippo signaling pathway (Varelas, 2014). Indeed, SPIA identified an over-representation of Hippo signaling pathway genes among the subgroup-specific DEGs in the Stromal/Mesenchymal subgroup (Supplemental Table 4). Further, differential analysis identified significantly higher mRNA expression of *YAP1* and *WWTR1* in the Stromal/Mesenchymal subgroup specimens compared to other PNENs or normal islets (Figure 2.16B). Given that YAP1 and WWTR1 act as transcriptional coactivators, a direct measurement of YAP1/ WWTR1 protein activity can be made by examining the transcriptional levels of their target genes. For this, I used a previously curated panel of 22 YAP1/WWTR1 target genes (Wang et al., 2018) as a reference gene set. Significantly higher YAP1/WWTR1 target enrichment scores in the Stromal/Mesenchymal subgroup specimens suggested the relative activation of YAP1/WWTR1 in this subgroup compared to other PNENs or normal islets (Figures 2.16C). Together, these results support the activation of the YAP1/WWTR1 signaling axis in the Stromal/Mesenchymal subgroup and mark the significance of the Hippo signaling pathway in PNENs.

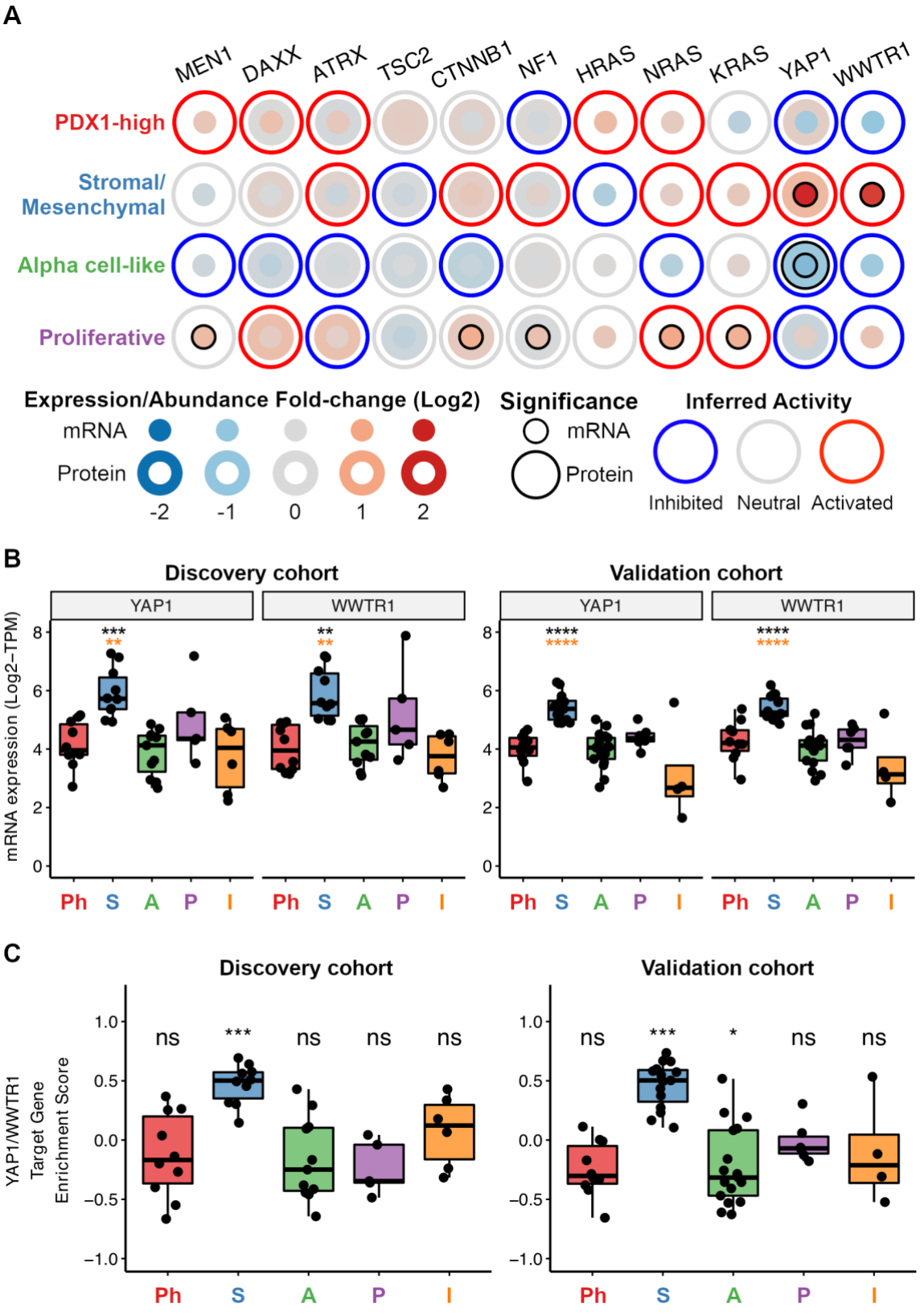
A
MEN1
DAXX
ATRX
TSC2
CTNNB1
NF1
HRAS
NRAS
KRAS
YAP1
WWTR1
PDX1-high
Stromal/
Mesenchymal
Alpha cell-like
Proliferative
Expression/Abundance Fold-change (Log2)
mRNA
Protein
-2
-1
0
1
2
Significance
mRNA
Protein
Inferred Activity
Inhibited
Neutral
Activated
B
Discovery cohort
Validation cohort
YAP1
WWTR1
mRNA expression (Log2−TPM)
Ph
S
A
P
I
C
Discovery cohort
Validation cohort
YAP1/WWTR1
Target Gene
Enrichment Score
ns
*
**
***
****

Figure 2.16. Inferred activities of cellular regulators are consistent with mutational differences and suggest involvement of the Hippo signaling pathway in the Stromal/Mesenchymal subgroup

(A) Inferred activity (outer ring) of select cellular regulators of interest are illustrated along with their mRNA expression (centre fill) and protein abundance (outer fill) fold-changes between the four proteotranscriptomic subgroups, among the 35 Discovery cohort specimens with paired transcriptome and proteome data. The mRNA expression of protein abundance of a gene is outlined in black if the fold-change was significant with an adjusted p-value less than 0.05. Only genes with an adjusted p-value < 0.05 from the inference analysis are considered as activated or inhibited. (B) mRNA expression levels of YAP1 and WWTR1 in each of the Discovery cohort (left) or Validation cohort (right) specimens, stratified by subgroup assignments, or in normal islet samples. mRNA expression levels shown as log2-TPM values. Statistical significance from differential expression analysis is shown for the Stromal/Mesenchymal subgroup vs. other PNENs (black asterisks) or normal islets (orange asterisks). Statistical significance from differential expression analysis is shown for the Stromal/Mesenchymal subgroup vs. other PNENs (black asterisks) or normal islets (orange asterisks). (C) YAP1/WWTR1 target gene enrichment score for each Discovery cohort (left) or Validation cohort (right) specimen, stratified by subgroup assignments, or for normal islet samples. Statistical significance was computed using Wilcoxon test to compare the scores from each subgroup of specimens to the rest. **: $p < 0.01$; ***: $p < 0.001$; ****: $p < 0.0001$. Ph: PDX1-high subgroup; S: Stromal/Mesenchymal subgroup; A: Alpha cell-like subgroup; P: Proliferative subgroup; I: Normal Islet. Each box marks the median, 25th quartile and 75th quartile, and the whiskers extend to 1.5 times the inter-quartile range.

2.3. Discussion

Using a multi-omics approach that combined exome-, transcriptome- and proteome- level data to portray an unselected group of PNENs, I identified four proteotranscriptomic subgroups. I also uncovered previously unrecognized metabolism-related molecular differences in an Alpha cell-like subgroup and involvement of the Hippo signaling pathway in a Stromal/Mesenchymal subgroup of PNENs. Combined with subgroup-specific cellular regulators and oncogenic features, my findings provide a basis for potential patient stratification strategies with therapeutic implications.

ARX and *PDX1* are two transcription factors that may distinguish pancreatic alpha versus beta cells, respectively, with *PDX1* also being expressed early during pancreas organogenesis (Shih et al., 2013). An *ARX*-high subtype of PNETs was shown to resemble pancreatic alpha cells, while a *PDX1*-high subtype of PNETs exhibited enhancer profiles resembling pancreatic beta cells but with more heterogeneity in intra-subtype GEPs and *PDX1* expression levels (Cejas et al., 2019; Chan et al., 2018). I similarly identified elevated *PDX1* or *ARX* mRNA expression levels in PDX1-high and Alpha-cell like subgroups, respectively. The Alpha cell-like specimens showed transcriptomic similarity to pancreatic alpha cells and enrichment of mutations in *ATRX, DAXX and MEN1*, consistent with the A-D-M mutant PNET subtype reported by Chan et

al. (2018) and the Type A subtype reported by Cejas et al. (2019). However, the PDX1-high subgroup did not exhibit any other molecular features suggestive of its similarity to pancreatic beta cells or any other endocrine cell types. These variations in the subset of PNENs with high *PDX1* mRNA expression across studies warrant further investigation using larger and broader cohorts of PNENs. Furthermore, the majority of PNENs in this and previous studies (Cejas et al., 2019; Chan et al., 2018) were clinically identified as nonfunctional PNENs. The discovery of a subset of PNENs with transcriptomic similarity to pancreatic alpha cells but without clinically significant glucagon detection suggests a disconnection between molecular characteristics and clinical phenotypes and the importance of employing an unbiased approach to fully understand PNENs as a disease.

In the Alpha cell-like subgroup specimens, I found previously unknown molecular features that revealed potential therapeutic angles. The Alpha cell-like subgroup showed mRNA- and protein- level enrichment of OxPhos-related genes as well as increased abundance of mitochondrial proteins, such as GLS, GLUL and ARG2. Some cancer types require utilization of GLS to catabolize glutamine and are susceptible to GLS inhibition (Cluntun et al., 2017). For example, in a hepatocellular carcinoma murine model with increased Gls mRNA expression and protein abundance, loss of a *Gls* allele or pharmacological inhibition of Gls using BPTES delayed tumour growth and prolonged survival (Xiang et al., 2015). The markedly higher abundance of glutamine and arginine metabolic enzymes in the Alpha cell-like subgroup may reflect the subgroup's reliance on these amino acids and therefore sensitivity to interventions that affect their supply/availability. Considering multiple groups have reported a subset of PNENs with elevated *ARX* expression or ARX IHC positivity (Cejas et al., 2019; Chan et al., 2018; Di Domenico et al., 2020; Hackeng et al., 2021) similar to the Alpha cell-like subgroup, therapeutic agents such as BPTES that inhibit glutamine metabolism may provide therapeutic benefit for patients within this subgroup. With the frequent mutation of *MEN1*, *DAXX* or *ATRX* and the high expression level of *ARX* in the Alpha cell-like subgroup of PNENs, the relationship between these genetic alterations and its distinct metabolism-related expression profile could be exploited for the discovery of potential targeted treatments and corresponding predictive biomarkers.

While I did not investigate the genomic landscapes of the PNEN specimens examined in this study, the Alpha cell-like subgroup may also correlate with other previously described subtypes without RNA-level characterization. Based on its

enrichment of specimens with mutant *MEN1* and *DAXX,* higher *ARX* expression and/or clustering with pancreatic α-cells, the Alpha cell-like subgroup may resemble the Group 1 subtype described by Lawrence et al. (2018), the Intermediate subtype by Di Domenico et al. (2020), the NF-Amp subtype by Hong et al. (2020), the T2 subtype by Lakis et al. (2021) and the Subtype A by Boons et al. (2020). Of note, three of these subtypes were characterized with recurrent LOH or loss in chromosomes 1, 2, 6, 10, 16 and 22 (Boons et al., 2020; Lakis et al., 2021; Lawrence et al., 2018), suggesting potential links between concurrent alterations in *MEN1* and *DAXX* and loss of these chromosomes.

PNETs are typically known as a “tumour-suppressor” disease, wherein potential driver mutations most often affect tumour suppressor genes and rarely proto-oncogenes (Jiao et al., 2011; Scarpa et al., 2017; Wong et al., 2018). I found a surprising number of PNET cases with hypermorphic variants of proto-oncogenes: *CTNNB1* (p.D32N), *HRAS* (p.Q61R), *NRAS* (p.Q61R), *KRAS* (p.L19F and p.Q22K), and *RET* (p.V292M) that result in either their constitutive activation or stabilization (Al-Fageeh et al., 2004; Burd et al., 2014; Castellone et al., 2010; Geyer et al., 2018; Smith et al., 2010a; Tsukuda et al., 2000). In particular, one third (3/9) of the PDX1-high subgroup specimens harboured gene variants that potentially lead to activated RAS signaling. Altogether, 5 out of 32 (15.6%) PNETs, or 5 out of 35 (14.3%) PNENs, and no PNECs, among the Discovery cohort specimens harboured hypermorphic mutations affecting proto-oncogenes. Through inference analysis, I also found accompanying transcriptomic changes consistent with relative activation of these genes in the corresponding subgroups. It remains uncertain what led to the higher-than-expected number of activating mutations in these sequenced PNETs, but the inclusive nature of the current study and the epidemiology of the included PNENs may contribute to the observed differences. Nonetheless, the clustering of the cases harbouring potentially oncogenic mutations with other PNENs lacking obvious driver genetic alterations could reflect common intra-subgroup molecular features.

The Hippo signaling pathway elicits downstream transcriptional effects through YAP1 and WWTR1 (Hansen et al., 2015). I identified an unexpected activation of the YAP1 and WWTR1 transcriptional coactivators in the Stromal/Mesenchymal subgroup. Phenotypic consequences of YAP1 and WWTR1 activation include a myriad of cancer hallmarks, among which are the induction of EMT (Lei et al., 2008), promotion of

angiogenesis (Choi et al., 2015; Kim et al., 2017a) and modification of the TME (Zanconato et al., 2019) - all of which were observed in the Stromal/Mesenchymal subgroup (Figures 2.10 and 2.12). Both increased mRNA expression and relative activation of YAP1 and WWTR1 were found in the Stromal/Mesenchymal subgroup and were further supported by transcriptomic signatures previously shown to correlate with YAP1 and WWTR1 activation in pan-cancer analysis (Wang et al., 2018). YAP1 and WWTR1 are favoured therapeutic targets among the Hippo signaling pathway due to their direct roles in transcriptional regulation. Investigative drugs targeting YAP1 and WWTR1 are being explored (Crawford et al., 2018). Verteporfin, a photosensitizer used in photodynamic therapies, has demonstrated YAP1 inhibitory effects and anti-tumour effects in hepatocellular carcinoma, retinoblastoma and glioblastoma (Brodowska et al., 2014; Liu-Chittenden et al., 2012; Vigneswaran et al., 2021), and may provide therapeutic benefit to patients with PNENs of the Stromal/Mesenchymal subgroup or exhibiting elevated *YAP1/WWTR1* expression. The observation of high expression and activity of YAP1 and WWTR1 in the Stromal/Mesenchymal subgroup specimens could indicate their reliance on the activation of these Hippo signaling pathway effectors and susceptibility to inhibition of YAP1/WWTR1 activity.

Epidemiological factors, the nonselective nature of case accrual, and an unprecedent multi-omic approach all likely contributed to the discovery of the new PNEN molecular features revealed in this study. Also, the PNEN specimens profiled in this study were mostly resected during the early stage of disease, as reflected by the few cases with metastases at the time of diagnosis. While the molecular landscapes of these early-stage PNEN specimens may partially differ from those of late-stage, metastatic disease, our study revealed biological subgroups that may aid treatment planning in the early stages of this highly heterogeneous disease. Given the rarity of PNENs and limitations of the specimens in the current studies, there may be additional PNEN subgroups not represented among our cohort specimens that could explain the distinct clustering of the NT-3 cell line samples. A meta-analysis combining the present study and previous PNEN profiling studies would be invaluable to more comprehensively understand the disease from both biological and therapeutic perspectives.

2.4. Methods

2.4.1. Case and clinical information accrual

Tumour specimens

The Discovery cohort consisted of PNEN cases included in a previously constructed pancreatic TMA (Riazy et al., 2015; Tessier-Cloutier et al., 2017). To identify PNEN cases for the Validation cohort, the pathology archives at Vancouver General were searched for PNEN cases, where the only criterion for inclusion in the study was a confirmed PNEN diagnosis. No exclusion criteria were implemented. For all identified cases with specimen availability, archival formalin-fixed paraffin-embedded (FFPE) tissue and corresponding data were retrieved and used in accordance with the ethical approval granted by the University of British Columbia (UBC) Clinical Research Ethics Board (H12-03484) and the UBC BC Cancer Research Ethics Board (H16-01577). The original slides were reviewed by a board certified pathologist (Dr. John Aird) to confirm the diagnosis, the pathological classification and the grade.

A total of 41 PNENs from the Discovery cohort and 51 PNENs from the Validation cohort were subjected to RNA-seq. Forty of the Discovery cohort PNENs were characterized with proteomic profiling. Samples that failed RNA-seq or yielded inferior sequencing quality were excluded (see the *RNA quantification and sample exclusion* subsection under Section 2.4.2), resulting in the final Discovery cohort of 36 PNENs and the final Validation cohort of 48 PNENs. Thirty-five of the Discovery cohort PNENs with both RNA-seq and proteomic data were additionally characterized with WES. The two cohorts included patients at various disease and pathological stages diagnosed between 1999 and 2016.

For molecular assays, tumour-rich regions from FFPE tumour blocks were marked and cored. Areas with the highest Ki67 proliferative index were targeted. Due to limited material, tissue scrolls were instead obtained for two cases where only biopsied materials were available. For sequencing and proteomic sample extractions, two cores (1 mm x1 mmx 10 mm) or three 10 µm scrolls (300~400 mm^2) were used for each assay.

Cell lines

BON-1 was a gift from Drs. Courtney Townsend and Mark Hellmich at the University of Texas Medical Branch, Texas, USA. QGP-1 was purchased from the Japanese Cancer Resource Bank. NT-3 was previously developed and provided by Dr. Jörg Schrader at University Medical Center Hamburg-Eppendorf, Hamburg, Germany (Benten et al., 2018). BON-1 cells were cultured in DMEM:F12 (Gibco) supplemented with 10% fetal bovine serum (FBS; Gibco) and 10 mM HEPES (Gibco). QGP-1 cells were cultured in RPMI 1640 (Gibco) supplemented with 10% FBS. NT-3 cells were cultured in RPMI 1640 supplemented with 10% FBS, 100 U/mL penicillin-streptomycin (Gibco), 20 ng/mL EGF (Sigma-Aldrich) and 10 ng/mL FGF2 (Sigma-Aldrich). For culturing NT-3 specifically, cell culture vessels were coated with collagen IV (Sigma-Aldrich) to ensure adherent growth. All three cell lines were developed from tumours from male patients. All cell cultures were maintained at 37°C with 5% CO_2 and were checked regularly to be free of mycoplasma. Cells were harvested at 70~90% confluence and immediately snap-frozen.

Normal islet samples

Islet extractions were obtained from the IsletCore at the Alberta Diabetes Institute, Alberta, Canada, between 2016 and 2018. All extractions were derived from cadaveric pancreas from individuals (age: 22~74; BMI: 21.5~32.5; 6 males and 3 females) without documented pancreas-related health conditions and of causes of death unrelated to cancer. All islet extractions were hand-picked after receipt to ensure maximum purity and snap-frozen immediately. An additional normal islet sample, matched to one of the FFPE tumour blocks was acquired by laser capture microdissection (LCM) of islets from fifteen 8 µm sections.

Clinicopathological characteristics

Where applicable, the grading (including the histological differentiation status and proliferative index) of the PNEN cases was updated to conform with the 2019 WHO classification system (Nagtegaal et al., 2020). The clinicopathological characteristics such as sex, tumour stage and WHO class of the study cohort are provided in Supplemental Table 1. The overall survival time was calculated by subtracting the date of diagnosis from the last follow-up date. pT and pN staging were defined according to the AJCC Staging Manual (8^{th} edition).

2.4.2. Sample processing

FFPE tissue nucleic acid extraction

Total nucleic acid extraction from FFPE specimens was performed using a modified version of Agencourt's FormaPure protocol developed in-house and described previously (Haile et al., 2017, 2018). Briefly, Agencourt® FFPE FormaPure Kit (Beckman Coulter) was used per manufacturer's instructions for total RNA extraction except 1) the DNase treatment step was excluded, 2) the deparaffinization/lysis step was extended to two hours, and 3) a reverse cross-linking step was included between proteinase K treatment and bead binding steps.

Snap-frozen tissue nucleic acid extraction

Frozen tissue or cell line pellets were homogenized in lysis buffer (RLT Plus + TCEP) for total nucleic acid (DNA and RNA) extraction using the EvoPure RNA Tissue Isolation kit (Aline Biosciences) automated on a Microlab NIMBUS liquid handler (Hamilton Robotics). Frozen tissue pieces were immersed in 420 µL of RLT Plus buffer (Qiagen) containing the reducing agent TCEP and a unique sample tracking DNA plasmid and gently agitated overnight at room temperature. Lysates were transferred from 2 mL tubes to wells of a 1.2 mL plate (Thermo Scientific, AB1127) into which was added 400 µL of 5x bind buffer (80 µL beads in 320 µL IPA). Following a 5 minute incubation at room temperature lysates were cleared on a magnet (Alpaqua, 96M-EX) for 6 minutes and the protein-containing supernatant removed. The beads, with bound nucleic acids, were washed by pipetting 10 times in wash buffer and returned to the magnet. Beads were washed three times in 70% ethanol then dried for 10 minutes. 40 µL nuclease-free water was added to the dried beads and returned to the magnet. The eluted total nucleic acids were transferred to a 96-well storage plate and aliquots taken for fluorometric quantification using Qubit 4 Fluorometer (Thermo Scientific).

RNA-seq

To remove cytoplasmic and mitochondrial ribosomal RNA (rRNA) species from total RNA, NEBNext® rRNA Depletion Kit was used (New England Biolabs, NEB). Enzymatic reactions were assembled in a 96-well plate on a Microlab NIMBUS liquid handler. 100 ng of DNase I-treated total RNA in 6 µL was hybridized to rRNA probes in a 7.5 µL reaction. Heat-sealed plates were incubated at 95°C for 2 minutes followed by

incremental reduction in temperature by 0.1°C per second to 22°C (730 cycles). The rRNA in DNA hybrids was digested using RNase H in a 10 µL reaction incubated in a thermocycler at 37°C for 30 minutes. To remove excess rRNA probes (DNA) and residual genomic DNA contamination, DNase I was added in a total reaction volume of 25 µL and incubated at 37°C for 30 minutes. RNA was purified using RNA MagClean DX beads (Aline Biosciences) with 15 minutes of binding time, 7 minutes clearing on a magnet followed by two 70% ethanol washes, 5 minutes to air dry the RNA pellet and elution in 36 µL DEPC water. The plate containing RNA was stored at -80°C prior to cDNA synthesis.

First-strand cDNA was synthesized from the purified RNA (minus rRNA) using the Maxima H Minus First Strand cDNA Synthesis kit (Thermo Scientific) and random hexamer primers at a concentration of 8 ng/µL along with a final concentration of 0.04 µg/µL Actinomycin D, followed by PCRClean DX bead (Aline Biosciences) purification on a Microlab NIMBUS liquid handler. The second strand cDNA was synthesized following the NEBNext® Ultra™ Directional Second Strand cDNA Synthesis Module (NEB) that incorporates dUTP in the dNTP mix, allowing the second strand to be digested using USER™ enzyme (NEB) in the post-adapter ligation reaction and thus achieving strand specificity.

cDNA was fragmented by sonication (Covaris, LE220) for 130 seconds (2x65 seconds) at a “Duty cycle” of 30%, 450 Peak Incident Power (W) and 200 Cycles per Burst in a 96-well microTUBE Plate (Covaris, 520078) to achieve 200-250 bp average fragment lengths. The paired-end sequencing library was prepared following the Genome Sciences Centre (BC Cancer, Canada) strand-specific, plate-based library construction protocol on a Microlab NIMBUS liquid handler. Briefly, the sheared cDNA was subject to end-repair and phosphorylation in a single reaction using an enzyme premix (NEB) containing T4 DNA polymerase, Klenow DNA Polymerase and T4 polynucleotide kinase, incubated at 20°C for 30 minutes. Repaired cDNA was purified in 96-well format using PCRClean DX beads and 3’ A-tailed (adenylation) using Klenow fragment (3’ to 5’ exo minus) and incubation at 37°C for 30 minutes prior to enzyme heat inactivation. Illumina PE adapters were ligated at 20°C for 15 minutes. The adapter-ligated products were purified using PCRClean DX beads, then digested with USER™ enzyme (1 U/µL) at 37°C for 15 minutes followed immediately by 13 cycles of indexed PCR using Phusion™ High-Fidelity DNA Polymerase (Thermo Scientific) and Illumina’s

PE primer set. PCR parameters: 98˚C for 1 minute followed by 13 cycles of 98˚C for 15 seconds, 65˚C for 30 seconds and 72˚C for 30 seconds, and then 72˚C for 5 minutes. The PCR products were purified and size-selected using a 1:1 PCRClean DX beads-to-sample ratio twice, and the eluted DNA quality was assessed with LabChip® GX (Caliper) for DNA samples using the DNA High Sensitivity Reagent Kit (PerkinElmer). Samples were then quantified using a Quant-iT™ dsDNA Assay Kit, high sensitivity (Thermo Scientific) on Qubit 4 Fluorometer prior to library pooling and size-corrected final molar concentration calculation for Illumina HiSeq2500 sequencing with paired-end 75 base reads. Library pooling was done in sets of three, with the exception of the library from the one LCM islet sample, which was not pooled with other libraries.

Protein extraction and digestion

FFPE tissues were first deparaffinized using xylene. Lysis buffer (500 mM Tris-Cl pH 8, 2% SDS, 1% NP40, 1% Triton X-100, 5mM EDTA, 50mM NaCl, 10mM TCEP and 40mM CAA) was then added to each sample. Proteins were denatured using heat (for 130 minutes at 95°C with shaking at 1,100 RPM), followed by a 30 minute incubation at room temperature in the dark to allow reduction and alkylation of disulfide bonds.

Protein clean-up and digestion was done using the SP3 protocol developed in-house (Hughes et al., 2014, 2019). Briefly, paramagnetic beads were prepared by mixing two types of Sera-Mag Speed beads (GE Life Sciences) at 1:1 ratio, and 20 µg of bead mix was added to each protein mixture. Ethanol was added to a final concentration of 50% (v/v), and the sample was mixed and incubated for 10 minutes at room temperature to ensure protein-bead binding. The samples were then placed on a magnetic rack to stabilize the beads, and the supernatants were discarded, and two rinses with 70% absolute ethanol and one rinse with 100% absolute ethanol were applied. The beads were reconstituted in aqueous buffer (50 mM HEPES pH 8) containing trypsin/LysC mix (Promega) at 1:50 (ug/ug) enzyme to protein amount and sonicated for 30 seconds in a water bath to disaggregate the beads. The mixtures were then incubated for 14 hours at 37°C, sonicated for 10 seconds to resuspend the beads, and the supernatants recovered.

Peptide labeling and fractionation

The digested peptide samples were prepared for mass spectrometry (MS) analysis in batches of 10, where each batch contained 8 randomly assigned patient samples and two common inter-batch controls. One control was a pooled all-sample mixture consisting of an aliquot of each patient sample. The second control was a universal standard consisting of digested peptides from thirteen cell lines. The peptide mixtures were labeled with tandem mass tag (TMT) using the TMT10plex labeling kit (Pierce) according to manufacturer's instructions. High-pH reversed phase analysis was performed on an Agilent 1100 HPLC system equipped with a diode array detector (254, 260, and 280 nm). Fractionation was performed on a Kinetix EVO C18 column (2.1 mm x 150 mm, 1.7 µm core shell, 100 Å, Phenomenex). Elution was performed at a flow rate of 0.2 mL per minute using a gradient of mobile phase A (10 mM ammonium bicarbonate, pH 8) and B (acetonitrile), from 3% to 35% over 60 minutes. Fractions were collected every minute across the elution window for a total of 48 fractions, which were concatenated to a final set of 12 (e.g. 1 + 13 + 25 + 37 = fraction 1). Fractions were dried in a SpeedVac centrifuge and reconstituted in 1% formic acid with 1% DMSO in water prior to MS analysis.

MS analysis

Analysis of TMT-labeled peptide fractions was carried out on an Orbitrap Fusion™ Tribrid™ MS platform (Thermo Scientific). Samples were introduced using an Easy-nLC 1000 system (Thermo Scientific). Columns used for trapping and separations were packed in-house. Trapping columns were packed in 100 µm internal diameter capillaries to a length of 25 mm with ReproSil-Pur C18 beads (3 µm particle size, Dr. Maisch). Trapping was carried out for a total volume of 10 µL at a pressure of 400 bar. After trapping, gradient elution of peptides was performed on a ReproSil-Pur C18 (1.9 µm particle size, Dr. Maisch) column packed in-house to a length of 15 cm in 100 µm internal diameter capillaries with a laser-pulled electrospray tip and heated to 45°C using AgileSLeeve column ovens (Analytical Sales & Service). Elution was performed with a gradient of mobile phase A (water and 0.1% formic acid) to 8% B (acetonitrile and 0.1% formic acid) over 5 minutes, to 25% B over 88 minutes, to 40% B over 20 minutes, with final elution (80% B) and equilibration (5% B) using a further 7 minutes at a flow rate of 375 nL per minute.

Data acquisition on the Orbitrap Fusion (control software v2.1.1565.20) was carried out using a data-dependent method with multi-notch synchronous precursor selection MS3 scanning for TMT tags. Survey scans covering the mass range of 350 – 1500 were acquired at a resolution of 120,000 (at m/z 200), with quadrupole isolation enabled, an S-Lens RF Level of 60%, a maximum fill time of 50 ms, and an automatic gain control (AGC) target value of 4^{e5}. For MS2 scan triggering, monoisotopic precursor selection was enabled, charge state filtering was limited to 2 – 4, an intensity threshold of 5^{e3} was employed, and dynamic exclusion of previously selected masses was enabled for 60 seconds with a tolerance of 20 ppm. MS2 scans were acquired in the ion trap in Rapid mode after CID fragmentation with a maximum fill time of 20 ms, quadrupole isolation, an isolation window of 1 m/z, collision energy of 30%, activation Q of 0.25, injection for all available parallelizable time turned OFF, and an AGC target value of 1^{e4}. Fragment ions were selected for MS3 scans based on a precursor selection range of 400-1600 m/z, ion exclusion of 20 m/z low and 5 m/z high, and isobaric tag loss exclusion for TMT. The top 10 precursors were selected for MS3 scans that were acquired in the Orbitrap after HCD fragmentation (NCE 60%) with a maximum fill time of 90 ms, 50,000 resolution, 120-750 m/z scan range, ion injection for all parallelizable time turned OFF, and an AGC target value of 1^{e5}. The total allowable cycle time was set to 4 seconds. MS1 and MS3 scans were acquired in profile mode, and MS2 in centroid format.

Genomic library construction

A 96-well library construction protocol was performed for library construction from genomic DNA as previously described (Haile et al., 2017, 2018). Since DNA extracted from FFPE tissues is damaged by the fixation process and prolonged storage in non-ideal conditions, variable DNA quality across the collection was expected with some highly degraded samples. An S1 nuclease treatment step was added to further remove single-stranded DNA as previously described (Haile et al., 2018). DNA was normalized to 300 ng in a volume of 62 µL elution buffer (Qiagen) and transferred into a 96-well microTUBE Plate (Covaris, 520078) for shearing on an LE220 (Covaris) acoustic sonicator using the conditions: Duty Factor - 20%, Peak Incident Power – 450W, Cycle per burst – 200, Duration – 2X 60 seconds with an intervening spin. The protocol for FFPE-derived DNA generates a dominant DNA peak in the 300-400 bp size range. Highly degraded DNAs can dominate the final amplified library. To improve library quality

of FFPE-derived DNA library, solid phase reversible immobilization (SPRI) bead-based size selection was performed before library construction to remove smaller fragments potentially from degraded DNAs. The NEBNext® FFPE End Repair Kit (NEB) was then used, followed by bead purification using a 0.8:1 (bead:sample) ratio to remove small FFPE-derived DNA fragments. Repaired DNA fragments were A-tailed and adaptor-ligated to paired-end, partial Illumina sequencing adapters using the NEB Paired-End Sample Prep Premix Kit – A Tail (NEB) and the NEB Paired-End Sample Prep Premix Kit – Ligation (NEB), respectively, then purified twice with PCRClean DX beads (0.9:1 ratio). Full-length, adaptor-ligated products were achieved by performing 8 cycles of PCR with primers, in which we introduced fault-tolerant hexamer "barcodes" to allow library multiplexing. Indexed PCR products were double purified with 0.9:1 ratio of library:beads. The concentrations of final library products were determined using size profiles obtained from a LabChip® GX using the DNA High Sensitivity Reagent Kit and quantified using the Quant-iT™ dsDNA Assay Kit with high sensitivity on the Qubit 4 Fluorometer.

WES

Eight different genomic libraries (total of >500 ng) were pooled prior to whole-exome capture using the xGen® Exome Research Panel v1.0 (Integrated DNA Technologies). The pooled libraries were hybridized to the capture probes at 65°C for a minimum of 4 hours. Following hybridization, Dynabeads™ M-270 Streptavidin (Thermo Scientific) was used for exome capture. Post-capture enrichment using 6 PCR cycles and primers that maintained the library-specific indices was performed. The pooled libraries were sequenced with paired-end 125 base reads in a single lane of an Illumina HiSeq2500 flowcell.

2.4.3. Data analysis

RNA quantification and sample exclusion

Raw RNA-seq data was aligned to the human reference genome hg19 using STAR in two-pass mode (Dobin et al., 2012), and duplicate reads were identified using Picard's MarkDuplicates. Gene counts were obtained using featureCounts (part of Subread) (Liao et al., 2013) using transcript annotations obtained from Ensembl (v87).

Transcripts per million (TPM) values were calculated from the gene counts using the formula: $\frac{(\text{Count}/\text{Effective length}) \times 1{,}000{,}000}{\text{Sum}(\text{Count}/\text{Effective length})}$.

As most of the samples were FFPE specimens, which typically yield degraded RNA, we excluded samples of inferior RNA-seq data quality based on strong deviation in quality measures from other FFPE samples within the same cohort. The decision to remove a sample was made based on a combination of factors including a low percentage of properly mapped reads, a much higher percentage of reads that were too short or mitochondrial, and a much higher percentage of duplicate reads. In addition, unsupervised clustering of the least variably expressed mRNAs (the 25% lowest ranking mRNAs based on coefficient of variation; n = 4,820) was used to identify outlier samples with strongly deviating mRNA expression profiles.

Protein quantification and preprocessing

Data from the Orbitrap Fusion were processed using Proteome Discoverer (Thermo Fisher) as previously described (Hughes et al., 2016). Briefly, Sequest HT was used to search for MS2 spectral matches against a combination of UniProt Human and *Escherichia coli* proteomes and a list of common contaminants. Percolator was used to determine peptide spectral match (PSM) error rates. A q-value cut-off of 0.05 was used to control for false discoveries. Reporter ions were quantified from MS3 scans where the output quantification values represented the signal-to-noise of the TMT value relative to the Orbitrap preamplifier.

Quantification outputs from Proteome Discoverer were exported and analyzed in R. PSM data were filtered to remove contaminant and decoy proteins and those that were mapped to more than one protein. The abundance of uniquely identified peptides were computed from the quantification values of the PSMs mapped to the peptides by taking the median of all mapped PSMs. Peptide abundances were then treated with variance-stabilization normalization using the vsn R package (Huber et al., 2002, 2019) and collapsed into normalized protein abundance by taking their median values. The normalized protein abundance (log2-scale) was used in differential protein abundance analysis.

For clustering and visualization, ComBat from the sva R package (Leek et al., 2019) was used on the normalized protein abundance values to adjust for batch covariates associated with different TMT batches.

cNMF

For initial cNMF analyses of the Discovery and Validation cohorts, I included normal human pancreatic islet samples and human PNEN cell lines as normal counterparts and to represent PNENs with known phenotypes and proliferative potential (Hofving et al., 2018), respectively. Six different normal (including one LCM) islet samples and BON-1 and QGP-1 cell line samples were included with the analysis of the Discovery cohort PNENs. For the analysis of the Validation cohort PNENs, four different normal islet samples and two biological replicate samples of NT-3 cell line were included. The final PNEN subgroups were identified among tumour specimens only.

cNMF was performed using the NMF R package (Gaujoux and Seoighe, 2010, 2020) using either the top 25% ranking genes (mRNAs or proteins) based on coefficient of variation or DEGs derived from the differential analysis between the four subgroups among the Discovery cohort (see the *Differential analysis* subsection below for details). cNMF analysis was done using either log2-transformed TPM values or normalized, batch-adjusted protein abundance values for mRNAs or proteins, respectively. mRNAs with expression level below 1 TPM in at least half of the sample cohort were excluded from the analysis. To survey the optimal rank and therefore the number of subgroups, 50 iterations of NMF were performed assuming a possible rank at 2~7, and an optimal rank was selected based on high cophenetic and silhouette coefficients. The rank survey was performed on all PNEN specimens where information was available to maximize sample variation: n = 36 for RNA-seq data from the Discovery cohort specimens, n = 40 for proteomic profiles (including 35 of the Discovery cohort specimens), and n = 48 for RNA-seq data from the Validation cohort specimens. To obtain the final subgroup assignment for each sample at the optimal rank, 200 iterations of NMF were performed followed by hierarchical cluster analysis of the resultant consensus matrix. Hierarchical cluster analysis was done using the *hclust* function from the stats R package (R Core Team, 2020) with distance computed from 1 – consensus matrix. Where applicable, an initial seed of 123456 was set for reproducibility in computation.

Differential analysis

Differential gene expression and protein abundance analyses were done using the limma R package (Ritchie et al., 2015; Smyth et al., 2020). For transcriptome data, RNAs expressed below 1 counts per million (CPM) in 10% of the samples were considered noise and removed. The read counts of the resultant 25,373 RNAs were transformed to log2-CPM using *voom* from the edgeR R package (Chen et al., 2020; Robinson et al., 2010). For proteome data, the normalized protein abundance was used, with the batch covariates associated with TMT-10 batches included in the design matrix to account for variations between different TMT-10 batches. DEGs or DAPs were identified between the PDX1-high, Stromal/Mesenchymal and Alpha cell-like subgroups. The Proliferative subgroup was analyzed independently and compared to the rest of the tumour samples to account for its higher intra-subgroup heterogeneity. Using a significance threshold of absolute log2-fold change (log2FC) > 2 and false discovery rate-adjusted p-value (p.FDR) < 0.05 for mRNAs, and absolute log2FC > 1 and p.FDR < 0.05 for proteins, 1,637 DEGs and 354 DAPs were identified.

Gene and protein ID conversions

Different software and algorithms may require different gene/protein identifiers. I used biomaRt (Durinck and Huber, 2020; Durinck et al., 2005, 2009) and org.Hs.eg.db (Carlson, 2019) for conversions of identifiers. In instances where an analysis referenced both mRNAs and proteins, the official gene symbols approved by HGNC were used, and the mRNAs and proteins without official gene symbols were excluded.

Enrichment analysis

GSA was performed using *Camera* (Wu and Smyth, 2012) from the limma R package. The Hallmark and cellular components gene ontology gene sets were obtained from the Molecular Signatures Database (Liberzon et al., 2015) (downloaded June 25th, 2019) and used as the reference gene sets.

Signaling pathway impact analysis (Tarca et al., 2008) was used to identify the list of KEGG pathways over-represented by the subgroup-specific DEGs using the iLINCS web-based platform (http://ilincs.org). Only pathways with adjusted p-value (SPIA pajd) less than 0.05 were considered, and the status of each enriched pathway was only considered if the topology p-value (Top pval) was less than 0.05.

ESTIMATE analysis was performed using the estimate R package (Yoshihara et al., 2013). Log2-TPM values were used as the input, and the analysis was run using default parameters.

TFEA was performed using the ChEA3 (Keenan et al., 2019) web portal (https://amp.pharm.mssm.edu/chea3/) using default parameters and the subgroup-specific DEGs.

PCA

PCA was performed using log2-transformed TPM values from protein-coding genes using the stats R package (R Core Team, 2020).

GSVA

GSVA was performed using the GSVA R package (Guinney and Castelo, 2019; Hänzelmann et al., 2013) using log2-TPM values from protein-coding genes. To measure the transcriptomic similarity of each sample to a panel of pancreatic cell types, cell type-specific gene sets were constructed from a previous report comparing single-cell RNA-seq data from different pancreatic cell types (Muraro et al., 2016). The genes found to be over-expressed (defined by a log2-fold change > 2 and an adjusted p-value < 0.05) in a cell type relative to others constituted the cell type-specific genes for that cell type. To estimate the transcriptional activity of YAP1/WWTR1, a panel of 22 YAP1/WWTR1 target genes from a previous report (Wang et al., 2018) was used as the reference, and GSVA was used to transform the gene expression profile of each sample into a YAP1/WWTR1 target enrichment score.

CIBERSORT

The CIBERSORT source code in R was requested from https://cibersort.stanford.edu/download.php (downloaded February 18th, 2019). To run CIBERSORT, TPM values from RNA-seq and the LM6 signature genes were used (Newman et al., 2015). CIBERSORT was run at the absolute mode without quantile normalization, using *sig.score* as the absolute method.

Cellular regulator activity inference analysis

Activities of cellular regulators were inferred using the viper R package (Alvarez, 2019; Alvarez et al., 2016) and a previously constructed neuroendocrine neoplasm-specific regulatory network (Alvarez et al., 2018). Subgroup-specific gene expression signatures were constructed from the moderated t-statistics from limma (described under the *Differential analysis* section), and the *msVIPER* function was used to infer the relative activities of cellular regulators between subgroups. The *ledge* function was used to perform leading edge analysis. A significance cut-off was set at an adjusted p-value of 0.005, at which the number of false positive roughly equals to one.

Variant calling and prioritization

To increase the detection while reducing the number of false positive variants, SNVs and Indels were identified from both WES and RNA-seq reads from the 35 Discovery cohort specimens with paired transcriptome and proteome data. WES and RNA-seq reads were aligned to hg19 with BWA-MEM (Li and Durbin, 2009) (parameters -M). Read duplicates were marked using sambamba (Tarasov et al., 2015). After alignment, RNA-seq reads that were aligned to exon junctions were repositioned in the genome as large-gapped alignments using JAGuaR (Butterfield et al., 2014). Four variant callers were used on the WES reads: Platypus (Rimmer et al., 2014), LoFreq (Wilm et al., 2012), Pisces (Dunn et al., 2019) and Mutect2 (Benjamin et al., 2019); all callers were run using default parameters including the respective quality filters. SNVs and Indels were identified in the RNA using SAMtools mpileup (Li et al., 2009) (parameters -C50 -ABuf) and filtered to remove variants with mapping quality score less than 20.

SnpEff (Cingolani et al., 2012) was used to annotate and predict the functional impacts of the identified variants using GRCh37 annotation (ensemble v69). Consensus variants called by two or more variant callers were then identified from the WES and RNA-seq variants. The identified variants were additionally annotated with minor allele frequencies from gnomAD v2 (Karczewski et al., 2020), COSMIC mutation identifiers and functional prediction scores from COSMIC Coding Mutation Data (Tate et al., 2018) (downloaded March 12th, 2020) and COSMIC Cancer Gene Census (Sondka et al., 2018) (downloaded October 18th, 2019).

Formalin fixation is known to cause sequencing artifacts (Do and Dobrovic, 2015; Haile et al., 2018) and can potentially lead to false discovery of sequence variants. Considering that we used FFPE tumour specimens, and to compensate for the absence of matched normal control samples to help subtract germline variants from somatic variants called from individual tumour samples, we introduced several exclusion criteria to filter out variants that were unlikely to be pathogenic. For this study, we assumed that a disease-causing variant would 1) affect known cancer-related genes, 2) be rare among populations, 3) be present in substantial fraction of the bulk tumour, and 4) be predicted to impact the function of the protein product. Specifically, we filtered out variants considered as small nucleotide polymorphisms or with minor allele frequencies greater than 0.1% in gnomAD (Karczewski et al., 2020) or variant allele frequencies less than 0.33 and focused on the variants affecting the 723 genes in the COSMIC Cancer Gene Census. Considering that PNENs generally have low mutation rates (Scarpa et al., 2017) and recurrent hotspot mutations are rare, we filtered out identical mutations (that cause identical nucleotide changes at exact same genomic locations) found in more than 10% of specimens in our cohort, which were likely due to technical artifacts. Variants in which the predicted functional impacts were benign according to COSMIC Coding Mutation Data (a FATHMM prediction of “Neutral”) were also filtered out. In addition, we filtered out variants with non-deleterious impacts (according to SnpEff) that affect the 500 most frequently mutated genes in public exomes (Shyr et al., 2014). Lastly, eight in-frame insertions or deletions affecting the two polymorphic trinucleotide repeat sites of the androgen receptor *(AR*) gene (Ferlin et al., 2005) were identified and excluded from further analysis. The result of incorporating these exclusion criteria and cancer focus was a list of more confident variants with presumptive oncogenic contributions. All 355 post-filtering variants were visually validated in IGV.

IHC analysis

IHC staining and scoring of markers were performed using the previously constructed TMA (Riazy et al., 2015; Tessier-Cloutier et al., 2017). Briefly, for each case, an epithelial rich area of an FFPE tissue specimen was cored twice with a 0.6 mm needle and inserted into a recipient block generating a duplicate 0.6 mm core TMA. For staining, 4 µm sections were mounted onto slides and used for IHC staining. IHC staining of CD31 and CD34 was performed using the Dako Omnis (Agilent Technologies, Inc.) and DAXX and ATRX using the Discovery XT (Ventana Medical

Systems, Inc.) automated staining platforms following manufactuers' recommendations. For CD31, slides were incubated with the JC70A clone (Agilent Technologies, Inc.) without dilution for 15 minutes at room temperature, then washed and incubated with mouse linker (Agilent Technologies, Inc.) for 10 minutes followed by polymer (Agilent Technologies, Inc.) for 15 minutes. For CD34, slides were incubated with the QBEnd/10 clone (Agilent Technologies, Inc.) without dilution for 25 minutes at room temperature, then washed and incubated with polymer for 25 minutes. For DAXX and ATRX, slides were incubated with rabbit polyclonal antibodies (Sigma-Aldrich) at a dilution of 1:50 (DAXX) or 1:100 (ATRX) for 60 minutes at room temperature, then washed and incubated with Universal Secondary antibody (Ventana Medical Systems, Inc.) for 32 minutes at room temperature.

CD31 and CD34 were quantified according to methods developed by Weidner (1995). DAXX and ATRX were quantified by H-Score which represents the product of percent (0-100) of epithelial cells staining positive and a subjective assessment of staining intensity (0-3) which yields a range of 0-300.

2.4.4. Data deposition and access

The sequencing datasets generated during this study are available at the European Genome-phenome Archive (EGA; EGAS00001005024). The mass spectrometry proteomics data have been deposited to the ProteomeXchange Consortium via the PRIDE (Perez-Riverol et al., 2019) partner repository with the dataset identifier PXD024175. Derivative datasets directly referred to in this study are provided as supplemental tables. No new software or algorithms were used during the study. Public datasets and software downloaded and used during the study are listed in the Key Resources Table.

2.4.5. Key Resources Table

REAGENT or RESOURCE	SOURCE	IDENTIFIER
Antibodies		
CD31, clone JC70A	Agilent Technologies, Inc.	Cat# GA610
CD34, clone QBEnd/10	Agilent Technologies, Inc.	Cat# GA632

REAGENT or RESOURCE	SOURCE	IDENTIFIER
DAXX, polyclonal	Sigma-Aldrich	Cat# HPA008736
ATRX, polyclonal	Sigma-Aldrich	Cat# HPA001906
Biological Samples		
FFPE PNEN tumour blocks	Pathology archive at Vancouver General Hospital	N/A
Cadaveric islet extractions	IsletCore, Alberta Diabetes Institute	https://www.ualberta.ca/alberta-diabetes/core-services/isletcore.html
Chemicals, Peptides, and Recombinant Proteins		
USER™ Enzyme	New England Biolabs	Cat# M5508
Phusion™ High-Fidelity DNA Polymerase	Thermo Scientific	Cat# F-530XL
Trypsin/LysC	Promega	Cat# V5071
Critical Commercial Assays		
Agencourt® FFPE FormaPure Kit	Beckman Coulter	Cat# A33343
EvoPure RNA Tissue Isolation kit	Aline Biosciences	SKU R-907T
NEBNext® rRNA Depletion Kit	New England Biolabs	Cat# E6310X
RNA MagClean DX beads	Aline Biosciences	SKU C-1005
Maxima H Minus First Strand cDNA Synthesis Kit	Thermo Scientific	Cat# K1652
PCRClean Dx beads	Aline Biosciences	SKU C-1003
NEBNext® Ultra™ Directional RNA Second Strand Synthesis Module	New England Biolabs	Cat# E7550
DNA High Sensitivity Reagent Kit	PerkinElmer	Part# CLS760672
Quant-iT™ dsDNA Assay Kit, high sensitivity	Thermo Scientific	Cat# Q33120
TMT10plex labeling kit	Pierce	Cat# 90406
Sera-Mag Speed beads, carboxylate modified	GE Life Sciences	Cat# 45152105050350
NEBNext® FFPE End Repair Kit GSC	New England Biolabs	Cat# E6615B-GSC
NEB Paired-End Sample Prep Premix Kit – A Tail	New England Biolabs	Cat# E6876B-GSC
NEB Paired-End Sample Prep Premix Kit – Ligation	New England Biolabs	Cat# E6877B-GSC
xGen® Exome Research Panel v1.0	Integrated DNA Technologies	Cat# 1056115
Dynabeads™ M-270 Streptavidin	Thermo Scientific	Cat# 65305
Deposited Data		
Molecular Signature Database gene sets	Liberzon et al., 2015	https://www.gsea-msigdb.org/gsea/index.jsp

REAGENT or RESOURCE	SOURCE	IDENTIFIER
Neuroendocrine neoplasm regulon	Alvarez et al., 2018	https://figshare.com/articles/GEP-NET_transcriptional_regulatory_network/6007232
gnomAD Exome variants v2	Karczewski et al., 2020	https://gnomad.broadinstitute.org
COSMIC Coding Mutation Data	Tate et al., 2018	https://cancer.sanger.ac.uk/cosmic
COSMIC Cancer Gene Census	Sondka et al., 2018	https://cancer.sanger.ac.uk/census
RNA-sequencing BAM files	This paper	EGAS00001005024 at https://www.ebi.ac.uk/ega/
Whole-exome sequencing BAM files	This paper	EGAS00001005024 at https://www.ebi.ac.uk/ega/
Mass spectrometry proteomics files	This paper	PXD024175 at https://www.ebi.ac.uk/pride/
Experimental Models: Cell Lines		
BON-1	Drs. Courtney Townsend and Mark Hellmich, University of Texas Medical Branch	N/A
NT-3	Benten et al., 2018	N/A
QGP-1	Japanese Cancer Resource Bank	Cat# JCRB0183
Software and Algorithms		
STAR v2.6.0c	Dobin et al., 2012	https://github.com/alexdobin/STAR
Subread v1.6.0	Liao et al., 2013	http://subread.sourceforge.net/
Picard v2.22.0	Broad Institute	https://broadinstitute.github.io/picard/

REAGENT or RESOURCE	SOURCE	IDENTIFIER
Proteome Discoverer v2.1.0.62	Thermo Fisher	https://www.thermofisher.com/ca/en/home/industrial/mass-spectrometry/liquid-chromatography-mass-spectrometry-lc-ms/lc-ms-software/multi-omics-data-analysis/proteome-discoverer-software.html
vsn v3.50.0	Huber et al., 2002, 2019	https://bioconductor.org/packages/release/bioc/html/vsn.html
sva v3.30.1	Leek et al., 2019	https://www.bioconductor.org/packages/release/bioc/html/sva.html
NMF v0.23.0	Gaujoux and Seoighe, 2010, 2020	https://cran.r-project.org/web/packages/NMF/index.html
R v3.6.3	R Core Team, 2020	https://www.r-project.org/
limma v3.42.2	Ritchie et al., 2015; Smyth et al., 2020	https://bioconductor.org/packages/release/bioc/html/limma.html
edgeR v3.28.1	Robinson et al., 2010; Chen et al., 2020	https://bioconductor.org/packages/release/bioc/html/edgeR.html
estimate v1.0.13	Yoshihara et al., 2013	https://bioinformatics.mdanderson.org/estimate/rpackage.html
GSVA v1.34.0	Hänzelmann et al., 2013; Guinney and Castelo, 2019	https://bioconductor.org/packages/release/bioc/html/GSVA.html
CIBERSORT v1.04		
viper v1.20.0	Alvarez et al., 2016; Alvarez, 2019	https://bioconductor.org/packages/release/bioc/html/viper.html

REAGENT or RESOURCE	SOURCE	IDENTIFIER
BWA-MEM v0.7.6a	Li and Durbin, 2009	http://bio-bwa.sourceforge.net/
sambamba v0.5.5	Tarasov et al., 2015	https://github.com/biod/sambamba
JAGuaR v1.7.5	Butterfield et al., 2014	https://www.bcgsc.ca/resources/software/jaguar
Platypus v0.8.1	Rimmer et al., 2014	https://www.well.ox.ac.uk/research/research-groups/lunter-group/lunter-group/platypus-a-haplotype-based-variant-caller-for-next-generation-sequence-data
LoFreq v2.1.3.1	Wilm et al., 2012	https://csb5.github.io/lofreq/
Pisces v5.2.10.49	Dunn et al., 2019	https://github.com/Illumina/Pisces
Mutect2 v4.0.10.0	Benjamin et al., 2019	https://gatk.broadinstitute.org/hc/en-us/articles/360036510132-Mutect2
SAMtools v0.1.19	Li et al., 2009	http://www.htslib.org/
SnpEff v4.1	Cingolani et al., 2012	https://pcingola.github.io/SnpEff/
survival v3.2-3	Therneau, 2020	https://cran.r-project.org/web/packages/survival/index.html
survminer v0.4.8	Kassambara et al., 2020	https://cran.r-project.org/web/packages/survminer/index.html
tidyverse v1.3.0	Wickham, 2019	https://cloud.r-project.org/web/packages/tidyverse/index.html
reshape2 v1.4.4	Wickham, 2020	https://cran.r-project.org/web/packages/reshape2/index.html

REAGENT or RESOURCE	SOURCE	IDENTIFIER
openxlsx v4.1.5	Schauberger and Walker, 2020	https://cran.r-project.org/web/packages/openxlsx/index.html
biomaRt v2.42.1	Durinck et al., 2005, 2009; Durink and Huber, 2020	https://bioconductor.org/packages/release/bioc/html/biomaRt.html
org.Hs.eg.db v3.10.0	Carlson, 2019	https://bioconductor.org/packages/release/data/annotation/html/org.Hs.eg.db.html

Chapter 3.

Whole-genome and transcriptome analyses of metastatic PNENs

This chapter is modified and expanded from a published report describing PNENs enrolled in the Personalized OncoGenomics (POG) program at BC Cancer (ClincalTrials.gov; NCT02155621). The individuals who contributed to this study and their specific contributions are outlined in the Acknowledgements. The first portion of the results in this chapter is adapted from the published report describing the whole-genome and whole-transcriptome characterization of five metastatic PNENs (Wong et al., 2018). A few updates to the published manuscript are implemented in this chapter to reflect advances in the field over the past 3 years. My specific roles in the published report included data curation and analysis, results interpretation, and preparation of the submitted manuscript. Later in this chapter, I expand the initial cohort of five metastatic PNENs to include four more recent PNEN cases enrolled in the POG program and compare them to the four proteotranscriptomic subgroups identified and characterized in Chapter 2.

3.1. Introduction

PNENs are rare pancreatic neoplasms commonly diagnosed at an advanced stage at which point distant metastases are evident or eventually ensue (Hallet et al., 2015; Niederle et al., 2010). The molecular landscape of PNETs was initially described in a seminal paper by Jiao et al. (2011), in which WES identified recurrent somatic mutations in *MEN1*, *DAXX*/*ATRX*, and PI3K/AKT/mTOR pathway genes, most commonly *PTEN*, *TSC2*, and *PIK3CA*. Mutations in these and other genes may occur in hereditary cancer syndromes, including MEN1 syndrome, TSC, NF1 disorder, and VHL syndrome, that increase susceptibility to PNEN development (Jensen et al., 2008). The recurrent somatic mutations in *MEN1*, *DAXX/ATRX* and the PI3K/AKT/mTOR pathway genes were subsequently confirmed in a WGS study by Scarpa et al. (2017), who categorized somatically altered genes into those involved in chromatin remodeling, DNA damage repair, PI3K/AKT/mTOR pathway activation, and telomere maintenance. Additionally, 17% of the patients were found to harbour germline mutations not only in

previously described *MEN1* and *VHL* but also in tumor suppressor genes *CHEK2*, *MUTYH*, and *CDKN1B* (Scarpa et al., 2017). PNECs, in contrast, often harbour alterations in *TP53*, *RB1* and *KRAS* (Yachida et al., 2012). Aside from sequence variants, recurrent chromosomal anomalies have been described and associated with mutational frequencies of *MEN1* and *DAXX/ATRX* in PNETs (Hong et al., 2020; Lawrence et al., 2018). Wide variations in CNV events have been observed between PNENs, and recurrent LOH in chromosomes 1, 2, 3, 6, 8, 10, 11, 16, 22 were observed in subsets of PNENs (Hong et al., 2020; Lawrence et al., 2018; Yao et al., 2019).

Most molecular profiling studies of PNENs to date, however, have focused on primary tumours. Despite the important implications of distant metastases in PNENs for prognosis and treatment (Kunz, 2015), the molecular characteristics of PNEN metastases are rarely reported and the existing studies only examined genomic aberrations or metastasis-associated genes (Raj et al., 2018; Scott et al., 2020). The whole-genome and whole-transcriptome landscapes of PNEN metastases have not been reported. In this chapter, I describe the whole-genome and whole-transcriptome profiles for five patients with metastatic PNENs who underwent sequencing analyses as part of an ongoing clinical trial – the POG program at BC Cancer (ClincalTrials.gov; NCT02155621). Together with Drs. Hui-Li Wong (former medical oncology resident at BC Cancer) and Yaoqing Shen (analyst in the POG program), we identified notable genomic and transcriptomic characteristics of each of the five POG PNENs, which are presented here along with their clinical histories. In addition to previously described recurrently altered genes and chromosomes with recurrent LOH, two cases were found with molecular aberrations novel to PNENs. One case harboured focal amplification of *MYCN* (MYCN proto-oncogene, bHLH transcription factor) concomitant with loss of *APC* (APC regulator of WNT signaling pathway) and *TP53* with wildtype *MEN1* and *DAXX*, while another case harboured a germline fusion gene involving the nth like DNA glycosylate (*NTHL1*) gene. Lastly, I correlate these 5 cases plus 4 more recent PNEN cases from the POG program with the proteotranscriptomic subgroups described in Chapter 2.

3.2. Results

3.2.1. Clinical Presentation and Treatment Outcomes

Clinical vignettes are described for each case below and summarized in Table 3.1 and Figure 3.1. Radiological responses are defined per RECIST (Response Evaluation Criteria in Solid Tumors) version 1.1 (Eisenhauer et al., 2009).

Table 3.1. Baseline characteristics of the five patients with metastatic PNENs.

	Case 1	Case 2	Case 3	Case 4	Case 5
Age (Year)	69	52	46	36	67
Gender	Male	Female	Female	Male	Male
Metastatic sites	Liver	Liver	Liver	Liver, lymph nodes	Liver
Functional status	Functional	Nonfunctional	Nonfunctional	Nonfunctional	Nonfunctional
Histological differentiation	Well	Well	Well	Well	Poor; LC
Ki67 index[a]	< 2%	10-15%	15%	20%	> 70%
Baseline chromogranin A[b]	110 µg/L	92 U/L	5200 µg/L	250 µg/L	4920 µg/L
^{111}In-labeled octreotide scan avidity	Yes	Yes	Not done	Yes	Not done

[a]Ki67 index was categorized according to the criteria of the WHO 2010 classification system, but the grades remain the same under the WHO 2017/2019 systems. [b]Normal range of baseline chromogranin A is < 94µg/L or < 40 U/L. LC: large-cell type.

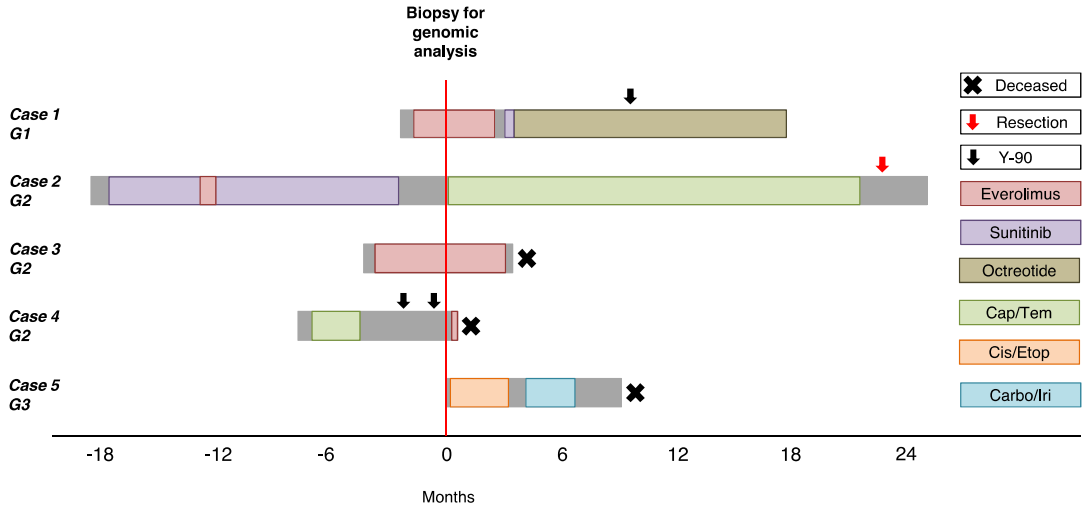

Figure 3.1. Clinical evolution and treatment of the five patients with metastatic PNENs.

Cap/Tem: capecitabine with temozolomide; Cis/Etop: cisplatin with etoposide; Carbo/Iri: carboplatin with irinotecan; Y-90: yttrium90 radioembolization.

Case 1

A 69 year-old man presented with hypercalcemia and was found on computed tomography (CT) imaging to have a pancreatic mass and liver lesions. Pathology examination of the pancreatic mass obtained under endoscopic ultrasound guidance confirmed a PNET-G1. Serum chromogranin A (CgA) was slightly elevated at 110 µg/L (normal range of < 94 µg/L), and the liver and pancreatic lesions were intensely avid on octreotide scan. He commenced treatment with everolimus and underwent core biopsy of a liver metastasis for molecular analyses after 7 weeks of therapy. He had radiologically stable disease, but treatment was discontinued after 4 months because of grade 2 pneumonitis. Second-line systemic therapy with sunitinib was initiated but also discontinued early because of congestive heart failure. He eventually received ^{90}yttrium (Y-90) radioembolization therapy to his liver metastases and had a partial radiological response. His hypercalcemia, which was initially refractory to bisphosphonates and required several hospital admissions for management, normalized and remained stable 5 months after Y-90 therapy. At the study cut-off time (20 months after diagnosis), he remained well on maintenance monthly long-acting octreotide.

Case 2

A 52 year-old female presented with several years of abdominal pain, which eventually led to abdominal ultrasound and CT that showed a pancreatic tail mass and multiple liver lesions. Pathological examination of the liver core biopsy showed a PNET-G2. CgA was slightly elevated at 92 U/L (normal range of < 40 U/L) and imaging with ^{111}Indium-labeled octreotide showed uptake in her known disease sites. She commenced treatment with sunitinib but required several dose reductions for grade 2 hand-foot syndrome. She had a brief trial of everolimus but switched back to sunitinib after 3 weeks because of mucositis and pneumonitis. She had a symptomatic response and radiologically stable disease that was sustained for 15 months before developing progressive liver metastases, which did not accumulate ^{18}F-DOPA. She underwent a liver biopsy for genomic analysis prior to starting second-line systemic therapy with Cap/Tem. She achieved a partial radiographic response and, after 20 months of chemotherapy, proceeded to resection of her pancreatic primary along with radiofrequency ablation of the liver metastases. Pathologic review of the resected pancreatic primary again confirmed a PNET-G2. Three of nine lymph nodes were involved. At the study cut-off time (43 months after diagnosis), she remained well with disease stability off chemotherapy.

Case 3

A 46 year-old female with a prior history of TSC, resected renal angiomyolipoma, and childhood epilepsy was noted to have liver masses on routine surveillance imaging. Due to progressive fatigue, leg edema, and abdominal discomfort related to massive hepatomegaly, a liver biopsy 9 months after initial presentation was done. IHC of the liver biopsy did not support metastatic angiomyolipoma but confirmed expression of paired box 8 (PAX8) in favour of a pancreatic origin (Sangoi et al., 2011), suggesting a PNET-G2 pathology. CgA was markedly elevated at 5200 µg/L. She commenced treatment with everolimus and underwent biopsy of a liver metastasis for molecular analyses after 16 weeks of therapy. She had an early symptomatic and marker response, where CgA decreased to 3780 µg/L from a peak of 8200 µg/L. Interestingly, her TSC-associated skin lesions (presumed facial angiofibromas), also improved on everolimus treatment. Radiological response could not be accurately assessed, as pretreatment imaging was performed 8 months prior to the start of the treatment. However, her treatment course was complicated by recurrent anemia, diarrhea, and

renal impairment. After nearly 7 months of everolimus treatment, she developed clinical progression and died 8 months after initial pathologic diagnosis. Referral to the Hereditary Cancer Program for clinical genetic testing had been discussed but was not pursued due to absence of significant family history, so this was not pursued.

Case 4

A 36 year-old man presented with a short history of right shoulder and chest pain was found on CT to have multiple liver lesions and a pancreatic tail mass. Pathological examination of the core liver biopsy suggested a PNET, both morphologically and on immunoprofile, with positive staining for synaptophysin and cytokeratin AE1/AE3. Although the tumor had < 2 mitotic rate (mitoses/10 HPF), the Ki67 index was up to 20% in some areas; hence this was classified as a PNET-G2. Octreotide scan identified additional disease within the retroperitoneal and supraclavicular lymph nodes, and CgA was modestly elevated at 250 µg/L. He commenced first-line systemic therapy with Cap/Tem, but the disease progressed after three cycles. He then received Y-90 radioembolization to the liver but progressed within 3 months. Prior to starting second-line systemic therapy with everolimus, he underwent liver biopsy for genomic analysis. He was also referred for PRRT, but his clinical status declined rapidly. He died 10 days after commencing everolimus, 8.4 months after initial diagnosis.

Case 5

A 67 year-old male presented with a short history of diarrhea and constitutional symptoms and was found on CT to have multiple liver masses and a pancreatic tail solid lesion that appeared suspicious for pancreatic ductal adenocarcinoma. He consented for genomic analysis at the time of his diagnostic liver biopsy, which showed a NEC-LC with positive staining for synaptophysin, chromogranin, and cytokeratin 19. The Ki67 index was > 70%. CgA was markedly elevated at 4920 µg/L. He received treatment with cisplatin and etoposide for four cycles before developing disease progression. He then received four cycles of carboplatin and irinotecan but also had upfront disease progression. He had ongoing clinical deterioration and died 9 months after initial diagnosis.

3.2.2. Genomic analyses

WGS of liver metastases and blood from the five patients was performed to identify somatic genomic alterations including chromosomal aberrations (Figure 3.2) and sequence variants (Figure 3.3A; Supplemental Table 9). Germline alterations in 98 cancer susceptibility genes were evaluated, as approved by the research ethics board. RNA-seq was performed to identify alterations in gene expression and molecular pathways. For comparison of gene expression levels, the expression levels of select genes were converted into percentile ranks against a collection of tumor transcriptomes from The Cancer Genome Atlas (TCGA) project (https://portal.gdc.cancer.gov/) (Figure 3.3A) or to a compendium of 16 normal tissue transcriptomes from the Illumina Human BodyMap 2.0 project (https://www.ebi.ac.uk/gxa/experiments/E-MTAB-513/Results) (Supplemental Table 11). The latter comparison provided a coarse list of putative disease-specific genes for each case and was used to identify prospective upstream regulators (Figure 3.3B) and pathways affected (Supplemental Table 10). Hereafter, description of individual gene expression level specifically refers to comparison with the TCGA tumor compendium unless otherwise noted.

The approved therapeutic drugs for the treatment of PNETs in Canada include everolimus, sunitinib, SSAs, and chemotherapy with Cap/Tem, whereas platinum-based chemotherapy is typically reserved for PNECs. I retrieved the list of proteins targeted by the aforementioned approved therapeutic agents from Santos et al. (2017) and examined the status of their gene and gene expression in addition to genes previously implicated in PNENs (Figure 3.3A).

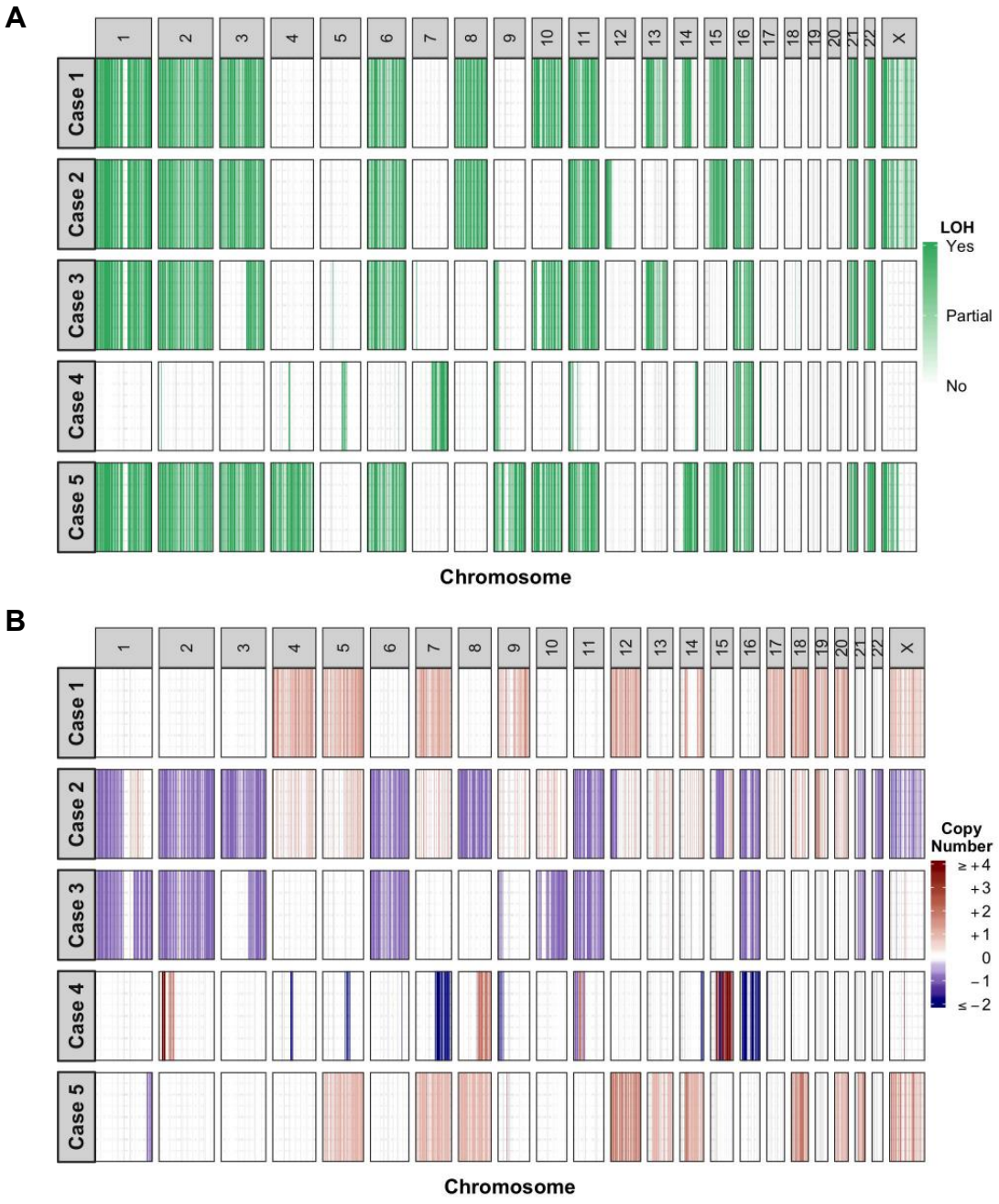

Figure 3.2. Genome-wide copy-number architectures across the five cases.
(A) Chromosomal regions with loss of heterozygosity events are depicted in green. The zygosity states at these regions are not discriminated. (B) Copy number deviations from the estimated ploidy in protein-coding regions are depicted in red (copy gain) or blue (copy loss). The magnitude of copy gains is capped at +4. Aside from Case 4 in which the estimated ploidy was 4, the other cases were estimated to be diploid.

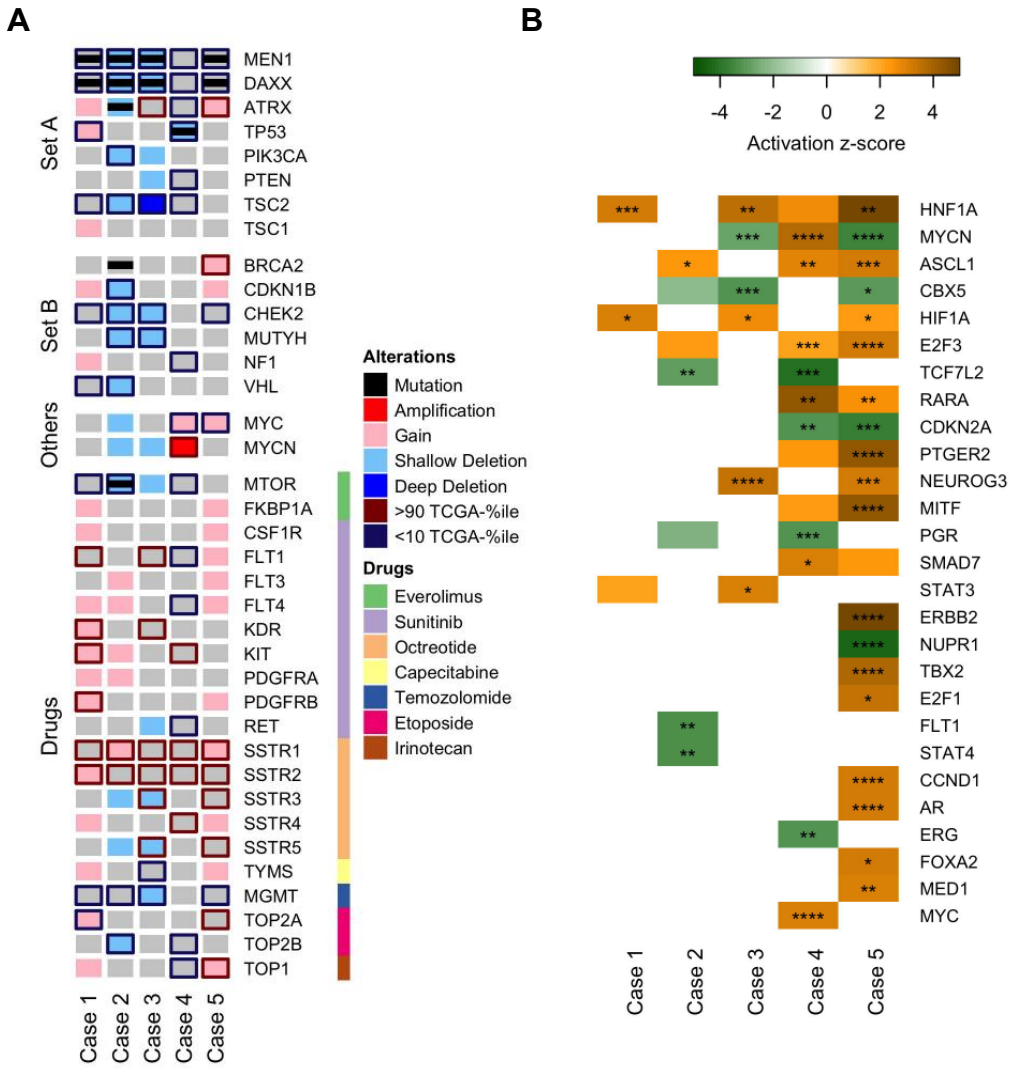

Figure 3.3. Key molecular alterations and predicted upstream regulators across the five cases.

(A) An OncoPrint depicting alterations in genes that have either been implicated in PNETs or are targets of conventional therapeutic agents used to treat PNETs. All alterations described here are somatic, aside from Case 3, which had germline one copy loss of *TSC2*. "Set A" contains genes recurrently mutated in sporadic PNETs (Jiao et al., 2011). "Set B" contains genes in which germline mutations were recently reported in PNET patients (Scarpa et al., 2017). "Others" contains genes of interest in this study. "Drugs" contains genes with protein products that are the molecular targets (color-coded) of the indicated therapeutic agents used to treat PNETs. Nonsynonymous mutations (black bar), copy-number aberrations (red/blue shade), and up- or down-regulated expressions (red/blue edge) of these genes are shown. All genes have gray background by default to facilitate visualization. Shallow and deep deletions refer to one- or two-copy losses, respectively. Up-regulated genes are defined as those expressed at levels > 90% of TCGA tumor compendium, and down-regulated genes as those expressed at levels < 10% of TCGA tumor compendium. (B) Using the Upstream Regulator Analysis tool from Ingenuity Pathway Analysis software, the activation states of prospective upstream regulators in each sample were predicted based on differentially regulated genes. Only upstream regulators with activation score of > 3 or < -3 were selected. Color and intensity indicate the predicted activation state and effect size, respectively. The overlap p-value of each prediction is also indicated. *: $p < 0.05$; **: $p < 0.01$; ***: $p < 0.001$; ****: $p < 0.0001$.

3.2.3. Shared molecular alterations

Several genomic alterations were shared within the cohort. LOH events were frequently observed in Cases 1, 2, 3, and 5, with chromosomes 1, 2, 3, 6, 11, 16, 21, and 22 largely affected. These include regions encoding for *MEN1* (11q13.1), *DAXX* (6p21.32), and *TSC2* (16p13.3) (Figure 3.2A). Frequent copy number gains were observed in Cases 1 and 5, whereas copy number losses, most of which were likely due to LOH, were more frequent in Cases 2 and 3. Gene amplification events, defined as the ploidy-corrected copy number gain being greater than the ploidy, were absent in Cases 1, 2, and 3 but were observed in Case 5 and more frequently in Case 4 (Figure 3.2B). Consistent with the reported low mutation burden in PNETs (Jiao et al., 2011), less than 50 nonsynonymous mutations in protein-coding genes were identified in three of the five cases (median = 39; range = 21~170; Supplemental Table 9). Somatic mutations in *MEN1* and *DAXX* were found in Cases 1, 2, 3, and 5. These comprised nonsense, frameshift, and splice site mutations as well as in-frame deletion or missense mutations predicted to be deleterious (Table 3.2). In conjunction with LOH events or copy number losses, these mutations resulted in biallelic loss of *MEN1* and *DAXX* in the four cases. The expression levels of both *MEN1* and *DAXX* were low across all five cases, whereas *TSC2* expression was low in Cases 1, 2, 3, and 4. Tumor suppressor gene *CHEK2* also had low expression in Cases 1, 2, 3, and 5 (Figure 3.3A).

The gene expression levels of the drug molecular targets varied across all five cases, but similar trends were observed in a few of the genes. All five cases had high expression of SSTR1/2, consistent with their neuroendocrine diagnosis and ^{111}In-labeled octreotide scan avidity. The gene encoding the core kinase of the mTOR pathway *MTOR* was expressed at low levels in cases 1, 2 and 4. Low expression of O-6-Methylguanine-DNA methyltransferase (*MGMT*), which indicates sensitivity to temozolomide in glioblastoma (Hegi et al., 2005), was observed in Cases 1, 2, 3 and 5 (Figure 3.3A).

High expression of neuroendocrine markers and pancreas-specific transcription factors confirmed the pancreatic origin of the metastases. In all five cases, high expression levels of the chromogranin A (*CHGA*) and the synaptophysin (*SYP*) genes were observed, and neuronal differentiation 1 (*NEUROD1*) and *PDX1* were expressed at high levels in four cases. In addition, each case exhibited increased expression of at

least one of the *INS*, glucagon (*GCG*), gastrin (*GAST*), *SST* or vasoactive intestinal peptide (*VIP*) genes, favouring a pancreatic endocrine cell origin (Supplemental Table 11).

Table 3.2. Sequence variants in genes previously implicated in PNENs.

Case	Gene	Chr	HGVS DNA	HGVS protein	Predicted effect	Genotype
Case 1	*MEN1*	1	c.1579C>T	p.R527*	Stop gain	Hom
Case 1	*DAXX*	6	c.1178delA	p.K393fs	Frameshift variant	Hom
Case 2	*MEN1*	11	c.245_259delA CCTGTCTA TCATCG	p.D82_I86del	Disruptive inframe deletion	
Case 2	*DAXX*	6	c.329_330delCT	p.S110fs	Frameshift variant	
Case 2	*ATRX*	X	c.1558G>T	p.V520F	Missense variant	Hom
Case 2	*MTOR*	1	c.6625C>G	p.L2209V	Missense variant	Hom
Case 2	*BRCA2*	13	c.3504G>T	p.M1168I	Missense variant	Het
Case 3	*MEN1*	11	c.798+1G>A		Splice donor variant + intron variant	Hom
Case 3	*DAXX*	6	c.850C>T	p.Pr284S	Missense variant	Hom
Case 4	*TP53*	17	c.818G>T	p.R273L	Missense variant	Hom
Case 5	*MEN1*	11	c.981_1006delCCAC TGTCGCAACCGC AATGTGCGGG	p.Y327fs	Frameshift variant	
Case 5	*DAXX*	6	c.801_824delTAACA GGCGCATTGAG CGGCTCAT	p.N268_I275del	Disruptive inframe deletion	

Chr: chromosome; Hom: homozygous; Het: heterozygous.

3.2.4. Case-specific molecular alterations of interest

Case 1

In addition to many of the shared molecular alterations, low expression levels of tumour suppressor genes *TP53* and *VHL* were observed in this case. Several receptor tyrosine kinases (RTKs) and targets of sunitinib including fms related receptor tyrosine kinase 1 (*FLT1*) and kinase insert domain receptor (*KDR*) that encode for vascular endothelial growth factor receptors 1 and 2, respectively, were expressed at high levels (Figure 3.3A). Moreover, several MAPK pathway genes including *MAP3K10*, *MAP3K12* and *MAP2K2* were highly expressed suggesting up-regulated activity of MAPK pathways

(Supplementary Table 11). The use of sunitinib as second-line therapy was supported by the high expression of several RTKs; however, treatment response was not assessable due to early discontinuation of therapy.

Case 2

Contrary to the other four cases where somatic mutations were only identified in *MEN1* and *DAXX*, additional somatic mutations in genes associated with PNENs were identified in Case 2. These include a heterozygous missense mutation in *BRCA2* and a homozygous missense mutation in *ATRX*, both of unknown significance (Table 3.2). Prediction of the damaging effects of the missense mutations using Polyphen-2 (Adzhubei et al., 2010) indicated that the *BRCA2* variant was likely benign (score = 0.000) while the *ATRX* variant p.V520F was likely damaging (score = 0.999). In addition, missense mutations resulting in amino acid substitutions adjacent to the identified *ATRX* variant (p.S519 and p.P521) had been reported and predicted to be pathogenic (http://cancer.sanger.ac.uk; COSM5878330, COSM5878331, COSM4993581, COSM4993582; Forbes et al., 2015). Collectively, these predictions suggested that the identified mutation in *ATRX* likely affected its protein functions. Mutations in *DAXX* and *ATRX* are typically mutually exclusive, and this case was the first reported instance of a PNEN with concurrent homozygous *DAXX* and *ATRX* loss. Examination of allelic frequencies of the *DAXX* and *ATRX* variants suggested that both were present in all tumour cells (Supplemental Table 9). The identified missense mutation in *MTOR*, which resulted p.L2209V, affected its kinase domain and had been previously characterised as an activating mutation that results in constitutively active mTOR signalling (Yamaguchi et al., 2015).

Case 3

In keeping with the clinical history of TSC in this case, one allele of *TSC2* was found altered in the germline. Combined with a somatic loss of the remaining copy, the biallelic loss of *TSC2* accompanied its very low expression (0 percentile) in the tumour. The germline inactivation of *TSC2* was due to structural variants in chromosome 16, which included a large deletion spanning *TSC2* and the base-excision repair gene *NTHL1*, and an inversion that caused a fusion between *NTHL1* and the TNF receptor associated factor 7 (*TRAF7*) gene (Figure 3.4), predicted to be non-functional. Comparison to previously described COSMIC mutational signatures (Alexandrov et al.,

2013) showed an unusually high contribution of Signature 30, characterized by a high proportion of C>T transitions (Figure 3.5). Similar mutational profiles were reported in *NTHL1*-mutated tumours related to polyposis syndromes (Rivera et al., 2015; Weren et al., 2015) and in *NTHL1* knock-out human colon organoids (Drost et al., 2017), but have not previously been described in PNENs. The TMB of this case was the highest among the PNETs in this cohort, with 7.47 somatic mutations per megabase *vs.* 1.17-2.17, with C>T transition accounting for 45% (77/170) of the coding variants.

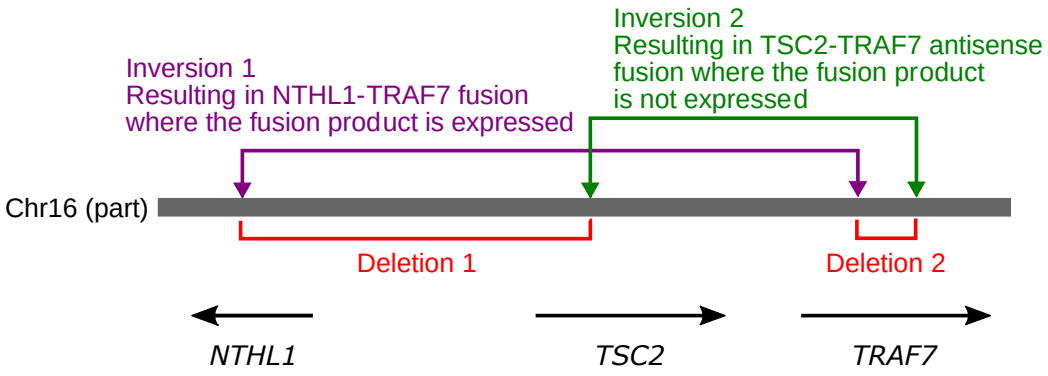

Breakpoints of Deletion 1: 16:2093920, 16:2126780
Breakpoints of Deletion 2: 16:2212355, 16:2214166

Breakpoints of Inversion 1: 16:2093920, 16:2212355
Breakpoints of Inversion 2: 16:2126780, 16:2214166

Figure 3.4. Illustration of the two structural variants involving *TSC2* identified in Case 3.
Only part of the chromosome 16 that is affected is shown. The lengths of the arrows shown are not to scale.

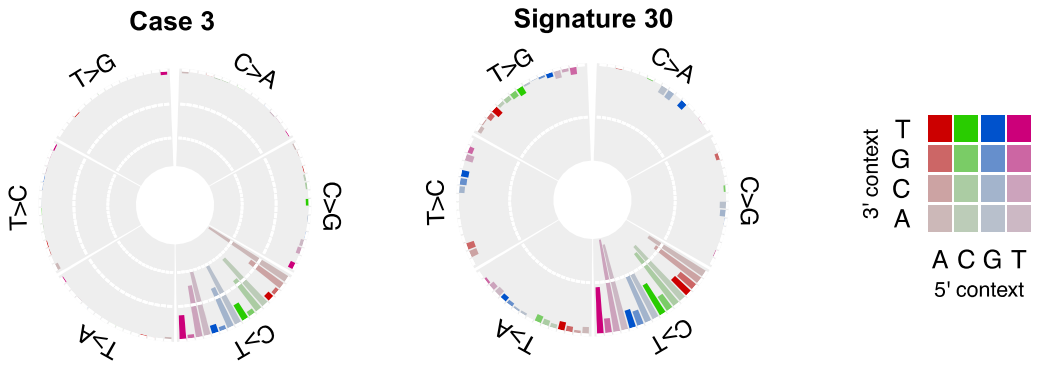

Figure 3.5. Comparison of mutation signature of case 3 to signature 30.
The base substitutions at all possible trinucleotide contexts are colour-coded as depicted on the right.

Case 4

Unlike the other cases in this cohort, CNV events were infrequent in Case 4 (Figure 3.2). Moreover, no mutations were observed in *MEN1*, *DAXX* and *ATRX*. Instead, the key genomic aberrations included a homozygous pathogenic *TP53* mutation (COSM10779), copy number loss and a gene fusion event involving the *APC*, and amplification of *MYCN*. Consistent with the observed genomic aberrations, both *TP53* and *APC* were expressed at low levels. *MYCN* had a 38-copy gain and was overexpressed (99 percentile; 48 fold-change relative to the BodyMap compendium expression) (Figure 3.3A). Gene expression analyses predicted activation of *MYCN* (Figure 3.3B) and identified enrichment of genes encoding ribosomal proteins (Supplemental Table 10), which are known to be regulated by *MYCN* (Boon et al., 2001). Together, these results suggested *MYCN*-driven transcriptomic changes in this case.

In view of the unusual genomic findings, pathology review was undertaken and confirmed the diagnosis of PNET-G2 in the liver biopsy samples taken at diagnosis and after progression on chemotherapy and Y-90. In particular, there was no evidence of transformation to a PNEC, or evidence of glandular or acinar components that may suggest an alternate diagnosis.

Case 5

Although Case 5 was histologically diagnosed as a PNEC, its genomic landscape was similar to that of PNETs as in Cases 1, 2 and 3. These include similar regions with LOH events (Figure 3.2A) and copy number aberrations (Figure 3.2B), as well as biallelic loss of *MEN1* and *DAXX* (Figure 3.3A). Gene expression analyses suggested a number of transcription factors and receptors were uniquely affected in this case. The cell cycle regulator cyclin D1 was predicted to be activated (Figure 3.3B), consistent with enrichment of genes involved in cell cycle pathway (Supplemental Table 10).

3.2.5. Proteotranscriptomic subgroup of metastatic PNENs

Having examined the whole-genome and whole-transcriptome landscapes of the PNEN metastases along with their clinical progression, I was interested in whether these metastases could be categorized into one of the four proteotranscriptomic subgroups described in Chapter 2. To determine the possible subgroup for each of the metastases,

I compared the transcriptomes of the PNENs from the POG program to the sequenced specimens from Chapter 2. Additional metastatic PNEN cases had been enrolled in the POG program since the publication of the report on the five cases described earlier in this chapter, so I expanded my POG PNEN cohort to include these four additional metastatic PNEN cases (available up to March 2021) for the comparisons. One of these newer cases was a PNET-G3 without alterations in *MEN1* and *DAXX/ATRX* and was described previously in a case report (Williamson et al., 2019). The inclusion of these more recent POG PNENs resulted in a total of 9 metastatic PNENs from which WGS and WTS data were available (Table 3.3).

Table 3.3. All metastatic PNENs enrolled in the POG program up to March 2021.

Study ID[a]	Differentiation status	Ki67 index	Biopsy site	Tumour content[b]
PN2 (Case 3)	Well	3-20	Liver	0.77
PN4 (Case 5)	Poor; LC	> 55	Liver	0.86
PN6 (Case 2)	Well	3-20	Liver	0.79
PN12 (Case 1)	Well	< 3	Liver	0.79
PN14 (Case 4)	Well	3-20	Liver	0.79
PN18	Mixed; Well	> 55	Pancreas	0.64
PN23	Well	21-55	Liver	0.95
PN25	Well	3-20	Liver	0.36
PN27	Well	3-20	Liver	0.30

[a]Case numbers were previously assigned arbitrarily based on Ki67 index-based grades for publication purposes. Instead of the case numbers, a Study ID was assigned to each NEN enrolled in POG in sequential order. The case numbers referred to in the 2018 publication are included in the brackets. [b]Tumour contents were estimated based on WGS data.

I first examined the global transcriptomic correlation of the 9 POG PNENs to the sequenced samples from Chapter 2. The samples from Chapter 2 used in this comparison included the 84 primary PNEN specimens with subgroup assignments, with the 10 normal islet and the 4 cell line samples serving as biological references. As expected, and similar to the unsupervised cluster analysis results showing normal islet and some of the cell line samples clustering away from PNEN specimens (Figures 2.1A and 2.5), the POG PNENs generally had lower transcriptomic correlation to normal islet

and cell line samples. On the contrary, greater correlations to primary PNENs of the Alpha cell-like subgroup were observed (p = 0.00042; Figure 3.6).

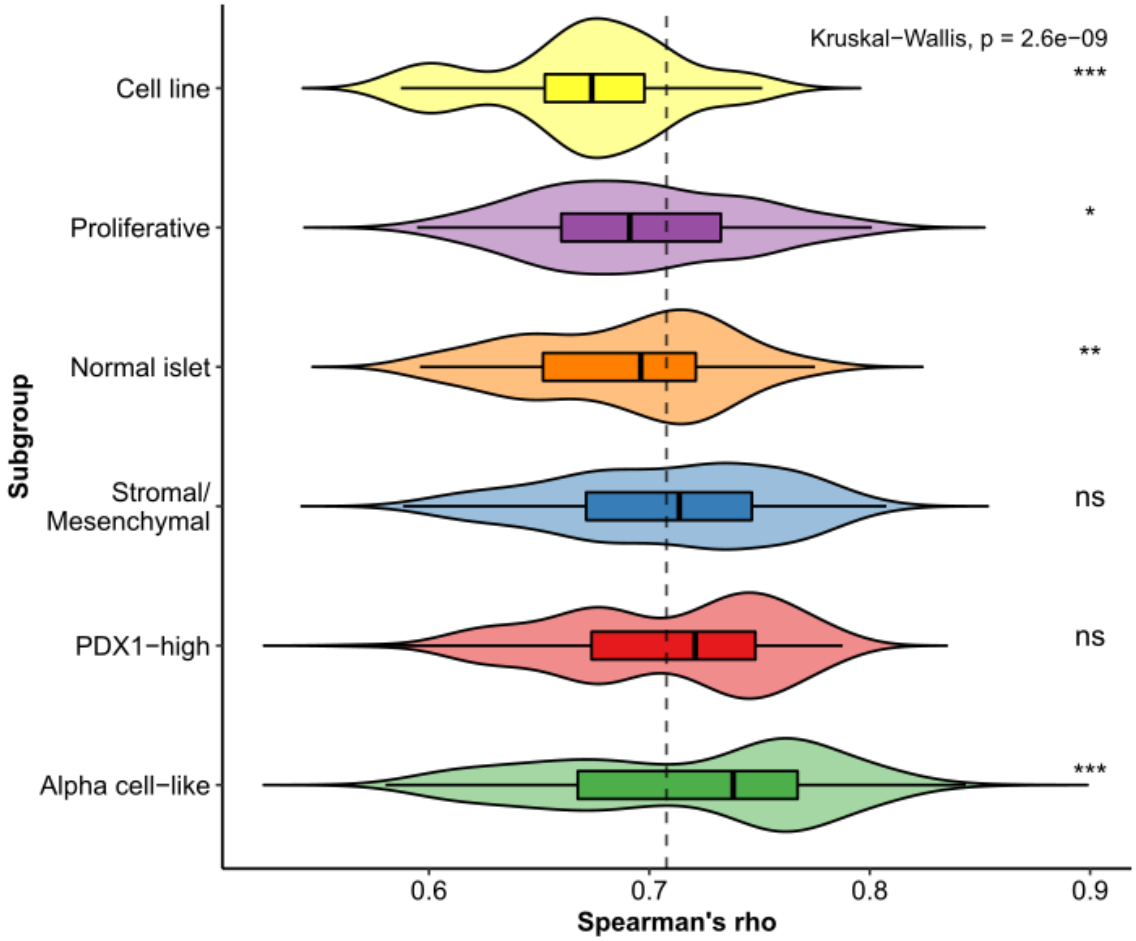

Figure 3.6 Correlation of POG PNENs to each of the proteotranscriptomic PNEN subgroups.

Transcriptomic correlation between the 9 analyzed POG PNENs and a total of 98 sequenced samples from Chapter 2 was evaluated using Spearman's rank correlation. The distributions of the correlations between the POG PNENs to PDX1-high subgroup (n = 20), Stromal/Mesenchymal subgroup (n = 25), Alpha cell-like subgroup (n = 28), Proliferative subgroup (n = 11), normal islet (n = 10) or cell line (n = 4) samples are shown. The dashed line denotes the median correlation for all comparisons. The statistical significance was computed using Kruskal-Wallis test to determine differences between the subgroups or using Wilcoxon test to compare between each subgroup/specimen type to the rest.

I next explored whether each of the POG PNENs could fit in any of the four proteotranscriptomic subgroups that I had identified. This entailed examining the 9 POG PNENs on an individual basis and evaluating their transcriptomic similarities to each of the subgroups. For this, I adapted the GSVA-based approach that I had employed in Chapter 2 for use with subgroup-specific genes. Here, subgroup-specific genes were

defined as DEGs exclusively up-regulated in a subgroup, and together represents the reference gene signature for the subgroup. Using GSVA against the reference gene signature from each of the four proteotranscriptomic subgroups enumerated an enrichment score that reflects the subgroup enrichment scores for a target GEP. Using the average score as the baseline for each subgroup enrichment, a higher transcriptomic similarity to the Alpha cell-like subgroup specimens was observed in 4 of the POG PNENs: PN2, PN4, PN6 and PN12 (Figure 3.7), corresponding to Cases 3, 5, 2 and 1 that had been previously characterized (Table 3.3). In addition, the mRNA expression of *ARX* was relatively high in these four cases, in keeping with their higher similarities to the Alpha cell-like subgroup specimens (Figure 3.8). These cases were also the only 4 POG PNENs among the cohort with concurrent mutations in *MEN1* and *DAXX* (Table 3.4), consistent with my previous observation of the Alpha cell-like subgroup enriched in specimens with mutant *MEN1* and *DAXX* (Figure 2.15).

Various combinations of subgroup signatures were observed in the POG PNENs. PN14 (previously referred to as Case 4), which had only been characterized with *MYCN* amplification and alterations in *APC* and *TP53*, had a GEP with a mixed signature of PDX1-high and Proliferative subgroups. PN18, a MiNEN, also displayed a mixed signature, but was of Stromal/Mesenchymal and Proliferative subgroups (Figure 3.7). Consistent with PN18 exhibiting the most pronounced Stromal/Mesenchymal subgroup signature among all POG PNENs, the mRNA expression of both *YAP1* and *WWTR1* were considerably higher in this PNEN. The only other POG PNEN also demonstrating a substantial Stromal/Mesenchymal subgroup signature, PN2, had a high *WWTR1* expression (Figure 3.8). Further, four POG PNENs displayed a pronounced Proliferative subgroup signature, either alone or in combination with another subgroup signature. These four cases: PN4, PN14, PN18 and PN23 exhibited various histology (including a PNEC-LC, a PNET-G2, a PNET-G3 and a MiNEN) but shared a common characteristic of high Ki67 indices (Table 3.3). This was consistent with my previous finding of the Proliferative subgroup associated with PNENs of higher Ki67 indices irrespective of histological differentiation (Table 2.2).

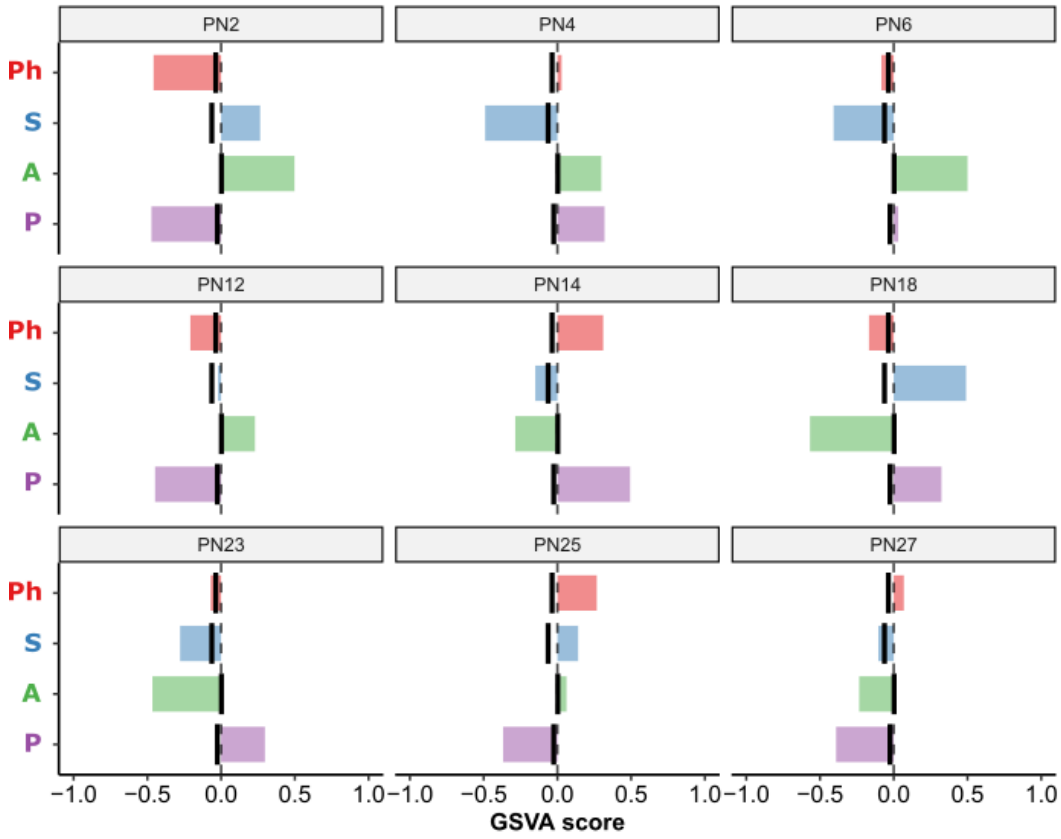

Figure 3.7. Transcriptomic similarity of each POG PNEN to the four proteotranscriptomic subgroups.

GSVA was used to evaluate the transcriptomic similarity of each POG PNEN to the four proteotranscriptomic subgroups using subgroup gene signatures. Each panel shows the enrichment results for a POG PNEN. The average enrichment score from all POG PNENs is indicated as a bold vertical line for each subgroup. Ph: PDX1-high; S: Stromal/Mesenchymal; A: Alpha cell-like; P: Proliferative.

Table 3.4. Mutational status of *MEN1*, *DAXX* and *ATRX* in the 9 POG PNENs.

Study ID	*MEN1*	*DAXX*	*ATRX*
PN2 (Case 3)	g.64575023C>T (splice variant)	p.P284S	-
PN4 (Case 5)	p.Tyr327fs	p.N268_I275del	-
PN6 (Case 2)	p.D82_I86del	p.S110fs	p.V520F
PN12 (Case 1)	p.R527*	p.K393fs	-
PN14 (Case 4)	-	-	-
PN18	p.D501fs	-	-
PN23	p.R420*	-	-
PN25	-	-	p.K1274*
PN27	-	-	-

Only identified somatic mutations in *MEN1*, *DAXX* and *ATRX* are shown. Cells indicated with a "-" denotes absence of mutations.

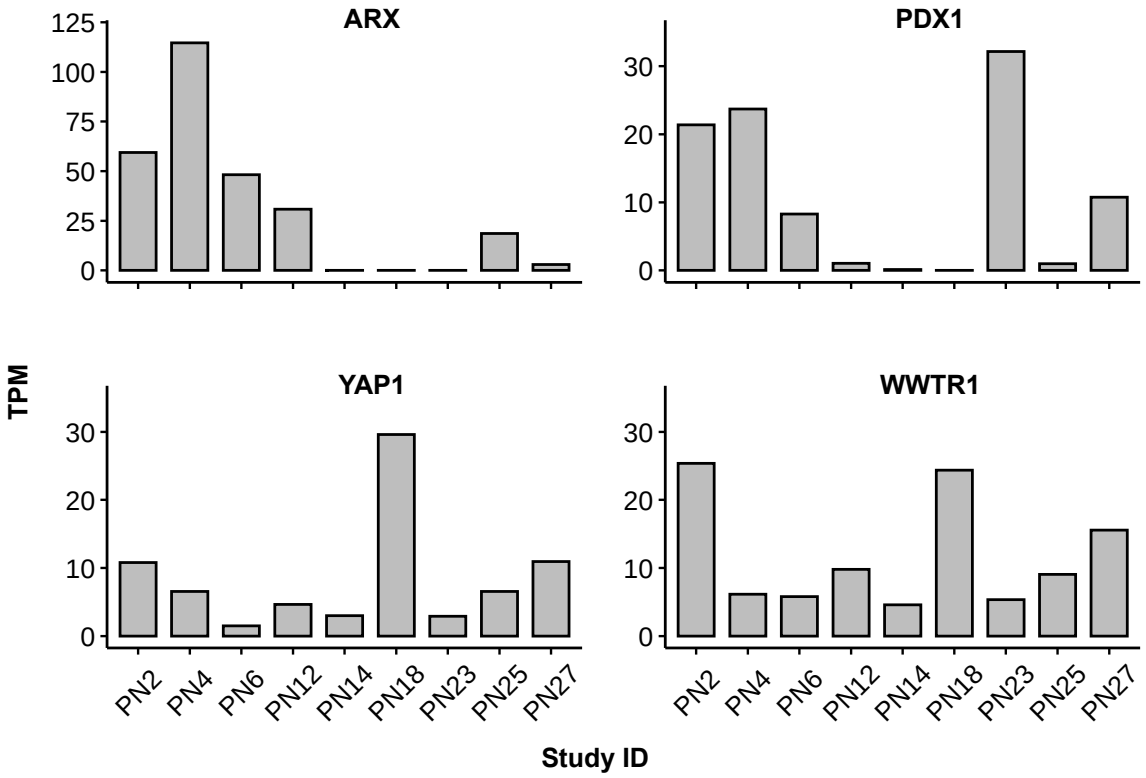

Figure 3.8. mRNA expression levels of *ARX*, *PDX1*, *YAP1* and *WWTR1* in the 9 POG PNENs.

The TPM value for each indicated gene from each of the 9 POG PNENs is shown. Aside from *ARX*, the y-axis is kept consistent across the genes.

3.3. Discussion

In the case series study in the earlier part of this chapter, the whole-genome and whole-transcriptome landscapes of liver metastases from five patients with metastatic PNENs were described. Previous studies on primary PNETs have identified recurrent somatic mutations in *MEN1*, *DAXX/ATRX* and mTOR pathway genes and germline mutations in genes involved in chromatin remodelling, DNA damage repair, mTOR signalling and telomere maintenance (Jiao et al., 2011; Scarpa et al., 2017). Consistent with these reports, we identified biallelic loss of *MEN1* and *DAXX* (due to deleterious mutations, copy number losses and/or LOH events) in three of the four PNETs characterized. Low mRNA expression of *MEN1*, *DAXX* and *TSC2* were observed in all five PNENs. These likely contributed to tumour development and progression. In addition, one or more cases exhibited low expression levels of tumour suppressor genes *CHEK2, CDKN1B*, *NF1* and *VHL*, in which germline mutations had been reported in PNETs (Scarpa et al., 2017). While we only identified one germline deletion affecting

TSC2 within our cohort (Case 3), the reduced expression of these genes likely also augmented disease development and progression.

Previous studies suggest that loss of nuclear DAXX/ATRX staining is associated with metastases, poor prognostic features and shorter survival (Marinoni et al., 2014; Singhi et al., 2017). While we are unable to make any definite conclusions about the prognostic impact of DAXX/ATRX in our cohort, it is clear that treatment and survival outcomes in PNENs were highly variable, and other drivers likely contributed to disease progression and treatment response.

For example, a liver metastasis (Case 4) with typical pathologic features of a PNET-G2 was characterized with unique genomic characteristics previously unreported in PNENs. The *MYCN* amplification and expression signature observed in this case had not previously been described in human PNENs, although ectopic targeted expression of *MYCN* in pancreatic islets or neural progenitor cells was shown sufficient to induce PNEN development in zebrafish and mice, respectively (Fielitz et al., 2016; Yang et al., 2004). *MYCN* promotes cell proliferation, and *MYCN* amplification was correlated with poor prognosis, particularly in neuroblastomas (Huang and Weiss, 2013). Similarly, the clinical picture for this case was characterized by treatment resistance and poor survival that may have been compounded by *TP53* loss, which may have negated the pro-apoptotic signals elicited by *MYCN* and augmented its oncogenic potential (Chen et al., 2010; Gamble et al., 2012). Of interest, a small interfering RNA targeting *MYC* (MYC proto-oncogene, bHLH transcription factor) was investigated as a potential therapeutic strategy in solid tumours including PNETs, where treatment responses observed in a phase I trial (Tolcher et al., 2015) have led to cohort expansion in this tumour type (ClinicalTrials.gov; NCT02110563) (Dicerna Pharmaceuticals Inc., 2015). The trial was unfortunately terminated as the pharmaceutical sponsor discontinued the program to focus on other candidates (Dicerna Pharmaceuticals Inc., 2016). However, given demonstrated anti-tumour activity of targeting *MYC* in PNENs, it would be important to explore any underlying molecular characteristics that may predict benefit to *MYC*-targeted therapy and regimens that target *MYCN*.

Conversely, another PNET within the cohort (Case 2) had relatively good treatment outcomes, with prolonged responses to sunitinib (15 months) and Cap/Tem (no progression after 20 months). We observed low expression of *MGMT* in the tumor,

which has previously been described and correlated with better responses to temozolomide in small PNET cohorts (Cros et al., 2016; Kulke et al., 2009).

Alterations and aberrant expression of PI3K/AKT/mTOR pathway genes have been frequently reported in PNETs (Jiao et al., 2011; Missiaglia et al., 2010), and the mTOR inhibitor everolimus is well-established as effective therapy in PNETs-G1/2 (Yao et al., 2011). However, no biomarkers that may predict for response to everolimus have yet been validated. Within our cohort, three patients received everolimus, and Case 3 had an early and sustained response to treatment, which would be supported by genomic evidence of biallelic *TSC2* inactivation. Decreased expression of *TSC2* and/or *PTEN* was observed in the other two patients (Cases 1 and 4); however, no conclusions can be made regarding the impact of these findings on response to everolimus treatment.

Previous study reported genomically distinct findings that differentiate pancreatic NETs from poorly differentiated NECs, with the latter frequently associated with *TP53* and *RB1* alterations and rarely with *DAXX* or *ATRX* loss (Yachida et al., 2012). Conversely, in a study comparing genomic characteristics of NECs from different primary sites, the majority PNECs did not harbour alterations in *TP53* or *RB1,* whereas 33% and 20% of the sequenced PNECs harboured genomic alterations (due to SNVs, SVs or CNVs) in *MEN1* and *DAXX*, respectively (Bergsland et al., 2016). The only PNEC in this study (Case 5) did not have *TP53* or *RB1* alterations but retained the pathognomonic mutations commonly observed in PNETs. Other genomic features in this case included a higher mutation burden and gene expression profile indicative of cell cycle activation that was not seen in the other cases (Figure 3.3B; Supplemental Table 10). The unusual observation of PNET-associated but not PNEC-associated genomic alterations in this PNEC-LC raises the hypothesis that it may have evolved from a PNET or that some PNECs may share genomic characteristics of PNETs. Either way, this suggested the patient would have been a candidate for therapy with targeted molecular therapy or temozolomide typically administered to PNETs rather than platinum therapy given for PNECs, which did not induce a response. This indicates an inadequacy of the conventional approach of treating PNETs and PNECs as distinct entities.

Of interest, the higher than expected TMB in a PNET-G2 (Case 3), coupled with an unusual mutational signature, drew our attention to the germline fusion event causing

NTHL1 loss. Germline mutations in *NTHL1* had been described in the context of polyposis syndromes (Rivera et al., 2015; Weren et al., 2015), similar to those associated with *MUTYH* loss, another base-excision repair gene (Al-Tassan et al., 2002; Shinmura et al., 2000). Analogous to Case 3, *MUTYH* loss was associated with a novel mutational signature in PNETs (Scarpa et al., 2017). While loss of the two base-excision repair genes resulted in different mutational patterns (C>T for *NTHL1* and C>A for *MUTYH*), the physiological similarities between the loss of these two genes highlight the potential utility of examining mutational signatures to determine mechanisms of tumorigenesis in PNETs. To our knowledge, this was the first reported PNET case associated with *NTHL1* loss and a somatic mutation pattern that resembles signature 30.

This was also the first study correlating response to systemic therapy with whole-genome and transcriptome analyses in PNEN patients and preceded many of the sequencing studies involving PNENs to date (Cejas et al., 2019; Chan et al., 2018; Hong et al., 2020; Lawrence et al., 2018; Raj et al., 2018). Notably, three of the PNENs in this study harboured LOH affecting chromosomes 1, 2, 3, 6, 11, 16, 21, and 22 (Figure 3.2A). Subsequent studies examining chromosomal aberrations in PNETs similarly identified recurrent LOH events in these chromosomes, concurrent with *MEN1* mutations. However, one study found the recurrent LOH events associated with lymphovascular invasion (Lawrence et al., 2018) while another observed association with a better overall survival probability (Yao et al., 2019). As we and others analogously found a subset of PNENs with recurrent LOH affecting chromosomes 1, 2, 3, 6, 11, 16, 21 and 22 coupled with *MEN1* mutations, the clinical outcomes between the affected PNET subsets varied and warrant further investigation using a bigger cohort of PNENs at various stages.

The clinical significance of the molecular changes identified among the PNENs sequenced in this study remains poorly understood, and to date, there are no known predictive biomarkers that are currently applicable in clinical practice. Aside from one case in which high expression of several RTKs and components of the MAPK pathway supported the use of sunitinib, genomic findings generally did not inform therapy decisions in real time. This was partly due to biopsy timing and relatively short disease course in three of the patients, as retrospective review suggested that the genomic results could potentially have informed treatment decisions. For the two patients who remained on follow-up at the completion of this study, high expression of *SSTR2* would

support the use of PRRT with radiolabeled somatostatin analogs (Hicks et al., 2017). Alternatively, four of the PNENs in this cohort had low expression of *MGMT* which may suggest their sensitivity to temozolomide-based regimens (Cros et al., 2016; Kulke et al., 2009). One of these cases (Case 2) indeed demonstrated exceptional response to Cap/Tem. The other three cases, however, were not treated with temozolomide, but the one case with normal *MGMT* expression (Case 4) did not respond to temozolomide.

Comparisons of the initial five and four additional POG PNENs to primary PNEN specimens from Chapter 2 showed stronger correlations with the Alpha cell-like subgroup. As mentioned in Chapter 2, the Alpha cell-like subgroup shared molecular characteristics of the A-D-M mutant and the Type A subtypes of PNETs with high *ARX* expression and/or transcriptomic similarity to pancreatic α-cells. These two subtypes were associated with a reduced recurrence-free or relapse-free survival rate (Cejas et al., 2019; Chan et al., 2018) and therefore a higher chance of refractory or metastatic disease. While I could not compare the recurrence-free or relapse-free survival rates between different PNEN subgroups in Chapter 2 due to limitations in available clinical data, the POG program generally enrolls metastatic, treatment-refractory cancer patients. Consequently, the POG PNENs may be inherently associated with a greater relapse rate explaining the higher correlation to the Alpha cell-like subgroup and in line with previous reports associating *ARX*-high PNETs with greater disease recurrence or relapse.

Four of the POG PNENs characterized with *MEN1* and *DAXX* alterations as well as high *ARX* expression demonstrated considerably higher transcriptomic similarity to the Alpha cell-like subgroup specimens. In all of these cases, recurrent LOH or loss could be observed in chromosomes 1, 2, 6, 10, 16 and 22 (Figure 3.2) as in the previously reported Group 1 subtype, T2 subtype and Subtype A (Boons et al., 2020; Lakis et al., 2021; Lawrence et al., 2018). Therefore, there is a possible relationship between concurrent *MEN1* and *DAXX* alterations, a pancreatic α-cell-like GEP including elevated expression of *ARX*, and recurrent LOH or loss of chromosomes 1, 2, 6, 10, 16 and 22. While further analysis combining specimens across studies for comparison is needed, the similar features shared by one subtype/subgroup across studies provides strong evidence that these studies have descended on the same subtype/subgroup of PNENs.

PNENs are associated with highly heterogeneous clinical outcomes and treatment sensitivities. The in-depth whole-genome and transcriptome analyses of the initial five cases demonstrated a number of shared and unique molecular aberrations that contribute to this observed heterogeneity. Transcriptomic comparisons with the primary PNENs suggested that the molecular characteristics observed in the four proteotranscriptomic subgroups were, at least partially, evident in PNEN metastases. And, the gene signatures from the proteotranscriptomic subgroups could be potentially employed to infer the molecular characteristics of a given PNEN. It is also worth mentioning that all 9 cases displayed an unique enrichment profile emphasizing the molecular heterogeneity of PNENs. Interestingly, a few of the POG PNENs adopted GEPs of hybrid subgroup gene signatures. This could point to a limitation in my subgrouping system due to the absence of metastasis specimens in the initial proteotranscriptomic subgroup identification process, or due to PNEN metastases embracing more composite GEPs. Further molecular analyses of metastatic PNENs with associated treatment and outcome information will be critical to improve our understanding of the prognostic and predictive implications of the various molecular features.

3.4. Methods

3.4.1. Sample collection and processing

Patients provided written informed consent for metastatic biopsies, sequencing, and publication of results as part of the POG program at BC Cancer (ClincalTrials.gov; NCT02155621). This study was approved by the UBC Clinical Research Ethics Board (H12-00137).

Following informed consent, patients underwent image-guided metastatic biopsies as part of the POG program at BC Cancer (ClincalTrials.gov; NCT02155621). As per protocol, biopsies could be undertaken at any time up to disease progression on first-line systemic therapy. Up to five biopsy cores were obtained using 18~22G biopsy needles and embedded in optimal cutting temperature compound. Tumour sections were reviewed by a pathologist to confirm the diagnosis, evaluate tumor content and cellularity, and select areas most suitable for DNA and RNA extraction. Peripheral

venous blood samples were obtained at the time of biopsy and leukocytes isolated for use as a germline reference.

3.4.2. Sequencing and Bioinformatics

DNA and RNA were extracted for genomic and transcriptomic library construction, which has been previously described in detail (Sheffield et al., 2015). Paired-end reads of 125 bp in length were generated on an Illumina HiSeq2500 sequencer and aligned to the human reference genome (GSCh37, available from http://www.bcgsc.ca/downloads/genomes/9606/hg19/1000genomes/bwa_ind/genome) by the BWA aligner (v0.5.7) (Li and Durbin, 2009). Somatic SNVs and Indels were processed using SAMtools (Li et al., 2009) and Strelka (v0.4.6.2) (Saunders et al., 2012). Regions of copy-number variations (CNV) were determined using CNASeq (v0.0.6) and LOH by APOLLOH (v0.1.1) (Ha et al., 2012). Tumour content and ploidy models were estimated from sequencing data through analysis of the CNV ratios and allelic frequencies of each chromosome. This was then compared to in-house theoretical models for different ploidy at various tumour contents. Tumour content and sequencing coverage as well as the estimated ploidy for each case are provided in Table 3.5. SVs were detected by de novo assembly of tumour reads using ABySS and Trans-ABySS (Robertson et al., 2010), followed by variant discovery using DELLY (Rausch et al., 2012). RNA-seq reads were processed and gene expression analyzed as previously described in (Sheffield et al., 2015).

Table 3.5. Tumour content and sequencing coverage for the five metastatic PNENs.

Case	WGS coverage – Tumour	WGS coverage – Normal	RNA-seq coverage (number of paired reads)	Tumour Content	Ploidy
Case 1	78X	41X	192M	79%	2
Case 2	94X	47X	246M	79%	2
Case 3	89X	42X	289M	77%	2
Case 4	87X	42X	187M	79%	4
Case 5	91X	43X	116M	86%	2

3.4.3. Gene expression analysis

In the absence of matched normal transcriptome data, the level of expression of each gene was determined as the number of reads per kilobase of transcript per million mapped reads (RPKM) and compared to a compendium of 16 normal transcriptomes from the Illumina BodyMap 2.0 project (https://www.ebi.ac.uk/gxa/experiments/E-MTAB-513/Results). Differential expression analysis between tumor and the normal compendium was performed as previously described (Sheffield et al., 2015). Up-regulated genes were defined as those with a fold change (FC) > 4 and a p.FDR < 0.05; down-regulated genes were defined as those with FC < −2 and a p-value < 0.1. Expression levels of select genes were converted into percentile ranks against a compendium of 5976 tumor transcriptomes across 25 cancer types from the TCGA project. KEGG signaling pathway gene set enrichment analysis was performed using the gage R package (Luo et al., 2009). Upstream regulator analysis was performed using Ingenuity Pathway Analysis to predict the activation/inhibition states of G-protein-coupled receptors, ligand-dependent nuclear receptors, transcription regulators, kinases, and phosphatases from the list of differentially expressed genes (Krämer et al., 2014). To increase prediction confidence, only candidates with activation scores > 3 or <−3 were selected. Molecular targets of drugs mentioned in this study were retrieved from Santos et al. (2017).

For comparisons with RNA-seq data from Chapter 2, TPM values from protein-coding genes were used. Correlation analyses were performed using Spearman's rho, and GSVA analyses were performed using log2-transformed TPM values. DEGs exclusively over-expressed in a subgroup (ie. subgroup signature genes) were used to construct the reference gene signature for the subgroup.

3.4.4. Sequencing result visualization

LOH events and CNAs were illustrated using the R package GenVisR (Skidmore et al., 2016). Heatmaps were generated using the R packages ComplexHeatmap (Gu et al., 2016) and gplots.

3.4.5. Data deposition and access

Sequencing data were deposited in the EGA as part of the study EGAS00001001159, accession IDs EGAD00001003048, EGAD00001003089, EGAD00001002591, EGAD00001003069 and EGAD00001002607. The variants reported were deposited in the ClinVar (http://www.ncbi.nlm.nih.gov/clinvar/) database with the following accession numbers: *MEN1* c.1579C>T (SCV000611142), c.245_259delACCTGTCTATCATCG (SCV000611144), c.798+1G>A (SCV000611149), c.981_1006delCCACTGTCGCAACCGCAATGTGCGGG (SCV000611152); *DAXX* c.1178delA (SCV000611143), c.329_330delCT (SCV000611145), c.850C>T (SCV000611150), c.801_824delTAACAGGCGCATTGAGCGGCTCAT (SCV000611153); *ATRX* c.1558G>T (SCV000611146); *MTOR* c.6625C>G (SCV000611147); *BRCA2* c.3504G>T (SCV000611148); *TP53* c.818G>T (SCV000611151).

Chapter 4.

Conclusions and future directions

PNENs are a group of rare pancreatic neoplasms with immense clinical, pathological and molecular heterogeneity. Increasing awareness of this disease has led to rising research interests in its etiology and pathology, yet the links between their wide-ranging clinicopathological presentations and diverse molecular characteristics remained fragmented. The drivers of PNEN development also remained elusive in some cases. In this thesis, I aimed to address these knowledge gaps by identifying potential pathogenic alterations in PNENs and elucidating connections between clinicopathological and molecular attributes of PNENs. Additionally, I investigated a potential molecular classification to help establish the basis for novel therapeutic approaches to better the management of this disease. In this concluding chapter, I highlight select key findings on PNENs throughout my doctoral study and describe their contributions to the field of PNEN research with emphases on their potential clinical utility. In addition, I present my insights on current limitations and potential future research directions that will help to improve the management of PNENs as well as NENs in general.

4.1. Novel alterations in PNENs

Novel dysregulated pathways or processes were found in the PDX1-high, Alpha cell-like and Stromal/Mesenchymal subgroups, including potential Ras pathway activation, metabolic dysregulation and YAP1/WWTR1 activation, respectively. Additionally, a metastatic PNEN carried *MYCN* alterations that likely contributed to its pathogenesis. The specific biological and therapeutic implications of these potential oncogenic drivers are described here.

4.1.1. Activation of HRAS and NRAS in PDX1-high PNENs

The RAS family of GTPases promotes oncogenic cellular functions through activation of signaling cascades including the mitogen-activated protein kinase (MAPK) pathway and the PI3K/AKT/mTOR pathway (Gimple and Wang, 2019). Three members of the family, *KRAS*, *NRAS* and *HRAS*, are proto-oncogenes frequently found with

activating mutations and promote tumour development in various cancer types (Akbani et al., 2015; Collisson et al., 2014; Muzny et al., 2012; Raphael et al., 2017a). From my analysis of primary PNENs, 11.4% (4 out of 35) of the specimens harboured genetic alterations potentially leading to RAS pathway activation. These included 3 PNETs with activating mutations in *KRAS*, *NRAS* or *HRAS* and another with a deleterious *NF1* mutation (Figure 2.15). Mutations in *KRAS* are rare in PNETs and, to my knowledge, there is no report of PNETs with mutant *HRAS* or *NRAS* except for a *NRAS* p.Q61R variant in the BON-1 NEN cell line (Vandamme et al., 2015) and a metastatic PNET with *BRAF* p.V600E variant that acquired an *NRAS* (p.Q61R) mutation after treatment with BRAF inhibitor vemurafenib (Raj et al., 2018). Aside from the *KRAS*-mutant case, all affected cases fell in the PDX1-high subgroup (Figure 2.15). Although only three of the 9 PDX1-high PNENs harboured RAS pathway-activating mutations, gene expression-based inference analysis identified higher activity of HRAS and NRAS in the PDX1-high subgroup suggesting a subgroup-wide dysregulation. This makes the potentially elevated RAS pathway activity a characteristic of the PDX1-high subgroup, which otherwise lacks obvious oncogenic drivers, and supplies a possible avenue for novel therapeutic intervention. Considering other groups had similarly reported PNET subtypes with high *PDX1* expression, and the PDX1-high subgroup expresses higher levels of *PDX1*, it would be interesting to investigate potential connections between *PDX1* and the RAS pathway in PNENs. The RAS pathway has been one of the most sought-after targets in anti-cancer therapeutics, and multiple inhibitors that have been approved for other indications or in clinical trials can be exploited to curb the activity of specific RAS protein variants, the MAPK pathway or the PI3K/AKT pathway (Moore et al., 2020). The identification of a subgroup of PNENs with elevated RAS pathway activity and high *PDX1* expression carries potential classification and therapeutic utility. A validated connection between *PDX1* expression, RAS pathway activation and possible susceptibility to RAS pathway inhibition could be explored to facilitate selection of patients with PNEN for RAS-targeting therapeutic options.

4.1.2. Activation of Hippo signaling pathway effectors in Stromal/Mesenchymal PNENs

The Hippo signaling pathway elicits downstream effects through transcription coactivators *YAP1* and *WWTR1*. In mammals, a kinase module comprising serine/threonine kinase 3/4 (STK3/4) and large tumor suppressor kinase 1/2 (LATS1/2)

acts downstream of NF2 and phosphorylates YAP1 and WWTR1 for cytoplasmic retention and degradation thereby inhibiting the transcription of genes mediated by YAP1/WWTR1 (Hansen et al., 2015). The Hippo signaling pathway is an emerging subject in cancer research, but its roles and implications in PNENs have never been described. Known mechanisms leading to dysregulation of YAP1/WWTR1 include mutations in upstream regulators such as *LATS1/2* and *NF2* in mesothelioma and amplification of *YAP1* and *WWTR1* in squamous cell carcinomas (Wang et al., 2018). Mutations in *YAP1* or *WWTR1* are rare (≤ 3% of all cancers) and include inactivating as well as activating mutations across cancers (Wang et al., 2018). IHC analyses revealed elevated YAP1/WWTR1 nuclear staining in cancer cells across multiple cancer types, suggesting YAP1/WWTR1 activation is not uncommon in cancer (Zanconato et al., 2016).

My identification of a Stromal/Mesenchymal subgroup of PNENs with the first molecular evidence of aberrant activation of YAP1/WWTR1 will hopefully spur interest in further investigating the roles of the Hippo signaling pathway in the context of PNENs. Also, the upstream alterations leading to YAP1/WWTR1 activation in PNENs remain elusive, and understanding the mechanisms by which YAP1 and WWTR1 are aberrantly activated in PNENs can provide additional details on PNEN pathogenesis and potential means for patient selection for YAP1/WWTR1-targeting therapeutics. Given the Stromal/Mesenchymal subgroup of PNENs demonstrated higher activity of YAP1/WWTR1, inhibiting the downstream function of these transcription coactivators may achieve anti-tumour effects and become an additional targeted therapeutic option for PNENs with evidence of aberrant YAP1/WWTR1 activation. The Hippo signaling pathway regulates angiogenesis, and *YAP1*/*WWTR1* expression promote endothelial cell proliferation and arrangements (Choi et al., 2015; Neto et al., 2018). Cell-type analysis suggested a higher endothelial cell proportion in the Stromal/Mesenchymal subgroup specimens which may have contributed to their elevated expression levels of *YAP1/WWTR1*. While it remains to be confirmed whether the higher expression and aberrant activation of YAP1/WWTR1 were restricted to tumour cells or due to endothelial cells, sunitinib, an existing agent that targets angiogenesis, achieves therapeutic benefits in PNETs (Raymond et al., 2011). Thus, suppressing the aberrant activities of YAP1/WWTR1 in either tumour or endothelial cells may be potentially effective in achieving anti-tumour effects in PNENs. Aberrant activation of YAP1/WWTR1 can lead

to dysregulated expression of genes associated with oncogenesis, including the target genes of the TEAD family of transcription factors (Liu-Chittenden et al., 2012; Ota and Sasaki, 2008; Zhao et al., 2008). As such, the YAP1/WWTR1-TEAD axis has gained enormous interest as a target to inhibit YAP1/WWTR1 function in cancer cells (Calses et al., 2019; Crawford et al., 2018). Although existing agents targeting the YAP1/WWTR1-TEAD interaction either lack clear mechanism of action or lead to off-target effects such as oligomerization of proteins involved in other cellular processes (Calses et al., 2019), the interaction axis itself remains a potential target to inhibit YAP1/WWTR1 activity, and such a strategy could be similarly employed to target PNENs with evidence of elevated YAP1/WWTR1 activity.

4.1.3. Dysregulated metabolism involving arginine and glutamine in Alpha cell-like PNENs

Metabolism represents one of the enabling cancer hallmarks in which cancer cells reprogram cellular energetics to sustain cell growth and proliferation (Hanahan and Weinberg, 2011). Interests in the field have led to explosive growth in our understanding and culminated in hallmarks of cancer metabolism including “deregulated uptake of glucose and amino acids” and “increased demand for nitrogen” (Pavlova and Thompson, 2016). Yet, there is virtually no published work on the possible metabolic dysregulation in PNENs nor metabolic variations between PNENs. The Alpha cell-like subgroup of PNENs that I identified showcased enrichment of OxPhos genes on both mRNA and protein levels (Figure 2.10) and had higher abundance of proteins involved in arginine and glutamine/glutamate metabolism (Supplemental Table 2). The OxPhos process is tightly connected to the tricarboxylic acid (TCA) cycle, and the two modules act in a feedback loop that ultimately produces ATP (Martínez-Reyes and Chandel, 2020). Glutamine is a major anaplerotic substrate in cancer cells that fuels the TCA cycle and supplies nitrogen for biosynthesis required during cancer cell growth (Hensley et al., 2013). Interestingly, glutaminolysis, the conversion of glutamine into α-ketoglutarate that involves GLS, is required for mTOR complex 1 (mTORC1) activation and downstream signaling that promotes cell growth (Durán et al., 2012; Jewell et al., 2015; Nicklin et al., 2009). In the context of glutamine deficit, arginine can sufficiently activate mTORC1 downstream signaling, though the activation mechanism remains to be investigated (Lowman et al., 2019). Given the Alpha cell-like subgroup exhibited higher abundance of glutamine/glutamate and arginine metabolic enzymes, the PNENs of this subgroup likely

had higher demands for these amino acids, and as such, may have higher mTORC1 activation. In line with this hypothesis, the Alpha cell-like subgroup was the only subgroup with PNENs in which deleterious mutations were found in *TSC1/2*, upstream negative regulators of mTORC1 (Huang and Manning, 2008).

A literature search identified only one conference abstract that describes metabolism-related work in PNENs. In that study, fresh tissue slices from 15 PNENs were treated with everolimus and subjected to transcriptomic profiling to identify potential molecular features of everolimus sensitivity/resistance. Apoptosis activation was evaluated based on IHC of caspase 3 (CASP3) for determining sensitivity or resistance to everolimus. Transcriptomic analysis identified enrichment of glycolytic signatures in the everolimus-resistant PNENs while everolimus-sensitive PNENs exhibited enrichment of OxPhos signatures. IHC analysis confirmed increased abundance of solute carrier family 2 member 1 (SLC2A1) and hypoxia inducible factor 1 subunit alpha (HIF1A) in the resistant specimens and mitochondrial respiratory chain components in the sensitive specimens (Cros et al., 2018). While the described work from this abstract is yet to be published (as of April 2021), the increased abundance of mitochondrial respiratory chain components and enrichment of OxPhos gene signature observed in their everolimus-sensitive PNENs match the characteristics of the Alpha cell-like PNENs. Further, two of the four patients from the analyzed POG PNENs exhibiting substantial Alpha cell-like subgroup signatures, PN2 (Case 3) and PN12 (Case 1), were treated and their neoplasms responded to everolimus during their clinical course. Future research is needed to confirm whether the Alpha cell-like subgroup of PNENs indeed exhibits higher mTORC1 signaling and is sensitive to everolimus treatment.

4.1.4. Focal amplification of *MYCN* concomitant with a *MCYN*-driven transcriptomic signature in a metastatic PNEN

The MYC family of transcription factors, including *MYC*, *MYCN* and *MYCL* (MYCL proto-oncogene, bHLH transcription factor), regulates the expression of a broad range of genes involved in a myriad of cellular processes, including ribosome biogenesis, DNA replication and inhibition of apoptosis, that contribute to cancer development (Dang, 2012). All three MYC family genes are proto-oncogenes. *Myc* overexpression promotes tumourigenesis in murine models (Dang, 2012), and *MYC* is frequently amplified across cancer types in human (Beroukhim et al., 2010). *MYCN* and

MYCL have tissue-specific expression patterns (Zimmerman et al., 1986) and are frequently amplified in neuroblastoma and small cell lung cancer, respectively (Huang and Weiss, 2013; Kim et al., 2016; Nau et al., 1985). Forced expression of *Mycn* and constitutively active Akt1 transforms prostate epithelial cells into metastatic neuroendocrine prostate cancer (Lee et al., 2016). In the context of PNENs, ectopically expressed *MYCN* induced PNEN development in animal models (Fielitz et al., 2016; Yang et al., 2004), but whether *MYCN* dysregulation contributes to PNEN development in human is unknown. The PNET-G2 with focally amplified *MYCN* from the POG program was the first instance of a human PNEN with evidence of *MYCN* amplification and resultant gene expression changes (Figure 3.3). While it is not possible to confirm the pathogenic roles of *MYCN* in this PNET, the absence of aberrations in PNET-associated genes or other obvious genomic alterations sufficient to induce neoplastic transformation (Figures 3.2~3.3) suggested a potential oncogenic contribution from the *MYCN* amplification in this case. In addition, this particular case of PNET was found in a relative young individual (< 50 year-old; Dasari et al., 2017) with rapid disease progression (Figure 3.1). This rather aggressive disease course may be related to its *MYCN*-driven nature. Although the aggressive clinical course of this PNET was unlike the most PNETs, pathology reviews confirmed its PNET diagnosis. Experimental assessments are needed to ascertain whether *MYCN* serves as a proto-oncogene in the context of pancreatic islets and promotes tumour aggressiveness in PNENs.

Murine studies showed *MYC* and *MYCN* are partially compensatory in functions yet are both required during development (Huang and Weiss, 2013) suggesting they have shared but also distinct transcriptional targets. In NEN-related studies, *MYC* has shown context-dependent roles. *MYC* promotes neuroendocrine marker expression and drug resistance in murine PDACs (Farrell et al., 2017) but induces neuroendocrine de-differentiation in a Notch pathway-dependent manner in small cell lung cancer (Ireland et al., 2020). Similar to *MYCN*, the oncogenic roles of *MYC* in PNENs are largely unknown, but 81% of 21 PNETs in a study were found with moderate to high MYC IHC score despite lack of association with clinicopathological characteristics (Chang et al., 2017). *MYC* overexpression confers resistance to everolimus, and pharmacological inhibition of MYC reduced the viability of everolimus-resistant PNEN cells (Terracciano et al., 2020). This provides a potential therapeutic avenue to target PNENs intrinsically resistant to everolimus by interfering with *MYC*. It is therefore important to elucidate the functional

roles and potential differences between *MYC* and *MYCN* in PNENs as well as their possible contributions to treatment sensitivity and resistance. It had been recognized that MYC-induced transcriptional activation is facilitated by members of the bromodomain and extra-terminal (BET) subfamily of proteins, and inhibition of BET proteins down-regulate the expression of *MYC* as well as *MYC* and *MYCN* target genes providing anti-tumour effects *in vivo* (Delmore et al., 2011; Puissant et al., 2013). Several phase 1/2 clinical trials are currently in progress to investigate the anti-cancer effects of BET inhibitors (Shorstova et al., 2021). While the functional roles of the MYC family in the context of PNENs are yet to be elucidated, the lessons to be learned from the BET inhibitor trials could be exploited to potentially repurpose those agents for PNENs with molecular evidence of MYC contribution.

4.2. Emerging molecularly based classifications

Traditional cancer classification systems such as the WHO Classification of Tumours project (Kleihues and Sobin, 2000) build upon clinical observations and experience of a given cancer type to guide the management of newly diagnosed patients with the same cancer type. This typically involves histopathological assessments of the tumours and has been the standard approach to classify tumours in order to facilitate clinical management of cancer patients, including those with PNENs (Kulke et al., 2010b; Nagtegaal et al., 2020). However, this traditional classification approach for PNENs is becoming insufficient as we begin to appreciate the vast clinical and pathological heterogeneity of these neoplasms. This problem is particularly evident from the generally poor responses to treatments observed in patients with PNENs despite basing treatment decisions on the recommendations surrounding the WHO classification of PNENs (Kunz et al., 2018; Li et al., 2020; Raymond et al., 2011; Sorbye et al., 2013; Yao et al., 2011). In conjunction with the lack of predictive biomarkers for PNENs to inform possible therapeutic regimens, a new approach to classify PNENs is imperative.

With an increasing number of molecular studies as well as targeted therapeutic agents surfacing over recent years, a new era of a molecularly guided classification approach to achieve more effective and precise management regimens for cancer patients seems imminent. In fact, clinical practices or ongoing initiatives have been harnessing the predictive utility of validated biomarkers or molecular data to inform therapeutic regimens. These include using single gene biomarkers such as *MGMT*, in

which promoter methylation or low expression confers sensitivity to temozolomide (Cros et al., 2016; Hegi et al., 2005; Kulke et al., 2009) and *BRCA1/2*, in which mutations confer sensitivity to poly(adenosine diphosphate-ribose) polymerase (PARP) inhibition (Golan et al., 2019; Robson et al., 2017), to identify therapeutic agents that are likely to result in a tumour response. A number of ongoing projects adopt a precision medicine approach which utilizes a tumour's unique sequencing data to identify its therapeutic vulnerabilities. Examples of such strategies include the POG program at BC Cancer (Laskin et al., 2015), the CAPTUR trial taking place across Canada (Skamene et al., 2018), the OncoTreat platform at Columbia University Irving Medical Center (Alvarez et al., 2018) and the MSK-IMPACT test at Memorial Sloan Kettering Cancer Center (Cheng et al., 2015). While these projects adopt different methodologies, they all engage a basket trial approach which sanctions the use of targeted therapeutic agents based on molecular evidence of treatment susceptibility, irrespective of the type of cancer in question. This transition towards using molecular evidence to support and inform treatment decisions can be similarly exploited for the classification and management of PNENs. The addition of molecular level data to cancer classification indirectly addresses the issues surrounding the clinicopathological heterogeneity of PNENs by identifying shared molecular characteristics and molecular aberrations suitable as therapeutic targets in PNENs regardless of their clinicopathological characteristics.

In Chapter 2, I used an unbiased approach to identify four subgroups of PNENs with distinct transcriptomic and proteomic profiles. The proteotranscriptomic subgroups demonstrated different mutational frequencies in genes associated with PNENs and variations in GEPs suggestive of different oncogenic drivers. Previous studies had attempted to classify PNENs using miRNA expression profiles, GEPs, CNVs and/or epigenomics, but the identified subtypes were limited to having prognostic significance and were either largely inconsistent or not comparable between studies. By coupling transcriptomic and proteomic variations, I confirmed an Alpha cell-like and a PDX1-high PNEN subgroup sharing features with previously described subtypes (Boons et al., 2020; Cejas et al., 2019; Chan et al., 2018; Di Domenico et al., 2020; Lakis et al., 2021; Lawrence et al., 2018). Moreover, I identified a Proliferative subgroup comprising PNENs with molecular characteristics suggestive of a higher proliferation (Figures 2.10~13 and 2.15; Table 2.2) and a Stromal/Mesenchymal subgroup of PNENs with novel implication of the Hippo signaling pathway (Figure 2.16). Applying my subgroup

classification to PNEN metastases confirmed select subgroup molecular characteristics but also reaffirmed the molecular heterogeneity of PNENs. Most notably, three of the subgroups that I identified exhibited certain dysregulated pathways or processes that may be exploited for novel therapeutic interventions, as discussed above.

Among the four proteotranscriptomic subgroups, the Proliferative subgroup was the only subgroup associated with known clinicopathological characteristics, including enrichment of PNECs. However, roughly half of the subgroup was PNETs. The conventional belief dictates that PNECs and PNETs are two independent entities and should be considered and managed differently (Kulke et al., 2010b; Kunz, 2015; Strosberg et al., 2010). My observation of a molecular subgroup comprising both PNETs and PNECs raises an important question surrounding this assumption. If a small subset of PNETs is genuinely more similar to PNECs than other PNETs on the molecular level, should PNETs and PNECs truly be considered distinct simply based on their differences in histological differentiation? While genetic differences between PNETs and PNECs had been previously reported (Yachida et al., 2012), and PNECs are more likely to respond to platinum-based therapy (Moertel et al., 1991), some PNETs were also found to harbour mutations in PNEC-associated genes: *KRAS*, *TP53* and *RB1*, albeit at lower frequencies (Vijayvergia et al., 2016). Similarly, the only PNEC (PN4; Case 5) among the 9 POG PNENs that I examined in Chapter 3 harboured mutations in PNET-associated genes, *MEN1* and *DAXX*, but not in PNEC-associated genes, *TP53*, *KRAS* or *RB1* (Table 3.5; Supplemental Table 9). These findings suggest some PNENs share molecular characteristics despite histological differences. In line with this argument, four of the POG PNENs analyzed in Chapter 3 presented with different histopathological characteristics yet all elicited a substantial degree of the Proliferative subgroup signature (Table 3.4; Figure 3.7). The addition of molecular evidence could augment histopathological assessments to better classify PNENs and predict whether a given neoplasm is likely to respond to a certain treatment.

4.3. Expanding to other NENs

NENs can arise from neuroendocrine cells found in most tissues and are categorized based on their organ of origin. However, NENs are perceived as distinct entities from their non-neuroendocrine counterparts arising from the same organ. Such distinction is reflected in the most recent WHO classification system which distinguishes

NENs in each organ-specific chapter (Nagtegaal et al., 2020). The current official nomenclatures for NENs in each primary anatomical site (PAS) differ due to historical conventions, and terminologies like “carcinoid” are still being used to refer to well-differentiated pulmonary NENs. That being said, clinically relevant features such as histological differentiation and proliferative indices are similarly used in NENs across different PASs for prognostic and therapeutic utility (Nagtegaal et al., 2020; Raphael et al., 2017b). An example of this is the use of platinum-based therapy for NECs of GI, pancreas and lung origin (Evans et al., 1985; Moertel et al., 1991). Generally, tumour grades based on proliferative indices are highly prognostic, but the presence of distant metastases remains the top contributor to inferior survival outcomes for patients with NENs (Dasari et al., 2017).

A recent initiative by international NEN experts proposed a consensus classification framework for NENs across different PASs (Rindi et al., 2018). This suggestion came in the wake of the various terminologies adopted for NENs of different PASs that are potentially confusing for interdisciplinary communication. The proposed consensus classification system largely resembled the current WHO classification for PNENs where a dichotomized histological definition distinguishes NETs from NECs. Similar to those of pancreatic origin, NETs were further classified into G1-3 based on proliferative index, and NECs may be of SC or LC type (Rindi et al., 2018). The nomenclatures from this proposed classification system is adopted hereafter for convenience.

Despite the initiative to consolidate and standardize the terminologies and some shared management regimens already in clinical practice for NENs across PASs, the vast majority of molecular studies to date have focused on primary NENs of certain PASs. Further, organ-specific NEN studies have identified molecular subtypes among NENs of pancreatic origin (as described in Chapter 2 and summarized in Section 1.4.4), pulmonary origin (Ireland et al., 2020) and the small intestine (Karpathakis et al., 2016). Yet, similar genetic alterations have been observed in NENs of different PASs. PNENs and pulmonary NENs, for example, share several mutational characteristics. *MEN1*, which is recurrently mutated in up to 56% of PNETs and rarely altered in PNECs, was found mutated in 13.6% of pulmonary NETs but not in pulmonary NECs. Similarly, tumour suppressors *TP53* and *RB1* that are frequently altered in PNECs were found recurrently altered in pulmonary NECs (26~98%) but rare in pulmonary NETs (< 5%)

(Fernandez-Cuesta et al., 2014; George et al., 2015; Jiao et al., 2011; Miyoshi et al., 2017; Scarpa et al., 2017; Yachida et al., 2012). In addition to genetic alterations, aberrations that affect signaling pathways such as the PI3K/AKT/mTOR pathway have been identified in both small intestinal NENs and pulmonary NECs-LC (Karpathakis et al., 2016; Miyoshi et al., 2017). Together, these observations suggest that despite vast heterogeneities among NENs of the same PASs, some NENs of different PASs share molecular features.

To explore potential commonalities and distinctions in the molecular profiles of NENs originating from different PASs, I conducted a preliminary analysis utilizing existing molecular data available from the POG program. I identified a total of 29 NENs (including the 9 PNENs explored in Section 3.5) enrolled in the POG programs with available WGS and WTS data. A consensus hierarchical cluster analysis, using Spearman's correlation calculated from the top 25% variably expressed RNAs between the samples, identified 3 hierarchical clusters, one of which may be further divided into two or three subclusters (Figure 4.1; green, red and orange at k = 5). One cluster consisted exclusively of pulmonary and thyroid NENs, and another contained mostly NECs or MiNENs with or without high Ki67 indices. The third cluster consisted of mostly NETs of pancreas or small intestine origin but also a few pulmonary/thyroid NETs and a NET originated from neck (Figure 4.1). For the majority of the cohort, biopsies from distant metastases were sequenced, and NENs of different PASs have distinct metastatic patterns (Hermans et al., 2020), so the biopsy sites were correlative with the PASs. Overall, the results suggest the clustering structure was largely associated with PASs/biopsy sites and grade or histological differentiation status. However, it is also evident that there are potential transcriptomic features not reflected in the clinicopathological characteristics as a few of the samples clustered away from others sharing the same PASs, grades or histological differentiation status. While this is a preliminary piece of data, it highlights the importance of elucidating potential commonalities and distinctions on the molecular level between NENs of different PASs. A comprehensive analysis of a large cohort with NENs of different PASs and various clinicopathological characteristics would provide valuable knowledge to better assess the adequacies of the current organ-specific practice in NEN management.

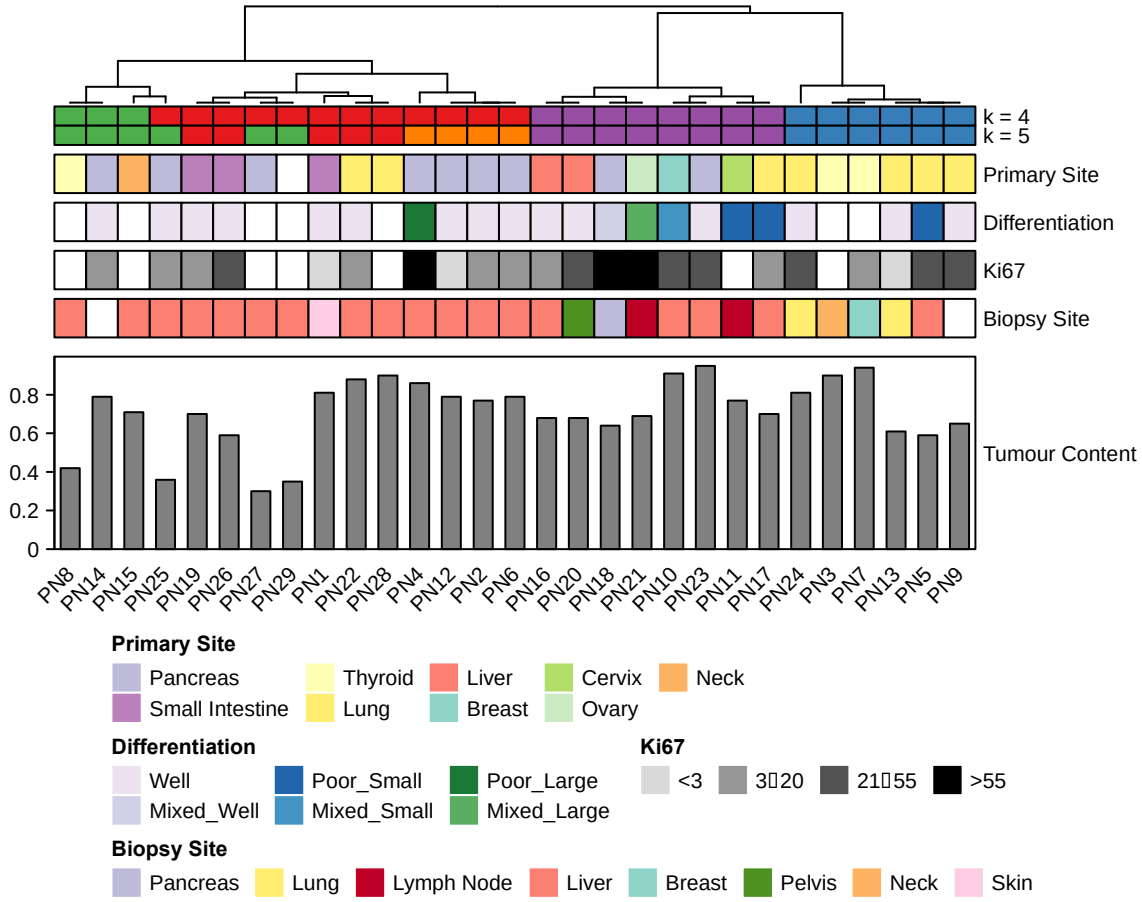

Figure 4.1. Consensus hierarchical clustering result of the POG NENs.
Consensus hierarchical cluster analysis was performed using Spearman's correlation for 1000 iterations. An optimal cluster solution was achieved at k = 3 (top dendrogram), after which there were relatively smaller changes in area under the consensus distribution function curves. The cluster solutions at k = 4 and 5 are shown for comparison. Where available, the available clinicopathological data and estimated tumour content are shown as coloured boxes with legends at the bottom. White boxes denote missing information.

4.4. Concluding remarks

Considerable clinical, translational and basic research advances in PNENs have led to improved detection, increased number of therapeutic options and better molecular understanding of this disease. However, the current cancer classification system and effective treatment regimens are still inadequate as demonstrated by the low treatment response rates and the lack of predictive markers to facilitate therapeutic decisions. In addition, putative drivers of PNEN development are unknown in a substantial number of cases. In Chapter 2, I show that PNENs can be stratified into four molecular subgroups characterized by mutational, transcriptomic and proteomic distinctions. Whereas other groups have reported subtypes of prognostic significance, I identified potential

therapeutic vulnerabilities suitable for clinical interventions in my subgroups. Due to the rarity of PNENs and heterogeneous nature of the disease, additional validation analyses using larger and international patient specimen cohorts are needed to affirm the applicability of my subgroup stratification system. Also, functional validation of subgroup-specific features, such as arginine/glutamine metabolism and YAP1/WWTR1 activity, could provide preclinical evidence for establishing novel therapeutic avenues for PNENs. This may entail genetic and pharmacological modulation of key factors of a cellular pathway/process of interest in cell line, patient-derived spheroids/organoids and genetically engineered mice. Experimental studies investigating select subgroup molecular characteristics are in the works.

Throughout Chapters 2 and 3, novel oncogenic events were identified in genes or pathways already implicated or utilized as therapeutic targets in other cancer types. The discoveries of these oncogenic contributors provide additional insights into the pathogenesis of PNENs and suggest potential for repurposing therapeutic agents approved for other cancers to be used for PNENs. This argument advocates the emerging precision medicine initiatives that leverage molecular evidence to aid therapeutic decision-making for patients with PNENs.

PNENs are heterogeneous yet may share molecular features with extrapancreatic NENs. The data and results from this thesis may help to foster the molecular understanding and clinical management of NENs in general. My findings herein provide a sizable contribution to the NEN field towards better clinical outcomes for patients with NENs.

References

Adzhubei, I.A., Schmidt, S., Peshkin, L., Ramensky, V.E., Gerasimova, A., Bork, P., Kondrashov, A.S., and Sunyaev, S.R. (2010). A method and server for predicting damaging missense mutations. Nat Meth *7*, 248–249.

Agarwal, S.K. (2017). The future: genetics advances in MEN1 therapeutic approaches and management strategies. Endocrine-Related Cancer *24*, T119–T134.

Akbani, R., Akdemir, K.C., Aksoy, B.A., Albert, M., Ally, A., Amin, S.B., Arachchi, H., Arora, A., Auman, J.T., Ayala, B., et al. (2015). Genomic Classification of Cutaneous Melanoma. Cell *161*, 1681–1696.

Al-Fageeh, M., Li, Q., Mohaiza Dashwood, W., Myzak, M.C., and Dashwood, R.H. (2004). Phosphorylation and ubiquitination of oncogenic mutants of β-catenin containing substitutions at Asp32. Oncogene *23*, 4839–4846.

Al-Tassan, N., Chmiel, N.H., Maynard, J., Fleming, N., Livingston, A.L., Williams, G.T., Hodges, A.K., Davies, D.R., David, S.S., Sampson, J.R., et al. (2002). Inherited variants of MYH associated with somatic G:C→T:A mutations in colorectal tumors. Nature Genetics *30*, 227–232.

Alexakis, N., Connor, S., Ghaneh, P., Lombard, M., Smart, H.L., Evans, J., Hughes, M., Garvey, C.J., Vora, J., Vinjamuri, S., et al. (2004). Hereditary pancreatic endocrine tumours. Pancreatology *4*, 417–435.

Alexandrov, L.B., Nik-Zainal, S., Wedge, D.C., Campbell, P.J., and Stratton, M.R. (2013). Deciphering signatures of mutational processes operative in human cancer. Cell Reports *3*, 246–259.

Ali, S.H., and DeCaprio, J.A. (2001). Cellular transformation by SV40 large T antigen: interaction with host proteins. Seminars in Cancer Biology *11*, 15–22.

Alkatout, I., Friemel, J., Sitek, B., Anlauf, M., Eisenach, P.A., Stühler, K., Scarpa, A., Perren, A., Meyer, H.E., Knoefel, W.T., et al. (2015). Novel prognostic markers revealed by a proteomic approach separating benign from malignant insulinomas. Modern Pathology *28*, 69–79.

Alvarez, M.J. (2019). viper: Virtual Inference of Protein-activity by Enriched Regulon analysis.

Alvarez, M.J., Shen, Y., Giorgi, F.M., Lachmann, A., Ding, B.B., Hilda Ye, B., and Califano, A. (2016). Functional characterization of somatic mutations in cancer using network-based inference of protein activity. Nature Genetics *48*, 838–847.

Alvarez, M.J., Subramaniam, P.S., Tang, L.H., Grunn, A., Aburi, M., Rieckhof, G., Komissarova, E. V., Hagan, E.A., Bodei, L., Clemons, P.A., et al. (2018). A precision oncology approach to the pharmacological targeting of mechanistic dependencies in neuroendocrine tumors. Nature Genetics *50*, 979–989.

Bahassi, E.M., Ovesen, J.L., Riesenberg, A.L., Bernstein, W.Z., Hasty, P.E., and Stambrook, P.J. (2008). The checkpoint kinases Chk1 and Chk2 regulate the functional associations between hBRCA2 and Rad51 in response to DNA damage. Oncogene *27*, 3977–3985.

Bailey, P., Chang, D.K., Nones, K., Johns, A.L., Patch, A.-M., Gingras, M.-C., Miller, D.K., Christ, A.N., Bruxner, T.J.C., Quinn, M.C., et al. (2016). Genomic analyses identify molecular subtypes of pancreatic cancer. Nature *531*, 47–52.

Banck, M.S., Kanwar, R., Kulkarni, A.A., Boora, G.K., Metge, F., Kipp, B.R., Zhang, L., Thorland, E.C., Minn, K.T., Tentu, R., et al. (2013). The genomic landscape of small intestine neuroendocrine tumors. The Journal of Clinical Investigation *123*, 2502–2508.

Bastidas-Ponce, A., Scheibner, K., Lickert, H., and Bakhti, M. (2017). Cellular and molecular mechanisms coordinating pancreas development. Development *144*, 2873 LP – 2888.

Basturk, O., Yang, Z., Tang, L.H., Hruban, R.H., Adsay, V., McCall, C.M., Krasinskas, A.M., Jang, K.-T., Frankel, W.L., Balci, S., et al. (2015). The high-grade (WHO G3) pancreatic neuroendocrine tumor category is morphologically and biologically heterogenous and includes both well differentiated and poorly differentiated neoplasms. The American Journal of Surgical Pathology *39*, 683–690.

Benjamin, D., Sato, T., Cibulskis, K., Getz, G., Stewart, C., and Lichtenstein, L. (2019). Calling Somatic SNVs and Indels with Mutect2. BioRxiv 861054.

Benten, D., Behrang, Y., Unrau, L., Weissmann, V., Wolters-Eisfeld, G., Burdak-Rothkamm, S., Stahl, F.R., Anlauf, M., Grabowski, P., Möbs, M., et al. (2018). Establishment of the First Well-differentiated Human Pancreatic Neuroendocrine Tumor Model. Molecular Cancer Research *16*, 496–507.

Bergsland, E.K., Roy, R., Stephens, P., Ross, J.S., Bailey, M., and Olshen, A. (2016). Genomic profiling to distinguish poorly differentiated neuroendocrine carcinomas arising in different sites. Journal of Clinical Oncology *34*, 4020.

Beroukhim, R., Mermel, C.H., Porter, D., Wei, G., Raychaudhuri, S., Donovan, J., Barretina, J., Boehm, J.S., Dobson, J., Urashima, M., et al. (2010). The landscape of somatic copy-number alteration across human cancers. Nature *463*, 899–905.

Bertolino, P., Tong, W.-M., Herrera, P.L., Casse, H., Zhang, C.X., and Wang, Z.-Q. (2003a). Pancreatic beta-cell-specific ablation of the multiple endocrine neoplasia type 1 (MEN1) gene causes full penetrance of insulinoma development in mice. Cancer Research *63*, 4836–4841.

Bertolino, P., Tong, W.-M., Galendo, D., Wang, Z.-Q., and Zhang, C.-X. (2003b). Heterozygous Men1 Mutant Mice Develop a Range of Endocrine Tumors Mimicking Multiple Endocrine Neoplasia Type 1. Molecular Endocrinology *17*, 1880–1892.

Bhaoighill, M.N., and Dunlop, E.A. (2019). Mechanistic target of rapamycin inhibitors: successes and challenges as cancer therapeutics. Cancer Drug Resistance *2*, 1069–1085.

Boon, K., Caron, H.N., van Asperen, R., Valentijn, L., Hermus, M.-C., van Sluis, P., Roobeek, I., Weis, I., Voûte, P.A., Schwab, M., et al. (2001). N-myc enhances the expression of a large set of genes functioning in ribosome biogenesis and protein synthesis. The EMBO Journal *20*, 1383–1393.

Boons, G., Vandamme, T., Ibrahim, J., Roeyen, G., Driessen, A., Peeters, D., Lawrence, B., Print, C., Peeters, M., Van Camp, G., et al. (2020). PDX1 DNA Methylation Distinguishes Two Subtypes of Pancreatic Neuroendocrine Neoplasms with a Different Prognosis. Cancers *12*.

Brabander, T., van der Zwan, W.A., Teunissen, J.J.M., Kam, B.L.R., Feelders, R.A., de Herder, W.W., van Eijck, C.H.J., Franssen, G.J.H., Krenning, E.P., and Kwekkeboom, D.J. (2017). Long-Term Efficacy, Survival, and Safety of [^{177}Lu-DOTA^{0},Tyr^{3}]octreotate in Patients with Gastroenteropancreatic and Bronchial Neuroendocrine Tumors. Clinical Cancer Research *23*, 4617 LP – 4624.

Brodowska, K., Al-Moujahed, A., Marmalidou, A., Meyer Zu Horste, M., Cichy, J., Miller, J.W., Gragoudas, E., and Vavvas, D.G. (2014). The clinically used photosensitizer Verteporfin (VP) inhibits YAP-TEAD and human retinoblastoma cell growth in vitro without light activation. Experimental Eye Research *124*, 67–73.

Burd, C.E., Liu, W., Huynh, M. V, Waqas, M.A., Gillahan, J.E., Clark, K.S., Fu, K., Martin, B.L., Jeck, W.R., Souroullas, G.P., et al. (2014). Mutation-Specific RAS Oncogenicity Explains NRAS Codon 61 Selection in Melanoma. Cancer Discovery *4*, 1418 LP – 1429.

Butterfield, Y.S., Kreitzman, M., Thiessen, N., Corbett, R.D., Li, Y., Pang, J., Ma, Y.P., Jones, S.J.M., and Birol, İ. (2014). JAGuaR: Junction Alignments to Genome for RNA-Seq Reads. PLOS ONE *9*, e102398.

Calses, P.C., Crawford, J.J., Lill, J.R., and Dey, A. (2019). Hippo Pathway in Cancer: Aberrant Regulation and Therapeutic Opportunities. Trends in Cancer *5*, 297–307.

Cantwell-Dorris, E.R., O'Leary, J.J., and Sheils, O.M. (2011). BRAF^{V600E}: Implications for Carcinogenesis and Molecular Therapy. Molecular Cancer Therapeutics *10*, 385 LP – 394.

Cao, Y., Gao, Z., Li, L., Jiang, X., Shan, A., Cai, J., Peng, Y., Li, Y., Jiang, X., Huang, X., et al. (2013). Whole exome sequencing of insulinoma reveals recurrent T372R mutations in YY1. Nature Communications *4*, 2810.

Capelli, P., Martignoni, G., Pedica, F., Falconi, M., Antonello, D., Malpeli, G., and Scarpa, A. (2009). Endocrine Neoplasms of the Pancreas: Pathologic and Genetic Features. Archives of Pathology & Laboratory Medicine *133*, 350–364.

Caplin, M.E., Pavel, M., Cwikla, J.B., Phan, A.T., Raderer, M., Sedlackova, E., Cadiot, G., Wolin, E.M., Capdevila, J., Wall, L., et al. (2014). Lanreotide in metastatic enteropancreatic neuroendocrine tumors. The New England Journal of Medicine *371*, 224–233.

Carbone, A. (2020). Cancer Classification at the Crossroads. Cancers *12*, 980.

Carlson, M. (2019). org.Hs.eg.db: Genome wide annotation for Human.

Casanovas, O., Hicklin, D.J., Bergers, G., and Hanahan, D. (2005). Drug resistance by evasion of antiangiogenic targeting of VEGF signaling in late-stage pancreatic islet tumors. Cancer Cell *8*, 299–309.

Castellone, M.D., Verrienti, A., Magendra Rao, D., Sponziello, M., Fabbro, D., Muthu, M., Durante, C., Maranghi, M., Damante, G., Pizzolitto, S., et al. (2010). A novel de novo germ-line V292M mutation in the extracellular region of RET in a patient with phaeochromocytoma and medullary thyroid carcinoma: functional characterization. Clinical Endocrinology *73*, 529–534.

Cejas, P., Drier, Y., Dreijerink, K.M.A., Brosens, L.A.A., Deshpande, V., Epstein, C.B., Conemans, E.B., Morsink, F.H.M., Graham, M.K., Valk, G.D., et al. (2019). Enhancer signatures stratify and predict outcomes of non-functional pancreatic neuroendocrine tumors. Nature Medicine.

Chamberlain, C.E., Scheel, D.W., McGlynn, K., Kim, H., Miyatsuka, T., Wang, J., Nguyen, V., Zhao, S., Mavropoulos, A., Abraham, A.G., et al. (2014). Menin determines K-RAS proliferative outputs in endocrine cells. The Journal of Clinical Investigation *124*, 4093–4101.

Chan, C.S., Laddha, S. V., Lewis, P.W., Koletsky, M.S., Robzyk, K., Da Silva, E., Torres, P.J., Untch, B.R., Li, J., Bose, P., et al. (2018). ATRX, DAXX or MEN1 mutant pancreatic neuroendocrine tumors are a distinct alpha-cell signature subgroup. Nature Communications *9*, 1–10.

Chang, T.-M., Shan, Y.-S., Chu, P.-Y., Jiang, S.S., Hung, W.-C., Chen, Y.-L., Tu, H.-C., Lin, H.-Y., Tsai, H.-J., and Chen, L.-T. (2017). The regulatory role of aberrant Phosphatase and Tensin Homologue and Liver Kinase B1 on AKT/mTOR/c-Myc axis in pancreatic neuroendocrine tumors. Oncotarget *8*, 98068–98083.

Chen, G., A, J., Wang, M., Farley, S., Lee, L.-Y., Lee, L.-C., and Sawicki, M.P. (2008). Menin Promotes the Wnt Signaling Pathway in Pancreatic Endocrine Cells. Molecular Cancer Research *6*, 1894 LP – 1907.

Chen, L., Iraci, N., Gherardi, S., Gamble, L.D., Wood, K.M., Perini, G., Lunec, J., and Tweddle, D.A. (2010). p53 is a direct transcriptional target of MYCN in neuroblastoma. Cancer Research *70*, 1377–1388.

Chen, Y., Lun, A.T.L., McCarthy, D.J., Ritchie, M.E., Phipson, B., Hu, Y., Zhou, X., Robinson, M.D., and Smyth, G.K. (2020). edgeR: Empirical Analysis of Digital Gene Expression Data in R.

Cheng, D.T., Mitchell, T.N., Zehir, A., Shah, R.H., Benayed, R., Syed, A., Chandramohan, R., Liu, Z.Y., Won, H.H., Scott, S.N., et al. (2015). Memorial Sloan Kettering-Integrated Mutation Profiling of Actionable Cancer Targets (MSK-IMPACT): A Hybridization Capture-Based Next-Generation Sequencing Clinical Assay for Solid Tumor Molecular Oncology. The Journal of Molecular Diagnostics : JMD *17*, 251–264.

Choi, H.-J., Zhang, H., Park, H., Choi, K.-S., Lee, H.-W., Agrawal, V., Kim, Y.-M., and Kwon, Y.-G. (2015). Yes-associated protein regulates endothelial cell contact-mediated expression of angiopoietin-2. Nature Communications *6*, 6943.

Christofori, G., Naik, P., and Hanahan, D. (1994). A second signal supplied by insulin-like growth factor II in oncogene-induced tumorigenesis. Nature *369*, 414–418.

Christofori, G., Naik, P., and Hanahan, D. (1995). Deregulation of both imprinted and expressed alleles of the insulin–like growth factor 2 gene during β–cell tumorigenesis. Nature Genetics *10*, 196–201.

Cingolani, P., Platts, A., Wang, L.L., Coon, M., Nguyen, T., Wang, L., Land, S.J., Lu, X., and Ruden, D.M. (2012). A program for annotating and predicting the effects of single nucleotide polymorphisms, SnpEff: SNPs in the genome of Drosophila melanogaster strain w1118; iso-2; iso-3. Fly *6*, 80–92.

Cloyd, J.M., and Poultsides, G.A. (2015). Non-functional neuroendocrine tumors of the pancreas: Advances in diagnosis and management. World Journal of Gastroenterology *21*, 9512–9525.

Cluntun, A.A., Lukey, M.J., Cerione, R.A., and Locasale, J.W. (2017). Glutamine Metabolism in Cancer: Understanding the Heterogeneity. Trends in Cancer *3*, 169–180.

Clynes, D., Jelinska, C., Xella, B., Ayyub, H., Scott, C., Mitson, M., Taylor, S., Higgs, D.R., and Gibbons, R.J. (2015). Suppression of the alternative lengthening of telomere pathway by the chromatin remodelling factor ATRX. Nature Communications *6*, 7538.

Collisson, E. a, Sadanandam, A., Olson, P., Gibb, W.J., Truitt, M., Gu, S., Cooc, J., Weinkle, J., Kim, G.E., Jakkula, L., et al. (2011). Subtypes of pancreatic ductal adenocarcinoma and their differing responses to therapy. Nat Med *17*, 500–503.

Collisson, E.A., Campbell, J.D., Brooks, A.N., Berger, A.H., Lee, W., Chmielecki, J., Beer, D.G., Cope, L., Creighton, C.J., Danilova, L., et al. (2014). Comprehensive molecular profiling of lung adenocarcinoma. Nature *511*, 543–550.

Conemans, E.B., Raicu-Ionita, G.M., Pieterman, C.R.C., Dreijerink, K.M.A., Dekkers, O.M., Hermus, A.R., de Herder, W.W., Drent, M.L., van der Horst-Schrivers, A.N.A., Havekes, B., et al. (2018). Expression of p27(Kip1) and p18(Ink4c) in human multiple endocrine neoplasia type 1-related pancreatic neuroendocrine tumors. Journal of Endocrinological Investigation *41*, 655–661.

Cook, R., Zoumpoulidou, G., Luczynski, M.T., Rieger, S., Moquet, J., Spanswick, V.J., Hartley, J.A., Rothkamm, K., Huang, P.H., and Mittnacht, S. (2015). Direct Involvement of Retinoblastoma Family Proteins in DNA Repair by Non-homologous End-Joining. Cell Reports *10*, 2006–2018.

Corbo, V., Beghelli, S., Bersani, S., Antonello, D., Talamini, G., Brunelli, M., Capelli, P., Falconi, M., and Scarpa, A. (2012). Pancreatic endocrine tumours: mutational and immunohistochemical survey of protein kinases reveals alterations in targetable kinases in cancer cell lines and rare primaries. Annals of Oncology *23*, 127–134.

Crawford, J.J., Bronner, S.M., and Zbieg, J.R. (2018). Hippo pathway inhibition by blocking the YAP/TAZ-TEAD interface: a patent review. Expert Opinion on Therapeutic Patents *28*, 867–873.

Cromer, M.K., Choi, M., Nelson-Williams, C., Fonseca, A.L., Kunstman, J.W., Korah, R.M., Overton, J.D., Mane, S., Kenneyg, B., Malchoff, C.D., et al. (2015). Neomorphic effects of recurrent somatic mutations in yin yang 1 in insulin-producing adenomas. Proceedings of the National Academy of Sciences of the United States of America *112*, 4062–4067.

Crona, J., Norlén, O., Antonodimitrakis, P., Welin, S., Stålberg, P., and Eriksson, B. (2016). Multiple and Secondary Hormone Secretion in Patients With Metastatic Pancreatic Neuroendocrine Tumours. The Journal of Clinical Endocrinology & Metabolism *101*, 445–452.

Cros, J., Hentic, O., Rebours, V., Zappa, M., Gille, N., Theou-Anton, N., Vernerey, D., Maire, F., Levy, P., Bedossa, P., et al. (2016). MGMT expression predicts response to temozolomide in pancreatic neuroendocrine tumors. Endocrine-Related Cancer *23*, 625–633.

Cros, J., Bucau, M., Raffenne, J., Soukeur, M., Dumont, F., De Koning, L., de Mestier, L., Hentic, O., Sauvanet, A., Sadanandam, A., et al. (2018). Mitochondrial or Aerobic Glycolysis Oriented Metabolism May Define Pancreatic Neuroendocrine Tumors (PanNET) Resistance to mTOR-Targeting Therapies. In Neuroendocrinology: Abstracts of the 15th Annual ENETS Conference for the DIagnosis and Treatment of Neuroendocrine Tumor, pp. 1–302.

Dang, C. V (2012). MYC on the Path to Cancer. Cell *149*, 22–35.

Dasari, A., Shen, C., Halperin, D., Zhao, B., Zhou, S., Xu, Y., Shih, T., and Yao, J.C. (2017). Trends in the Incidence, Prevalence, and Survival Outcomes in Patients With Neuroendocrine Tumors in the United States. JAMA Oncology *77030*, 1335–1342.

Delmore, J.E., Issa, G.C., Lemieux, M.E., Rahl, P.B., Shi, J., Jacobs, H.M., Kastritis, E., Gilpatrick, T., Paranal, R.M., Qi, J., et al. (2011). BET bromodomain inhibition as a therapeutic strategy to target c-Myc. Cell *146*, 904–917.

Dicerna Pharmaceuticals Inc. (2015). DCR-MYC-101 study, a phase 1 study in advanced solid tumors and hematological malignancies.

Dicerna Pharmaceuticals Inc. (2016). Dicerna prioritizes resources to advance GalXC product candidates [Press release].

Do, H., and Dobrovic, A. (2015). Sequence artifacts in DNA from formalin-fixed tissues: causes and strategies for minimization. Clinical Chemistry *61*, 64–71.

Dobin, A., Davis, C.A., Schlesinger, F., Drenkow, J., Zaleski, C., Jha, S., Batut, P., Chaisson, M., and Gingeras, T.R. (2012). STAR: ultrafast universal RNA-seq aligner. Bioinformatics *29*, 15–21.

Dolenšek, J., Rupnik, M.S., and Stožer, A. (2015). Structural similarities and differences between the human and the mouse pancreas. Islets *7*, e1024405–e1024405.

Di Domenico, A., Pipinikas, C.P., Maire, R.S., Bräutigam, K., Simillion, C., Dettmer, M.S., Vassella, E., Thirlwell, C., Perren, A., and Marinoni, I. (2020). Epigenetic landscape of pancreatic neuroendocrine tumours reveals distinct cells of origin and means of tumour progression. Communications Biology *3*, 740.

Drané, P., Ouararhni, K., Depaux, A., Shuaib, M., and Hamiche, A. (2010). The death-associated protein DAXX is a novel histone chaperone involved in the replication-independent deposition of H3.3. Genes & Development *24*, 1253–1265.

Drost, J., van Boxtel, R., Blokzijl, F., Mizutani, T., Sasaki, N., Sasselli, V., de Ligt, J., Behjati, S., Grolleman, J.E., van Wezel, T., et al. (2017). Use of CRISPR-modified human stem cell organoids to study the origin of mutational signatures in cancer. Science *358*, 234 LP – 238.

Dunn, T., Berry, G., Emig-Agius, D., Jiang, Y., Lei, S., Iyer, A., Udar, N., Chuang, H.-Y., Hegarty, J., Dickover, M., et al. (2019). Pisces: an accurate and versatile variant caller for somatic and germline next-generation sequencing data. Bioinformatics (Oxford, England) *35*, 1579–1581.

Durán, R. V, Oppliger, W., Robitaille, A.M., Heiserich, L., Skendaj, R., Gottlieb, E., and Hall, M.N. (2012). Glutaminolysis activates Rag-mTORC1 signaling. Molecular Cell *47*, 349–358.

Durinck, S., and Huber, W. (2020). biomaRt: Interface to BioMart databases (i.e. Ensembl).

Durinck, S., Moreau, Y., Kasprzyk, A., Davis, S., De Moor, B., Brazma, A., and Huber, W. (2005). BioMart and Bioconductor: a powerful link between biological databases and microarray data analysis. Bioinformatics *21*, 3439–3440.

Durinck, S., Spellman, P.T., Birney, E., and Huber, W. (2009). Mapping identifiers for the integration of genomic datasets with the R/Bioconductor package biomaRt. Nature Protocols *4*, 1184–1191.

Efrat, S., Teitelman, G., Anwar, M., Ruggiero, D., and Hanahan, D. (1988). Glucagon gene regulatory region directs oncoprotein expression to neurons and pancreatic a cells. Neuron *1*, 605–613.

Eisenhauer, E.A., Therasse, P., Bogaerts, J., Schwartz, L.H., Sargent, D., Ford, R., Dancey, J., Arbuck, S., Gwyther, S., Mooney, M., et al. (2009). New response evaluation criteria in solid tumours: revised RECIST guideline (version 1.1). European Journal of Cancer (Oxford, England : 1990) *45*, 228–247.

Evans, W.K., Shepherd, F.A., Feld, R., Osoba, D., Dang, P., and Deboer, G. (1985). VP-16 and cisplatin as first-line therapy for small-cell lung cancer. Journal of Clinical Oncology : Official Journal of the American Society of Clinical Oncology *3*, 1471–1477.

Ezziddin, S., Khalaf, F., Vanezi, M., Haslerud, T., Mayer, K., Al Zreiqat, A., Willinek, W., Biersack, H.-J., and Sabet, A. (2014). Outcome of peptide receptor radionuclide therapy with 177Lu-octreotate in advanced grade 1/2 pancreatic neuroendocrine tumours. European Journal of Nuclear Medicine and Molecular Imaging *41*, 925–933.

Farrell, A.S., Joly, M.M., Allen-Petersen, B.L., Worth, P.J., Lanciault, C., Sauer, D., Link, J., Pelz, C., Heiser, L.M., Morton, J.P., et al. (2017). MYC regulates ductal-neuroendocrine lineage plasticity in pancreatic ductal adenocarcinoma associated with poor outcome and chemoresistance. Nature Communications *8*, 1728.

Ferlin, A., Garolla, A., Bettella, A., Bartoloni, L., Vinanzi, C., Roverato, A., and Foresta, C. (2005). Androgen receptor gene CAG and GGC repeat lengths in cryptorchidism. European Journal of Endocrinology Eur j Endocrinol *152*, 419–425.

Fernandez-Cuesta, L., Peifer, M., Lu, X., Sun, R., Ozretić, L., Seidal, D., Zander, T., Leenders, F., George, J., Müller, C., et al. (2014). Frequent mutations in chromatin-remodelling genes in pulmonary carcinoids. Nature Communications *5*, 3518.

Feyrter, F. (1938). Uber diffuse endokrine epitheliale Organe. Zentralbl Innere Med *545*, 31–41.

Fielitz, K., Althoff, K., De Preter, K., Nonnekens, J., Ohli, J., Elges, S., Hartmann, W., Kloppel, G., Knosel, T., Schulte, M., et al. (2016). Characterization of pancreatic glucagon-producing tumors and pituitary gland tumors in transgenic mice overexpressing MYCN in hGFAP-positive cells. Oncotarget *7*, 74415–74426.

Folkman, J., Watson, K., Ingber, D., and Hanahan, D. (1989). Induction of angiogenesis during the transition from hyperplasia to neoplasia. Nature *339*, 58–61.

Forbes, S.A., Beare, D., Gunasekaran, P., Leung, K., Bindal, N., Boutselakis, H., Ding, M., Bamford, S., Cole, C., Ward, S., et al. (2015). COSMIC: exploring the world's knowledge of somatic mutations in human cancer. Nucleic Acids Research *43*, D805–D811.

Forsburg, S.L. (2004). Eukaryotic MCM proteins: beyond replication initiation. Microbiology and Molecular Biology Reviews : MMBR *68*, 109–131.

Gamble, L.D., Kees, U.R., Tweddle, D.A., and Lunec, J. (2012). MYCN sensitizes neuroblastoma to the MDM2-p53 antagonists Nutlin-3 and MI-63. Oncogene *31*, 752–763.

Gaujoux, R., and Seoighe, C. (2010). A flexible R package for nonnegative matrix factorization. BMC Bioinformatics *11*.

Gaujoux, R., and Seoighe, C. (2020). NMF: Algorithms and Framework for Nonnegative Matrix Factorization (NMF).

George, J., Lim, J.S., Jang, S.J., Cun, Y., Ozretić, L., Kong, G., Leenders, F., Lu, X., Fernández-Cuesta, L., Bosco, G., et al. (2015). Comprehensive genomic profiles of small cell lung cancer. Nature *524*, 47–53.

Geyer, F.C., Li, A., Papanastasiou, A.D., Smith, A., Selenica, P., Burke, K.A., Edelweiss, M., Wen, H.-C., Piscuoglio, S., Schultheis, A.M., et al. (2018). Recurrent hotspot mutations in HRAS Q61 and PI3K-AKT pathway genes as drivers of breast adenomyoepitheliomas. Nature Communications *9*, 1816.

Gimple, R.C., and Wang, X. (2019). RAS: Striking at the Core of the Oncogenic Circuitry . Frontiers in Oncology *9*, 965.

Glenn, S.T., Jones, C.A., Sexton, S., LeVea, C.M., Caraker, S.M., Hajduczok, G., and Gross, K.W. (2014). Conditional deletion of p53 and Rb in the renin-expressing compartment of the pancreas leads to a highly penetrant metastatic pancreatic neuroendocrine carcinoma. Oncogene *33*, 5706–5715.

Golan, T., Hammel, P., Reni, M., Van Cutsem, E., Macarulla, T., Hall, M.J., Park, J.-O., Hochhauser, D., Arnold, D., Oh, D.-Y., et al. (2019). Maintenance Olaparib for Germline BRCA-Mutated Metastatic Pancreatic Cancer. New England Journal of Medicine *381*, 317–327.

Goldberg, A.D., Banaszynski, L.A., Noh, K.-M., Lewis, P.W., Elsaesser, S.J., Stadler, S., Dewell, S., Law, M., Guo, X., Li, X., et al. (2010). Distinct Factors Control Histone Variant H3.3 Localization at Specific Genomic Regions. Cell *140*, 678–691.

Gu, Z., Eils, R., and Schlesner, M. (2016). Complex heatmaps reveal patterns and correlations in multidimensional genomic data. Bioinformatics *32*, 2847–2849.

Guinney, J., and Castelo, R. (2019). GSVA: Gene Set Variation Analysis for microarray and RNA-seq data.

Guinney, J., Dienstmann, R., Wang, X., de Reyniès, A., Schlicker, A., Soneson, C., Marisa, L., Roepman, P., Nyamundanda, G., Angelino, P., et al. (2015). The consensus molecular subtypes of colorectal cancer. Nature Medicine *21*, 1350–1356.

Günther, T., Tulipano, G., Dournaud, P., Bousquet, C., Csaba, Z., Kreienkamp, H.-J., Lupp, A., Korbonits, M., Castaño, J.P., Wester, H.-J., et al. (2018). International Union of Basic and Clinical Pharmacology. CV. Somatostatin Receptors: Structure, Function, Ligands, and New Nomenclature. Pharmacological Reviews *70*, 763 LP – 835.

Guru, S.C., Goldsmith, P.K., Burns, A.L., Marx, S.J., Spiegel, A.M., Collins, F.S., and Chandrasekharappa, S.C. (1998). Menin, the product of the MEN1 gene, is a nuclear protein. Proceedings of the National Academy of Sciences *95*, 1630 LP – 1634.

Ha, G., Roth, A., Lai, D., Bashashati, A., Ding, J., Goya, R., Giuliany, R., Rosner, J., Oloumi, A., Shumansky, K., et al. (2012). Integrative analysis of genome-wide loss of heterozygosity and monoallelic expression at nucleotide resolution reveals disrupted pathways in triple-negative breast cancer. Genome Research *22*, 1995–2007.

Hackeng, W.M., Brosens, L.A.A., Kim, J.Y., O'Sullivan, R., Sung, Y.-N., Liu, T.-C., Cao, D., Heayn, M., Brosnan-Cashman, J., An, S., et al. (2021). Non-functional pancreatic neuroendocrine tumours: ATRX/DAXX and alternative lengthening of telomeres (ALT) are prognostically independent from ARX/PDX1 expression and tumour size. Gut gutjnl-2020-322595.

Haile, S., Pandoh, P., McDonald, H., Corbett, R.D., Tsao, P., Kirk, H., MacLeod, T., Jones, M., Bilobram, S., Brooks, D., et al. (2017). Automated high throughput nucleic acid purification from formalin-fixed paraffin-embedded tissue samples for next generation sequence analysis. PloS One *12*, e0178706.

Haile, S., Corbett, R.D., Bilobram, S., Bye, M.H., Kirk, H., Pandoh, P., Trinh, E., MacLeod, T., McDonald, H., Bala, M., et al. (2018). Sources of erroneous sequences and artifact chimeric reads in next generation sequencing of genomic DNA from formalin-fixed paraffin-embedded samples. Nucleic Acids Research *47*, e12–e12.

Halfdanarson, T.R., Rabe, K.G., Rubin, J., Petersen, G.M., Farnell, M.B., Grant, C.S., and Petersen, G.M. (2008). Pancreatic endocrine neoplasms: Epidemiology and prognosis of pancreatic endocrine tumors. Endocrine-Related Cancer *15*, 409–427.

Hallet, J., Law, C.H.L., Cukier, M., Saskin, R., Liu, N., and Singh, S. (2015). Exploring the rising incidence of neuroendocrine tumors: A population-based analysis of epidemiology, metastatic presentation, and outcomes. Cancer *121*, 589–597.

Halperin, D.M., Shen, C., Dasari, A., Xu, Y., Chu, Y., Zhou, S., Shih, Y.-C.T., and Yao, J.C. (2017). Frequency of carcinoid syndrome at neuroendocrine tumour diagnosis: a population-based study. The Lancet Oncology *18*, 525–534.

Hammel, P.R., Vilgrain, V., Terris, B., Penfornis, A., Sauvanet, A., Correas, J., Chauveau, D., Balian, A., Beigelman, C., O'Toole, D., et al. (2000). Pancreatic involvement in von Hippel-Lindau disease. Gastroenterology *119*, 1087–1095.

Hanahan, D. (1985). Heritable formation of pancreatic beta-cell tumours in transgenic mice expressing recombinant insulin/simian virus 40 oncogenes. Nature *315*, 115–122.

Hanahan, D., and Folkman, J. (1996). Patterns and Emerging Mechanisms of the Angiogenic Switch during Tumorigenesis. Cell *86*, 353–364.

Hanahan, D., and Weinberg, R.A. (2000). The Hallmarks of Cancer. Cell *100*, 57–70.

Hanahan, D., and Weinberg, R.A. (2011). Hallmarks of cancer: The next generation. Cell *144*, 646–674.

Hansen, C.G., Moroishi, T., and Guan, K.-L. (2015). YAP and TAZ: a nexus for Hippo signaling and beyond. Trends in Cell Biology *25*, 499–513.

Hänzelmann, S., Castelo, R., and Guinney, J. (2013). GSVA: Gene set variation analysis for microarray and RNA-Seq data. BMC Bioinformatics *14*.

Heaphy, C.M., de Wilde, R.F., Jiao, Y., Klein, A.P., Edil, B.H., Shi, C., Bettegowda, C., Rodriguez, F.J., Eberhart, C.G., Hebbar, S., et al. (2011). Altered telomeres in tumors with ATRX and DAXX mutations. Science (New York, N.Y.) *333*, 425.

Hegi, M.E., Diserens, A.-C., Gorlia, T., Hamou, M.-F., de Tribolet, N., Weller, M., Kros, J.M., Hainfellner, J.A., Mason, W., Mariani, L., et al. (2005). MGMT gene silencing and benefit from temozolomide in glioblastoma. The New England Journal of Medicine *352*, 997–1003.

Heitz, P.U., Komminoth, P., Perren, A., Klimstra, D.S., and Dayal, Y. (2004). Pathology and genetic:tumors of endocrine organs. In WHO Classification of Tumors, R.A. DeLellis, R. V Lloyd, P.U. Heitz, and C. Eng, eds. (Lyon, France: IARC Press), pp. 177–182.

Hensley, C.T., Wasti, A.T., and DeBerardinis, R.J. (2013). Glutamine and cancer: cell biology, physiology, and clinical opportunities. The Journal of Clinical Investigation *123*, 3678–3684.

Hermans, B.C.M., de Vos-Geelen, J., Derks, J.L., Latten, L., Liem, I.H., van der Zwan, J.M., Speel, E.-J.M., Dercksen, M.W., and Dingemans, A.-M.C. (2020). Unique Metastatic Patterns in Neuroendocrine Neoplasms of Different Primary Origin. Neuroendocrinology.

Hicks, R.J., Kwekkeboom, D.J., Krenning, E., Bodei, L., Grozinsky-Glasberg, S., Arnold, R., Borbath, I., Cwikla, J., Toumpanakis, C., Kaltsas, G., et al. (2017). ENETS Consensus Guidelines for the Standards of Care in Neuroendocrine Neoplasia: Peptide Receptor Radionuclide Therapy with Radiolabeled Somatostatin Analogues. Neuroendocrinology.

Hofland, J., Kaltsas, G., and de Herder, W.W. (2020a). Advances in the Diagnosis and Management of Well-Differentiated Neuroendocrine Neoplasms. Endocrine Reviews *41*, 371–403.

Hofland, J., Kaltsas, G., and De Herder, W.W. (2020b). Advances in the diagnosis and management of well-differentiated neuroendocrine neoplasms. Endocrine Reviews *41*, 371–403.

Hofving, T., Arvidsson, Y., Almobarak, B., Inge, L., Pfragner, R., Persson, M., Stenman, G., Kristiansson, E., Johanson, V., and Nilsson, O. (2018). The neuroendocrine phenotype, genomic profile and therapeutic sensitivity of GEPNET cell lines. Endocrine-Related Cancer *25*, 367–380.

Hong, X., Qiao, S., Li, F., Wang, W., Jiang, R., Wu, H., Chen, H., Liu, L., Peng, J., Wang, J., et al. (2020). Whole-genome sequencing reveals distinct genetic bases for insulinomas and non-functional pancreatic neuroendocrine tumours: leading to a new classification system. Gut *69*, 877 LP – 887.

Huang, J., and Manning, B.D. (2008). The TSC1-TSC2 complex: a molecular switchboard controlling cell growth. The Biochemical Journal *412*, 179–190.

Huang, M., and Weiss, W.A. (2013). Neuroblastoma and MYCN. Cold Spring Harbor Perspectives in Medicine *3*, a014415.

Huber, W., von Heydebreck, A., Sueltmann, H., Poustka, A., and Vingron, M. (2002). Variance Stabilization Applied to Microarray Data Calibration and to the Quantification of Differential Expression. Bioinformatics *18 Suppl.*, S96–S104.

Huber, W., with contributions from Anja von Heydebreck. Many comments, suggestions by users are acknowledged, among them Dennis Kostka, Kreil, D., Klein, H.-U., Gentleman, R., Sarkar, D., and Smyth, G. (2019). vsn: Variance stabilization and calibration for microarray data.

Hughes, C.S., Foehr, S., Garfield, D.A., Furlong, E.E., Steinmetz, L.M., and Krijgsveld, J. (2014). Ultrasensitive proteome analysis using paramagnetic bead technology. Molecular Systems Biology *10*, 757.

Hughes, C.S., McConechy, M.K., Cochrane, D.R., Nazeran, T., Karnezis, A.N., Huntsman, D.G., and Morin, G.B. (2016). Quantitative Profiling of Single Formalin Fixed Tumour Sections: proteomics for translational research. Scientific Reports *6*, 34949.

Hughes, C.S., Sorensen, P.H., and Morin, G.B. (2019). A Standardized and Reproducible Proteomics Protocol for Bottom-Up Quantitative Analysis of Protein Samples Using SP3 and Mass Spectrometry. Methods in Molecular Biology (Clifton, N.J.) *1959*, 65–87.

Imhof, A., Brunner, P., Marincek, N., Briel, M., Schindler, C., Rasch, H., Mäcke, H.R., Rochlitz, C., Müller-Brand, J., and Walter, M.A. (2011). Response, Survival, and Long-Term Toxicity After Therapy With the Radiolabeled Somatostatin Analogue [90Y-DOTA]-TOC in Metastasized Neuroendocrine Cancers. Journal of Clinical Oncology *29*, 2416–2423.

Inzani, F., Petrone, G., and Rindi, G. (2018). The New World Health Organization Classification for Pancreatic Neuroendocrine Neoplasia. Endocrinology and Metabolism Clinics of North America *47*, 463–470.

Ionescu-Tirgoviste, C., Gagniuc, P.A., Gubceac, E., Mardare, L., Popescu, I., Dima, S., and Militaru, M. (2015). A 3D map of the islet routes throughout the healthy human pancreas. Scientific Reports *5*, 14634.

Ireland, A.S., Micinski, A.M., Kastner, D.W., Guo, B., Wait, S.J., Spainhower, K.B., Conley, C.C., Chen, O.S., Guthrie, M.R., Soltero, D., et al. (2020). MYC Drives Temporal Evolution of Small Cell Lung Cancer Subtypes by Reprogramming Neuroendocrine Fate. Cancer Cell *38*, 60-78.e12.

Ito, T., Igarashi, H., and Jensen, R.T. (2012). Pancreatic neuroendocrine tumors: Clinical features, diagnosis and medical treatment: Advances. Best Practice and Research: Clinical Gastroenterology *26*, 737–753.

Jass, J.R., Sobin, L.H., and Watanabe, H. (1990). The World Health Organization's histologic classification of gastrointestinal tumors. A commentary on the second edition. Cancer *66*, 2162–2167.

Jennings, R.E., Berry, A.A., Kirkwood-Wilson, R., Roberts, N.A., Hearn, T., Salisbury, R.J., Blaylock, J., Piper Hanley, K., and Hanley, N.A. (2013). Development of the Human Pancreas From Foregut to Endocrine Commitment. Diabetes *62*, 3514 LP – 3522.

Jensen, R.T., Berna, M.J., Bingham, D.B., and Norton, J.A. (2008). Inherited pancreatic endocrine tumor syndromes: advances in molecular pathogenesis, diagnosis, management, and controversies. Cancer *113*, 1807–1843.

Jewell, J.L., Kim, Y.C., Russell, R.C., Yu, F.-X., Park, H.W., Plouffe, S.W., Tagliabracci, V.S., and Guan, K.-L. (2015). Differential regulation of mTORC1 by leucine and glutamine. Science *347*, 194 LP – 198.

Jiang, L., Wang, M., Lin, S., Jian, R., Li, X., Chan, J., Dong, G., Fang, H., Robinson, A.E., Snyder, M.P., et al. (2020). A Quantitative Proteome Map of the Human Body. Cell 269–283.

Jiao, Y., Shi, C., Edil, B.H., de Wilde, R.F., Klimstra, D.S., Maitra, A., Schulick, R.D., Tang, L.H., Wolfgang, C.L., Choti, M.A., et al. (2011). DAXX/ATRX, MEN1, and mTOR pathway genes are frequently altered in pancreatic neuroendocrine tumors. Science (New York, N.Y.) *331*, 1199–1203.

Juhász, S., Elbakry, A., Mathes, A., and Löbrich, M. (2018). ATRX Promotes DNA Repair Synthesis and Sister Chromatid Exchange during Homologous Recombination. Molecular Cell *71*, 11-24.e7.

Karczewski, K.J., Francioli, L.C., Tiao, G., Cummings, B.B., Alföldi, J., Wang, Q., Collins, R.L., Laricchia, K.M., Ganna, A., Birnbaum, D.P., et al. (2020). The mutational constraint spectrum quantified from variation in 141,456 humans. Nature *581*, 434–443.

Karnik, S.K., Hughes, C.M., Gu, X., Rozenblatt-Rosen, O., McLean, G.W., Xiong, Y., Meyerson, M., and Kim, S.K. (2005). Menin regulates pancreatic islet growth by promoting histone methylation and expression of genes encoding p27^{Kip1} and p18^{INK4c} Proceedings of the National Academy of Sciences of the United States of America *102*, 14659 LP – 14664.

Karpathakis, A., Dibra, H., Pipinikas, C., Feber, A., Morris, T., Francis, J., Oukrif, D., Mandair, D., Pericleous, M., Mohmaduvesh, M., et al. (2016). Prognostic impact of novel molecular subtypes of small intestinal neuroendocrine tumor. Clinical Cancer Research *22*, 250–258.

Kasajima, A., Yazdani, S., and Sasano, H. (2015). Pathology diagnosis of pancreatic neuroendocrine tumors. Journal of Hepato-Biliary-Pancreatic Sciences *22*, 586–593.

Keenan, A.B., Torre, D., Lachmann, A., Leong, A.K., Wojciechowicz, M.L., Utti, V., Jagodnik, K.M., Kropiwnicki, E., Wang, Z., and Ma'ayan, A. (2019). ChEA3: transcription factor enrichment analysis by orthogonal omics integration. Nucleic Acids Research *47*, W212–W224.

Kim, D.-W., Wu, N., Kim, Y.-C., Cheng, P.F., Basom, R., Kim, D., Dunn, C.T., Lee, A.Y., Kim, K., Lee, C.S., et al. (2016). Genetic requirement for Mycl and efficacy of RNA Pol I inhibition in mouse models of small cell lung cancer. Genes & Development *30*, 1289–1299.

Kim, J., Kim, Y.H., Kim, J., Park, D.Y., Bae, H., Lee, D.-H., Kim, K.H., Hong, S.P., Jang, S.P., Kubota, Y., et al. (2017a). YAP/TAZ regulates sprouting angiogenesis and vascular barrier maturation. The Journal of Clinical Investigation *127*, 3441–3461.

Kim, J.Y., Brosnan-Cashman, J.A., An, S., Kim, S.J., Song, K.-B., Kim, M.-S., Kim, M.-J., Hwang, D.W., Meeker, A.K., Yu, E., et al. (2017b). Alternative Lengthening of Telomeres in Primary Pancreatic Neuroendocrine Tumors Is Associated with Aggressive Clinical Behavior and Poor Survival. Clinical Cancer Research *23*, 1598 LP – 1606.

Kleihues, P., and Sobin, L.H. (2000). World Health Organization classification of tumors. Cancer *88*, 2887.

Kobayashi, S., Contractor, T., Vosburgh, E., Du, Y.-C.N., Tang, L.H., Clausen, R., and Harris, C.R. (2019). Alleles of Insm1 determine whether RIP1-Tag2 mice produce insulinomas or nonfunctioning pancreatic neuroendocrine tumors. Oncogenesis *8*, 16.

Komori, Y., Yada, K., Ohta, M., Uchida, H., Iwashita, Y., Fukuzawa, K., Kashima, K., Yokoyama, S., Inomata, M., and Kitano, S. (2014). Mammalian target of rapamycin signaling activation patterns in pancreatic neuroendocrine tumors. Journal of Hepato-Biliary-Pancreatic Sciences *21*, 288–295.

Krämer, A., Green, J., Pollard, J., and Tugendreich, S. (2014). Causal analysis approaches in Ingenuity Pathway Analysis. Bioinformatics *30*, 523–530.

Kulke, M.H., Hornick, J.L., Frauenhoffer, C., Hooshmand, S., Ryan, D.P., Enzinger, P.C., Meyerhardt, J.A., Clark, J.W., Stuart, K., Fuchs, C.S., et al. (2009). O6-methylguanine DNA methyltransferase deficiency and response to temozolomide-based therapy in patients with neuroendocrine tumors. Clinical Cancer Research : An Official Journal of the American Association for Cancer Research *15*, 338–345.

Kulke, M.H., Anthony, L.B., Bushnell, Þ.D.L., Herder, W.W. De, Goldsmith, S.J., Klimstra, D.S., Marx, S.J., and Pasieka, L.J.L. (2010a). NANETS Treatment Guidelines of the Stomach and Pancreas. Pancreas *39*, 735–752.

Kulke, M.H., Anthony, L.B., Bushnell, D.L., de Herder, W.W., Goldsmith, S.J., Klimstra, D.S., Marx, S.J., Pasieka, J.L., Pommier, R.F., Yao, J.C., et al. (2010b). NANETS Treatment Guidelines: Well-Differentiated Neuroendocrine Tumors of the Stomach and Pancreas. Pancreas *39*.

Kulke, M.H., Siu, L.L., Tepper, J.E., Fisher, G., Jaffe, D., Haller, D.G., Ellis, L.M., Benedetti, J.K., Bergsland, E.K., Hobday, T.J., et al. (2011). Future directions in the treatment of neuroendocrine tumors: Consensus report of the National Cancer Institute Neuroendocrine Tumor Clinical Trials Planning Meeting. Journal of Clinical Oncology *29*, 934–943.

Kunz, P.L. (2015). Carcinoid and neuroendocrine tumors: building on success. Journal of Clinical Oncology : Official Journal of the American Society of Clinical Oncology *33*, 1855–1863.

Kunz, P.L., Catalano, P.J., Nimeiri, H., Fisher, G.A., Longacre, T.A., Suarez, C.J., Yao, J.C., Kulke, M.H., Hendifar, A.E., Shanks, J.C., et al. (2018). A randomized study of temozolomide or temozolomide and capecitabine in patients with advanced pancreatic neuroendocrine tumors: A trial of the ECOG-ACRIN Cancer Research Group (E2211). Journal of Clinical Oncology *36*, 4004.

Kvols, L.K., Buck, M., Moertel, C.G., Schutt, A.J., Rubin, J., O'Connell, M.J., and Hahn, R.G. (1987). Treatment of metastatic islet cell carcinoma with a somatostatin analogue (SMS 201-995). Annals of Internal Medicine *107*, 162–168.

Lakis, V., Lawlor, R.T., Newell, F., Patch, A.-M., Mafficini, A., Sadanandam, A., Koufariotis, L.T., Johnston, R.L., Leonard, C., Wood, S., et al. (2021). DNA methylation patterns identify subgroups of pancreatic neuroendocrine tumors with clinical association. Communications Biology *4*, 155.

Lamberts, S.W., van der Lely, A.J., de Herder, W.W., and Hofland, L.J. (1996). Octreotide. The New England Journal of Medicine *334*, 246–254.

Larson, A.M., Hedgire, S.S., Deshpande, V., Stemmer-Rachamimov, A.O., Harisinghani, M.G., Ferrone, C.R., Shah, U., and Thiele, E.A. (2012). Pancreatic neuroendocrine tumors in patients with tuberous sclerosis complex. Clinical Genetics *82*, 558–563.

Laskin, J., Jones, S., Aparicio, S., Chia, S., Ch'ng, C., Deyell, R., Eirew, P., Fok, A., Gelmon, K., Ho, C., et al. (2015). Lessons learned from the application of whole-genome analysis to the treatment of patients with advanced cancers. Cold Spring Harbor Molecular Case Studies *1*, a000570–a000570.

Lawrence, B., Blenkiron, C., Parker, K., Tsai, P., Fitzgerald, S., Shields, P., Robb, T., Yeong, M.L., Kramer, N., James, S., et al. (2018). Recurrent loss of heterozygosity correlates with clinical outcome in pancreatic neuroendocrine cancer. Npj Genomic Medicine *3*.

Lee, J.K., Phillips, J.W., Smith, B.A., Park, J.W., Stoyanova, T., McCaffrey, E.F., Baertsch, R., Sokolov, A., Meyerowitz, J.G., Mathis, C., et al. (2016). N-Myc Drives Neuroendocrine Prostate Cancer Initiated from Human Prostate Epithelial Cells. Cancer Cell *29*, 536–547.

Leek, J.T., Johnson, W.E., Parker, H.S., Fertig, E.J., Jaffe, A.E., Storey, J.D., Zhang, Y., and Torres, L.C. (2019). sva: Surrogate Variable Analysis.

Lei, Q.-Y., Zhang, H., Zhao, B., Zha, Z.-Y., Bai, F., Pei, X.-H., Zhao, S., Xiong, Y., and Guan, K.-L. (2008). TAZ Promotes Cell Proliferation and Epithelial-Mesenchymal Transition and Is Inhibited by the Hippo Pathway. Molecular and Cellular Biology *28*, 2426 LP – 2436.

Lewis, P.W., Elsaesser, S.J., Noh, K.-M., Stadler, S.C., and Allis, C.D. (2010). Daxx is an H3.3-specific histone chaperone and cooperates with ATRX in replication-independent chromatin assembly at telomeres. Proceedings of the National Academy of Sciences of the United States of America *107*, 14075–14080.

Li, H., and Durbin, R. (2009). Fast and accurate short read alignment with Burrows-Wheeler transform. Bioinformatics (Oxford, England) *25*, 1754–1760.

Li, D., Rock, A., Kessler, J., Ballena, R., Hyder, S., Mo, C., Chang, S., and Singh, G. (2020). Understanding the Management and Treatment of Well-Differentiated Pancreatic Neuroendocrine Tumors: A Clinician's Guide to a Complex Illness. JCO Oncology Practice *16*, 720–728.

Li, H., Handsaker, B., Wysoker, A., Fennell, T., Ruan, J., Homer, N., Marth, G., Abecasis, G., and Durbin, R. (2009). The Sequence Alignment/Map format and SAMtools. Bioinformatics *25*, 2078–2079.

Liao, Y., Smyth, G.K., and Shi, W. (2013). featureCounts: an efficient general purpose program for assigning sequence reads to genomic features. Bioinformatics *30*, 923–930.

Liberzon, A., Birger, C., Thorvaldsdóttir, H., Ghandi, M., Mesirov, J.P., and Tamayo, P. (2015). The Molecular Signatures Database Hallmark Gene Set Collection. Cell Systems *1*, 417–425.

Lichtenauer, U.D., Di Dalmazi, G., Slater, E.P., Wieland, T., Kuebart, A., Schmittfull, A., Schwarzmayr, T., Diener, S., Wiese, D., Thasler, W.E., et al. (2015). Frequency and Clinical Correlates of Somatic Ying Yang 1 Mutations in Sporadic Insulinomas. The Journal of Clinical Endocrinology & Metabolism *100*, E776–E782.

Liu-Chittenden, Y., Huang, B., Shim, J.S., Chen, Q., Lee, S.-J., Anders, R.A., Liu, J.O., and Pan, D. (2012). Genetic and pharmacological disruption of the TEAD-YAP complex suppresses the oncogenic activity of YAP. Genes & Development *26*, 1300–1305.

Lloyd, R. V, Osamura, R.Y., Kloppel, G., and Rosai, J. (2017). WHO Classification of Tumours of Endocrine Organs (IARC Press).

Lopez, T., and Hanahan, D. (2002). Elevated levels of IGF-1 receptor convey invasive and metastatic capability in a mouse model of pancreatic islet tumorigenesis. Cancer Cell *1*, 339–353.

Lowman, X.H., Hanse, E.A., Yang, Y., Ishak Gabra, M.B., Tran, T.Q., Li, H., and Kong, M. (2019). p53 Promotes Cancer Cell Adaptation to Glutamine Deprivation by Upregulating Slc7a3 to Increase Arginine Uptake. Cell Reports *26*, 3051-3060.e4.

Lubensky, I.A., Pack, S., Ault, D., Vortmeyer, A.O., Libutti, S.K., Choyke, P.L., Walther, M.M., Linehan, W.M., and Zhuang, Z. (1998). Multiple neuroendocrine tumors of the pancreas in von Hippel-Lindau disease patients: histopathological and molecular genetic analysis. The American Journal of Pathology *153*, 223–231.

Luo, W., Friedman, M.S., Shedden, K., Hankenson, K.D., and Woolf, P.J. (2009). GAGE: generally applicable gene set enrichment for pathway analysis. BMC Bioinformatics *10*, 161.

Mafficini, A., and Scarpa, A. (2019). Genetics and Epigenetics of Gastroenteropancreatic Neuroendocrine Neoplasms. Endocrine Reviews *40*, 506–536.

Marinoni, I., Kurrer, A.S., Vassella, E., Dettmer, M., Rudolph, T., Banz, V., Hunger, F., Pasquinelli, S., Speel, E.-J.J., and Perren, A. (2014). Loss of DAXX and ATRX are associated with chromosome instability and reduced survival of patients with pancreatic neuroendocrine tumors. Gastroenterology *146*, 453-460.e5.

Marshall, A.E., Roes, M. V, Passos, D.T., DeWeerd, M.C., Chaikovsky, A.C., Sage, J., Howlett, C.J., and Dick, F.A. (2019). RB1 Deletion in Retinoblastoma Protein Pathway-Disrupted Cells Results in DNA Damage and Cancer Progression. Molecular and Cellular Biology *39*, e00105-19.

Martínez-Reyes, I., and Chandel, N.S. (2020). Mitochondrial TCA cycle metabolites control physiology and disease. Nature Communications *11*, 102.

Mertins, P., Mani, D.R., Ruggles, K. V., Gillette, M.A., Clauser, K.R., Wang, P., Wang, X., Qiao, J.W., Cao, S., Petralia, F., et al. (2016). Proteogenomics connects somatic mutations to signalling in breast cancer. Nature *534*, 55–62.

Missiaglia, E., Dalai, I., Barbi, S., Beghelli, S., Falconi, M., Della Peruta, M., Piemonti, L., Capurso, G., Di Florio, A., Delle Fave, G., et al. (2010). Pancreatic endocrine tumors: Expression profiling evidences a role for AKT-mTOR pathway. Journal of Clinical Oncology *28*, 245–255.

Miyoshi, T., Umemura, S., Matsumura, Y., Mimaki, S., Tada, S., Makinoshima, H., Ishii, G., Udagawa, H., Matsumoto, S., Yoh, K., et al. (2017). Genomic Profiling of Large-Cell Neuroendocrine Carcinoma of the Lung. Clinical Cancer Research : An Official Journal of the American Association for Cancer Research *23*, 757–765.

Modlin, I.M., Shapiro, M.D., and Kidd, M. (2004). Siegfried oberndorfer: Origins and perspectives of carcinoid tumors. Human Pathology *35*, 1440–1451.

Modlin, I.M., Oberg, K., Chung, D.C., Jensen, R.T., de Herder, W.W., Thakker, R. V, Caplin, M., Delle Fave, G., Kaltsas, G.A., Krenning, E.P., et al. (2008). Gastroenteropancreatic neuroendocrine tumours. The Lancet. Oncology *9*, 61–72.

Moertel, C.G., Kvols, L.K., O'Connell, M.J., and Rubin, J. (1991). Treatment of neuroendocrine carcinomas with combined etoposide and cisplatin. Evidence of major therapeutic activity in the anaplastic variants of these neoplasms. Cancer *68*, 227–232.

Moertel, C.G., Lefkopoulo, M., Lipsitz, S., Hahn, R.G., and Klaassen, D. (1992). Streptozocin-doxorubicin, streptozocin-fluorouracil or chlorozotocin in the treatment of advanced islet-cell carcinoma. The New England Journal of Medicine *326*, 519–523.

Moore, A.R., Rosenberg, S.C., McCormick, F., and Malek, S. (2020). RAS-targeted therapies: is the undruggable drugged? Nature Reviews Drug Discovery *19*, 533–552.

Muñoz-Maldonado, C., Zimmer, Y., and Medová, M. (2019). A Comparative Analysis of Individual RAS Mutations in Cancer Biology . Frontiers in Oncology *9*, 1088.

Muraro, M.J., Dharmadhikari, G., Grün, D., Groen, N., Dielen, T., Jansen, E., van Gurp, L., Engelse, M.A., Carlotti, F., de Koning, E.J.P., et al. (2016). A Single-Cell Transcriptome Atlas of the Human Pancreas. Cell Systems *3*, 385–394.

Muzny, D.M., Bainbridge, M.N., Chang, K., Dinh, H.H., Drummond, J.A., Fowler, G., Kovar, C.L., Lewis, L.R., Morgan, M.B., Newsham, I.F., et al. (2012). Comprehensive molecular characterization of human colon and rectal cancer. Nature *487*, 330–337.

Nagano, Y., Kim, D.H., Zhang, L., White, J.A., Yao, J.C., Hamilton, S.R., and Rashid, A. (2007). Allelic alterations in pancreatic endocrine tumors identified by genome-wide single nucleotide polymorphism analysis. Endocrine-Related Cancer Endocr Relat Cancer *14*, 483–492.

Nagtegaal, I.D., Odze, R.D., Klimstra, D., Paradis, V., Rugge, M., Schirmacher, P., Washington, K.M., Carneiro, F., Cree, I.A., and Board, the W.H.O.C. of T.E. (2020). The 2019 WHO classification of tumours of the digestive system. Histopathology *76*, 182–188.

Nau, M.M., Brooks, B.J., Battey, J., Sausville, E., Gazdar, A.F., Kirsch, I.R., McBride, O.W., Bertness, V., Hollis, G.F., and Minna, J.D. (1985). L-myc, a new myc-related gene amplified and expressed in human small cell lung cancer. Nature *318*, 69–73.

Neto, F., Klaus-Bergmann, A., Ong, Y.T., Alt, S., Vion, A.-C., Szymborska, A., Carvalho, J.R., Hollfinger, I., Bartels-Klein, E., Franco, C.A., et al. (2018). YAP and TAZ regulate adherens junction dynamics and endothelial cell distribution during vascular development. ELife *7*, e31037.

Newman, A.M., Liu, C.L., Green, M.R., Gentles, A.J., Feng, W., Xu, Y., Hoang, C.D., Diehn, M., and Alizadeh, A.A. (2015). Robust enumeration of cell subsets from tissue expression profiles. Nature Methods *12*, 453–457.

Nicklin, P., Bergman, P., Zhang, B., Triantafellow, E., Wang, H., Nyfeler, B., Yang, H., Hild, M., Kung, C., Wilson, C., et al. (2009). Bidirectional Transport of Amino Acids Regulates mTOR and Autophagy. Cell *136*, 521–534.

Niederle, M.B., Hackl, M., Kaserer, K., and Niederle, B. (2010). Gastroenteropancreatic neuroendocrine tumours: the current incidence and staging based on the WHO and European Neuroendocrine Tumour Society classification: an analysis based on prospectively collected parameters. Endocrine-Related Cancer *17*, 909–918.

O'Toole, D., Ducreux, M., Bommelaer, G., Wemeau, J.L., Bouché, O., Catus, F., Blumberg, J., and Ruszniewski, P. (2000). Treatment of carcinoid syndrome: a prospective crossover evaluation of lanreotide versus octreotide in terms of efficacy, patient acceptability, and tolerance. Cancer *88*, 770–776.

Oberndorfer, S. (1907). Karzinoide tumoren des dónndarms. Frankfurt Z Path *1*, 426–432.

Oka, S., Leon, J., Tsuchimoto, D., Sakumi, K., and Nakabeppu, Y. (2014). MUTYH, an adenine DNA glycosylase, mediates p53 tumor suppression via PARP-dependent cell death. Oncogenesis *3*, e121.

Olson, P., Lu, J., Zhang, H., Shai, A., Chun, M.G., Wang, Y., Libutti, S.K., Nakakura, E.K., Golub, T.R., and Hanahan, D. (2009). MicroRNA dynamics in the stages of tumorigenesis correlate with hallmark capabilities of cancer. Genes & Development *23*, 2152–2165.

Oronsky, B., Ma, P.C., Morgensztern, D., and Carter, C.A. (2017). Nothing But NET: A Review of Neuroendocrine Tumors and Carcinomas. Neoplasia (New York, N.Y.) *19*, 991–1002.

Ota, M., and Sasaki, H. (2008). Mammalian Tead proteins regulate cell proliferation and contact inhibition as transcriptional mediators of Hippo signaling. Development (Cambridge, England) *135*, 4059–4069.

Pàez-Ribes, M., Allen, E., Hudock, J., Takeda, T., Okuyama, H., Viñals, F., Inoue, M., Bergers, G., Hanahan, D., and Casanovas, O. (2009). Antiangiogenic Therapy Elicits Malignant Progression of Tumors to Increased Local Invasion and Distant Metastasis. Cancer Cell *15*, 220–231.

Pavlova, N.N., and Thompson, C.B. (2016). The Emerging Hallmarks of Cancer Metabolism. Cell Metabolism *23*, 27–47.

Perez-Riverol, Y., Csordas, A., Bai, J., Bernal-Llinares, M., Hewapathirana, S., Kundu, D.J., Inuganti, A., Griss, J., Mayer, G., Eisenacher, M., et al. (2019). The PRIDE database and related tools and resources in 2019: improving support for quantification data. Nucleic Acids Research *47*, D442–D450.

Perl, A.-K., Wilgenbus, P., Dahl, U., Semb, H., and Christofori, G. (1998). A causal role for E-cadherin in the transition from adenoma to carcinoma. Nature *392*, 190–193.

Pietras, K., and Hanahan, D. (2005). A Multitargeted, Metronomic, and Maximum-Tolerated Dose “Chemo-Switch” Regimen is Antiangiogenic, Producing Objective Responses and Survival Benefit in a Mouse Model of Cancer. Journal of Clinical Oncology *23*, 939–952.

Pipinikas, C.P., Berner, A.M., Sposito, T., and Thirlwell, C. (2019). The evolving (epi)genetic landscape of pancreatic neuroendocrine tumours. Endocrine-Related Cancer *26*, R519–R544.

Porta, C., Paglino, C., and Mosca, A. (2014). Targeting PI3K/Akt/mTOR Signaling in Cancer. Frontiers in Oncology *4*, 64.

Puissant, A., Frumm, S.M., Alexe, G., Bassil, C.F., Qi, J., Chanthery, Y.H., Nekritz, E.A., Zeid, R., Gustafson, W.C., Greninger, P., et al. (2013). Targeting MYCN in neuroblastoma by BET bromodomain inhibition. Cancer Discovery *3*, 308–323.

R Core Team (2020). R: A language and environment for statistical computing.

Raj, N., Shah, R., Stadler, Z., Mukherjee, S., Chou, J., Untch, B., Li, J., Kelly, V., Saltz, L.B., Mandelker, D., et al. (2018). Real-Time Genomic Characterization of Metastatic Pancreatic Neuroendocrine Tumors Has Prognostic Implications and Identifies Potential Germline Actionability. JCO Precision Oncology *2018*.

Raphael, B.J., Hruban, R.H., Aguirre, A.J., Moffitt, R.A., Yeh, J.J., Stewart, C., Robertson, A.G., Cherniack, A.D., Gupta, M., Getz, G., et al. (2017a). Integrated Genomic Characterization of Pancreatic Ductal Adenocarcinoma. Cancer Cell *32*, 185-203.e13.

Raphael, M.J., Chan, D.L., Law, C., and Singh, S. (2017b). Principles of diagnosis and management of neuroendocrine tumours. Cmaj *189*, E398–E404.

Rausch, T., Zichner, T., Schlattl, A., Stütz, A.M., Benes, V., and Korbel, J.O. (2012). DELLY: structural variant discovery by integrated paired-end and split-read analysis. Bioinformatics *28*, i333–i339.

Raymond, E., Dahan, L., Raoul, J.-L., Bang, Y.-J., Borbath, I., Lombard-Bohas, C., Valle, J., Metrakos, P., Smith, D., Vinik, A., et al. (2011). Sunitinib Malate for the Treatment of Pancreatic Neuroendocrine Tumors. New England Journal of Medicine *364*, 501–513.

Riazy, M., Kalloger, S.E., Sheffield, B.S., Peixoto, R.D., Li-Chang, H.H., Scudamore, C.H., Renouf, D.J., and Schaeffer, D.F. (2015). Mismatch repair status may predict response to adjuvant chemotherapy in resectable pancreatic ductal adenocarcinoma. Modern Pathology *28*, 1383–1389.

Rimmer, A., Phan, H., Mathieson, I., Iqbal, Z., Twigg, S.R.F., Wilkie, A.O.M., McVean, G., Lunter, G., and Consortium, W. (2014). Integrating mapping-, assembly- and haplotype-based approaches for calling variants in clinical sequencing applications. Nature Genetics *46*, 912–918.

Rindi, G., and Solcia, E. (2007). Endocrine hyperplasia and dysplasia in the pathogenesis of gastrointestinal and pancreatic endocrine tumors. Gastroenterology Clinics of North America *36*, 851–865, vi.

Rindi, G., Arnold, R., Bosman, F.T., and Capella, C. (2010). Nomenclature and classification of neuroendocrine neoplasms of the digestive system. In WHO Classification of Tumours of the Digestive System, F. Bosman, F. Carnerio, R. Hruban, and N. Theise, eds. (Lyon, France: IARC Press), pp. 13–14.

Rindi, G., Petrone, G., and Inzani, F. (2014). The 2010 WHO Classification of Digestive Neuroendocrine Neoplasms: a Critical Appraisal four years after Its Introduction. Endocrine Pathology *25*, 186–192.

Rindi, G., Klimstra, D.S., Abedi-Ardekani, B., Asa, S.L., Bosman, F.T., Brambilla, E., Busam, K.J., de Krijger, R.R., Dietel, M., El-Naggar, A.K., et al. (2018). A common classification framework for neuroendocrine neoplasms: an International Agency for Research on Cancer (IARC) and World Health Organization (WHO) expert consensus proposal. Modern Pathology *31*, 1770–1786.

Ritchie, M.E., Phipson, B., Wu, D., Hu, Y., Law, C.W., Shi, W., and Smyth, G.K. (2015). Limma powers differential expression analyses for RNA-sequencing and microarray studies. Nucleic Acids Research *43*, e47.

Rivera, B., Castellsague, E., Bah, I., van Kempen, L.C., and Foulkes, W.D. (2015). Biallelic NTHL1 Mutations in a Woman with Multiple Primary Tumors. The New England Journal of Medicine *373*, 1985–1986.

Robertson, G., Schein, J., Chiu, R., Corbett, R., Field, M., Jackman, S.D., Mungall, K., Lee, S., Okada, H.M., Qian, J.Q., et al. (2010). De novo assembly and analysis of RNA-seq data. Nat Meth *7*, 909–912.

Robinson, M.D., McCarthy, D.J., and Smyth, G.K. (2010). edgeR: a Bioconductor package for differential expression analysis of digital gene expression data. Bioinformatics *26*, 139–140.

Robson, M., Im, S.-A., Senkus, E., Xu, B., Domchek, S.M., Masuda, N., Delaloge, S., Li, W., Tung, N., Armstrong, A., et al. (2017). Olaparib for Metastatic Breast Cancer in Patients with a Germline BRCA Mutation. New England Journal of Medicine *377*, 523–533.

Roldo, C., Missiaglia, E., Hagan, J.P., Falconi, M., Capelli, P., Bersani, S., Calin, G.A., Volinia, S., Liu, C.-G.G., Scarpa, A., et al. (2006). MicroRNA expression abnormalities in pancreatic endocrine and acinar tumors are associated with distinctive pathologic features and clinical behavior. Journal of Clinical Oncology *24*, 4677–4684.

Roskoski, R.J. (2007). Sunitinib: a VEGF and PDGF receptor protein kinase and angiogenesis inhibitor. Biochemical and Biophysical Research Communications *356*, 323–328.

Sadanandam, A., Wullschleger, S., Lyssiotis, C.A., Grotzinger, C., Barbi, S., Bersani, S., Korner, J., Wafy, I., Mafficini, A., Lawlor, R.T., et al. (2015). A cross-species analysis in pancreatic neuroendocrine tumors reveals molecular subtypes with distinctive clinical, metastatic, developmental, and metabolic characteristics. Cancer Discovery *5*, 1296–1313.

Sangoi, A.R., Ohgami, R.S., Pai, R.K.R.K.R.K.R.K., Beck, A.H., McKenney, J.K., and Pai, R.K.R.K.R.K.R.K. (2011). PAX8 expression reliably distinguishes pancreatic well-differentiated neuroendocrine tumors from ileal and pulmonary well-differentiated neuroendocrine tumors and pancreatic acinar cell carcinoma. Modern Pathology : An Official Journal of the United States and Canadian Academy of Pathology, Inc *24*, 412–424.

Sankar, S., and Lessnick, S.L. (2011). Promiscuous partnerships in Ewing's sarcoma. Cancer Genetics *204*, 351–365.

Santos, R., Ursu, O., Gaulton, A., Bento, A.P., Donadi, R.S., Bologa, C.G., Karlsson, A., Al-Lazikani, B., Hersey, A., Oprea, T.I., et al. (2017). A comprehensive map of molecular drug targets. Nat Rev Drug Discov *16*, 19–34.

Saunders, C.T., Wong, W.S.W., Swamy, S., Becq, J., Murray, L.J., and Cheetham, R.K. (2012). Strelka: accurate somatic small-variant calling from sequenced tumor-normal sample pairs. Bioinformatics (Oxford, England) *28*, 1811–1817.

Scarpa, A., Chang, D.K., Nones, K., Corbo, V., Patch, A.-M., Bailey, P., Lawlor, R.T., Johns, A.L., Miller, D.K., Mafficini, A., et al. (2017). Whole-genome landscape of pancreatic neuroendocrine tumours. Nature *543*, 65–71.

Scott, A.T., Weitz, M., Breheny, P.J., Ear, P.H., Darbro, B., Brown, B.J., Braun, T.A., Li, G., Umesalma, S., Kaemmer, C.A., et al. (2020). Gene Expression Signatures Identify Novel Therapeutics for Metastatic Pancreatic Neuroendocrine Tumors. Clinical Cancer Research : An Official Journal of the American Association for Cancer Research *26*, 2011–2021.

Sheffield, B.S., Tinker, A. V, Shen, Y., Hwang, H., Li-Chang, H.H., Pleasance, E., Ch'ng, C., Lum, A., Lorette, J., McConnell, Y.J., et al. (2015). Personalized oncogenomics: clinical experience with malignant peritoneal mesothelioma using whole genome sequencing. PloS One *10*, e0119689.

Shih, H.P., Wang, A., and Sander, M. (2013). Pancreas Organogenesis: From Lineage Determination to Morphogenesis. Annual Review of Cell and Developmental Biology *29*, 81–105.

Shimura, M., Mizuma, M., Takadate, T., Katoh, Y., Suzuki, T., Iseki, M., Hata, T., Aoki, S., Suzuki, Y., Sakata, N., et al. (2018). A novel liver metastasis-correlated protein of pancreatic neuroendocrine neoplasm (PanNEN) discovered by proteomic analysis. Oncotarget *9*, 24291–24303.

Shinmura, K., Yamaguchi, S., Saitoh, T., Takeuchi-Sasaki, M., Kim, S.R., Nohmi, T., and Yokota, J. (2000). Adenine excisional repair function of MYH protein on the adenine:8-hydroxyguanine base pair in double-stranded DNA. Nucleic Acids Research *28*, 4912–4918.

Shorstova, T., Foulkes, W.D., and Witcher, M. (2021). Achieving clinical success with BET inhibitors as anti-cancer agents. British Journal of Cancer *124*, 1478–1490.

Shyr, C., Tarailo-Graovac, M., Gottlieb, M., Lee, J.J.Y., van Karnebeek, C., and Wasserman, W.W. (2014). FLAGS, frequently mutated genes in public exomes. BMC Medical Genomics *7*, 64.

Singhi, A.D., Liu, T.-C.C., Roncaioli, J.L., Cao, D., Zeh, H.J., Zureikat, A.H., Tsung, A., Marsh, J.W., Lee, K.K., Hogg, M.E., et al. (2017). Alternative Lengthening of Telomeres and Loss of DAXX/ATRX Expression Predicts Metastatic Disease and Poor Survival in Patients with Pancreatic Neuroendocrine Tumors. Clinical Cancer Research *23*, 600–609.

Skamene, T., Siu, L.L., Renouf, D.J., Laskin, J.J., Bedard, P.L., Jones, S.J.M., Ferrario, C., Whitlock, J., Petrie, J., Sullivan, P., et al. (2018). Canadian profiling and targeted agent utilization trial (CAPTUR/PM.1): A phase II basket precision medicine trial. Journal of Clinical Oncology *36*, TPS12127–TPS12127.

Skidmore, Z.L., Wagner, A.H., Lesurf, R., Campbell, K.M., Kunisaki, J., Griffith, O.L., and Griffith, M. (2016). GenVisR: Genomic Visualizations in R. Bioinformatics *32*, 3012–3014.

Smith, G., Bounds, R., Wolf, H., Steele, R.J.C., Carey, F.A., and Wolf, C.R. (2010a). Activating K-Ras mutations outwith “hotspot” codons in sporadic colorectal tumours - implications for personalised cancer medicine. British Journal of Cancer *102*, 693–703.

Smith, J., Mun Tho, L., Xu, N., and A. Gillespie, D. (2010b). Chapter 3 - The ATM–Chk2 and ATR–Chk1 Pathways in DNA Damage Signaling and Cancer. G.F. Vande Woude, and G.B.T.-A. in C.R. Klein, eds. (Academic Press), pp. 73–112.

Smyth, G., Hu, Y., Ritchie, M., Silver, J., Wettenhall, J., McCarthy, D., Wu, D., Shi, W., Phipson, B., Lun, A., et al. (2020). limma: Linear Models for Microarray Data.

Sobin, L.H. (1981). The international histological classification of tumours. Bulletin of the World Health Organization *59*, 813–819.

Sobin, L.H. (1989). International histological classification of tumours, second edition. Cancer *63*, 907.

Sondka, Z., Bamford, S., Cole, C.G., Ward, S.A., Dunham, I., and Forbes, S.A. (2018). The COSMIC Cancer Gene Census: describing genetic dysfunction across all human cancers. Nature Reviews Cancer *18*, 696–705.

Song, Y.L., Yu, R., Qiao, X.W., Bai, C.M., Lu, C.M., Xiao, Y., Zhong, D.R., Chen, J., Zhao, Y.P., Zhang, T.P., et al. (2017). Prognostic relevance of UCH-L1 and α-internexin in pancreatic neuroendocrine tumors. Scientific Reports *7*, 1–15.

Sorbye, H., Welin, S., Langer, S.W., Vestermark, L.W., Holt, N., Osterlund, P., Dueland, S., Hofsli, E., Guren, M.G., Ohrling, K., et al. (2013). Predictive and prognostic factors for treatment and survival in 305 patients with advanced gastrointestinal neuroendocrine carcinoma (WHO G3): The NORDIC NEC study. Annals of Oncology *24*, 152–160.

Sørlie, T., Perou, C.M., Tibshirani, R., Aas, T., Geisler, S., Johnsen, H., Hastie, T., Eisen, M.B., van de Rijn, M., Jeffrey, S.S., et al. (2001). Gene expression patterns of breast carcinomas distinguish tumor subclasses with clinical implications. Proceedings of the National Academy of Sciences of the United States of America *98*, 10869–10874.

Strosberg, J., El-Haddad, G., Wolin, E., Hendifar, A., Yao, J., Chasen, B., Mittra, E., Kunz, P.L., Kulke, M.H., Jacene, H., et al. (2017). Phase 3 Trial of 177Lu-Dotatate for Midgut Neuroendocrine Tumors. The New England Journal of Medicine *376*, 125–135.

Strosberg, J.R., Coppola, D., Klimstra, D.S., Phan, A.T., Kulke, M.H., Wiseman, G.A., and Kvols, L.K. (2010). The NANETS Consensus Guidelines for the Diagnosis and Management of Poorly Differentiated (High-Grade) Extrapulmonary Neuroendocrine Carcinomas. Pancreas *39*.

Takahashi, D., Kojima, M., Suzuki, T., Sugimoto, M., Kobayashi, S., Takahashi, S., Konishi, M., Gotohda, N., Ikeda, M., Nakatsura, T., et al. (2018). Profiling the Tumour Immune Microenvironment in Pancreatic Neuroendocrine Neoplasms with Multispectral Imaging Indicates Distinct Subpopulation Characteristics Concordant with WHO 2017 Classification. Scientific Reports *8*, 13166.

Tang, L.H., Contractor, T., Clausen, R., Klimstra, D.S., Du, Y.-C.N., Allen, P.J., Brennan, M.F., Levine, A.J., and Harris, C.R. (2012). Attenuation of the Retinoblastoma Pathway in Pancreatic Neuroendocrine Tumors Due to Increased Cdk4/Cdk6. Clinical Cancer Research *18*, 4612 LP – 4620.

Tang, L.H., Basturk, O., Sue, J.J., and Klimstra, D.S. (2016). A Practical Approach to the Classification of WHO Grade 3 (G3) Well-differentiated Neuroendocrine Tumor (WD-NET) and Poorly Differentiated Neuroendocrine Carcinoma (PD-NEC) of the Pancreas. The American Journal of Surgical Pathology *40*, 1192–1202.

Tarasov, A., Vilella, A.J., Cuppen, E., Nijman, I.J., and Prins, P. (2015). Sambamba: fast processing of NGS alignment formats. Bioinformatics (Oxford, England) *31*, 2032–2034.

Tarca, A.L., Draghici, S., Khatri, P., Hassan, S.S., Mittal, P., Kim, J., Kim, C.J., Kusanovic, J.P., and Romero, R. (2008). A novel signaling pathway impact analysis. Bioinformatics *25*, 75–82.

Tate, J.G., Bamford, S., Jubb, H.C., Sondka, Z., Beare, D.M., Bindal, N., Boutselakis, H., Cole, C.G., Creatore, C., Dawson, E., et al. (2018). COSMIC: the Catalogue Of Somatic Mutations In Cancer. Nucleic Acids Research *47*, D941–D947.

Teitelman, G., Alpert, S., and Hanahan, D. (1988). Proliferation, senescence, and neoplastic progression of beta cells in hyperplasic pancreatic islets. Cell *52*, 97–105.

Terracciano, F., Capone, A., Montori, A., Rinzivillo, M., Partelli, S., Panzuto, F., Pilozzi, E., Arcidiacono, P.G., Sette, C., and Capurso, G. (2020). MYC Upregulation Confers Resistance to Everolimus and Establishes Vulnerability to Cyclin-Dependent Kinase Inhibitors in Pancreatic Neuroendocrine Neoplasm Cells. Neuroendocrinology.

Tessier-Cloutier, B., Kalloger, S.E., Al-Kandari, M., Milne, K., Gao, D., Nelson, B.H., Renouf, D.J., Sheffield, B.S., and Schaeffer, D.F. (2017). Programmed cell death ligand 1 cut-point is associated with reduced disease specific survival in resected pancreatic ductal adenocarcinoma. BMC Cancer *17*, 618.

Thorslund, T., and West, S.C. (2007). BRCA2: a universal recombinase regulator. Oncogene *26*, 7720–7730.

Tolcher, A.W., Papadopoulos, K.P., Patnaik, A., Rasco, D.W., Martinez, D., Wood, D.L., Fielman, B., Sharma, M., Janisch, L.A., Brown, B.D., et al. (2015). Safety and activity of DCR-MYC, a first-in-class Dicer-substrate small interfering RNA (DsiRNA) targeting MYC, in a phase I study in patients with advanced solid tumors. Journal of Clinical Oncology *33*, 11006.

Tsukuda, K., Tanino, M., Soga, H., Shimizu, N., and Shimizu, K. (2000). A novel activating mutation of the K-ras gene in human primary colon adenocarcinoma. Biochemical and Biophysical Research Communications *278*, 653–658.

Vandamme, T., Peeters, M., Dogan, F., Pauwels, P., Van Assche, E., Beyens, M., Mortier, G., Vandeweyer, G., de Herder, W., Van Camp, G., et al. (2015). Whole-exome characterization of pancreatic neuroendocrine tumor cell lines BON-1 and QGP-1. Journal of Molecular Endocrinology *54*, 137–147.

Varelas, X. (2014). The Hippo pathway effectors TAZ and YAP in development, homeostasis and disease. Development *141*, 1614 LP – 1626.

Vigneswaran, K., Boyd, N.H., Oh, S.-Y., Lallani, S., Boucher, A., Neill, S.G., Olson, J.J., and Read, R.D. (2021). YAP/TAZ Transcriptional Coactivators Create Therapeutic Vulnerability to Verteporfin in EGFR-mutant Glioblastoma. Clinical Cancer Research : An Official Journal of the American Association for Cancer Research *27*, 1553–1569.

Vijayvergia, N., Boland, P.M., Handorf, E., Gustafson, K.S., Gong, Y., Cooper, H.S., Sheriff, F., Astsaturov, I., Cohen, S.J., and Engstrom, P.F. (2016). Molecular profiling of neuroendocrine malignancies to identify prognostic and therapeutic markers: a Fox Chase Cancer Center Pilot Study. British Journal of Cancer *115*, 1–7.

Vinik, A.I., Woltering, E.A., Warner, R.R.P., Caplin, M., O'Dorisio, T.M., Wiseman, G.A., Coppola, D., and Go, V.L.W. (2010). NANETS Consensus Guidelines for the Diagnosis of Neuroendocrine Tumor. Pancreas *39*.

Wang, H., Bender, A., Wang, P., Karakose, E., Inabnet, W.B., Libutti, S.K., Arnold, A., Lambertini, L., Stang, M., Chen, H., et al. (2017). Insights into beta cell regeneration for diabetes via integration of molecular landscapes in human insulinomas. Nature Communications *8*, 1–14.

Wang, S.-E., Su, C.-H., Kuo, Y.-J., Shyr, Y.-M., Li, A.F.-Y., Chen, T.-H., Wu, C.-W., and Lee, C.-H. (2011a). Comparison of functional and nonfunctional neuroendocrine tumors in the pancreas and peripancreatic region. Pancreas *40*, 253–259.

Wang, Y., Ozawa, A., Zaman, S., Prasad, N.B., Chandrasekharappa, S.C., Agarwal, S.K., and Marx, S.J. (2011b). The Tumor Suppressor Protein Menin Inhibits AKT Activation by Regulating Its Cellular Localization. Cancer Research *71*, 371 LP – 382.

Wang, Y., Xu, X., Maglic, D., Dill, M.T., Mojumdar, K., Ng, P.K.-S., Jeong, K.J., Tsang, Y.H., Moreno, D., Bhavana, V.H., et al. (2018). Comprehensive Molecular Characterization of the Hippo Signaling Pathway in Cancer. Cell Reports *25*, 1304-1317.e5.

Weidner, N. (1995). Current pathologic methods for measuring intratumoral microvessel density within breast carcinoma and other solid tumors. Breast Cancer Research and Treatment *36*, 169–180.

Weren, R.D.A., Ligtenberg, M.J.L., Kets, C.M., de Voer, R.M., Verwiel, E.T.P., Spruijt, L., van Zelst-Stams, W.A.G., Jongmans, M.C., Gilissen, C., Hehir-Kwa, J.Y., et al. (2015). A germline homozygous mutation in the base-excision repair gene NTHL1 causes adenomatous polyposis and colorectal cancer. Nature Genetics *47*, 668–671.

de Wilde, R.F., Edil, B.H., Hruban, R.H., and Maitra, A. (2012). Well-differentiated pancreatic neuroendocrine tumors: from genetics to therapy. Nature Reviews Gastroenterology & Hepatology *9*, 199–208.

Williams, A.B., and Schumacher, B. (2016). p53 in the DNA-Damage-Repair Process. Cold Spring Harbor Perspectives in Medicine *6*, a026070.

Williams, E.D., and Sandler, M. (1963). THE CLASSIFICATION OF CARCINOID TUMOURS. The Lancet *281*, 238–239.

Williamson, L.M., Steel, M., Grewal, J.K., Thibodeau, M.L., Zhao, E.Y., Loree, J.M., Yang, K.C., Gorski, S.M., Mungall, A.J., Mungall, K.L., et al. (2019). Genomic characterization of a well-differentiated grade 3 pancreatic neuroendocrine tumor. Molecular Case Studies *5*.

Wilm, A., Aw, P.P.K., Bertrand, D., Yeo, G.H.T., Ong, S.H., Wong, C.H., Khor, C.C., Petric, R., Hibberd, M.L., and Nagarajan, N. (2012). LoFreq: a sequence-quality aware, ultra-sensitive variant caller for uncovering cell-population heterogeneity from high-throughput sequencing datasets. Nucleic Acids Research *40*, 11189–11201.

Wong, H.L., Yang, K.C., Shen, Y., Zhao, E.Y., Loree, J.M., Kennecke, H.F., Kalloger, S.E., Karasinska, J.M., Lim, H.J., Mungall, A.J., et al. (2018). Molecular characterization of metastatic pancreatic neuroendocrine tumors (PNETs) using whole-genome and transcriptome sequencing. Molecular Case Studies *4*, a002329.

Wong, L.H., McGhie, J.D., Sim, M., Anderson, M.A., Ahn, S., Hannan, R.D., George, A.J., Morgan, K.A., Mann, J.R., and Choo, K.H.A. (2010). ATRX interacts with H3.3 in maintaining telomere structural integrity in pluripotent embryonic stem cells. Genome Research *20*, 351–360.

Wu, D., and Smyth, G.K. (2012). Camera: a competitive gene set test accounting for inter-gene correlation. Nucleic Acids Research *40*, e133–e133.

Xiang, Y., Stine, Z.E., Xia, J., Lu, Y., O'Connor, R.S., Altman, B.J., Hsieh, A.L., Gouw, A.M., Thomas, A.G., Gao, P., et al. (2015). Targeted inhibition of tumor-specific glutaminase diminishes cell-autonomous tumorigenesis. The Journal of Clinical Investigation *125*, 2293–2306.

Yachida, S., Vakiani, E., White, C.M., Zhong, Y., Saunders, T., Morgan, R., de Wilde, R.F., Maitra, A., Hicks, J., Demarzo, A.M., et al. (2012). Small Cell and Large Cell Neuroendocrine Carcinomas of the Pancreas are Genetically Similar and Distinct From Well-differentiated Pancreatic Neuroendocrine Tumors. The American Journal of Surgical Pathology *36*, 173–184.

Yamaguchi, H., Kawazu, M., Yasuda, T., Soda, M., Ueno, T., Kojima, S., Yashiro, M., Yoshino, I., Ishikawa, Y., Sai, E., et al. (2015). Transforming somatic mutations of mammalian target of rapamycin kinase in human cancer. Cancer Science *106*, 1687–1692.

Yang, H., Jeffrey, P.D., Miller, J., Kinnucan, E., Sun, Y., Thoma, N.H., Zheng, N., Chen, P.-L., Lee, W.-H., and Pavletich, N.P. (2002). BRCA2 function in DNA binding and recombination from a BRCA2-DSS1-ssDNA structure. Science *297*, 1837–1848.

Yang, H.W., Kutok, J.L., Lee, N.H., Piao, H.Y., Fletcher, C.D.M., Kanki, J.P., and Look, A.T. (2004). Targeted expression of human MYCN selectively causes pancreatic neuroendocrine tumors in transgenic zebrafish. Cancer Research *64*, 7256–7262.

Yang, K.C., Kalloger, S.E., Aird, J.J., Lee, M.K., Rushton, C., Mungall, K.L., Mungall, A.J., Gao, D., Chow, C., Xu, J., et al. Proteotranscriptomic classification and characterization of pancreatic neuroendocrine neoplasms. Cell Reports (In Revision).

Yao, J., Garg, A., Chen, D., Capdevila, J., Engstrom, P., Pommier, R., Cutsem, E. Van, Singh, S., Fazio, N., He, W., et al. (2019). Genomic profiling of NETs: a comprehensive analysis of the RADIANT trials. Endocrine-Related Cancer *26*, 391–403.

Yao, J.C., Hassan, M., Phan, A., Dagohoy, C., Leary, C., Mares, J.E., Abdalla, E.K., Fleming, J.B., Vauthey, J.N., Rashid, A., et al. (2008). One Hundred Years After " Carcinoid ": Epidemiology of and Prognostic Factors for Neuroendocrine Tumors in 35 , 825 Cases in the United States. Journal of Clinical Oncology *26*, 3063–3072.

Yao, J.C., Shah, M.H., Ito, T., Bohas, C.L., Wolin, E.M., Van Cutsem, E., Hobday, T.J., Okusaka, T., Capdevila, J., de Vries, E.G.E., et al. (2011). Everolimus for advanced pancreatic neuroendocrine tumors. The New England Journal of Medicine *364*, 514–523.

Yoshihara, K., Shahmoradgoli, M., Martínez, E., Vegesna, R., Kim, H., Torres-Garcia, W., Treviño, V., Shen, H., Laird, P.W., Levine, D.A., et al. (2013). Inferring tumour purity and stromal and immune cell admixture from expression data. Nature Communications *4*.

Yu, R. (2016). Animal models of spontaneous pancreatic neuroendocrine tumors. Molecular and Cellular Endocrinology *421*, 60–67.

Zanconato, F., Cordenonsi, M., and Piccolo, S. (2016). YAP/TAZ at the Roots of Cancer. Cancer Cell *29*, 783–803.

Zanconato, F., Cordenonsi, M., and Piccolo, S. (2019). YAP and TAZ: a signalling hub of the tumour microenvironment. Nature Reviews Cancer *19*, 454–464.

Zhang, B., Wang, J., Wang, X., Zhu, J., Liu, Q., Shi, Z., Chambers, M.C., Zimmerman, L.J., Shaddox, K.F., Kim, S., et al. (2014). Proteogenomic characterization of human colon and rectal cancer. Nature *513*, 382–387.

Zhao, B., Ye, X., Yu, J., Li, L., Li, W., Li, S., Yu, J., Lin, J.D., Wang, C.-Y., Chinnaiyan, A.M., et al. (2008). TEAD mediates YAP-dependent gene induction and growth control. Genes & Development *22*, 1962–1971.

Zimmerman, K.A., Yancopoulos, G.D., Collum, R.G., Smith, R.K., Kohl, N.E., Denis, K.A., Nau, M.M., Witte, O.N., Toran-Allerand, D., and Gee, C.E. (1986). Differential expression of myc family genes during murine development. Nature *319*, 780–783.

Appendix

Supplemental Data File

The following files can be found in the Appendix file “Supplemental Data File.xlsx”.

Supplemental Table 1. Clinicopathological and subgroup information for each of the 84 PNENs in the Discovery and Validation cohorts. List of sample identifiers, clinical and pathological characteristics, and the cohort and subgroup assignment for each of the 84 cases of PNENs included in this study.

Supplemental Table 2. The list of DEGs and DAPs and their differential expression or abundance analysis statistics. The Accession column refers to the Ensembl Gene ID (for mRNAs) or the UniProt Accession ID (for proteins) of each gene entry.

Supplemental Table 3. The mRNA- and protein- based gene set enrichment results for the complete list of MSigDB Hallmark gene sets. Includes mRNA-based results from the Discovery and Validation cohort specimens, and protein-based results from the Discovery cohort specimens.

Supplemental Table 4. Significantly over-represented pathways from SPIA results. Only over-represented pathways with adjusted p-value less than 0.05 are shown, and the status of a pathway is indicated as activated or inhibited based on topology score and p-value threshold of 0.05.

Supplemental Table 5. The mRNA- and protein- based gene set enrichment results for the cellular components gene ontologies. Only ontologies with an FDR-adjusted p-value less than 0.05 in either mRNA- or protein- based analysis are included.

Supplemental Table 6. TFEA results from ChEA3Only the top 10% ranked transcription factors are included.

Supplemental Table 7. Filtered variants in cancer-related genes identified from each of the Discovery cohort specimens.

Supplemental Table 8. VIPER results. Only regulators with an FDR-adjusted p-value less than 0.05 in at least one subgroup are shown**.**

Supplemental Table 9. Somatic sequence variants identified from each of the five metastatic PNEN cases.

Supplemental Table 10. KEGG pathway enrichment results for each of the five metastatic PNEN cases.

Supplemental Table 11. RNA expression and comparison of select genes of interest for each of the five metastatic PNEN cases.

Filename: Yang-Appendix.xlsx